The work described in this thesis was carried out at the Stratingh Institute for Chemistry, University of Groningen, The Netherlands.

This work was financially supported by the European Research Council (ERC).

Cover design by: R. Göstl, D. J. van Dijken and P. de Mendoza.

Printed by Ipskamp Drukkers BV, Enschede, The Netherlands.

ISBN: 978-90-367-7454-3
eISBN: 978-90-367-7453-6

university of groningen

Responsive Supramolecular Systems

PhD thesis

to obtain the degree of PhD at the
University of Groningen
on the authority of the
Rector Magnificus Prof. E. Sterken
and in accordance with
the decision by the College of Deans.

This thesis will be defended in public on

Friday 21 November 2014 at 11.00 h

by

Derk Jan van Dijken

born on 20 May 1984
in Soltau, Germany

Supervisor
Prof. B. L. Feringa

Assessment Committee
Prof. W. R. Browne
Prof. R. J. M. Nolte
Prof. J. J. L. M. Cornelissen

"Jedes erreichte Ziel ist wieder
Anfang einer neuen Laufbahn,
und so ins Unendliche."
(A. Schopenhauer, 19th century)

Table of Contents

Chapter 1

Photochromic Supramolecular Systems

In this introductory chapter, a literature overview of photochromic supramolecular systems is given, with the focus on molecular switches, incorporated into supramolecular assemblies. The first part highlights supramolecular chemistry, describing strategies for self-assembly, based on different interactions. In the second part of this chapter, an overview of various classes of photoswitches and their use in supramolecular assemblies is illustrated with recent literature examples. At the end of this chapter, an outline of this thesis is presented.

Part of the research presented in this chapter will be published:
D. J. van Dijken, B. L. Feringa, *manuscript in preparation*

1.1 Introduction

In this chapter, recent progress on photochromic supramolecular assemblies is discussed. Key concepts such as supramolecular chemistry and non-covalent interactions will be briefly explained and a short general overview of different classes of photoresponsive molecules will be given. Relevant literature examples will be given where these photoresponsive molecules have been employed in the realization of different photoresponsive supramolecular assemblies.

1.2 Supramolecular chemistry

Supramolecular chemistry is a specialized field in chemistry that specifically revolves around non-covalent interactions between different molecules, i.e. intermolecular bonds and interactions. The foundations have been laid by Cram,[1,2] Pedersen[3,4] and Lehn[5] and their work has been awarded the Nobel Prize in Chemistry in 1987, given for the development and use of molecules with structure-specific interactions of high selectivity.[6] Common interactions that "hold molecules together" are for example electrostatic interactions,[7–10] hydrogen bonding,[11–18] metal coordination,[19–24] hydrophobic forces,[25–27] π-π interactions,[28–34] ion-π interactions[35–37] and van der Waals forces.[38,39] In most cases, a combination of several of these forces is involved in the self-assembly process and responsible for preserving the supramolecular structure.

1.2.1 Complementarity and hydrogen bonds

The most well-known and perhaps the most important supramolecular assembly that is held together by complementary hydrogen bonds is deoxyribonucleic acid (DNA). DNA is a nucleic acid and consists of two polymeric strands that are coiled around each other to give the typical double helix structure. The two DNA strands consist of nucleotide building blocks.[40,41] The nucleotides contain a monosaccharide, phosphate and nucleobase moiety. The nucleobase moieties, i.e. guanine (G), adenine (A), thymine (T) or cytosine (C), have either a purine (G and A) or a pyrimidine (T and C) core. Guanine and adenine can form complementary hydrogen bonds with the pyrimidine nucleobases (T and C) and due to dimensional requirements in DNA, base pairs are normally formed between G-C and A-T.[40]

In recent years, supramolecular chemistry has received much attention as a tool to increase complexity in artificial systems. Self-assembly allows the design of molecules that can interact with each other to form a supramolecular macroscopic system with a level of complexity and/or functionality that would be very difficult to assemble by means of classical covalent synthesis.[42–45] Complementarity, which is defined as 'hosts must have binding sites which can simultaneously contact and attract the binding sites of the guests without generating internal strains or strong non-bonded repulsions",[46] is a key concept in designing molecules that are to self-assemble into a supramolecular complex as effective host-guest complexation requires that weak non-covalent interactions between the host and the guest outcompete solvation.

An example of (self)complementarity was reported by the group of Meijer[47] and consists of ureidopyrimidinone (**1.1**) and ureidotriazine (**1.2**) molecules (Figure 1.1). These molecules contain two hydrogen bond donor (D) and two hydrogen bond acceptor (A) moieties in a DADA and AADD array, respectively. The molecules are thereby self-complementary and this gives rise to the formation of dimers with high association constants (log K_a = 7 for **1.1** and log K_a = 4 for **1.2** in chloroform) in the solid state and solution. Utilizing the self-assembling properties of these cleverly designed molecules has led to the development of highly interesting supramolecular polymers[16,47–49] and recently hydrogels.[50]

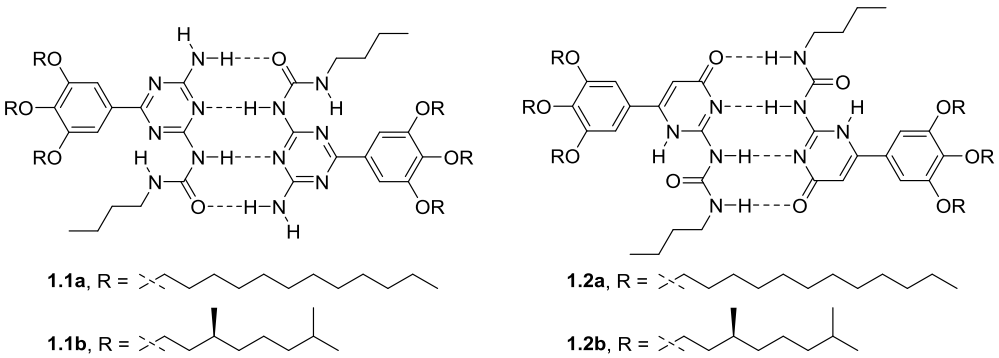

Figure 1.1. Structure of self-complementary ureidopyrimidinone **1.1** and ureidotriazine molecules **1.2** by Meijer and coworkers.[47]

1.2.2 Metal coordination

A different approach to supramolecular assemblies is based on metal coordination. In particular, chelating ligands are of interest and have been studied since the discovery and early work on crown ethers by Pedersen and coworkers.[3,51,52] Soon after the concept was established, Sauvage and Lehn studied the synthesis and stability of a wide variety of [2]-cryptates[53–56] and paved the way for metal coordination chemistry.[57–59] An increasingly popular class of metal-chelating ligands are pyridine-based, such as bipyridines[60] and terpyridines.[61] Complexes between (bis)terpyridine ligands and metal ions such as iron(II), copper(II), ruthenium(II), zinc(II), nickel(II) and cobalt(II) are readily formed.[61,62] A large variety of systems and intriguing structures have been prepared by design. One example is a giant supramolecular cube (Figure 1.2), reported by the group of Li.[63]

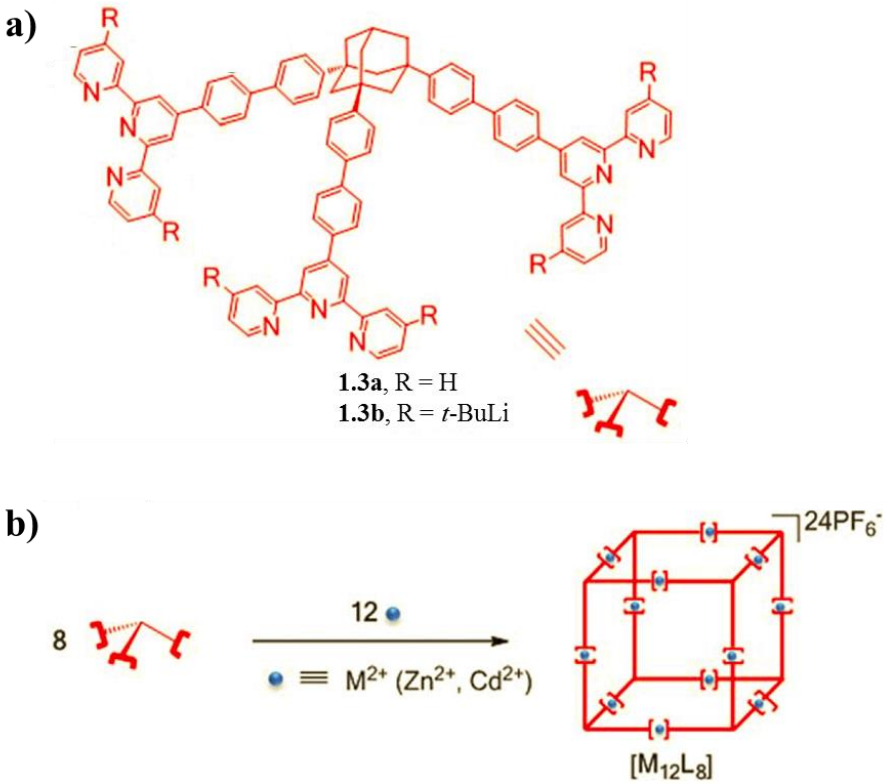

Figure 1.2. Giant supramolecular cube, containing eight terpyridine ligands **1.3** (L_8) as vertices and twelve metal ions (M_{12}; Cd^{2+} or Zn^{2+}) on edges. a) Structure of the ligand. b) Mixing the ligand with the metal ions yields the $M_{12}L_8$ cube. (Figure reproduced from reference 63)

The cube is the largest metallo-supramolecular cube reported to date. In most designs of metallo-cubes, the metal centres are used as vertices and the ligands that are able to coordinate to the metal, as edges. By reversing this synthetic strategy (Figure 1.2), mixing the ligand **1.3** with the metal ions yields the $M_{12}L_8$ cube with an edge length of ~4.9 nm, where the eight terpyridine ligands serve as vertices and twelve metal ions (Cd^{2+} or Zn^{2+}) as edges.

A recent and impressive example of using supramolecular assemblies, based on metal coordination was reported by the group of Fujita.[64] Using porous metal frameworks with large cavities (so called "crystalline sponges"), compounds that are hard to crystallize may enter the cavities and form an ordered array that can be studied by X-ray crystallography (Figure 1.3).

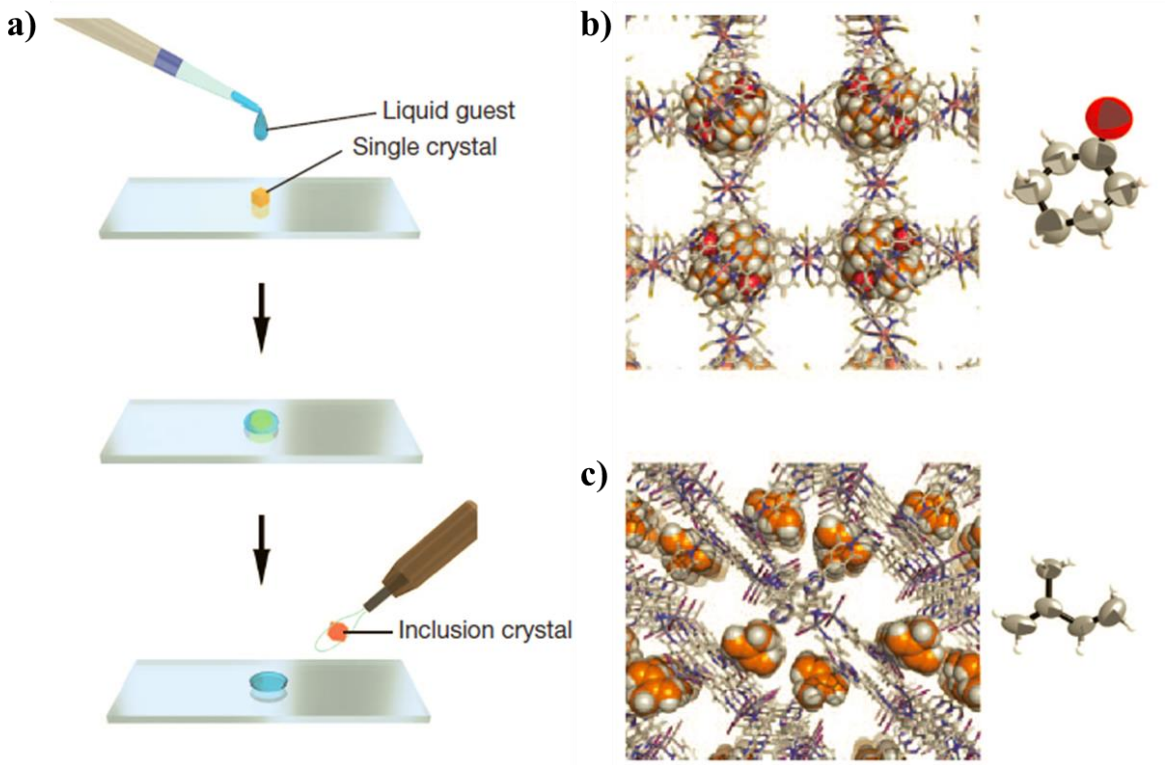

Figure 1.3. Crystal-free crystallography.[65] a) Schematic outline of the guest-included network complex: a piece of crystal of the porous metal complex host is treated for 2 d with a drop of liquid guest and subjected to X-ray data collection. b) X-ray crystal structure of cyclohexanone observed in the cavities of the host. c) X-ray crystal structure of isoprene in the pores of a different host. (Figure reproduced from reference 64)

The method has been termed "crystal-free crystallography"[65,66] and despite the fact that the power of the method was somewhat oversold[67] (the stereochemical assignment of a natural product turned out to be wrong), Fujita and coworkers demonstrated that by smart design and using non-covalent interactions, important problems in structure analysis can be addressed.[20] While the method is in its infancy, crystal-free crystallography may lead to a rapid and more convenient method for tentative crystallographic analysis than traditional X-ray crystallography, although the obtained results should be interpreted with caution.

1.2.3 π-π Interactions

Aromatic molecules have attracted a lot of attention due to their specific nature. In particular, the electronic and physiochemical properties of molecules such as fullerene, graphene and hexa-*peri*-hexabenzocoronene[68–71] (HBC) have prompted many research groups to study the chemical reactivity and possible modification of these molecules in the hope of finding practical applications in the fields of (nano)materials and biology. Supramolecular interactions between fullerene and synthetic hosts or receptors has recently emerged as an upcoming field.[72–75] Complexation of fullerene with macrocyclic host molecules such as crown ethers, cyclodextrins and calix[*n*]arenes is facile due to the concave-convex complementarity. It was reported by the groups of de Mendoza and Martín that complexation can be greatly increased when using three 2-[9-(1,3-dithiol-2-ylidene)anthracen-10(9*H*)-ylidene]-1,3-dithiole (exTTF) moieties, linked together in the cyclotriveratrylene (CTV) host molecule (Figure 1.4a, **1.4**).[76]

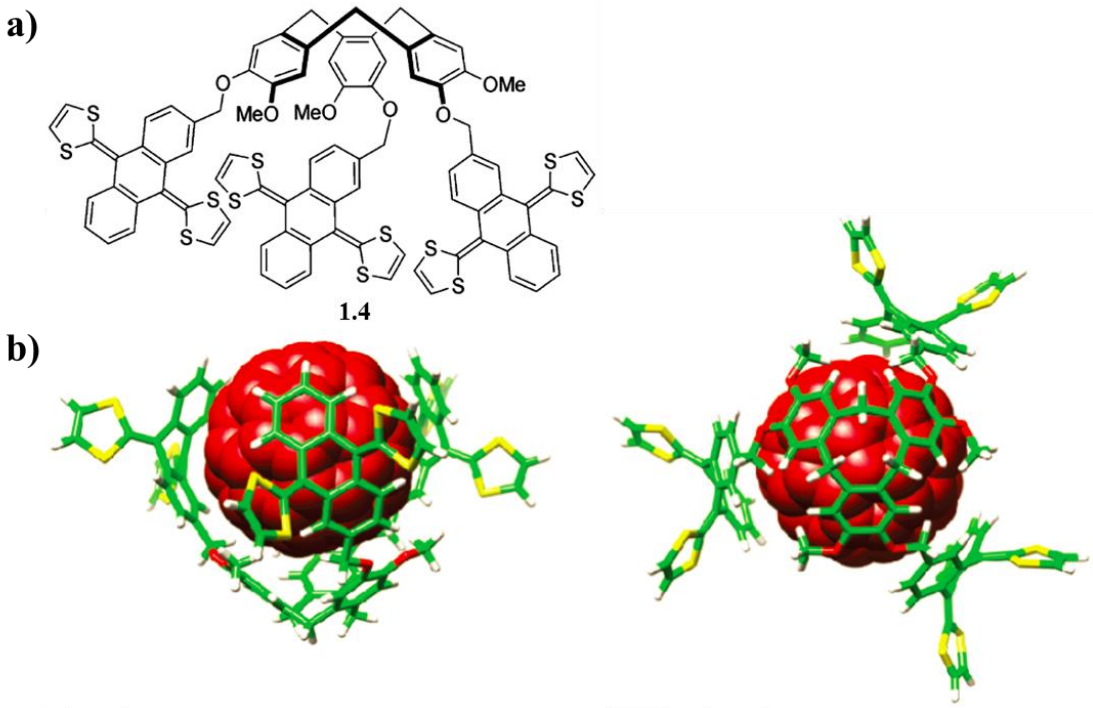

Figure 1.4. Complexation of host exTTF-CTV **1.4** and guest C_{60} fullerene. a) Structure of exTTF-CTV **1.4**, having four binding moieties for C_{60}. b) Energy-minimized structure (DFT) of C_{60}@exTTF-CTV; side view and top view. (Figure reproduced from reference 76)

It was envisioned that the CTV moiety would complex with C_{60} or C_{70} fullerene guest molecules and that the three exTTF moieties would wrap around the guest to effect very efficient binding (Figure 1.4b). Very stable complexes of the exTTF-CTV **1.4** and fullerenes were indeed found and the very high association constants were calculated to be log K_a = 5.3 ± 0.2 for C_{60} and log K_a = 6.3 ± 0.6 for C_{70}.

1.2.4 Hydrophobic forces

The tendency of apolar molecules to aggregate in aqueous solution in order to minimize the contact with water molecules is referred to as the hydrophobic effect.[77] The hydrophobic effect is very important for a variety of processes, including protein folding, the formation of micelles and bilayers and the insertion of membrane proteins into bilayer membranes.[78,79] Although the hydrophobic effect is to date not fully understood, it has been used in the design of artificial supramolecular systems.[80] The design of these type of systems is not trivial due to the aforementioned reason and focuses on host-guest complexes where the host is usually hydrophilic on the outside and has a far less hydrophilic cavity. Hydrophobic guests of appropriate size will have the tendency to enter the cavity due to the favourable hydrophobic interactions. Examples include, but are not limited to, cyclodextrins, porphyrins, crown ethers, calixarenes and cucurbiturils. In an example from Isaacs and coworkers,[81,82] it was shown that matching the size of a cucurbituril (CB) host, compared to the size of the guest, is very important and leads to large differences in binding (Figure 1.5).

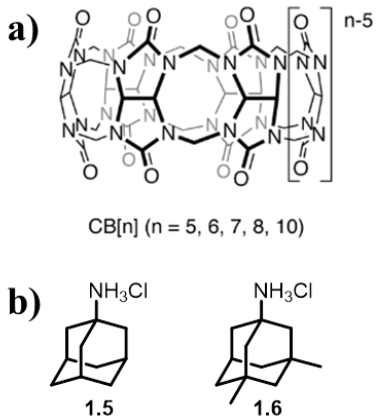

Figure 1.5. Host-guest binding based on cucurbituril hosts and adamantane guests. a) Structure of host CB[*n*]. b) Structures of adamantane guests **1.5** and **1.6**. (Figure in part reproduced from reference 82)

For adamantane **1.5**, association constants were found of log K_a = 12.6 for CB[7] and log K_a = 8.9 for CB[8]. For the more bulky adamantane **1.6**, association constants were found of log K_a = 4.4 for CB[7] and log K_a = 11.6 for CB[8] under identical conditions.[82] The higher association constant of CB[7] with **1.5** compared to **1.6** on one hand and the higher association constant of CB[8] with **1.5** compared to **1.6** on the other hand, show that seemingly small differences in structure have a large effect on association.

Despite the fact the hydrophobic effect is not completely understood to date, clever design has led to the development of complexes with very high association constants and as our knowledge of hydrophobic forces grows, supramolecular systems based on hydrophobic interactions could see increasing popularity in the coming years.

1.2.5 Amphiphiles

In Nature, aggregation processes play a crucial role. The membranes of all living cells consist of aggregated molecules, most notably lipids and proteins.[83] The lipids found in biological membranes are mainly phospholipids but non-phospholipids are also known. These amphiphilic, phospholipid molecules self-assemble into lipid bilayers in water and facilitate compartmentalization in cells. Without compartmentalization, i.e. the separation of different parts of the cell, specific function within these compartments without interfering with other cell functions would not be possible.[40]

The amphiphile, or surfactant, industry is huge[84–86] and these molecules have found wide spread use, ranging from household detergents to explosives.[87,88] Amphiphilic molecules contain a hydrophilic (water soluble) and hydrophobic (water insoluble) part (Figure 1.6a) and generally have the tendency to self-assemble in water in order to minimize unfavorable interactions with the solvent. The amphiphiles orient in such a way that the hydrophilic part of the molecule is facing the water (or other polar solvent), while the other part of the molecule aligns in such a way that interactions with the solvent are mostly avoided and other, more favorable interactions can be achieved. Following this principle, amphiphilic molecules have the tendency to give well-defined aggregates upon self-assembly in water, leading to the formation of for example rods, micelles, vesicles and inversed micelles (Figure 1.6b), depending on the amphiphile and the conditions.[89]

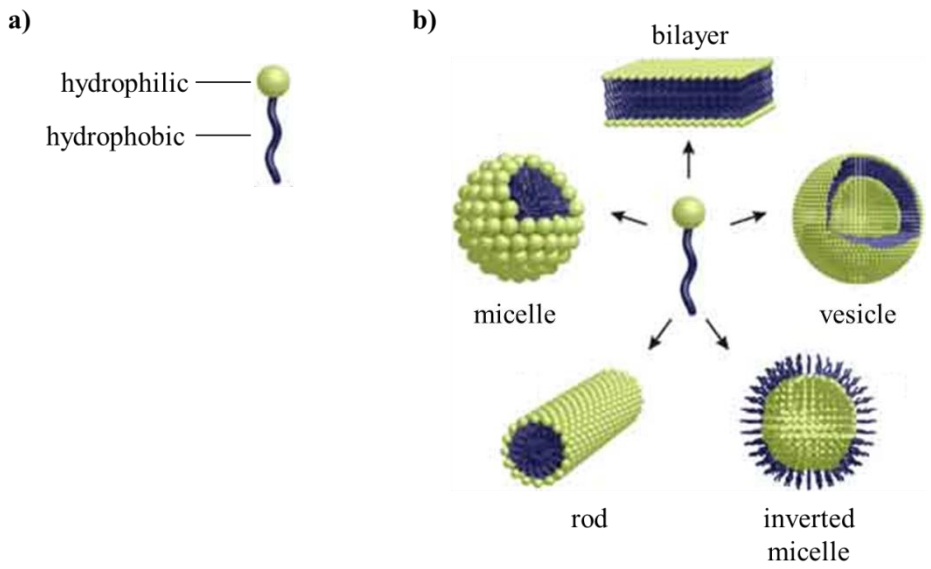

Figure 1.6. General structure and self-assembly of amphiphiles.[90] a) Schematic representation of an amphiphile. b) Different self-assembled morphologies. (Figure in part reproduced from reference 90)

The obtained morphology of the self-assembled amphiphile, depends on the way the amphiphiles organize in the solvent. This is directly correlated to their structure and the packing of the individual molecules, dependent on the so called "packing parameter" as introduced by Israelachvili and coworkers.[91] This model allows the prediction of aggregate morphology by calculating the headgroup area and the volume and length of the hydrophobic part of the amphiphile (Equation 1.1).

$$P = \frac{V}{a_0 \cdot l_c}$$

Equation 1.1. Packing parameter as introduced by Israelachvili and coworkers.[91]

In this equation,[91] the packing parameter is defined as the volume of the hydrophobic part of the amphiphile (V), divided by the cross-section of the headgroup (a_0) times the chain length (l_c). While V and l_c can be calculated relatively easily for a simple surfactant such as sodium dodecylsulphate (SDS), the value for the cross-section of the headgroup a_0, is more complicated to obtain as the effective size of the headgroup is dependent on the concentration of the amphiphile, the medium and the possible counterion. The packing parameter gives an indication for relatively simple amphiphiles on the self-assembled morphology as a function of their structure (Figure 1.7).

Effective shape of the surfactant molecule	Packing parameter	Aggregate morphology
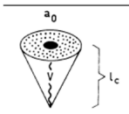 cone	<1/3	spherical micelles
 truncated cone	1/3 – 1/2	wormlike micelles
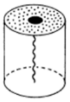 cylinder	1/2 – 1	bilayers, vesicles
 inverted (truncated) cone	>1	inverted micelles

Figure 1.7. Predicted morphology as a function of the packing parameter P.[92,93] (Figure reproduced from reference 93)

As the headgroup of an amphiphile gets smaller (Figure 1.7), relative to the hydrophobic volume of the amphiphile, self-assembly will change from spherical micelles, to stretched wormlike micelles and bilayers to ultimately inverted micelles. While the packing parameter gives a good estimate for relatively simple molecules and is very useful, it is often difficult to use for more complex molecules and synthesis and study of new classes of amphiphiles is often necessary.[94] New models or adaptations to the existing models are being developed,[95–98] to improve the ability to explain, rationalize or even predict self-assembly based on the molecular structure of the amphiphile, but one will eventually always have to prepare any new amphiphiles in the lab and study their morphology.

1.3 Cryo-transmission electron microscopy

Cryo-transmission electron microscopy (cryo-TEM) generally is the technique of choice to visualize and study the structure of dilute aggregated soft matter.[99] A thin film of the sample is prepared by rapidly freezing a blotted grid, containing a small drop of a dispersion, in liquid ethane. Due to the fact that TEM relies on the detection of transmitted electrons, the sample needs to be thin (<500 nm). The cooling with liquid ethane is fast enough to prevent reorganization and the sample is vitrified. This means that the sample can in principle be observed under the microscope as it was in the originally dispersed state. Caution should be taken when interpreting (cryo-)TEM data as artefacts may arise from sample preparation and sample impurities.

1.4 Photochromic moieties

Light is thought to be an important stimulus to trigger events for several reasons. Firstly, light can be controlled with high spatial and temporal precision. Secondly, light is non-invasive and does not leave any residues behind, unlike for example chemical stimuli, which can be an important aspect when addressing photoresponsive gelators for example.[92] Photochromic switches, or photoswitches, are a class of compounds that can undergo reversible photochemistry and are mostly based on isomerizations around double bonds or ring-opening

and -closing reactions. The most widely used photoswitches and their advantages and disadvantages are described briefly below.

1.4.1 Azobenzenes

Azobenzenes undergo *trans-cis* isomerization around the central double bond when irradiated with light of different wavelengths.[100] Generally, irradiation with UV light isomerizes *trans*-azobenzene to the *cis* form and the back reaction can be effected by irradiation with visible light. The *cis* isomer of azobenzenes is generally less stable than the *trans* isomer and a thermal back reaction from *cis* to *trans* usually occurs (Scheme 1.1). The photochemical isomerization is, however, much faster.

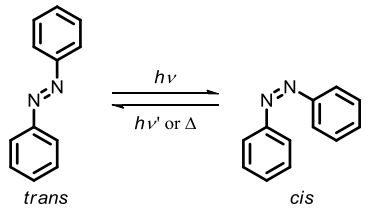

Scheme 1.1. Reversible photoisomerization of *trans* to *cis* azobenzene.

The two isomers of azobenzenes have significantly different dipole moments and a large geometrical change occurs upon isomerization from one form to the other. Azobenzenes are relatively easy to synthesize and have good fatigue resistance. One drawback is the usually modest thermal stability of the *cis* isomer, although in some cases this may be used as an advantage.[101–103]

1.4.2 Stilbenes

Much like their azo-analogs, stilbenes undergo *trans-cis* isomerization when irradiated with light. Isomerization of *trans* stilbene to its *cis* isomer or the reverse, is usually achieved by irradiation with UV light of different wavelengths (Scheme 1.2).

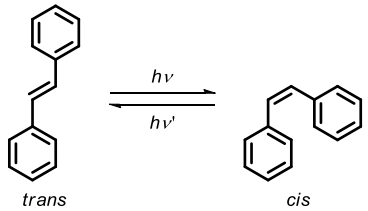

Scheme 1.2. Reversible photoisomerization of *trans* and *cis* stilbene.

The major drawback of stilbenes, compared to azobenzenes, is their tendency to undergo side reactions when isomerized from *trans* to *cis*. In particular, ring-closing reactions leading to the formation of dihydrophenanthrene side products from *cis* stilbene[104] is a common issue and has limited the use of stilbenes in complex, photoresponsive supramolecular assemblies.

1.4.3 Diarylethenes

Diarylethenes consist of a triene core that can undergo a reversible cyclization reaction (Scheme 1.3), giving rise to a ring-open and ring-closed form of the photoswitches. Irradiation with UV light yields the closed form, while ring-opening can be achieved by irradiation of the closed form with visible light.[105,106]

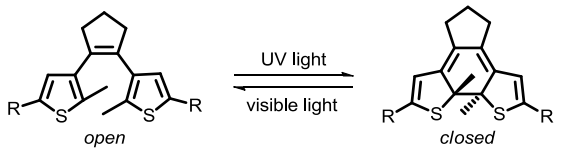

Scheme 1.3. Reversible photoisomerization of open and closed diarylethenes.

Diarylethenes count amongst the most widely used photoswitches, mainly due to the distinct differences in optical and electronic properties of the open and the closed form.[105,106] Another attractive aspect of diarylethenes is that their synthesis is relatively straightforward[107] and desired modifications are generally readily accomplished. Both the ring-open and -closed isomer of diarylethenes generally have good thermal stabilities and fatigue resistance.

1.4.4 Spiropyrans

Consisting of two heterocyclic moieties, spiropyrans can undergo reversible ring-opening to their merocyanine isomers upon irradiation with light (Scheme 1.4).[108]

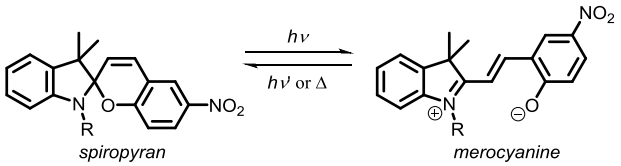

Scheme 1.4. Reversible photoisomerization of spiropyran.

The merocyanine form of the spiropyran is (predominantly) zwitterionic and a large change in dipole moment occurs. Usually, the merocyanine form is much more coloured than the thermally favoured spiropyran. The main drawback of spiropyrans is that the open merocyanine isomer suffers from relatively low thermal stability and a consecutively low lifetime.[109–111]

In addition to the most commonly used, aforementioned photoswitches, others are known but will not be treated here. Some examples are hemithioindigos[112] and fulgides.[113]

Photocleavable protecting groups have found widespread use in organic chemistry. This is due to the advantages light has over chemical means for deprotection.[114] Although sophisticated supramolecular systems have been reported where light is used as a trigger, these systems are not photochromic and as such will not be treated in this chapter.

1.5 Photoresponsive supramolecular systems

In this paragraph, a comprehensive literature overview of representative, recent examples of photoresponsive supramolecular assemblies is given. The focus lies on how the molecular functionality influences the supramolecular system as a whole when light is applied as an external stimulus.

1.5.1 Polymers

Supramolecular polymers are constructed by designing the monomers in such a way that intermolecular interactions hold the monomeric units together in a directional fashion so that a polymer can be formed. Typical interactions are described in paragraph 1.2 of this chapter.[115–117] While a disadvantage of supramolecular polymers, compared to conventional polymers, is the relatively weak interactions holding the polymer together, one of the major advantages is the ability to introduce specific functions in the polymer by functionalizing the monomers appropriately. Responsiveness of various supramolecular polymers to external stimuli such as a change in pH or light has been realized and reviewed recently in detail.[118,119] An illustrative example of light-responsive polymers by the group of Tian is shown in Figure 1.8.[120]

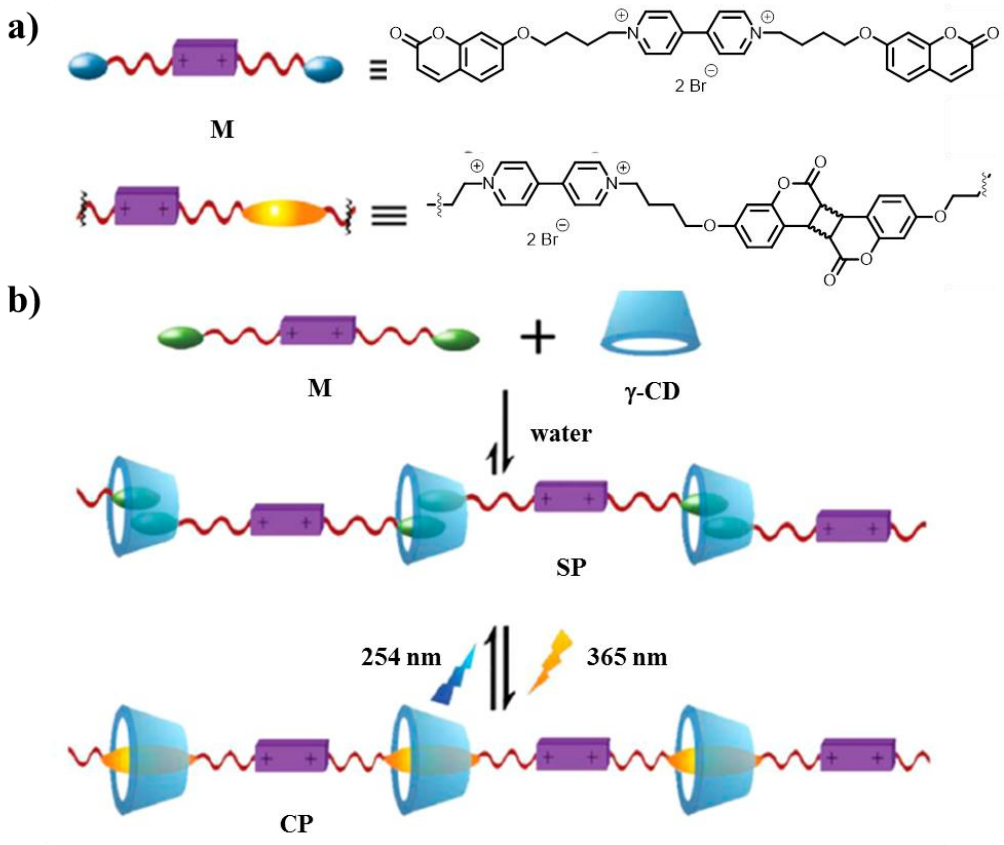

Figure 1.8. Dual-modality photoswitchable polymer. a) Molecular structures of the monomer **M** and the photo-dimerized covalent polymer. b) Schematic overview of the complexation and photo-dimerization and photochemical cleavage of the different complexes. **M** = monomer, γ-CD = γ-cyclodextrin, **SP** = supramolecular polymer, **CP** = covalent polymer. (Figure reproduced from reference 118)

The dual-modality photoswitchable polymer is based on a monomeric unit (**M**) bearing two terminal coumarin moieties, linked by a viologen unit (Figure 1.8a).[120] The coumarin moieties

can be accommodated by the γ-cyclodextrin (γ-CD) and this interaction is favorable in aqueous medium. The hydrophobic cavity of γ-CD is large enough to accommodate two coumarin moieties and a supramolecular polymer (**SP**) is formed in which γ-cyclodextrin acts as a linker between the monomeric units (Figure 1.8b). Upon irradiation with UV light (λ = 365 nm), the coumarins dimerize inside the γ-CD cavity and a covalent polymer (**CP**) is formed. Photochemical cleavage of the coumarin dimer by irradiation with UV light (λ = 254 nm), leads back to the supramolecular polymer **SP**, showing the reversibility of the system. Noteworthy, even at high concentration of **M** in aqueous solution, dimerization does not occur upon UV irradiation (λ = 365 nm). This finding proves that the γ-cyclodextrin is crucial for bringing the coumarins in close enough proximity for the photoreaction to occur, i.e. without formation of the supramolecular polymer **SP**, the covalent polymer **CP** cannot be formed.

Functional supramolecular polymers offer the possibility to integrate dynamics and order in one system and show promise for future applications.[116]

1.5.2 Liquid crystals

Liquid crystals (LCs) are self-assembled dynamic, functional, soft materials, which possess both mobility and order at the molecular, supramolecular and macroscopic level.[121] The fundamental liquid crystal forming structural unit is called a mesogen and, much like an amphiphile, usually consists of two (or more) separate parts, i.e. flexible and rigid moieties. LCs display unique, intermediate phase behavior between the liquid and solid phase and these materials therefore have properties that are common to both liquids and solids. All kinds of supramolecular interactions can be found in liquid crystals.[121,122] Specific intermolecular interactions play a major role in the supramolecular assembly of LCs. In addition, a mesogen can consist of self-assembled molecules itself and this concept has received much attention in recent years. A major advantage of these supramolecular mesogens is that complex structures can be built from molecular components by taking advantage of relatively simple and predictable assembly processes (Figure 1.9).[123]

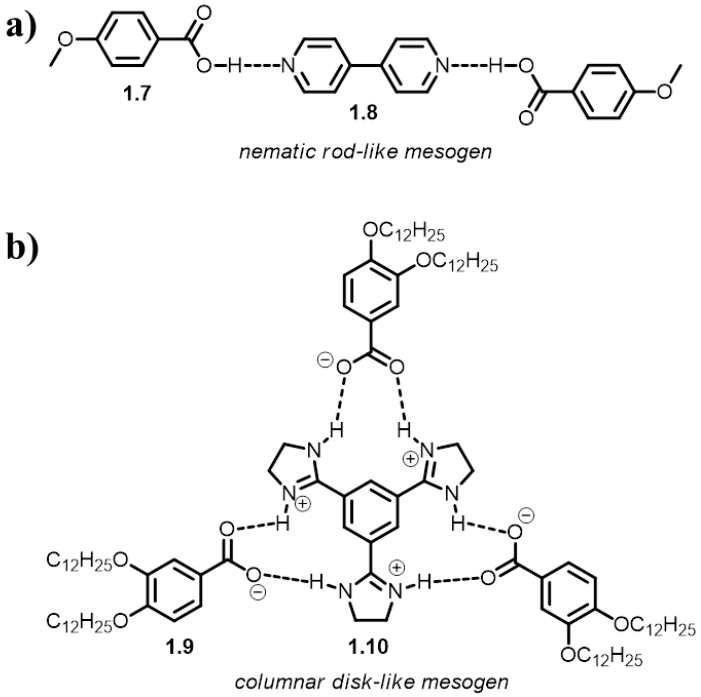

Figure 1.9. Mesogens that consist of self-assembled molecules that undergo specific supramolecular interactions to form a mesogen that gives well-defined LC phases.[123] a) Nematic rod-like mesogen, obtained by self-assembly of two components **1.7** and **1.8** (ratio 2:1) through hydrogen bonding. b) Columnar disk-like mesogen, obtained by self-assembly of two components **1.9** and **1.10** (ratio: 3:1) through hydrogen bonding.

Classically, temperature and concentration trigger liquid crystal phase transitions. Over the last decades, light has been added as a stimulus for these phase transitions, as pioneered by the group of Feringa,[124] through the incorporation of a variety of photoresponsive molecules either as dopant in LC mixtures[125–129] or the use of photoswitches that exhibit LC properties by themselves.[130,131] An illustrative example is given in Figure 1.10.

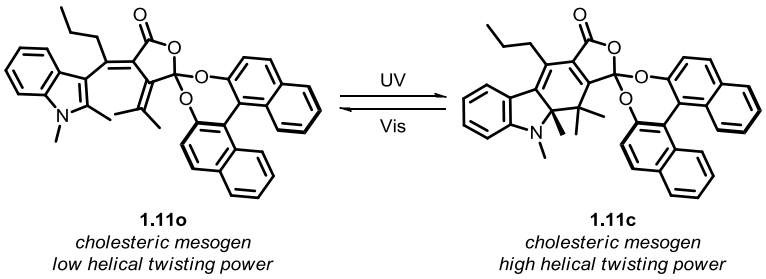

Figure 1.10. Photochromic dopant for switchable LCs.[127,132] The open (fulgide) form of the cholesteric mesogen **1.11o** has a low helical twisting power (β_M = -28 μm^{-1}), whereas the closed form **1.11c** has a very high helical twisting power (β_M = -175.3 μm^{-1}).

The efficiency of a dopant to induce a helical organization in an LC material is termed the helical twisting power, β_M. The open form of fulgide **1.11o** (Figure 1.10), has a low helical twisting power (β_M = -28 μm^{-1}) when mixed with a nematic LC.[127,132] The closed form **1.11c**, obtained by irradiation with UV light, has a very high helical twisting power (β_M = -175.3 μm^{-1}).

The authors report that the pitch of a cholesteric phase, doped with the photochromic fulgide **1.11**, can be changed to a large extend by irradiation with light of different wavelengths as a result of a change in the helical twisting power.

1.5.3 Gels

The effectiveness of a gelator to form a gel, as well as other properties of gelators, is in general very dependent on their molecular structure and small changes can have a significant effect on the properties. Molecular gelators, based on photoswitches, have therefore been developed as switching induces a structural change.[92,133–135]

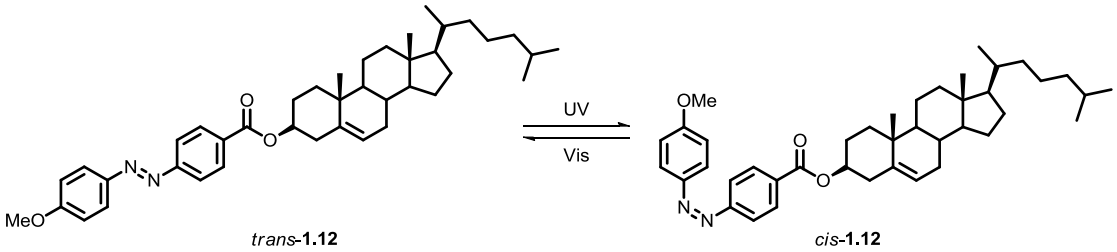

trans-**1.12** *cis*-**1.12**

Scheme 1.5. Photochromic gelator **1.12**, based on an azobenzene photoswitch.[133]

Azobenzene-derived molecular gelator **1.12** (Scheme 1.5) was reported by Shinkai and coworkers.[136] Gel to solution transitions in a variety of organic solvents could be tuned for this photoswitch, using light irradiation to trigger *trans*-*cis* isomerization. This further demonstrates the potential photoswitches have in macroscopic systems with the advantage of using light as the external trigger to induce changes.

In another design by the group of Feringa,[137] cholesteryl-appended diarylethene photoswitch **1.13** showed remarkable aggregation behavior in both organic and aqueous media (Figure 1.11). The development of systems that are able to form supramolecular aggregates in aqueous media takes the concept a step further in the direction of biocompatibility.[92,137,138]

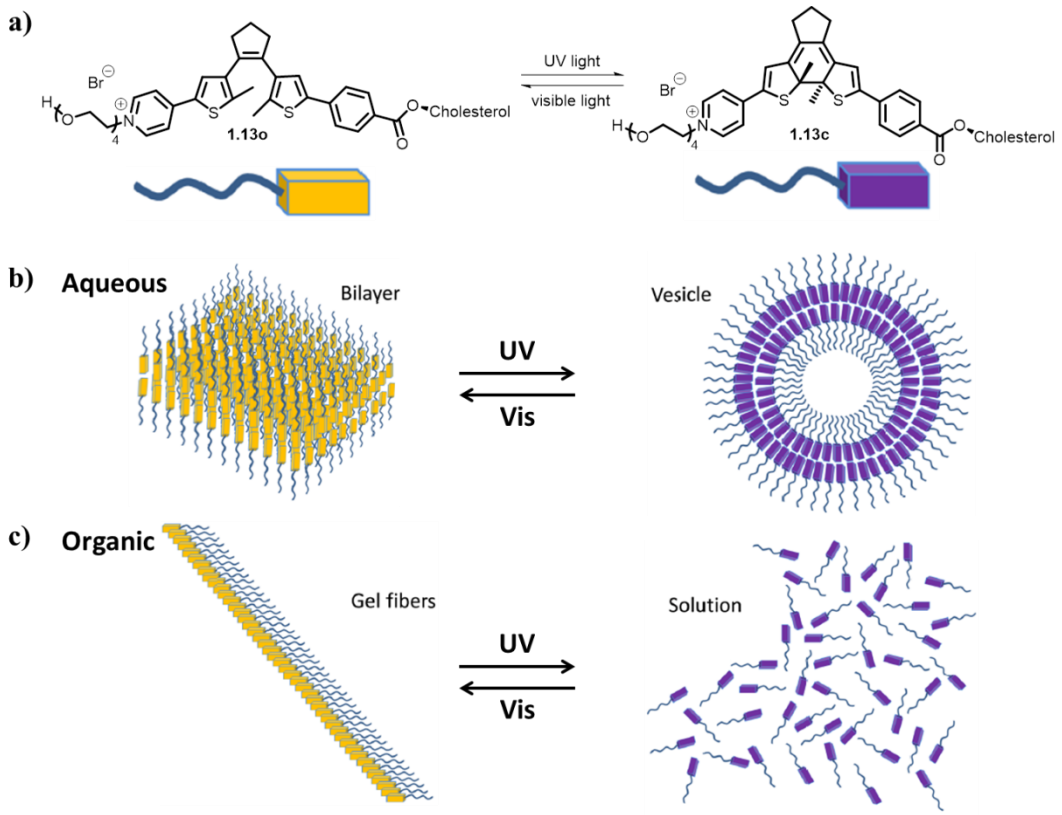

Figure 1.11. Dynamic self-assembly behavior of cholesterol-appended diarylethene **1.13**.[92,137] a) Structure and photoisomerization of **1.13**. b) Self-assembly behavior in aqueous media. c) Self-assembly behavior in organic media. (Figure reproduced from reference 92)

Photoswitch **1.13o** self-assembles into bilayers in aqueous media. Upon ring-closing with UV light, **1.13c** forms vesicles, presumably due to less tight packing of **1.13c** in the supramolecular aggregate, compared to **1.13o**, induced by a change in the packing parameter as a consequence of the ring-closure.[137] Remarkably, in organic media, different changes were observed upon photoisomerization of **1.13**. A gel was formed from **1.13o** and upon irradiation with UV light, the gel fibers were dissolved as confirmed by cryo-TEM measurements. Both changes in aqueous and organic media were found to be reversible and could be repeated several times.

1.5.4 Bilayer structures and micelles

The self-assembly properties of amphiphiles are strongly dependent on the structure and packing of the amphiphile (*vide supra*). Therefore, the packing can be disturbed by introducing a change in the structure of the amphiphilic molecule, resulting in a change of the self-assembly. The groups of Engberts and Poolman demonstrated this by synthesizing photochromic amphiphiles, bearing a hydrophilic phosphate headgroup and one (**1.14**) or two (**1.15**) hydrophobic chains that contain an azobenzene moiety (Figure 1.12).[139]

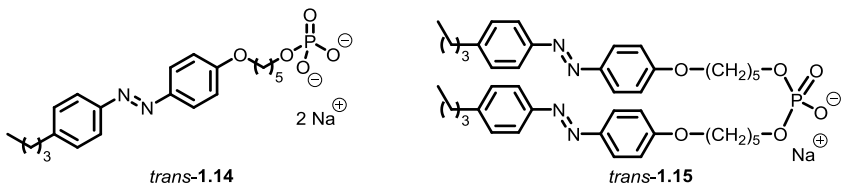

trans-**1.14** *trans*-**1.15**

Figure 1.12. Structure of amphiphilic azobenzenes reported by the groups of Engberts and Poolman.[139,140]

The effect of *trans-cis* isomerization on the aggregation and packing behaviour was studied. It was found that in all cases, photoisomerization disturbed the packing showing that photocontrol over bilayers that resemble biological membranes can be achieved. The prospect of such a system was further highlighted by the same groups in a system where a 1,2-dioleoyl-sn-glycero-3-phosphocholine (DOPC) membrane was doped with 20% of photochromic amphiphile **1.15** and a membrane channel, i.e. the mechanosensitive channel of large conductance (MscL), was reconstituted into this membrane.[140] Photoisomerization of *trans*-**1.15** to *cis*-**1.15** led to reversible activation and deactivation of the embedded MscL.

Micelles are self-assembled structures that are typically >1.5 nm in diameter and have a packing parameter P <1/3 – 1/2 (Figure 1.7). As micelles have a hydrophobic core that is shielded from water, these nanocontainers are capable of solubilizing hydrophobic compounds. Photoswitchable micelles have been reported and are mainly based on polymeric systems.[141,142] In an example by the group of Sakai,[141] following a molecular approach, fluid viscosity could be changed by irradiating azobenzene-based amphiphile **1.16** (Figure 1.13).

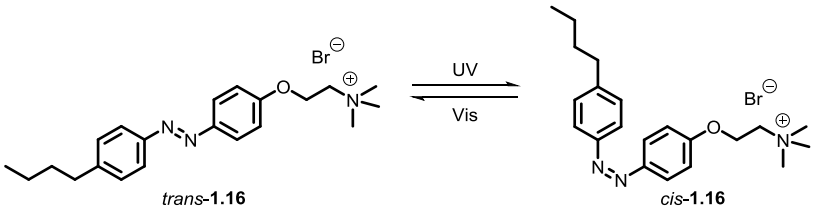

trans-**1.16** *cis*-**1.16**

Figure 1.13. Structure and photochromism of azobenzene-based amphiphile **1.16**.

A dispersion of wormlike micelles of cetyltrimethylammonium bromide (CTAB) was doped with photoswitch **1.16**.[141] The viscous mixture was irradiated with UV light to induce photoisomerization of the azobenzene amphiphile to give *cis*-**1.16** and this led to a significant drop in the viscosity of the mixture. This example shows the power of photoresponsive supramolecular systems in which doping a mixture with a small amount of photoresponsive material, that is able to interact in an intermolecular manner with the bulk material, leads to an overall photoresponsive system that can be made to change macroscopic properties with light as a stimulus.

1.6 Conclusions

Since supramolecular chemistry was introduced some decades ago,[1–5] the field has become increasingly more popular. The main reason for this is the ability of supramolecular chemistry to increase complexity of artificial systems by design. Based on non-covalent interactions such as hydrogen bonding, metal coordination, π-π interactions and hydrophobic interactions, increasingly complex supramolecular assemblies have been realized. In addition, over the years, more sophisticated techniques have been developed to analyze supramolecular structures and their morphology. Noteworthy, cryo-transmission electron microscopy has opened up the possibility to look at samples in their native state at very high spatial resolution.[143]

By incorporating functional molecules, such as photoswitches, into supramolecular assemblies, responsiveness into the larger system as a whole can be introduced, based on the molecular building block. Using light as an external stimulus to induce (macroscopic) changes in supramolecular complexes offers the advantages of high spatial and temporal precision as well as the non-invasive character of light. Towards this goal, the introduction of photoswitches into supramolecular building blocks has become an important field and many fascinating systems have been reported where different macroscopic properties of for example polymers, liquid crystals, gels and various bilayer structures can be changed with light.

Photochromic supramolecular systems have potential to be used in a wide variety of future applications. One could envision the use of these systems as photoresponsive materials, where a macroscopic object could for example be “healed” due to the rearranging of its molecular building blocks, triggered by light. Other applications that come to mind are dynamic sensing, as major events such as gelation can be triggered by light, or delivery systems in which photoresponsive capsules can be loaded, emptied and reloaded on demand by using light and heat (or light of a different wavelength) as orthogonal stimuli. The dynamic character of supramolecular assemblies and the non-invasive character of light as a stimulus, together with the growing knowledge and understanding of self-assembly and tunability of absorption wavelengths, has made the ongoing evolution of these type of systems possible. Due to the relative synthetic ease to create increasingly complex (photochromic) supramolecular systems, the limits of such systems are virtually only hampered by one’s creativity and effort.

1.7 Aim and outline of this thesis

The aim of this thesis work is the use of designed, (photo)responsive molecules and their self-assembly into supramolecular assemblies that have new properties, based on the molecular functionalities of the individual building blocks. The remaining chapters of this thesis can be divided into three general, but interconnected topics.

In chapter 2 and 3, chiral molecules were designed that can undergo non-covalent interactions with their achiral analogues, in order to induce chirality in the supramolecular assembly as a whole. In chapter 2, autoamplification of molecular chirality *via* induction of supramolecular chirality is described. The synthesis of enantiopure ring-closed diarylethenes and their use as chiral dopant in the co-assembly with their prochiral open counterparts, leading to the formation of a chirally biased, supramolecular gel is discussed. Subsequent ring-closure of the prochiral open diarylethenes leads to the preferential formation of one enantiomer that is the same compound as the chiral dopant. Chapter 3 is focussed around the synthesis and use of a chiral and achiral nanotube-forming amphiphile. For the chiral analogue, the chiral information is present in the hydrophobic, interacting part of the amphiphile and self-assembly is not inhibited. The nanotubes that are formed as a co-assembly with DOPC, from either chiral or achiral amphiphile, show characteristic differences and we studied the co-assemblies of the two amphiphiles at different ratios. The chiral (mixed) nanotubes are CD-active and the chiral information can be erased with light as the molecules undergo an irreversible photochemical ring-closing reaction and the resulting molecules are CD-silent.

In chapter 4, the synthesis of a small library of novel aromatic, amphiphilic molecules is described. We introduced systematic changes in the hydrophilic and hydrophobic parts of the amphiphiles as well as changes in the aromatic cores. Morphological changes as a function of structural changes in the amphiphiles were studied by cryo-TEM and the results are discussed. Some of the amphiphiles described in chapter 4 showed remarkable properties and a study of their properties in the formation of semi-permeable, ion-conducting membranes is presented in chapter 5. It is also discussed how the amphiphiles can form stable unilamellar vesicles of different sizes that have comparable properties as natural phospholipids, by using standard techniques.

In chapter 6, the design and properties of amphiphilic molecular motors, based on overcrowded alkenes is explored. It was observed that the molecular motors are able to self-assemble into nanotubular structures of different morphology, depending on the aromatic core. A large effect of the counterion on the structure of the aggregates was found and three different molecular motors were studied. The effect of the isomerization of the self-assembled molecular motors on the morphology and the reversibility of this process was investigated.

1.8 References

[1] D. J. Cram, J. M. Cram, *Container Molecules and Their Guests*, Royal Society Of Chemistry, Cambridge, UK, **1997**.

[2] D. J. Cram, *Angew. Chem. Int. Ed. Engl.* **1988**, *27*, 1009–1020.

[3] C. J. Pedersen, *J. Am. Chem. Soc.* **1967**, *89*, 7017–7036.

[4] C. J. Pedersen, *Angew. Chem. Int. Ed. Engl.* **1988**, *27*, 1021–1027.

[5] J. -M. Lehn, *Angew. Chem. Int. Ed. Engl.* **1988**, *27*, 89–112.

[6] *"Press Release: The 1987 Nobel Prize in Chemistry". Nobelprize.org.*, **2013**.

[7] L. Fabbrizzi, A. Poggi, *Chem. Soc. Rev.* **1995**, *24*, 197–202.

[8] J. A. Tilney, T. J. Sørensen, B. P. Burton-Pye, S. Faulkner, *Dalton Trans.* **2011**, *40*, 12063–12066.

[9] L. R. Hill, T. J. Sørensen, O. A. Blackburn, A. Brown, P. D. Beer, S. Faulkner, *Dalton Trans.* **2013**, *42*, 67–70.

[10] A. J. Harte, P. Jensen, S. E. Plush, P. E. Kruger, T. Gunnlaugsson, *Inorg. Chem.* **2006**, *45*, 9465–9474.

[11] L. C. Gilday, P. D. Beer, *Chem. – Eur. J.* **2014**, *20*, 8379–8385.

[12] J. J. D. de Jong, L. N. Lucas, R. M. Kellogg, J. H. Van Esch, B. L. Feringa, *Science* **2004**, *304*, 278–281.

[13] J. J. D. de Jong, T. D. Tiemersma-Wegman, J. H. van Esch, B. L. Feringa, *J. Am. Chem. Soc.* **2005**, *127*, 13804–13805.

[14] J. J. D. de Jong, P. van Rijn, T. D. Tiemersma-Wegeman, L. N. Lucas, W. R. Browne, R. M. Kellogg, K. Uchida, J. H. Van Esch, B. L. Feringa, *Tetrahedron* **2008**, *64*, 8324–8335.

[15] D. J. van Dijken, J. M. Beierle, M. C. A. Stuart, W. Szymański, W. R. Browne, B. L. Feringa, *Angew. Chem. Int. Ed.* **2014**, *53*, 5073–5077.

[16] W. P. J. Appel, M. M. L. Nieuwenhuizen, M. Lutz, B. F. M. de Waal, A. R. A. Palmans, E. W. Meijer, *Chem. Sci.* **2014**, *5*, 3735–3745.

[17] L. Brunsveld, A. Schenning, M. A. C. Broeren, H. M. Janssen, J. Vekemans, E. W. Meijer, *Chem. Lett.* **2000**, *29*, 292–293.

[18] G. Schaeffer, O. Fuhr, D. Fenske, J. -M. Lehn, *Chem. – Eur. J.* **2014**, *20*, 179–186.

[19] E. Elacqua, D. S. Lye, M. Weck, *Acc. Chem. Res.* **2014**, *47*, 2405–2416.

[20] Y. Inokuma, S. Yoshioka, J. Ariyoshi, T. Arai, M. Fujita, *Nat. Protoc.* **2014**, *9*, 246–252.

[21] T. Sawada, A. Matsumoto, M. Fujita, *Angew. Chem. Int. Ed.* **2014**, *53*, 7228–7232.

[22] M. Yoneya, S. Tsuzuki, T. Yamaguchi, S. Sato, M. Fujita, *ACS Nano* **2014**, *8*, 1290–1296.

[23] A. -M. Stadler, J. -M. Lehn, *J. Am. Chem. Soc.* **2014**, *136*, 3400–3409.

[24] G. Vantomme, J. -M. Lehn, *Angew. Chem. Int. Ed.* **2013**, *52*, 3940–3943.

[25] M. Lee, B. -K. Cho, K. J. Ihn, W. -K. Lee, N. -K. Oh, W. -C. Zin, *J. Am. Chem. Soc.* **2001**, *123*, 4647–4648.

[26] E. Obert, M. Bellot, L. Bouteiller, F. Andrioletti, C. Lehen-Ferrenbach, F. Boué, *J. Am. Chem. Soc.* **2007**, *129*, 15601–15605.

[27] M. Lee, D. -W. Lee, B. -K. Cho, J. -Y. Yoon, W. -C. Zin, *J. Am. Chem. Soc.* **1998**, *120*, 13258–13259.

[28] V. Percec, M. Glodde, T. K. Bera, Y. Miura, I. Shiyanovskaya, K. D. Singer, V. S. K. Balagurusamy, P. A. Heiney, I. Schnell, A. Rapp, H. -W. Spiess, S. D. Hudson, H. Duan, *Nature* **2002**, *419*, 384–387.

[29] C. A. Hunter, J. K. M. Sanders, *J. Am. Chem. Soc.* **1990**, *112*, 5525–5534.

[30] C. A. Hunter, M. N. Meah, J. K. M. Sanders, *J. Am. Chem. Soc.* **1990**, *112*, 5773–5780.

[31] J. P. Hill, W. S. Jin, A. Kosaka, T. Fukushima, H. Ichihara, T. Shimomura, K. Ito, T. Hashizume, N. Ishii, T. Aida, *Science* **2004**, *304*, 1481–1483.
[32] W. Jin, T. Fukushima, M. Niki, A. Kosaka, N. Ishii, T. Aida, *Proc. Natl. Acad. Sci. U. S. A.* **2005**, *102*, 10801–10806.
[33] T. Yamamoto, T. Fukushima, A. Kosaka, W. Jin, Y. Yamamoto, N. Ishii, T. Aida, *Angew. Chem.* **2008**, *120*, 1696–1699.
[34] T. Yamamoto, T. Fukushima, T. Aida, in *Self-Assembled Nanomaterials II*, Springer-Verlag Berlin, Heidelberg, Germany, **2008**, pp. 1–27.
[35] M. M. Watt, M. S. Collins, D. W. Johnson, *Acc. Chem. Res.* **2013**, *46*, 955–966.
[36] D. A. Dougherty, *Acc. Chem. Res.* **2013**, *46*, 885–893.
[37] J. C. Ma, D. A. Dougherty, *Chem. Rev.* **1997**, *97*, 1303–1324.
[38] S. U. N. Zipei, D. Xuelin, Z. Yan, L. Ziyan, H. Yaodong, *Front. Chem. Sci. Eng.* **2014**, *8*, 219–224.
[39] Y. Sun, X. Huang, *Supramol. Chem.* **2014**, DOI 10.1080/10610278.2014.904044.
[40] B. Alberts, A. Johnson, J. Lewis, M. Raff, K. Roberts, P. Walter, *Molecular Biology of the Cell, 4th Edition*, Garland Science, New York, USA, **2002**.
[41] J. D. Watson, F. H. C. Crick, *Nature* **1953**, *171*, 737–738.
[42] G. M. Whitesides, M. Boncheva, *Proc. Natl. Acad. Sci. U. S. A.* **2002**, *99*, 4769–4774.
[43] M. M. Boyle, R. A. Smaldone, A. C. Whalley, M. W. Ambrogio, Y. Y. Botros, J. F. Stoddart, *Chem. Sci.* **2011**, *2*, 204–210.
[44] J. -M. Lehn, *Top. Curr. Chem.* **2012**, *322*, 1–32.
[45] J. -M. Lehn, *Angew. Chem. Int. Ed.* **2013**, *52*, 2836–2850.
[46] J. B. Wittenberg, L. Isaacs, in *Supramolecular Chemistry: From Molecules to Materials*, John Wiley & Sons, Ltd, Chichester, UK, **2011**.
[47] A. R. Palmans, E. W. Meijer, *Angew. Chem. Int. Ed.* **2007**, *46*, 8948–8968.
[48] H. Kautz, D. J. M. van Beek, R. P. Sijbesma, E. W. Meijer, *Macromolecules* **2006**, *39*, 4265–4267.
[49] D. J. M. van Beek, A. J. H. Spiering, G. W. M. Peters, K. te Nijenhuis, R. P. Sijbesma, *Macromolecules* **2007**, *40*, 8464–8475.
[50] M. Guo, L. M. Pitet, H. M. Wyss, M. Vos, P. Y. Dankers, E. W. Meijer, *J. Am. Chem. Soc.* **2014**, *136*, 6969–6977.
[51] C. J. Pedersen, *J. Am. Chem. Soc.* **1967**, *89*, 2495–2496.
[52] C. J. Pedersen, *Org. Synth.* **1972**, *52*, 66–66.
[53] B. Dietrich, J. -M. Lehn, J. -P. Sauvage, *Tetrahedron Lett.* **1969**, 2885–&.
[54] B. Dietrich, J. -M. Lehn, J. -P. Sauvage, *Tetrahedron Lett.* **1969**, 2889–&.
[55] B. Dietrich, J. -M. Lehn, J. -P. Sauvage, *Tetrahedron* **1973**, *29*, 1647–1658.
[56] J. -M. Lehn, J. -P. Sauvage, *J. Am. Chem. Soc.* **1975**, *97*, 6700–6707.
[57] J. -P. Sauvage, *Acc. Chem. Res.* **1998**, *31*, 611–619.
[58] B. Champin, P. Mobian, J. -P. Sauvage, *Chem. Soc. Rev.* **2007**, *36*, 358–366.
[59] J. -P. Sauvage, C. Dietrich-Buchecker, *Molecular Catenanes, Rotaxanes and Knots: A Journey Through the World of Molecular Topology*, Wiley-VCH, Weinheim, Germany, **1999**.
[60] G. R. Newkome, A. K. Patri, E. Holder, U. S. Schubert, *Eur. J. Org. Chem.* **2004**, 235–254.
[61] H. Hofmeier, U. S. Schubert, *Chem. Soc. Rev.* **2004**, *33*, 373–399.
[62] U. S. Schubert, C. Eschbaumer, *Angew. Chem. Int. Ed.* **2002**, *41*, 2892–2926.
[63] C. Wang, X. -Q. Hao, M. Wang, C. Guo, B. Xu, E. N. Tan, Y. -Y. Zhang, Y. Yu, Z. -Y. Li, H. -B. Yang, M. -P. Song, X. Li, *Chem. Sci.* **2014**, *5*, 1221–1226.

[64] Y. Inokuma, S. Yoshioka, J. Ariyoshi, T. Arai, Y. Hitora, K. Takada, S. Matsunaga, K. Rissanen, M. Fujita, *Nature* **2013**, *495*, 461–466.
[65] B. Halford, *Chem. Eng. News Arch.* **2013**, *91*, 9–9.
[66] P. Stallforth, J. Clardy, *Nature* **2013**, *495*, 456–457.
[67] Y. Inokuma, S. Yoshioka, J. Ariyoshi, T. Arai, Y. Hitora, K. Takada, S. Matsunaga, K. Rissanen, M. Fujita, *Nature* **2013**, *501*, 262–262.
[68] A. Saeki, Y. Koizumi, T. Aida, S. Seki, *Acc. Chem. Res.* **2012**, *45*, 1193–1202.
[69] J. Wu, W. Pisula, K. Müllen, *Chem. Rev.* **2007**, *107*, 718–747.
[70] H. Duran, B. Hartmann-Azanza, M. Steinhart, D. Gehrig, F. Laquai, X. Feng, K. Müllen, H. -J. Butt, G. Floudas, *ACS Nano* **2012**, *6*, 9359–9365.
[71] W. Pisula, Ž. Tomović, M. D. Watson, K. Müllen, J. Kussmann, C. Ochsenfeld, T. Metzroth, J. Gauss, *J. Phys. Chem. B* **2007**, *111*, 7481–7487.
[72] S. -X. Fa, L. -X. Wang, D. -X. Wang, L. Zhao, M. -X. Wang, *J. Org. Chem.* **2014**, *79*, 3559–3571.
[73] F. Langa De La Puente, J. -F. Nierengarten, *Fullerenes: Principles and Applications*, Royal Society Of Chemistry, Cambridge, UK, **2007**.
[74] T. Kawase, H. Kurata, *Chem. Rev.* **2006**, *106*, 5250–5273.
[75] F. Diederich, M. Gómez-López, *Chem. Soc. Rev.* **1999**, *28*, 263–277.
[76] E. Huerta, H. Isla, E. M. Pérez, C. Bo, N. Martín, J. de Mendoza, *J. Am. Chem. Soc.* **2010**, *132*, 5351–5353.
[77] W. Blokzijl, J. B. F. N. Engberts, *Angew. Chem. Int. Ed. Engl.* **1993**, *32*, 1545–1579.
[78] C. Tanford, *Science* **1978**, *200*, 1012–1018.
[79] W. T. Wickner, H. F. Lodish, *Science* **1985**, *230*, 400–407.
[80] Z. Laughrey, B. C. Gibb, *Chem. Soc. Rev.* **2011**, *40*, 363–386.
[81] S. Liu, C. Ruspic, P. Mukhopadhyay, S. Chakrabarti, P. Y. Zavalij, L. Isaacs, *J. Am. Chem. Soc.* **2005**, *127*, 15959–15967.
[82] L. Isaacs, *Acc. Chem. Res.* **2014**, *47*, 2052–2062.
[83] H.T. Tien, A. Ottova-Leitmannova, *Membr. Sci. Technol.* **2003**, *7*, 1–73.
[84] E. W. Flick, *Industrial Surfactants: An Industrial Guide*, William Andrew, Park Ridge, N.J., U.S.A, **1994**.
[85] L. L. Schramm, *Surfactants. Fundamentals and Applications in the Petroleum Industry.*, Cambridge University Press, Cambridge, UK, **2010**.
[86] R. Nagarajan, *Amphiphiles: Molecular Assembly and Applications*, American Chemical Society, Washington, DC, USA, **2011**.
[87] P. L. Swisstack, *Aerated Aqueous Explosive Composition with Surfactant*, **1966**, US3288661 (A).
[88] T. F. Tadros, in *Applied Surfactants*, Wiley-VCH Verlag GmbH & Co. KGaA, Weinheim, Germany **2005**, pp. 1–17.
[89] K. Velonia, J. J. L. M. Cornelissen, M. C. Feiters, A. E. Rowan, R. J. M. Nolte, in *Nanoscale Assembly* (Ed.: W.T.S. Huck), Springer US, New York, USA, **2005**, pp. 119–185.
[90] D. Vriezema, H. Elemans, E. Pierson, H. Geurts, "Amphiphiles," can be found under http://www.vcbio.science.ru.nl/en/fesem/applets/amphiphiles/, **2014**.
[91] J. N. Israelachvili, D. J. Mitchell, B. W. Ninham, *J. Chem. Soc. Faraday Trans. 2 Mol. Chem. Phys.* **1976**, *72*, 1525–1568.
[92] J. T. van Herpt, *PhD Thesis: Photo- and Mechano-Responsive Supramolecular Systems*, University of Groningen, **2013**.

[93] R. T. Buwalda, *PhD Thesis: Molecular Aggregation in Water: The Interplay of Hydrophobic and Electrostatic Interactions*, University of Groningen, **2001**.
[94] J. M. Kuiper, *PhD Thesis: Azobenzene-Substituted Phosphate Amphiphiles*, University of Groningen, **2005**.
[95] R. Nagarajan, *Langmuir* **2002**, *18*, 31–38.
[96] G. K. Bourov, A. Bhattacharya, *J. Chem. Phys.* **2007**, *127*, 2449051–2449057.
[97] C. -I. Huang, Y. -J. Chiou, Y. -K. Lan, *Polymer* **2007**, *48*, 877–886.
[98] R. Lipowsky, E. Sackmann, *Structure and Dynamics of Membranes: I. From Cells to Vesicles/II. Generic and Specific Interactions*, Elsevier, Amsterdam, The Netherlands, **1995**.
[99] D. B. Williams, C. B. Carter, *Transmission Electron Microscopy: A Textbook for Materials Science*, Springer, New York, USA, **2011**.
[100] H. Rau, *Photoisomerization of Azobenzenes*, CRC Press: Boca Raton, FL, USA, **1990**.
[101] A. A. Beharry, G. A. Woolley, *Chem. Soc. Rev.* **2011**, *40*, 4422–4437.
[102] W. A. Velema, J. P. van der Berg, M. J. Hansen, W. Szymanski, A. J. M. Driessen, B. L. Feringa, *Nat. Chem.* **2013**, *5*, 924–928.
[103] W. A. Velema, W. Szymanski, B. L. Feringa, *J. Am. Chem. Soc.* **2014**, *136*, 2178–2191.
[104] D. H. Waldeck, *Chem. Rev.* **1991**, *91*, 415–436.
[105] M. Irie, *Chem. Rev.* **2000**, *100*, 1685–1716.
[106] B. L. Feringa, W. R. Browne, *Molecular Switches*, John Wiley & Sons, Weinheim, Germany, **2011**.
[107] L. N. Lucas, J. J. D. de Jong, J. H. van Esch, R. M. Kellogg, B. L. Feringa, *Eur. J. Org. Chem.* **2003**, *2003*, 155–166.
[108] G. Berkovic, V. Krongauz, V. Weiss, *Chem. Rev.* **2000**, *100*, 1741–1754.
[109] J. C. Crano, R. J. Guglielmetti, *Organic Photochromic and Thermochromic Compounds: Volume 2: Physicochemical Studies, Biological Applications, and Thermochromism*, Springer, New York, USA, **1999**.
[110] H. Dürr, H. Bouas-Laurent, *Photochromism: Molecules and Systems: Molecules and Systems*, Gulf Professional Publishing, Amsterdam, The Netherlands, **2003**.
[111] R. Guglielmetti, in *Photochromism* (Eds.: H. Dürr, H. Bouas-Laurent), Elsevier Science, Amsterdam, The Netherlands, **2003**, pp. 855–878.
[112] J. Plötner, A. Dreuw, *J. Phys. Chem. A* **2009**, *113*, 11882–11887.
[113] Y. Yokoyama, T. Gushiken, T. Ubukata, in *Molecular Switches* (Eds.: B. L. Feringa, W. R. Browne), Wiley-VCH Verlag GmbH & Co. KGaA, Weinheim, Germany, **2011**, pp. 81–95.
[114] A. G. Griesbeck, M. Oelgemöller, F. Ghetti, *CRC Handbook of Organic Photochemistry and Photobiology*, CRC Press, **2012**.
[115] L. Brunsveld, B. J. B. Folmer, E. W. Meijer, R. P. Sijbesma, *Chem. Rev.* **2001**, *101*, 4071–4098.
[116] T. Aida, E. W. Meijer, S. I. Stupp, *Science* **2012**, *335*, 813–817.
[117] T. F. A. De Greef, M. M. J. Smulders, M. Wolffs, A. P. H. J. Schenning, R. P. Sijbesma, E. W. Meijer, *Chem. Rev.* **2009**, *109*, 5687–5754.
[118] X. Ma, H. Tian, *Acc. Chem. Res.* **2014**, *47*, 1971–1981.
[119] X. Yan, F. Wang, B. Zheng, F. Huang, *Chem. Soc. Rev.* **2012**, *41*, 6042–6065.
[120] Q. Zhang, D. -H. Qu, J. Wu, X. Ma, Q. Wang, H. Tian, *Langmuir* **2013**, *29*, 5345–5350.
[121] H. K. Bisoyi, S. Kumar, *Chem. Soc. Rev.* **2011**, *40*, 306–319.

[122] D. Demus, J. W. Goodby, G. W. Gray, H. W. Spiess, V. Vill, *Handbook of Liquid Crystals, Low Molecular Weight Liquid Crystals I: Calamitic Liquid Crystals*, John Wiley & Sons, Weinheim, Germany, **2011**.
[123] T. Kato, N. Mizoshita, K. Kishimoto, *Angew. Chem. Int. Ed.* **2006**, *45*, 38–68.
[124] B. L. Feringa, N. P. M. Huck, H. A. van Doren, *J. Am. Chem. Soc.* **1995**, *117*, 9929–9930.
[125] S. J. Aßhoff, S. Iamsaard, A. Bosco, J. J. L. M. Cornelissen, B. L. Feringa, N. Katsonis, *Chem. Commun.* **2013**, *49*, 4256–4258.
[126] R. Eelkema, M. M. Pollard, J. Vicario, N. Katsonis, B. S. Ramon, C. W. M. Bastiaansen, D. J. Broer, B. L. Feringa, *Nature* **2006**, *440*, 163–163.
[127] R. Eelkema, B. L. Feringa, *Org. Biomol. Chem.* **2006**, *4*, 3729–3745.
[128] C. Denekamp, B. L. Feringa, *Adv. Mater.* **1998**, *10*, 1080–1082.
[129] R. Eelkema, *PhD Thesis: Liquid Crystals as Amplifiers of Molecular Chirality*, University of Groningen, **2006**.
[130] Y. Li, Q. Li, in *Nanosci. Liq. Cryst.* (Ed.: Q. Li), Springer International Publishing, New York, USA, **2014**, pp. 135–177.
[131] K. Ichimura, *Chem. Rev.* **2000**, *100*, 1847–1874.
[132] T. Sagisaka, Y. Yokoyama, *Bull. Chem. Soc. Jpn.* **2000**, *73*, 191–196.
[133] X. Yang, G. Zhang, D. Zhang, *J. Mater. Chem.* **2011**, *22*, 38–50.
[134] J. J. D. de Jong, *PhD Thesis: Dithienylcyclopentene Optical Switches*, University of Groningen, **2006**.
[135] J. H. van Esch, B. L. Feringa, *Angew. Chem. Int. Ed.* **2000**, *39*, 2263–2266.
[136] K. Murata, M. Aoki, T. Suzuki, T. Harada, H. Kawabata, T. Komori, F. Ohseto, K. Ueda, S. Shinkai, *J. Am. Chem. Soc.* **1994**, *116*, 6664–6676.
[137] J. T. van Herpt, J. Areephong, M. C. A. Stuart, W. R. Browne, B. L. Feringa, *Chem. – Eur. J.* **2014**, *20*, 1737–1742.
[138] W. A. Velema, M. C. A. Stuart, W. Szymanski, B. L. Feringa, *Chem. Commun.* **2013**, *49*, 5001–5003.
[139] J. M. Kuiper, M. C. A. Stuart, J. B. F. N. Engberts, *Langmuir* **2008**, *24*, 426–432.
[140] J. H. A. Folgering, J. M. Kuiper, A. H. de Vries, J. B. F. N. Engberts, B. Poolman, *Langmuir* **2004**, *20*, 6985–6987.
[141] H. Sakai, Y. Orihara, H. Kodashima, A. Matsumura, T. Ohkubo, K. Tsuchiya, M. Abe, *J. Am. Chem. Soc.* **2005**, *127*, 13454–13455.
[142] J. Jiang, Q. Shu, X. Chen, Y. Yang, C. Yi, X. Song, X. Liu, M. Chen, *Langmuir* **2010**, *26*, 14247–14254.
[143] H. v. Berlepsch, K. Ludwig, B. Schade, R. Haag, C. Böttcher, *Adv. Colloid Interface Sci.* **2014**, *208*, 279–292.

Chapter 2

Autoamplification of Molecular Chirality through the Induction of Supramolecular Chirality

Doping a mixture of prochiral, open diarylethenes with their enantiopure, closed counterparts, led to formation of gel fibers of preferred helicity. This supramolecular chirality was transferred to the molecular level by photochemical ring-closing, yielding a chiral product that is enhanced in the same enantiomer as was used as a template.

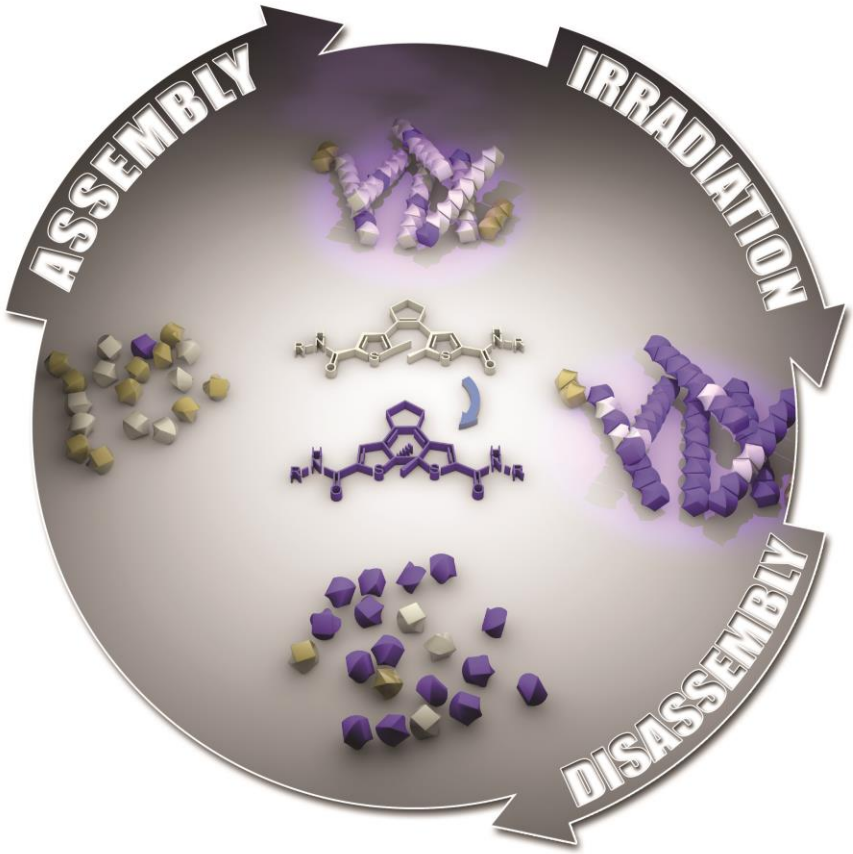

Part of the research presented in this chapter has been published:
D. J. van Dijken, J. M. Beierle, M. C. A. Stuart, W. Szymański, W. R. Browne, B. L. Feringa, *Angew. Chem. Int. Ed.* **2014**, *53*, 5073–5077.

2.1 Introduction

The origin of homochirality in biological systems has been the topic of research and debate for many decades.[1,2] Going from an initial imbalance in racemates, creating very small enantiomeric excesses (*e.e.*), in the prebiotic world to the homochiral, biological world we live in now, must imply an amplification mechanism to propagate and enhance the chiral bias.[3,4] One of the principles that can underlie this process, asymmetric autocatalysis, is that a reaction forms a chiral product that can act as a chiral catalyst for its own formation (Scheme 2.1) while suppressing the formation of the other chiral product.

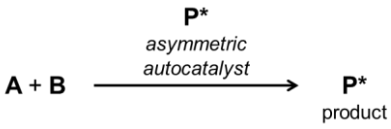

Scheme 2.1. Principle of asymmetric autocatalysis.

This model, first proposed by Frank,[5] was experimentally demonstrated in the so called Soai reaction (Scheme 2.2). In the seminal work by Soai *et al.*[6–8] on asymmetric autocatalysis it is shown that auto-amplification of *molecular chirality* can be achieved by the product of a reaction acting as a chiral ligand for a metal, forming a complex that catalyzes the enantioselective formation of this product.

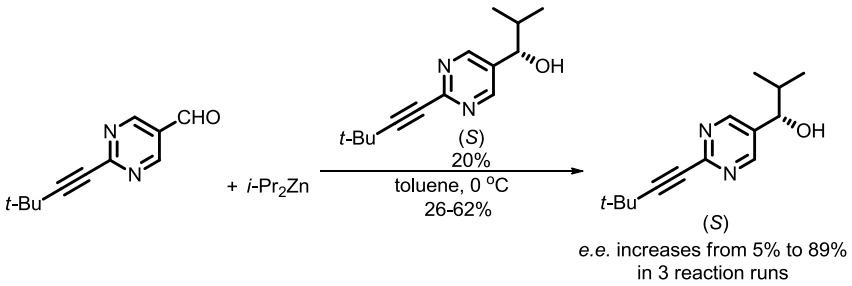

Scheme 2.2. Autoamplification of molecular chirality in the Soai reaction.[8]

When the aldehyde starting material reacts with diisopropylzinc in the presence of catalytic amounts of the chiral alcohol with small enantiomeric excess, more of the alcohol is formed through an autocatalytic reaction.[8] The enantiomeric excess of the product is enhanced as the chiral catalyst is the product generated from this reaction and because the reaction is enantioselective.[9,10] This reaction stands out as the first example that employed a catalyst with very low enantiomeric excess, while yielding catalyst as product with very high *e.e*. Blackmond and Brown provided a mechanistic model for this chiral amplification, involving a catalyst that is able to accelerate its own formation, while simultaneously suppressing other catalytic species that would lead to the formation of the opposite enantiomer.[3,11,12] Finding and understanding reactions that can follow such autocatalytic pathways has been the goal of many research groups since the original proposal and discoveries.[6,7,13,14]

The concept of chiral amplification has been extended to noncovalent macromolecular systems and the emergence and induction of *supramolecular chirality* in dynamic macromolecular aggregates was pioneered by Meijer and co-workers.[15,16] It was shown that doping of achiral, disc-shaped molecules with small quantities of chiral analogues results in the formation of long, chiral, columnar stacks held together by hydrogen bonding.[17]

In the columnar stacks, the chiral dopant is distinct from the majority of the achiral entity, as opposed to the Soai system that shows autoamplification of chirality based on a chiral catalyst in which the product is identical to the chiral ligand in the catalyst. Moreover, the achiral molecule is not a precursor for the chiral molecule and there is no conversion of one into the other.

For the transfer of chirality, most supramolecular systems (including the previously-mentioned example by the group of Meijer[17]) rely on the "sergeant-soldier principle" as introduced by Green and coworkers.[18] According to this mechanism of chiral amplification, a minor amount of the chiral compound (sergeant), used as dopant, dictates the overall chirality of a system that is made up of mainly achiral material (soldiers). In recent years, this principle has been exploited in the field of supramolecular chemistry in preparation of supramolecular polymers,[19–25] gels,[26] organic nanotubes[27–29] and other assemblies.[30–35]

Another example from the group of Meijer[36] is based on the coassembly of achiral, amide-functionalized porphyrins with small quantities of the chiral analogue, forming helical, columnar stacks (Figure 2.1) and it nicely illustrates the concept and power of the sergeant-soldiers principle applied in supramolecular systems. Successful coaggregation was shown and chiral amplification *via* the sergeant-soldier principle was achieved, i.e., the overall chirality of the helical columns can be dictated by incorporation of small quantities of chiral zinc-porphyrin (**S-Zn**; sergeant) into the coaggregated column that mainly consists of achiral copper-porphyrin (**A-Cu**; soldier). Aggregates of pure **A-Cu** are CD-silent and show no bias in helicity.

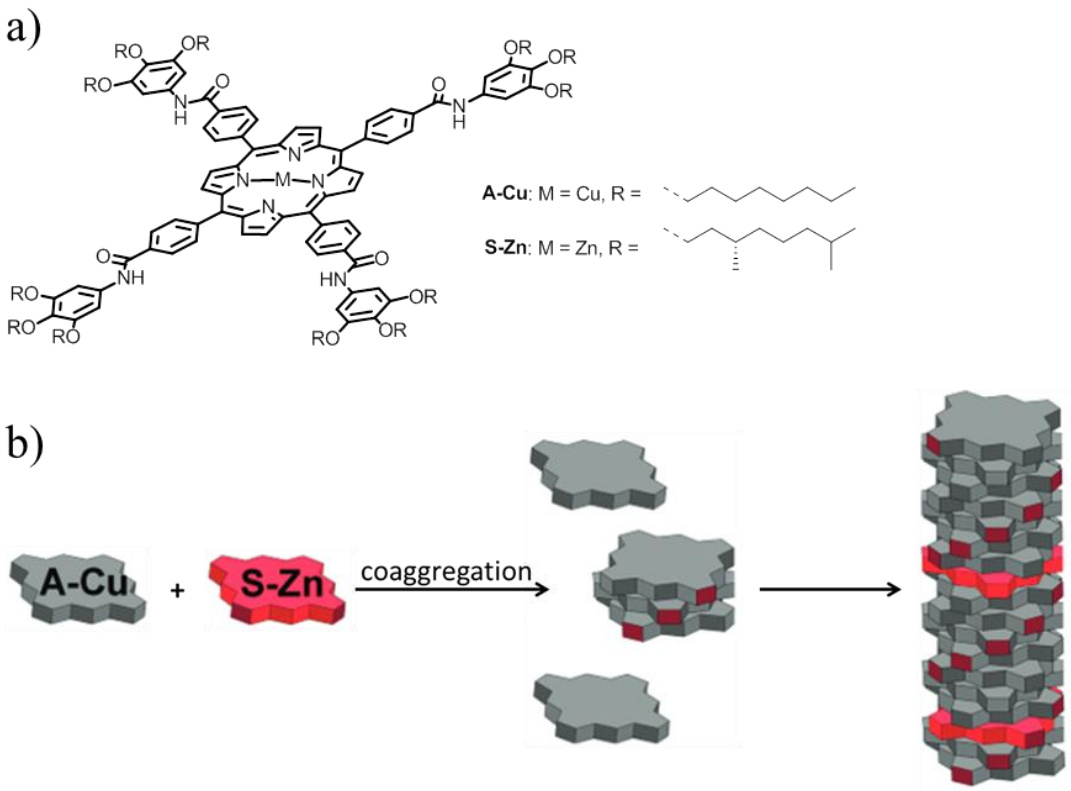

Figure 2.1. Sergeant-soldier principle in supramolecular, helical, columnar stacks of coaggregates of chiral and achiral porphyrins, presented by Meijer and coworkers.[36] (Figure reproduced from reference 36)

The key question is: can supramolecular chirality result in induction of chirality at the molecular level in the constituting molecular component of the chiral supramolecular aggregate? The research described in this chapter aims at the development of such a system, combining the concept of autoamplification of chirality and that of supramolecular amplification of chirality. The main novelty of this system, as compared to for example the work of Meijer and coworkers,[15,16,36] resides in the fact that the soldier is a precursor of the sergeant, and can be converted into it after the amplification of supramolecular chirality is established. This allows the autoamplification of molecular chirality *via* induction of supramolecular chirality. The system presented here is based on amide-modified diarylethene molecular photoswitches.[37–41]

Diarylethenes consist of a triene core that can undergo a reversible cyclization reaction (Scheme 2.3), giving rise to a ring-open and ring-closed form of the photoswitches. Due to the presence of the two methyl substituents and the freedom of rotation between the ethene moiety and the aryl groups, diarylethenes in their open form are not planar and exist in two conformations (Scheme 2.3). The two aryl groups can either be in the parallel (mirror symmetry) or anti-parallel (C_2 symmetry) conformation.

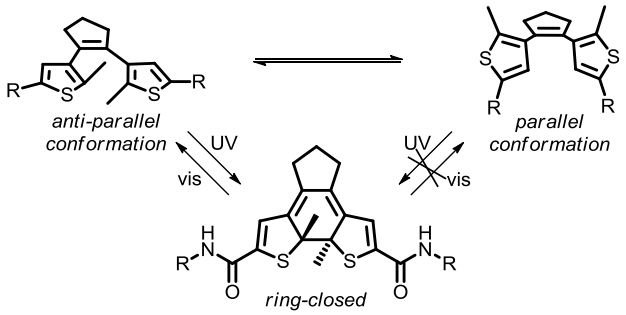

Scheme 2.3. Conformations and cyclization reaction of the most common diarylethenes.

In addition, diarylethenes in their open form **2.1o** (**o** = open form) exist in two, rapidly exchanging, chiral conformations ((*P*)- and (*M*)-helicity) in solution.[42] During ring-closing, which results from irradiation with UV light, two stereogenic centers are generated, giving rise to two enantiomers (Scheme 2.4): (*R*,*R*)-**2.1c*** from (*P*)-**2.1o** and (*S*,*S*)-**2.1c*** from (*M*)-**2.1o** (**c** = closed form; ***** denotes that the compound is a single enantiomer). Ring-closure is only possible in the anti-parallel conformation (Scheme 2.3). Upon ring-closure of prochiral **2.1o** in solution, a racemic mixture of **2.1c** is obtained due to the fast interconversion of the two conformations of **2.1o** in solution.

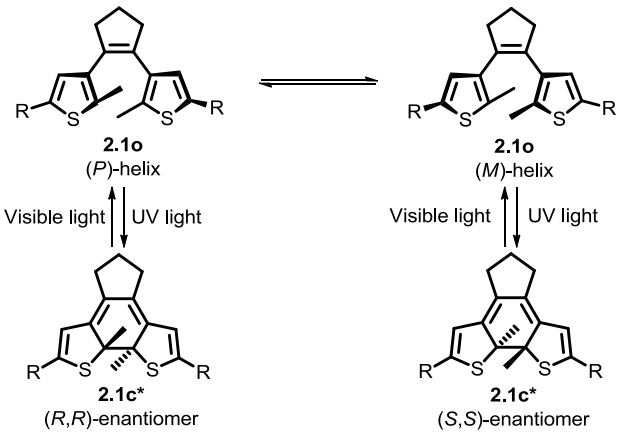

Scheme 2.4. Helical conformations of diarylethene **2.1o** and the formation of two enantiomers of **2.1c** upon photochemical ring-closing; **o** = open form, **c** = closed form, ***** = single enantiomer.

Due to fast equilibrium between the anti-parallel and parallel conformations, full conversion to the ring-closed form of the diarylethene can in principle be obtained. Irradiation of the closed form with visible light, results in the reverse reaction to the open form.[43]

The fact that diarylethenes are widely used is mainly due to the distinct differences in optical and electronic properties of the open and the closed form.[37,44] Another attractive aspect of diarylethenes is that their synthesis is relatively straightforward[40] and desired modifications are generally readily accomplished. Moreover, functionalization of diarylethenes with amide moieties allows the photoswitches to assemble through hydrogen bonding and undergo highly specific self-assembly.[39,41,45,46] The self-assembly, that is a consequence of the hydrogen bonding, results in low molecular weight gelators (LMWGs).[47–52] LMWGs form non-covalent interactions that allow monomers to aggregate and entrap solvent molecules, thereby forming a gel (Figure 2.2).

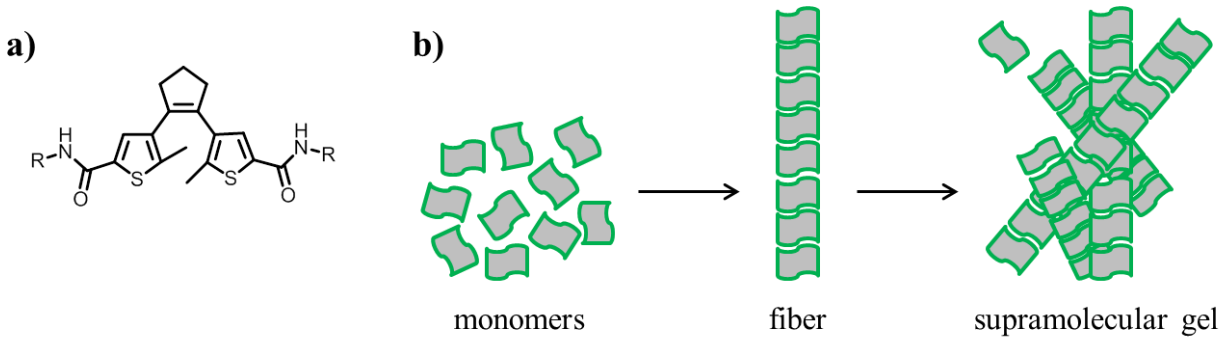

Figure 2.2. Schematic representation of self-assembly of amide-functionalized diarylethenes a) Monomer diarylethene, appended with amide moieties. b) The monomers interact with each other through hydrogen bonding, self-assembling into fibers. The fibers aggregate and entrap solvent molecules, thereby forming a gel.

To prepare a gel, solvent is added to the LMWG monomers, but not enough to dissolve all monomers. When heated, the gelator molecules dissolve and, upon cooling, aggregate to form fibers. These fibers interact with each other and form a gel. Properties of the gels can be fine-tuned by chemical modifications of the monomers,[53–56] but understanding the processes that occur within the gel is often difficult.[49]

2.2 Concept

The goal of the research, presented in this chapter, is to induce a templated bias for one of the product enantiomers in the photochemical ring-closing reaction of a prochiral diarylethene photoswitch. The use of an enantiopure template in "catalytic" amounts, that is also the product of the reaction (the ring-closed photoswitch), means that this reaction is analogous to autocatalytic reactions such as the Soai reaction.[8] A simplified version of the concept is shown in Scheme 2.5.

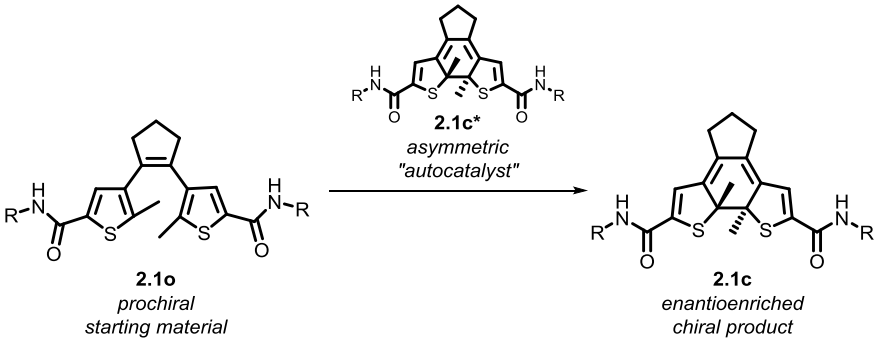

Scheme 2.5. Simplified concept for autoamplification using diarylethene photoswitches (R = achiral side chain).

We propose the use of prochiral diarylethene molecular photoswitches **2.1o**, which co-aggregate with a small fraction of their enantiomerically pure closed counterparts **2.1c***, resulting in the formation of chiral supramolecular gels (Figure 2.3, templated pathway). The (*S,S*) molecular chirality present in the dopant ((*S,S*)-**2.1c***) is translated into a preferred helicity in the chiral supramolecular gel ((*M*)-helicity in Figure 2.3) consisting of **2.1o** (soldier). In the gel state, the prochiral switches **2.1o** can be photochemically ring-closed to **2.1c** by UV irradiation, thereby locking the chirality at the molecular level and completing the cycle from *molecular chirality*, *via* induction of *supramolecular chirality*, and finally back to *molecular chirality*, leading to an enriched mixture in the templated enantiomer (*S,S* in Figure 2.3). If no chiral dopant is added to the system (Figure 2.3, non-templated pathway), the gel consists of an equal amount of (*P*)- and (*M*)-helical fibers and, upon irradiation, a statistical 1:1 mixture of the (*S,S*)- and (*R,R*)-enantiomer of **2.1c** (*rac*-**2.1c**) is formed.

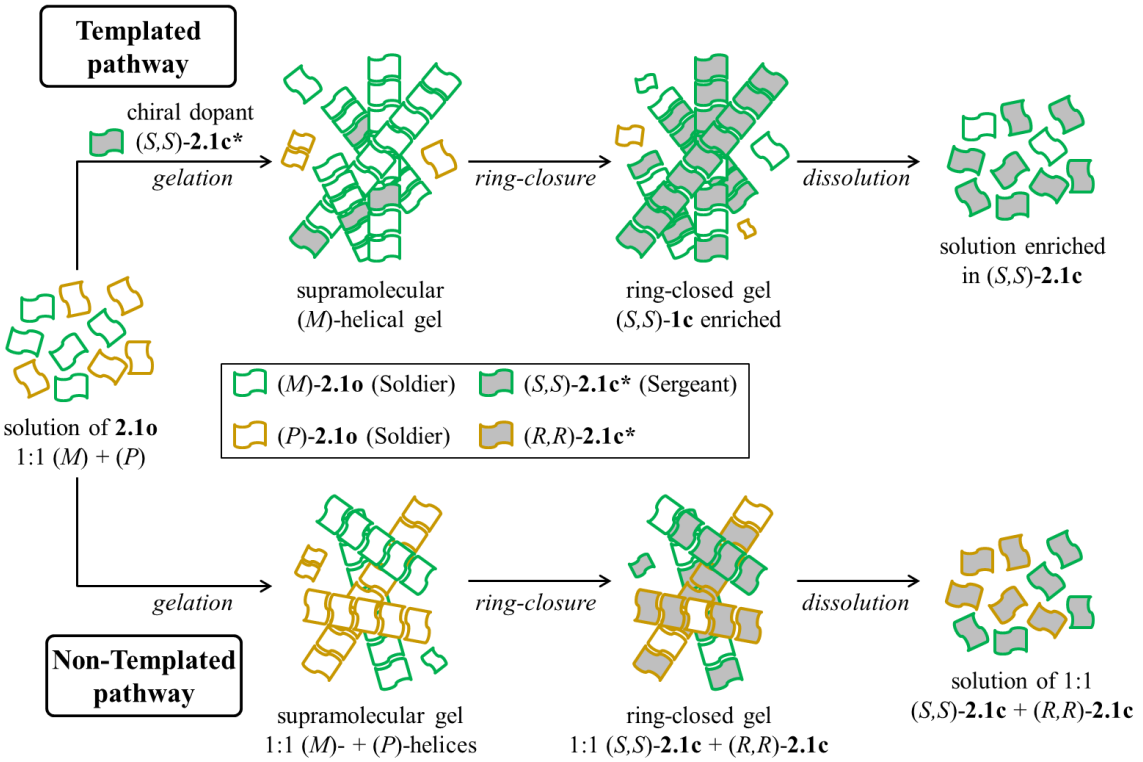

Figure 2.3. Concept for autoamplification of molecular chirality through the induction of supramolecular chirality. For the templated pathway, a small fraction of chiral dopant (*S,S*)-**2.1c*** is added to a mixture of prochiral photoswitches ((*M*)-**2.1o** and (*P*)-**2.1o**) prior to gelation. The formed fibers that result in gel formation are templated by the chiral dopant (*S,S*)-**2.1c*** and one helicity (*M*) is dominant. Upon ring-closing of the photoswitches with UV light, the chirality of the fibers results predominantly in the formation of the templated enantiomer (*S,S*)-**2.1c**. If no chiral dopant is added to the mixture of prochiral photoswitches (non-templated pathway), the gel is made up of an equal mixture of (*P*)- and (*M*)-conformers in the fibers. Subsequent ring-closure results in a statistical 1:1 mixture of products.

In our earlier study of LMWGs of type **2.1o** (Scheme 2.4) we have shown how **2.1o**, bearing chiral side chains (R = (*R*)-phenylethylamine), can undergo ring-closure in the gel state to give **2.1c** with 96% diastereomeric excess (Scheme 2.6).[57] It was also shown that these chiral compounds can co-aggregate with compounds of the same type that have achiral R-groups (R = *c*-hexyl) and induce an enantiomeric excess of up to 94% after ring-closing of the mixture in the gel.[39]

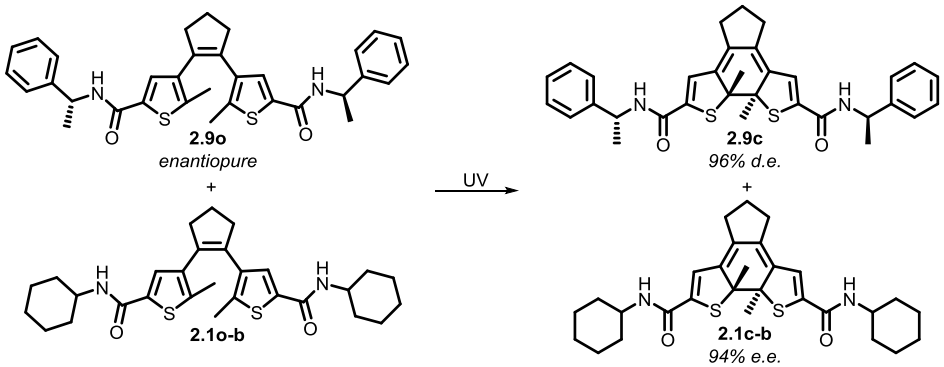

Scheme 2.6. Diastereoselective ring-closing of chiral auxiliary-appended diarylethene **2.9o** in the gel state and induction of *e.e.* by co-aggregation of achiral open switch **2.1o-b** with chiral open switch **2.9o**.[39] The absolute chirality of the products was not determined and is depicted arbitrarily in this Scheme.

This is an impressive example of supramolecular "asymmetric amplification". Predicting the outcome of chiral amplification in supramolecular systems is, however, a daunting task.[58] Small structural changes in the chiral dopant can result in complete changes in selectivity[39] or even loss of amplification.[59] Taking this concept one step further, we designed the sergeant **2.1c*** to be one of the enantiomers of the ring-closed soldier **2.1o**, i.e. the product of the reaction is the template for its own formation (Figure 2.3). The fact that the soldier and sergeant in our system are the same molecule may have outstanding implications for autoamplification of chirality.

We envisioned a system in which the chiral information is exclusively transferred from the ring-closed diarylethene core, rather than from auxiliary, peripheral stereogenic centers adjacent to the amide group.[39,58] *n*-Hexyl and *c*-hexyl substituents were chosen in order to prevent any additional influence from non-innocent groups such as for instance phenyl moieties.

One of the main challenges is the preparation and isolation of the enantiopure, ring-closed sergeant. Although the closed form of diarylethenes are generally stable, any exposure to visible light will ring-open the photoswitch and cause loss of chiral information. Furthermore, aggregation of ring-closed diarylethenes has not been studied extensively and the possible success relies on successful co-aggregation of the enantiopure closed form with the prochiral open counterpart of the same photoswitch.

2.3 Synthesis

Soldiers **2.1o-a** and **2.1o-b** and enantiopure sergeants **2.1c*-a** and **2.1c*-b** were synthesized to investigate the potential for **2.1c*** to act as a template in the gel state. The soldiers **2.1o-a** and **2.1o-b** are readily prepared following our reported procedure (Scheme 2.7).[40,58]

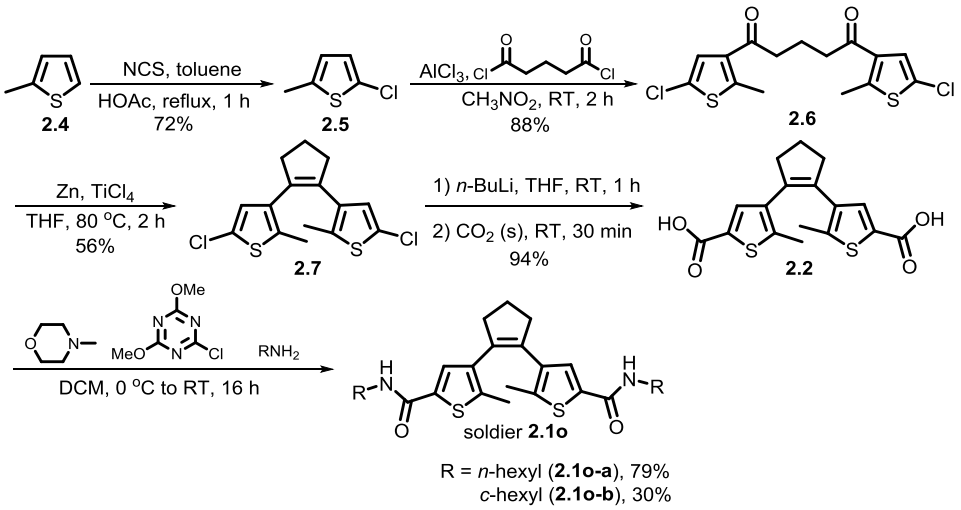

Scheme 2.7. Synthesis of soldiers **2.1o-a** and **2.1o-b** based on a literature procedure.[40]

Chlorination in the 5-position of commercially available 2-methylthiophene with *N*-chlorosuccinimide gives **2.5** in good yield. Friedel-Crafts acylation with glutaryl chloride gives diketone **2.6**, which can be directly converted into building block **2.7** on large scale, using the intramolecular McMurry reaction. Lithium-halogen exchange of **2.7** with *n*-BuLi at

room temperature and subsequent quenching with solid CO_2 yields diacid **2.2**. Conversion into diamides (soldiers) **2.1o-a** and **2.1o-b** can be achieved using *N*-methylmorpholine, 2-chloro-4,6-dimethoxy-1,3,5-triazine and the desired amine under mild conditions. The conversion of acid **2.2** into the amides **2.1o** proceeds with good conversion, but the yield suffers from purification issues. The removal of 2-hydroxy-4,6-dimethoxy-1,3,5-triazine was accomplished by washing the amide product with small amounts of MeOH in ether. As the product **2.1o** is also soluble in this mixture, some product is lost.

The soldiers were obtained in 5 steps from commercially available starting materials. The chiral sergeant, however, undergoes fast ring-opening to the achiral (open) form when exposed to visible light[60,61] and its synthesis proved to be highly challenging.

We envisioned to functionalize precursor **2.2** with a chiral auxiliary group in a manner that not only resulted in separation of the closed isomers, but also allowed for facile synthesis of the desired enantiomers of amides **2.1c***. Our first approach was the functionalization of diacid **2.2** with chiral auxiliary groups. Photochemical ring-closure would then give diastereomers. If the diastereoselectivity of this reaction is sufficient, or the diastereomers can be readily separated, one of the diastereomers might be obtained and converted into enantiopure sergeant after cleavage of the auxiliary groups, providing that no ring-opening occurred in the process. l-Menthol was chosen as an auxiliary group, because of its availability in enantiopure form and because esters are usually readily converted into amides under mild conditions. Synthesis of menthol-appended **2.8o** from **2.2** was achieved by Steglich esterification, employing DMAP and EDC (Scheme 2.8). Upon irradiation with UV light, diastereomers of **2.8c** were indeed formed (conversion was monitored by UV-vis spectroscopy), but only with low selectivity (ratio 4:6). Since diastereomers have different physical properties, we then hoped to separate them from each other by ordinary purification techniques. In this way, both enantiomers of the sergeant can be obtainable after conversion to the corresponding diamides.

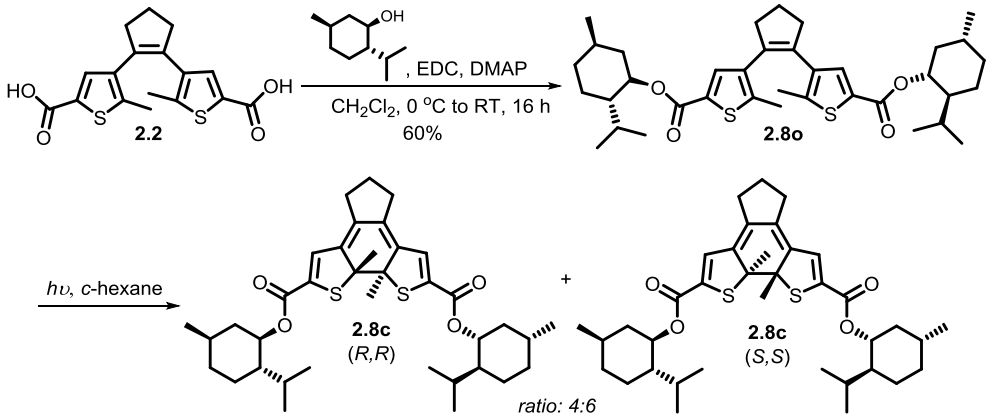

Scheme 2.8. Synthesis of l-menthol-derived diarylethene **2.8**. The absolute chirality of the products was not determined and is depicted arbitrarily in this Scheme.

Compound **2.8c** is obtained as an oil and does not crystallize. Therefore, column chromatography was an obvious choice for the separation of both isomers of **2.8c**. A wide variety of common eluents was tested, but TLC revealed that the diastereomers were inseparable with any solvent combination of *n*-pentane, *n*-hexane, *n*-heptane, cyclohexane or toluene with Et_2O, TBME, EtOAc, DCM or MeOH examined. Combinations of chiral (+)-2-carvene

with polar solvents were also tried as eluent, but to no avail. Formation of diastereomeric salts of ring-closed diacid **2.2c** with (*R*)-1-phenylethylamine and a variety of amino acids did not result in isolation of enantiopure material either.

Separation of the diastereomers of **2.8c** in *c*-hexane was found to be possible using chiral HPLC. If **2.8c** could be converted to the corresponding diamides under mild conditions (to ensure that no ring-opening takes place), enantiopure **2.1c*** could in principle be obtained. Several procedures were investigated (Table 2.1).

Table 2.1. Attempted conversion of **2.8c** into ring-closed diacid or diamide.

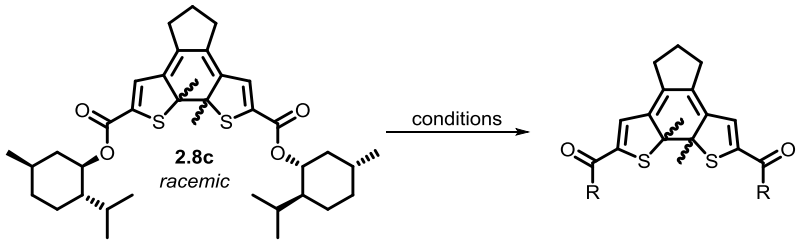

Entry	R	Conditions	Result
1[a]	*n*-hexylamine	$NH_2C_6H_{13}$-DIBAL-H (1.1 equiv), THF, RT, 16 h	no conversion
2	*n*-hexylamine	$NH_2C_6H_{13}$-DIBAL-H (1.1 equiv), THF, RT, 3 d	no conversion
3	*c*-hexylamine	$NH_2C_6H_{11}$-DIBAL-H (1.1 equiv), THF, RT, 16 h	no conversion
4	*c*-hexylamine	$NH_2C_6H_{11}$, MeOH, 5 d	no conversion
5	OH	LiOH (10 equiv), THF/H_2O (1:1), 16 h	no conversion
6	OH	LiOH (10 equiv), THF/H_2O (1:1), sonicate, 30 min	no conversion
7	OH	LiOH (30 equiv), THF/H_2O (1:1), sonicate, 30 min	no conversion

[a] Based on a literature procedure.[62]

Direct conversion of bulky esters to the corresponding amides through aminolysis, using mild conditions, has been reported.[62] In the original procedure, esters and lactones are readily converted into the amines by reaction with a preformed DIBAL-H-H_2NR complex that is generated by the reaction of DIBAL-H with the amine. The authors show that the reaction of, for example, γ-butyrolactone and benzylamine at 45 °C resulted in 28% yield of the desired amide after 20 h. When using a preformed complex of benzylamine with DIBAL-H, aminolysis reactions of a variety of substrates proceeded smoothly at room temperature and the correspondings amides were obtained in high yields in 30 min. As several amines, esters and lactones gave good results, this procedure gave us hope for the conversion of **2.8c** into **2.1c**.

Using this method, after 16 h, no conversion for either linear (Table 2.1, entry 1) or cyclic amine (Table 2.1, entry 3) was obtained. Prolonging the reaction time up to 3 d (Table 2.1, entry 2) did not give any conversion either. Preparation of enantiopure diamide from enantiopure diacid after hydrolysis of **2.8c** adds one step and the risk of ring-opening is increased, but it was considered to be a viable method. Stirring a solution of **2.8c** in a mixture of THF/H_2O with LiOH for 16 h, did not give any conversion (Table 2.1, entry 5). Sonication can speed up chemical reactions tremendously[63] and is a commonly used method for hydrolysis of esters with LiOH in our lab, but this procedure gave no conversion in the case of **2.8c** (Table 2.1, entry 6 and 7).

Although many more methods for hydrolysis and aminolysis exist, at this point the l-menthol-appended switch **2.8** was concluded to be too unreactive and an alternative was proposed. l-Cystein was thought to be a better choice as chiral auxiliary than l-menthol. The amino acid is commercially available and should facilitate separation of the ring-closed diastereomers in a similar way as was shown for the diarylethene functionalized with l-menthol. A major advantage in the case of l-cystein is the nature of the linker, being a thioester moiety rather than an oxo-ester. Thioesters are more labile, compared to oxo-esters[64,65] and we envisioned easier conversion of the thioester to the desired amide. The synthesis of dithioester **2.3** is given in Scheme 2.9.

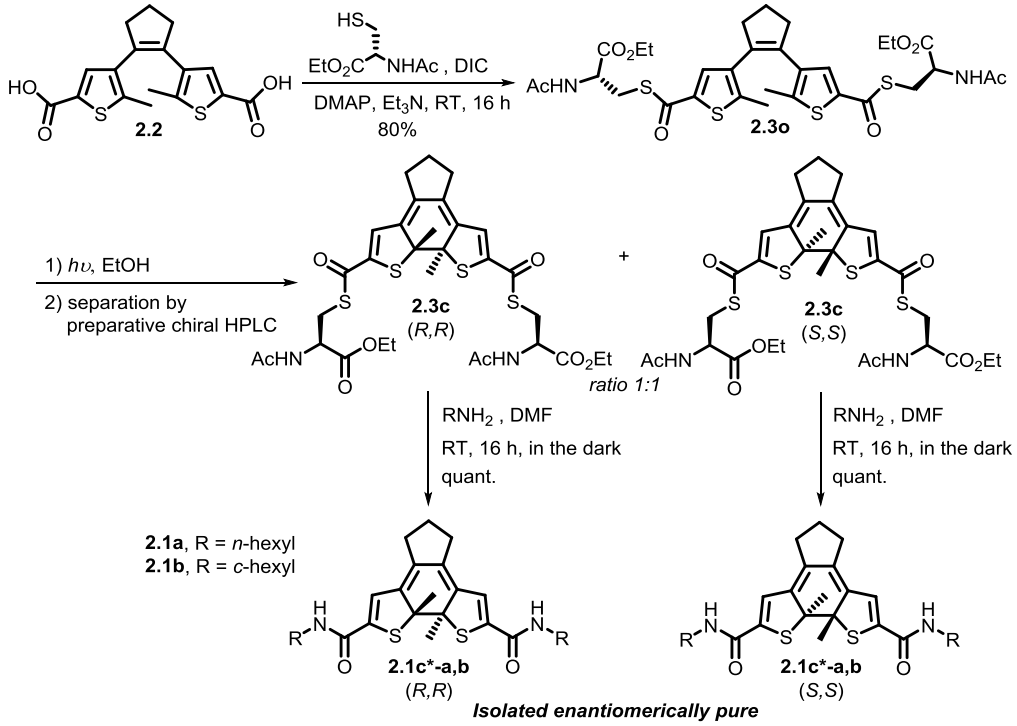

Scheme 2.9. Synthesis of sergeants **2.1c*-a** and **2.1c*-b**.

Chiral dithioester **2.3** was synthesized by coupling dicarboxylic acid **2.2** with Ac-(*R*)-Cys-OEt. Compound **2.3o** was then photo-cyclized with UV light (λ = 312 nm) to form a 1:1 mixture of diastereomers of **2.3c**. Separation of the diastereomers by column chromatography or crystallization was unsuccessful. However, separation of the diastereomers by chiral HPLC could be achieved and was followed by reaction of **2.3c-a**, or **2.3c-b**, with an excess of *n*-hexyl or *c*-hexyl amine, respectively, at room temperature and shielded from light, to provide enantiopure amides **2.1c*-a** and **2.1c*-b**. These mild conditions resulted in full conversions for the last step and no ring-opening was observed.

2.4 Photochromic properties

The photochromic properties of compounds **2.1o** were studied using UV-vis spectroscopy (Figure 2.4a-b). Upon irradiation with UV light (λ = 312 nm), the band at λ = 262 nm decreases and new bands of *rac*-**2.1c-a** and rac-**2.1c-b** appear at λ = 347 and 528 nm and λ = 347 and 531 nm, respectively. This observation is consistent with the formation of the closed form of the switches.[41]

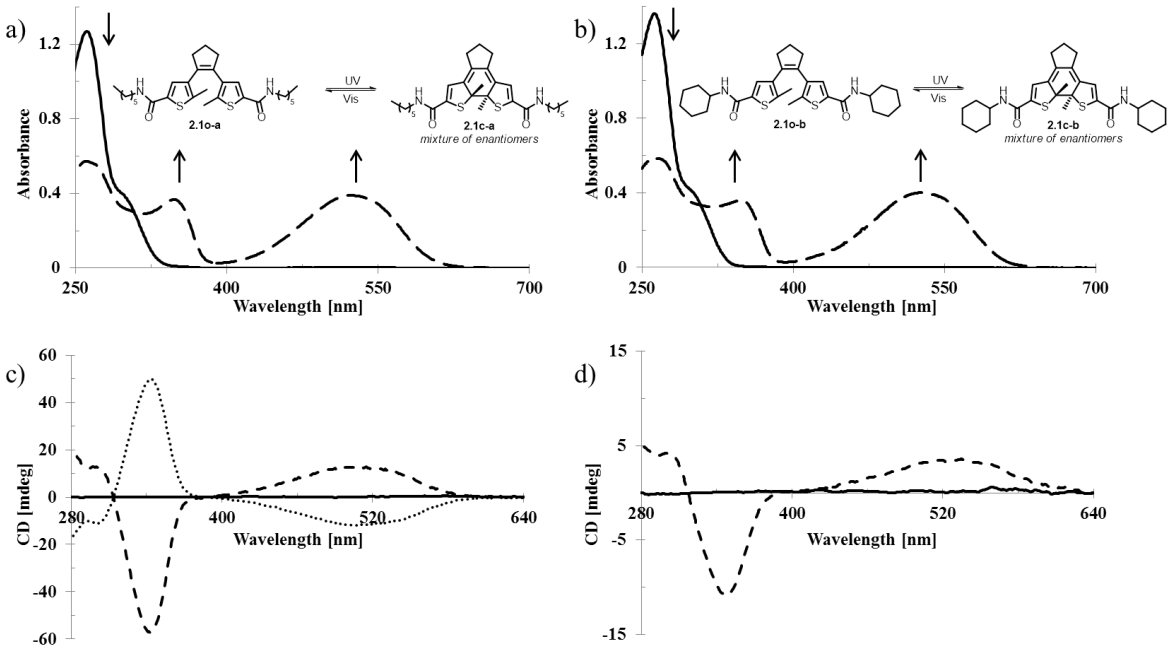

Figure 2.4. Photochromic properties of **2.1o** and **2.1c**. a) UV-vis absorption spectra prior to and after irradiation (λ = 312 nm) of **2.1o-a** (solid line, $5.3 \cdot 10^{-4}$ M) to form *rac*-**2.1c-a** (dashed line) in EtOH. b) UV-vis absorption spectra upon irradiation (λ = 312 nm) of **2.1o-b** (solid line, $5.0 \cdot 10^{-4}$ M) to form *rac*-**2.1c-b** (dashed line) in EtOH. c) CD spectra of enantiomer 1 (dashed line, $1.9 \cdot 10^{-4}$ M) and 2 (dotted line, $1.5 \cdot 10^{-4}$ M) of sergeant **2.1c*-a** and ring-closed soldier *rac*-**2.1c-a** (solid line, $1.7 \cdot 10^{-4}$ M) in EtOH. d) CD spectra of enantiomer 1 (dashed line, $3.7 \cdot 10^{-5}$ M) of sergeant **2.1c*-b** and racemic ring-closed soldier *rac*-**2.1c-b** (solid line, $3.7 \cdot 10^{-5}$ M) in EtOH.

CD spectroscopy (Figure 2.4c-b) confirmed that **2.1o** closes in a racemic fashion and has no influence on the outcome of the sergeant-soldier asymmetric induction experiment. As expected, no Cotton effect was observed for a solution of neither the open (**2.1o-a** and **2.1o-b**), nor the closed soldiers (*rac*-**2.c-a** and *rac*-**2.1c-b**). The enantiopure **2.1c*-a**, on the other hand, shows a positive Cotton effect with a maximum at λ = 528 nm and a minimum at λ = 347 nm for enantiomer 1 (and the inverse for enantiomer 2). Enantiopure **2.1c*-b** shows a positive Cotton effect with a maximum at λ = 531 nm and a minimum at λ = 347 nm for enantiomer 1. The absolute configuration of the sergeants was not determined and the names (enantiomer 1 and 2) refer to the order of elution of the enantiomer from the chiral HPLC.

2.5 Sergeant-soldier experiments

With both enantiopure sergeants **2.1c*** and soldiers **2.1o** in hand we set out to probe the concept presented in Figure 2.3. A suspension of soldier **2.1o-a** in toluene was doped with a small amount of enantiomerically pure **2.1c*-a**. The gelation experiments were performed by weighing a known amount of enantiopure (sergeant) **2.1c*-a**, or **2.1c*-b**, and achiral (soldier) **2.1o-a**, or **2.1o-b**, in a 2 mL glass GC vial. After addition of the solvent (either 250 μL for 1.75 mg was used to give a total concentration of 7.0 mg/mL (0.8% w/v) or 250 μL for 3.75 mg was used to give a total concentration of 15.0 mg/mL (1.5% w/v)), the vial was tightly closed and heated until the solids dissolved. Subsequently, the vial was allowed to cool and age for 1 h at room temperature, upon which a gel formed. Gelation is considered to have occurred when a homogeneous material is obtained that does not exhibit gravitational flow. Irradiation with UV light (λ = 312 nm) for 10 min resulted in ring-closure of the aggregated mixture. The sample was redissolved in ethanol (usually 0.5 mL) for HPLC analysis.

If induction of the enantiopure sergeant on the ring-closed soldier does not take place, i.e. the ring-closure of the soldier molecules proceeds in a racemic fashion, the amount of added enantiopure sergeant is directly reflected in the observed *e.e.*[66] The difference between the observed *e.e.* and the *e.e.* if no asymmetric induction occurs, shows the *e.e.* that was induced by the chiral sergeant (Δ *e.e.*) and is referred to henceforth as "induction". To our delight, we found that the sergeant was able to induce a bias in its own formation in toluene (Table 2.2), providing, for the first time, the proof-of-concept for the autoamplification of molecular chirality *via* induction of supramolecular chirality.

Table 2.2. Sergeant-soldier experiments of **2.1-a** in toluene.

Entry	Total concentration **2.1o** + **2.1c*** [% w/v]	*e.e.* at no induction / % sergeant	*e.e.* observed	Δ *e.e.*
1	1.5	0	0	0
2	1.5	3.2	25	22
3	**1.5**	**9.5**	**50**	**40**
4	1.5	12.5	44	32
5	1.5	16.9	48	31
6	1.5	37.8	84	46
7	0.8	9.0	47	38
8	0.3	15.7	29	13
9	0.2	14.5	31	16
10[a]	0.8	-19.5	-45	25
11[a]	1.5	-19.6	-54	35
12[b]	1.0	9.0	47	38

[a] The opposite enantiomer of the sergeant was used as dopant and the other enantiomer of the product was obtained accordingly. [b] The *c*-hexyl-appended soldier **2.1o-b** and sergeant **2.1c*-b** were used instead of *n*-hexyl **2.1o-a** and **2.1c*-a**.

It was found that the sergeant was able to induce its own formation with 40% (Table 2.2, entry 3) induction (*e.e.* observed = 50%, Δ *e.e.* = 40%), compared to the system in the absence of sergeant (Table 2.2, entry 1), after correction for the amount of sergeant initially

added. Decreasing the amount of sergeant to 3.2% led to a lower induction of 22% (Table 2.2, entry 2). Increasing the amount of sergeant (up to 37.8%), on the other hand, did not significantly increase the asymmetric induction (Table 2.2, entries 4-6). Cryo-transmission electron microscopy (cryo-TEM) revealed a fibrous network of very high density in both the open and closed gel (Figure 2.5). We therefore envisioned that decreasing the total concentration of the gelator might have an effect on the outcome of the experiment as the gel would become less dense, but lowering the concentration from 1.5% w/v to 0.8% did not increase the induction (Table 2.2, entry 7). Further decrease in the concentration below a certain threshold (0.3% w/v) resulted in a drop in induction to approximately 15% (Table 2.2, entries 8 and 9). When the opposite enantiomer of the sergeant **2.1c*-a** was used as the dopant, the other enantiomer of the product was obtained (Table 2.2, entries 10 and 11), providing evidence that the sergeant is responsible for templating its own formation and that one of the enantiomers is not simply favored for other reasons. The system gives comparable results for **2.1-b**, functionalized with *c*-hexyl instead of *n*-hexyl side chains (Table 2.2, entry 12), demonstrating that the nature of the alkyl moieties has a minor influence. In each case, doping the gels with enantiopure sergeant **2.1c*** resulted in an increase in *e.e.* (after correcting for the initial amount of sergeant **2.1c*** added), compared to cases where no dopant was added.

We found that the product samples racemize if left for longer periods of time when dissolved in EtOH. Therefore, caution was taken in the analysis and reproducibility. Experiments with samples of **2.1o-a** with 9% of sergeant **2.1c*-a** at a concentration of 1.5% w/v in toluene were repeated several times under nearly identical conditions. The results were statistically analyzed and gave an induction value of 35 ± 6% (n = 7), showing that the induction is significant and reproducible.

As the solvent is an integral part of organogels,[55,67] a range of other solvents were investigated to assess their effect on the asymmetric auto-induction (Table 2.3).

Table 2.3. Sergeant-soldier experiments of **2.1-a** in different solvents.[a]

Entry	Solvent	*e.e.* at no induction / % sergeant	*e.e.* observed	Δ *e.e.*
1[b]	**Toluene**	**9.5**	**50**	**35 ± 6**
2[b]	*c*-Hexane	11.0	44	33
3	Benzene	9.6	27	17
4[b]	Decalin	10.0	24	14
5	1-Phenyloctane	12.5	rac.	-
6	Dibutylether	6.0	rac.	-
7[c]	Acetonitrile	11.3	-	-
8[c]	Hexadecane	11.9	-	-

[a] The total gelator concentration was 1.5% w/v. [b] At a concentration of 0.8% w/v, Δ *e.e.* was the same. [c] Solid precipitated from the solution upon cooling.

The use of toluene or *c*-hexane gave the best results in these asymmetric autoamplification experiments (Table 2.3, entries 1 and 2). Benzene and decalin facilitate asymmetric induction, but lower Δ *e.e.* values (~15%) were observed (Table 2.3, entries 3 and 4). In 1-phenyloctane,

the product was formed as a racemate (Table 2.3, entry 5). Although a gel can still be formed in the more polar dibutylether, the product was obtained as a racemate (Table 2.3, entry 6). The use of acetonitrile and hexadecane resulted in a precipitate, rather than a gel (Table 2.3, entries 7 and 8). In conclusion, hydrophobic solvents were required for the observation of *e.e.* enhancement (with toluene being the preferred solvent), as the use of more polar solvents resulted in poor gel formation or racemic mixtures. This observation supports the hypothesis that hydrogen bonding in the supramolecular gel state helps to preorganize the achiral **2.1o** (soldier) with a preferred helical conformation. In other words, one of the dynamic (and interconverting) helical conformers (Scheme 2.4) is selected in the supramolecular aggregate, governed by the chirality of the dopant **2.1c***.

One explanation for the modest induction could be inefficient co-aggregation of the sergeants and soldiers. Since the presence of sergeant favors the formation of one ring-closed photoswitch over the other, we conclude that co-aggregation between the open and closed form of the photoswitch is successful to a certain extent. When increasing the fraction of enantiopure sergeant in the mixture, however, no increase in induction is observed (Table 2.3, entry 3-6). If enough sergeant is present, distinct fibers may form that are enriched in sergeant molecules. This would limit the amount of sergeant available to co-aggregate with the prochiral soldier and hence limit the templating effect on selective gel fiber formation and ultimately induction. In order to provide evidence for this hypothesis, we employed transmission electron microscopy (TEM). We performed cryo-TEM measurements on a gel sample before and after irradiation as well as a gel made of racemic ring-closed soldier to see if different fibers or aggregates could be seen for open and closed photoswitches (Figure 2.5). A difference between the samples could, however, not be detected and the dense fibrous networks seem identical. These findings indicate that issues with co-aggregation are unlikely, although the possibility for sergeant-enriched fibers cannot be excluded based on these measurements. Possible differences between gels of sergeant and ring-closed soldier were not studied due to lack of material. Results obtained were therefore interpreted with due caution.

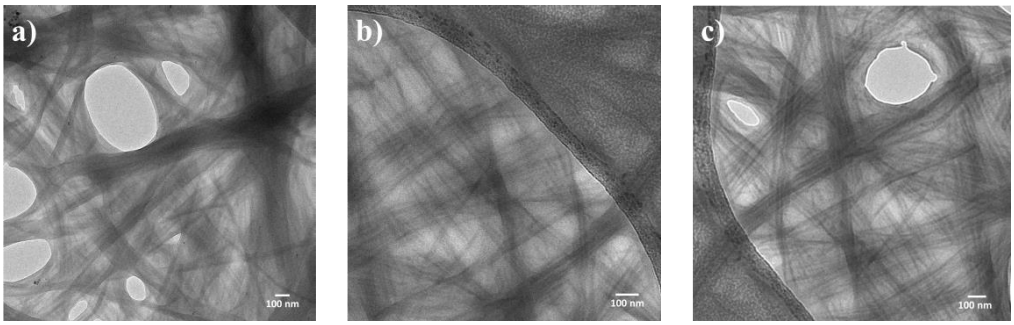

Figure 2.5. TEM images of self-assembled gel morphologies. a) Gel fibers of ring-open soldier **2.1o-b** (1.5% w/v in toluene). b) Gel fibers of ring-closed soldier **2.1c-b** (1.5% w/v in toluene) after irradiation with UV light (λ = 312 nm). c) Gel fibers of ring-closed soldier **2.1c-b** (1.5% w/v in toluene, irradiated with UV light (λ = 312 nm) prior to gelation.

The gel-to-solution temperature (T_{gel}) of gelated **2.1o-b** and *rac*-**2.1c-b**, using dropping-ball experiments were also determined. In this experiment, a small metal ball is placed on a gel and the temperature of the gel slowly increased until the gel can no longer support the weight of the ball.[68] The temperature at which the ball dropped to the bottom of the gel was recorded as the gel melting temperature T_{gel}. The gel of **2.1o-b** has a T_{gel} of 82 °C and the gel of *rac*-**2.1c-b** has a

T_{gel} of 74 °C, suggesting a lower stability of the aggregates of the closed form, in agreement with earlier findings.[39,41] The data suggest that upon irradiation of the gel, the closed form goes into solution preferentially over the open form; a process that would limit the amount of sergeant present in the gel fibers and be a possible origin of a modest asymmetric induction. Indeed, it has been shown by the groups of Sijbesma and Meijer that the presence of chiral monomers in solution has little or no effect on the chirality of assemblies if the monomers are not part of the assembly.[69,70] Therefore, we believe that the difference in solubility between the open and the closed photoswitch may be the main reason for the modest induction.

2.6 Control experiments

A range of control experiments were performed to validate the method of analysis and gelation.

Induction in solution

To establish that no induction takes place in solution, the sergeant-soldier experiment was performed in EtOH (total gelator concentration of 7.8 mM) for **2.1o-a** and **2.1o-b** with a small amount of **2.1c*-a** and **2.1c*-b**, respectively. After irradiation, the samples were analyzed by HPLC and no induction was found. In addition, portions of gels of **2.1o-a** and **2.1o-b**, doped with a small amount of **2.1c*-a** and **2.1c*-b**, respectively, were taken and dissolved in EtOH. After irradiation, the remainder gel-samples showed induction as reported in Table 2.2, but the solutions of the samples, taken out of the original gel, showed no induction.

Addition of sergeant or soldier after the sergeant-soldier experiment

Not all molecules become part of the fibers and a certain percentage remains in solution. These molecules still undergo ring-closure and experiments were performed to confirm that the presence of either open or closed photoswitch did not influence the outcome of the sergeant-soldier experiment. Therefore, soldiers **2.1o-a** or **2.1o-b** were deliberately added to a sample after analysis for induction. This spiked sample was analyzed again under the same conditions. In both cases, the chromatograms were identical to those obtained before addition of **2.1o-a** or **2.1o-b**. Similarly, adding sergeant **2.1c*-a** or **2.1c*-b** to the sample after the sergeant-soldier experiment led to an increased amount of the templated enantiomer. The originally measured *e.e.* was obtained after subtraction of the post-experiment added sergeant in both cases.

Racemization

Leaving the dissolved samples for longer periods of time in EtOH (4.5 or 9.8 mM) after the sergeant-soldier experiment led to loss of induction. The *e.e.* dropped by ~10% after one week in the dark at room temperature. Therefore, all samples were kept in the dark at all times and immediately analyzed after irradiation and dissolution.

Cooling and aging

Gels that are made up of LMWGs are known to be dependent on cooling rate and are easily disturbed by mechanical stress.[47–52] After heating the suspensions in the sergeant-soldier experiments, the vials were left to stand for 1 h at room temperature. In all cases, a gel formed. Aging[39,41] for longer periods of time (up to 24 h) or at lower temperatures (4 °C or -18 °C) did not result in higher inductions.

2.7 Conclusions

In summary, we present herein, to the best of our knowledge, the first example of autoamplification of molecular chirality *via* induction of supramolecular chirality. We have shown how diarylethene photochemical switches can be used in autocatalytic induction. A small amount of chiral sergeant **2.1c*** can be added to its precursor **2.1o** without inhibiting gel formation. The chirality of the gel is controlled by the chiral sergeant, thereby favoring the formation of either (*P*)- or (*M*)-helical gel. The chiral information is subsequently locked to the molecular level as the prochiral soldiers undergo ring-closure by irradiation of the gel with UV light to form one of the enantiomers in excess. This completes the cycle from molecular chirality *via* supramolecular chirality back to molecular chirality of the same molecules and places this system among the very few examples where a chiral product of a reaction can template its own asymmetric synthesis. This process is reminiscent of so-called "autocatalytic reactions", however here the autoamplification takes place in a kinetically trapped state.

2.8 Experimental section

General remarks

Starting materials and reagents were commercially available and used as obtained from Sigma-Aldrich or Acros without further purification. All solvents used for spectroscopic measurements, chromatography and the sergeant-soldier experiments were of analytical grade and degassed prior to use. Melting points were determined on a Büchi melting point B-545 apparatus. ^{1}H-NMR spectra were recorded on a Varian VXR-300 spectrometer (at 300 MHz) or a Varian MR400 (at 400 MHz) at ambient temperature. The splitting patterns are designated as follows: s (singlet); d (doublet); dd (double doublet); t (triplet); q (quartet); m (multiplet) and br (broad). ^{13}C-NMR spectra were recorded on a Varian VXR-300 spectrometer (at 75.4 MHz) or a Varian MR400 (100.6 MHz) at ambient temperature. Chemical shifts are denoted in δ (ppm), referenced to the residual protic solvent peak. Coupling constants *J*, are denoted in Hz. Masses were recorded with a Thermo scientific LTQ Orbitrap XL mass spectrometer. Silicycle Siliaflash P60, 40-63 m, (230-400 mesh) was used for column chromatography. Thin-layer chromatography (TLC) was performed on commercial Kieselgel 60F, 254 silica gel plates and compounds were visualized with UV light (λ = 254 nm) or $KMnO_4$ stain. The diarylethene derivatives are light-sensitive and were therefore exclusively kept in the dark, and column chromatography was performed in yellow light. Irradiations were performed with Spectroline ENB-280C/FE UV lamp. CD spectra were recorded on a JASCO J-715 spectropolarimeter and UV-vis measurements were performed on a Agilent 8453 UV-vis Spectrophotometer. Weighing of small quantities was performed on a Mettler MT5 analytical microbalance.

Dropping ball experiments

Gel-to-solution temperatures T_{gel} were determined by using the dropping ball method.[68] After the gel was formed, a steel ball (65.0 mg, 2.5 mm in diameter) was placed on top of the gel in a 2 mL glass vial. The vial was subsequently placed in a heating block. The temperature of the heating block was increased by 1 °C/min and the T_{gel} was defined as the temperature at which the steel ball reached the bottom of the vial, as observed by a CCD camera.

Cryo-transmission electron microscopy

A suspension (2.5 µL) was placed on a holy carbon coated grid (Quantifoil 3.5/1, QUANTIFOIL Micro Tools GmbH, Großlöbichau, Germany). After blotting, the grid was rapidly frozen in liquid ethane (Vitrobot, FEI, Eindhoven, The Netherlands) and stored in liquid nitrogen until observed. Grids were observed in a Gatan model 626 cryo-stage in a Philips CM120 cryo-electron microscope operating at 120 KeV. Images were recorded under low-dose conditions on a slow-scan CCD camera.

Synthesis

2-Chloro-5-methylthiophene (2.5)

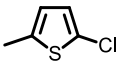

This compound was prepared as described in literature.[40] 2-Methylthiophene (100 mL, 1.04 mol, 1.0 equiv) and *N*-chlorosuccinimide (152 g, 1.14 mol, 1.1 equiv) were added to a vigorously stirred mixture of benzene (400 mL) and acetic acid (400 mL). The suspension was stirred for 30 min at room temperature. After 1 h of heating at reflux, the cooled mixture was poured into a 3 M aq. NaOH solution (300 mL). The organic phase was washed with 3 M aq NaOH solution (3 x 300 mL), dried over Na_2SO_4 and filtered. Evaporation of the solvent gave a pale yellow liquid. Purification of the product by vacuum distillation (19 Torr, 55 °C) afforded **2.5** as a colourless liquid (111 g, 0.850 mol, 82%). b.p. 55 °C (19 Torr); ^{1}H NMR (300 MHz, $CDCl_3$): δ = 6.58 (d, *J* = 3.6 Hz, 1H), 6.39 – 6.44 (m, 1H), 2.30 (s, 3H) ppm; ^{13}C NMR (75.4 MHz, $CDCl_3$) δ = 138.4, 126.4, 125.7, 124.3, 15.2 ppm. Data is in accordance with literature.[40]

1,5-Bis(5-chloro-2-methylthiophen-3-yl)pentane-1,5-dione (2.6)

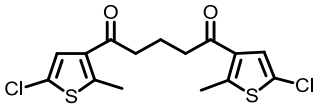

This compound was prepared according to an adapted literature procedure.[40] Under vigorous stirring, $AlCl_3$ (62 g, 0.47 mol, 1.2 equiv) was added in portions to an ice-cooled solution of **2.5** (51 g, 0.39 mol, 1.0 equiv) and glutaryl chloride (25 mL, 0.20 mol, 0.5 equiv) in nitromethane (400 mL). After addition of $AlCl_3$, the reaction mixture was stirred at room temperature for 2 h. Ice-cold water (100 mL) was carefully added to the reaction mixture and the aqueous layer was extracted with Et_2O (3 x 150 mL). The combined organic layers were washed with water (100 mL), dried over Na_2SO_4, filtered and the solvent was removed in vacuo to yield **2.6** as a brown semisolid (91 g, 0.25 mol, 64%). The product was used without further purification. ^{1}H NMR (200 MHz, $CDCl_3$): δ = 7.19 (s, 2H), 2.86 (t, *J* = 6.8 Hz, 4H), 2.66 (s, 6H), 2.01 (quint, *J* = 7.5 Hz, 2H) ppm; ^{13}C NMR (75.4 MHz, $CDCl_3$): δ = 194.7, 147.6, 134.7, 126.7, 125.2, 40.4, 18.1, 16.0 ppm. Data is in accordance with literature.[40]

1,2-Bis(5-chloro-2-methylthiophen-3-yl)cyclopent-1-ene (2.7)

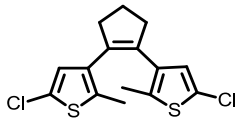

This compound was prepared as described in the literature.[40] THF (300 mL) and Zn dust (2.5 g, 0.17 mol, 1.5 equiv) were placed in a three-necked flask equipped with stirring bar under a nitrogen atmosphere. $TiCl_4$ (18 mL, 0.17 mol, 1.5 equiv) was added cautiously using a dropping funnel. The solution turned deep blue and was heated at reflux for 1 h. Next, it was cooled in an ice bath and **2.6** (40 g, 0.11 mol, 1.0 equiv) was added in portions. This mixture was heated at reflux for 2 h, subsequently quenched with 1 M aq. NH_4Cl (300 mL) and extracted with Et_2O (4 x 120 mL). The combined organic layers were washed with water (150 mL), dried over Na_2SO_4, filtered and the solvent was removed in vacuo to yield a yellow solid. Flash column chromatography (SiO_2, petroleum ether) yielded **2.7** as an off-white solid (18 g, 62 mmol, 56%). m.p. 75 – 78 °C; ^{1}H NMR (200 MHz, $CDCl_3$): δ = 6.58 (s, 2H), 2.71 (t, *J* = 7.5 Hz, 4H), 2.01 (quint, *J* = 7.5 Hz, 2H), 1.98 (s, 6H) ppm; ^{13}C NMR (75.4 MHz, $CDCl_3$): δ = 135.5, 135.1, 134.0, 127.4, 125.9, 39.1, 23.6, 14.9 ppm. Data is in accordance with literature.[40]

4,4'-(Cyclopent-1-ene-1,2-diyl)bis(5-methylthiophene-2-carboxylic acid) (2.2)

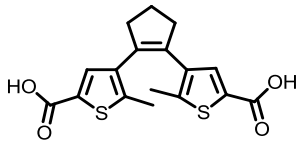

This compound was prepared as described in the literature.[40] In a round-bottomed flask equipped with stirring bar, **2.7** (2.0 g, 6.0 mmol, 1.0 equiv) was dissolved in dry THF (60 mL). Then *n*-BuLi (9.4 mL, 1.6 M in hexanes, 2.5 equiv) was added dropwise and the black mixture was stirred for 1 h. Solid CO_2 (excess) was added, after which a brown suspension was formed which was stirred for 30 min. Water (60 mL) was added and the aqueous layer was washed with Et_2O (60 mL) and subsequently acidified to pH = 1 with 30% aq. HCl. After extraction with CH_2Cl_2 (3 x 60 mL), the combined organic layers were dried over $MgSO_4$, filtered and concentrated to yield **2.2** as a brown solid (2.0 g, 5.8 mmol, 94%). The product was used without further purification in subsequent reactions. ^{1}H NMR (300 MHz, DMSO-d_6): δ = 7.40 (s, 2H), 2.77 (t, *J* = 7.8 Hz, 4H), 2.01 (quint, *J* = 7.5 Hz, 2 H), 1.91 (s, 6H) ppm; ^{13}C NMR (75.4 MHz, DMSO-d_6): δ = 162.6, 141.7, 136.4, 134.3, 133.8, 130.4, 37.9, 22.3, 14.3 ppm. Data is in accordance with literature.[40]

4,4'-(Cyclopent-1-ene-1,2-diyl)bis(*N*-hexyl-5-methylthiophene-2-carboxamide) (2.1o-a)

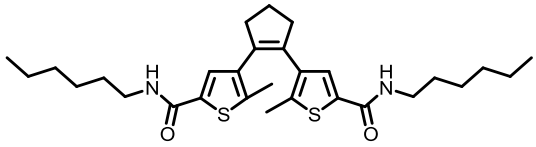

A suspension of compound **2.2** (0.40 g, 1.2 mmol, 1.0 equiv) in CH_2Cl_2 (5 mL) was placed in an ice bath. Subsequently, *N*-methylmorpholine (0.25 mL, 2.4 mmol, 2.0 equiv) was added after which compound **2.2** dissolved. 2-Chloro-4,6-dimethoxytriazine (0.40 g, 2.3 mmol, 2.0 equiv) was added and a milky suspension was formed immediately after this addition. The reaction mixture was stirred for 2 h at 0 °C and another 2 equiv of *N*-methylmorpholine (0.25 mL, 2.3 mmol, 2.0 equiv) was added, followed by *n*-hexylamine (0.30 mL, 2.3 mmol, 2.0 equiv). Stirring was continued for 1 h at 0 °C, and the mixture was

allowed to warm to room temperature overnight. CH_2Cl_2 (50 mL) was added and the solution was washed with 1 M aq. HCl (2 x 20 mL), brine (20 mL), saturated aq. $NaHCO_3$ solution (20 mL) and water (40 mL). The organic phase was dried over Na_2SO_4 and filtered. Evaporation of the solvent gave a solid residue. After purification by flash column chromatography (SiO_2, 1.5% MeOH in CH_2Cl_2) and washing with a small quantity of ether with a drop of MeOH, **2.1o-a** was obtained as an off-white solid (0.47 g, 0.91 mmol, 79%). m.p. 124 – 130 °C (dec); ^{1}H NMR (300 MHz, $CDCl_3$) δ = 7.18 (s, 2H), 5.78 (t, *J* = 5.6 Hz, 2H), 3.37 (apparent quartet, *J* = 13.1, 7.1 Hz, 4H), 2.77 (t, *J* = 7.5 Hz, 4H), 2.01 (quint, *J* = 7.5 Hz, 2 H), 1.93 (s, 6H), 1.58 – 1.52 (m, 4H), 1.40 – 1.22 (m, 12H), 0.88 (t, *J* = 6.8 Hz, 6H) ppm; ^{13}C NMR (75.4 MHz, $CDCl_3$) δ = 161.7, 139.5, 136.2, 134.7, 134.4, 129.2, 40.0, 38.4, 31.5, 29.6, 26.6, 22.9, 22.5, 14.7, 14.0 ppm; HRMS-ESI+ *m/z* calculated for $C_{29}H_{43}N_2O_2S_2$ $[M + H]^+$ 515.2761, found 515.2754.

4,4'-(Cyclopent-1-ene-1,2-diyl)bis(*N*-cyclohexyl-5-methylthiophene-2-carboxamide) (2.1o-b)

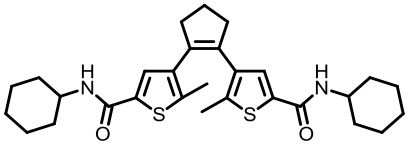

A suspension of compound **2.2** (0.50 g, 1.4 mmol, 1.0 equiv) in CH_2Cl_2 (6 mL) was placed in an ice bath. Subsequently, *N*-methylmorpholine (0.32 mL, 2.8 mmol, 2.0 equiv) was added and the solid material dissolved. Then 2-chloro-4,6-dimethoxytriazine (0.50 g, 2.8 mmol, 2.0 equiv) was added and a milky suspension was formed immediately after this addition. The reaction mixture was stirred for 2 h at 0 °C and another 2 equiv of *N*-methylmorpholine (0.32 mL, 2.8 mmol, 2.0 equiv) was added, followed by *c*-hexylamine (0.33 mL, 2.8 mmol, 2.0 equiv). Stirring was continued for 1 h at 0 °C, and the mixture was allowed to warm to room temperature overnight. CH_2Cl_2 (50 mL) was added and the solution was washed with 1 M aq. HCl (2 x 20 mL), brine (20 mL), saturated aq. $NaHCO_3$ solution (20 mL) and water (40 mL). The organic phase was dried over Na_2SO_4 and filtered. Evaporation of the solvent gave a solid residue. After purification by flash column chromatography (SiO_2, 1.5% MeOH in CH_2Cl_2) and washing with a small quantity of ether with a drop of MeOH, **2.1o-b** was obtained as an off-white solid (0.22 g, 0.43 mmol, 30%). m.p. 250 – 255 °C (dec); ^{1}H NMR (400 MHz, $CDCl_3$) δ = 7.17 (s, 2H), 5.58 (d, *J* = 7.8 Hz, 2H), 3.97 – 3.83 (m, 2H), 2.78 (t, *J* = 7.4 Hz, 4H), 1.98 (d, *J* = 12.1 Hz, 4H), 1.93 (s, 6H), 1.73 (d, *J* = 13.6 Hz, 4H), 1.64 (d, *J* = 12.7 Hz, 2H), 1.40 (dd, *J* = 24.7, 12.1 Hz, 4H), 1.28 – 1.13 (m, 8H) ppm; ^{13}C NMR (75.4 MHz, DMSO-d_6) δ = 159.9, 146.2, 138.5, 136.0, 134.0, 128.6, 48.2, 38.3, 32.5, 25.2, 24.9, 22.3, 14.2 ppm; HRMS-ESI+ *m/z* calculated for $C_{29}H_{39}N_2O_2S_2$ $[M + H]^+$ 511.2448, found 511.2437.

Di-l-menthol diarylethene (2.8o)

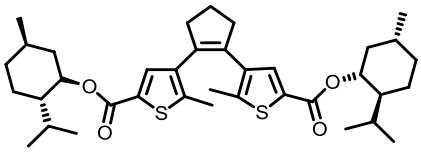

Compound **2.2** (1.5 g, 4.3 mmol, 1.0 equiv.) was dissolved in CH_2Cl_2 (50 mL). Subsequently, DMAP (0.53 g, 4.3 mmol, 1.0 equiv) and l-menthol (1.5 g, 9.5 mmol, 2.2 equiv) were added. After cooling in an ice bath and stirring for 10 min, EDC (1.8 g, 9.5 mmol, 2.2 equiv.) was added and the mixture was allowed to warm to room temperature and stirred for 16 h. The mixture was washed with water (50 mL), dried over Na_2SO_4 and filtered. Evaporation of the solvent gave an off-white solid. After purification by flash column chromatography (SiO_2, 5% Et_2O in *n*-heptane), **2.8o** was obtained as a colorless oil (1.6 g, 2.6 mmol, 60%). ^{1}H NMR (400 MHz, $CDCl_3$) δ = 7.49 (s, 2H), 4.82 (td, *J* = 10.9, 4.4 Hz, 2H), 2.79 (t, *J* = 7.5 Hz, 4H), 2.14 – 2.01 (m, 2H), 1.92 (s, 6H), 1.70 (ad, *J* = 11.4 Hz, 2H), 1.58 – 1.41 (m, 6H), 1.34 – 1.23 (m, 2H), 1.18 – 1.00 (m, 4H), 0.90 (d, *J* = 6.3 Hz, 12H), 0.88 – 0.82 (m, 4H), 0.78 (d, *J* = 6.9 Hz, 6H) ppm.

Di-l-menthol diarylethene (2.8c)

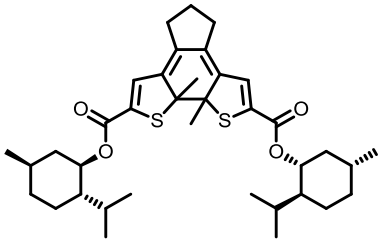

Di-ester **2.8o** was dissolved in *c*-hexane and the solution was irradiated in a quartz tube with UV light (λ = 312 nm) to cyclize the compound. The cyclization was followed by UV-vis spectroscopy. The resulting diastereomers could be separated by chiral HPLC (ChiralPak AD, 4.6 x 250 mm, particle size 1 µm, 95:5 heptane/i-PrOH, 1 mL/min.); retention times (min): 6.4, 9.3.

***N*-acetyl-L-cystein ethyl ester**

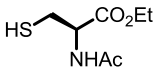

This compound was prepared as described in literature.[71] *N*-acetyl-L-cystein (5.0 g, 26 mmol, 1.0 equiv.) was suspended in EtOH (150 mL) and $SOCl_2$ (5.0 mL, 69 mmol, 2.6 equiv.) was added dropwise. The mixture was stirred at room temperature for 4 h. Water (300 mL) was added and the aqueous phase was extracted with EtOAc (3 x 200 mL). The combined organic layer was dried over Na_2SO_4 and evaporation of the solvent gave ***N*-acetyl-L-cystein ethyl ester** as an off-white solid (4.5 g, 24 mmol, 91%). ^{1}H NMR (400 MHz, $CDCl_3$) δ = 6.42 (bs, 1H), 4.83 – 4.89 (m, 1H), 4.26 (q, *J* = 7.2 Hz, 2H), 3.03 (dd, *J* = 9.0, 4.0 Hz, 2H), 2.08 (s, 3H), 1.26 – 1.35 (m, 4H) ppm; ^{13}C NMR (100.6 MHz, $CDCl_3$) δ = 170.1, 169.8, 62.0, 53.5, 26.9, 23.1, 14.1 ppm. Data is in accordance with literature.[71]

(2R,2'R)-Diethyl 3,3'-((4,4'-(cyclopent-1-ene-1,2-diyl)bis(5-methylthiophene-2,2'-carbonyl))-bis(sulfanediyl))bis(2-acetamidopropanoate) (2.3o)

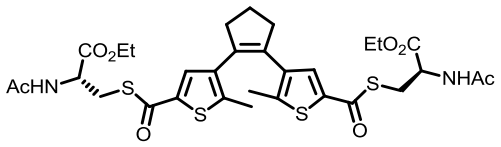

Compound **2.2** (0.34 g, 0.97 mmol, 1.0 equiv) was dissolved in DMF (10 mL). Subsequently, DMAP (24 mg, 0.020 mmol, 0.2 equiv) and NEt_3 (0.28 mL, 0.20 mmol, 2.0 equiv) were added at room temperature. DIC (0.89 mL, 5.8 mmol, 5.8 equiv) was added dropwise and the reaction mixture was stirred for 15 min. Ac-(*R*)-Cys-OEt (1.4 g, 7.8 mmol, 7.8 equiv) was then added and the solution was left at ambient temperature for 16 h. The reaction mixture was taken up in EtOAc (30 mL) and water (50 mL) and the organic phase was separated. The aqueous layer was extracted with EtOAc (2 x 30 mL). The organic layers were combined and washed with water (30 mL) and brine (30 mL) to remove remaining DMF. The organic phase was dried over $MgSO_4$ and filtered. Evaporation of the solvent gave a solid residue. After purification by flash column chromatography (dry load, SiO_2, 40%–100% EtOAc in *n*-pentane) **2.3o** was obtained as a white foam (0.58 g, 0.83 mmol, 86%). m.p. not determinable (dec); ^{1}H NMR (400 MHz, $CDCl_3$) δ = 7.41 (s, 2H), 6.61 (d, *J* = 7.6 Hz, 2H), 4.90 – 4.69 (m, 2H), 4.15 (q, *J* = 7.1 Hz, 4H), 3.57 – 3.38 (m, 4H), 2.75 (t, *J* = 7.5 Hz, 4H), 2.05 – 2.00 (m, 2H), 1.96 (s, 6H), 1,95 (s, 6H), 1.23 (t, *J* = 7.1 Hz, 6H) ppm; ^{13}C NMR (100.6 MHz, $CDCl_3$) δ = 182.4, 170.2, 170.2, 144.4, 136.9, 136.8, 135.0, 132.7, 62.0, 52.3, 38.3, 30.7, 23.0, 22.8, 15.0, 14.1 ppm; HRMS-TOF+ *m/z* calculated for $C_{31}H_{39}N_2O_8S_4$ $[M+H]^+$ 695.1584, found 695.1580.

(2R,2'R)-Diethyl 3,3'-((9a,9b-dimethyl-5,6,9a,9b-tetrahydro-4*H*-indeno[5,4-b:6,7-b']dithiophene-2,8-dicarbonyl)bis(sulfanediyl))bis(2-acetamidopropanoate) (2.3c)

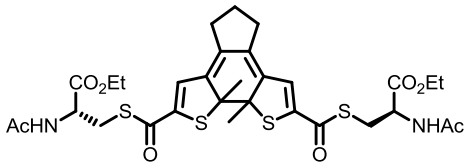

Dithioester **2.3o** was dissolved in EtOAc and the solution was irradiated in a quartz tube with UV light (λ = 365 nm) to cyclize the compound. The cyclization was followed by UV-vis spectroscopy (EtOAc, λ_{max} = 590 nm). The resulting diastereomers were separated by preparative HPLC (ChiralPak AD, 4.6 x 250 mm, particle size 1 µm, 70:30 heptane/i-PrOH, 1 mL/min.); retention times (min): 10.0, 12.0. The solvent was then evaporated at ambient temperature in the dark to give diastereomerically pure **2.3c** as a blue solid.

(9aR,9bR)-*N*2,*N*8-Dihexyl-9a,9b-dimethyl-5,6,9a,9b-tetrahydro-4*H*-indeno[5,4-b: 6,7-b']dithiophene-2,8-dicarboxamide 2.1c*-a)

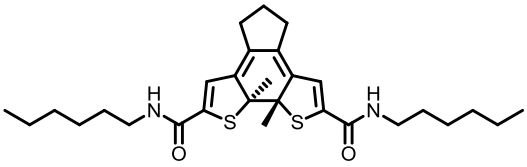

Diastereomerically pure dithioester diarylethene **2.3c** (27 mg, 0.041 mmol, 1.0 equiv) was dissolved in dry DMF (3 mL) and *n*-hexylamine (86 µL, 0.65 mmol, 16 equiv) was added at room temperature. The vessel was protected from light and left stirring at ambient temperature for 24 h. The colour of the reaction mixture changed from blue to purple, then finally red. The DMF solution was taken up in EtOAc (10 mL) and saturated aq. NH_4Cl solution (10 mL). The organic phase was separated and the aqueous layer was washed with EtOAc (2 x 10 mL). The combined organic layers were washed with water (10 mL) and brine (10 mL). The organic layer was then dried over $MgSO_4$, filtered and concentrated in vacuo at room temperature (see Note 1). The red crude product was purified by flash column chromatography (SiO_2, 30%–50% EtOAc in *n*-pentane) and then evaporated to dryness to yield **2.1c*-a** as a red solid (21 mg, 0.041 mmol, quant.). The compounds were confirmed to be enantiopure by chiral HPLC; retention times (min): 31, 40. ^{1}H NMR (400 MHz, $CDCl_3$) δ = 7.63 (s, 2H), 5.71 (t, *J* = 5.5 Hz, 2H), 3.43 – 3.25 (m, 4H), 2.82 – 2.74 (m, 2H), 2.43 (t, *J* = 7.3 Hz, 4H), 1.95 (s, 6H), 1.63 – 1.48 (m, 4H), 1.43 – 1.19 (m, 12H), 0.89 (t, *J* = 6.6 Hz, 6H). Data are identical to the racemic compound *rac*-**2.1c-a** in all respects.

(9aS,9bS)-*N*2,*N*8-Dicyclohexyl-9a,9b-dimethyl-5,6,9a,9b-tetrahydro-4*H*-indeno[5,4-b:6,7-b']dithiophene-2,8-dicarboxamide (2.1c*-b)

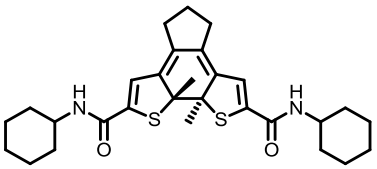

Diastereomerically pure dithioester diarylethene **2.3c** (34 mg, 0.051 mmol, 1.0 equiv) was dissolved in dry DMF (3 mL) and *c*-hexylamine (94 µL, 0.82 mmol, 18 equiv) was added at room temperature. The vessel was protected from light and left stirring at ambient temperature for 24 h. The colour of the reaction mixture changed from blue to purple, then finally red. The DMF solution was taken up in EtOAc (10 mL) and saturated aq. NH_4Cl solution (10 mL). The organic phase was separated and the aqueous layer was washed with EtOAc (2 x 10 mL). The combined organic layers were washed with water (10 mL) and brine (10 mL). The organic layer was then dried over $MgSO_4$, filtered and concentrated in vacuo at RT (see Note 1). The red crude was purified by flash column chromatography (SiO_2, 40% EtOAc in *n*-pentane) and then evaporated to dryness to yield **2.1c*-b** as a red solid (17 mg, 0.051 mmol, quant.). The compounds were confirmed to be enantiopure by chiral HPLC; retention times (min): 24, 45. ^{1}H NMR (400 MHz, $CDCl_3$) δ = 6.66 (s, 2H), 5.56 (d, *J* = 8.0 Hz, 2H), 3.92 – 3.79 (m, 2H), 2.44 (t, *J* = 7.3 Hz, 4H), 1.95 (s, 6H), 1.72 (dd, *J* = 9.9, 3.5 Hz, 4H), 1.63 (d, *J* = 12.8 Hz, 2H), 1.38 (m, 6H), 1.30 – 1.11 (m, 10H) ppm. Data are identical to the racemic compound *rac*-**2.1c-a** in all respects.

Representative HPLC chromatograms

Chromatogram of *rac*-**2.1c-a**

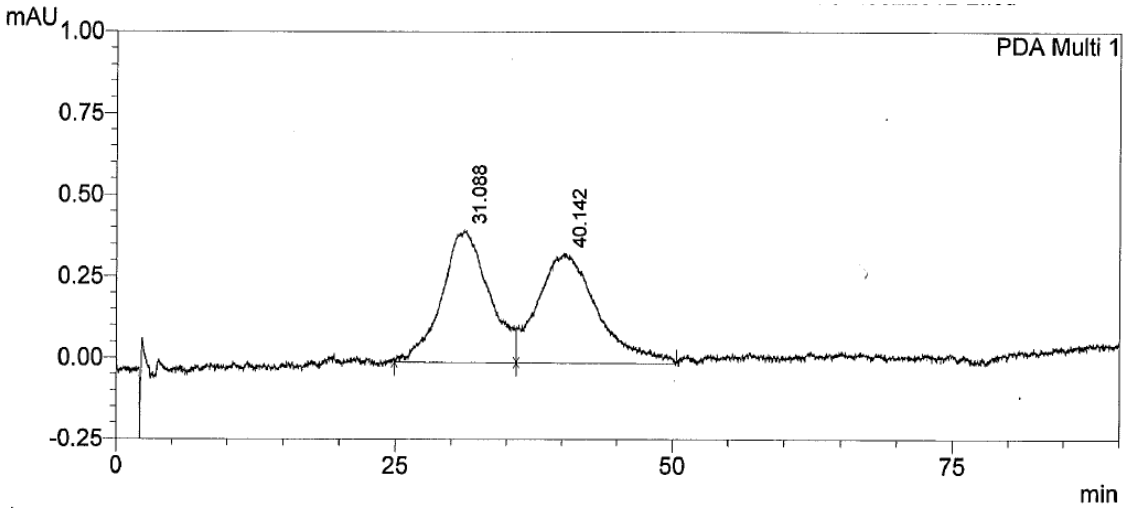

Column: ChiralCel OJ 4.6 x 250 mm, particle size 1 µm, 98:2 heptane/*i*-PrOH, 1.5 mL/min., temperature: 50 °C, PDA: 540 nm. Retention times: 31.1 and 40.1 min. In this example the ratio of the two enantiomers is 50:50 and the induction is 0%. See Note 2.

Example of Sergeant-Soldier experiment of **2.1o-a** with **2.1c*-a** (Sergeant % = 19.6%)

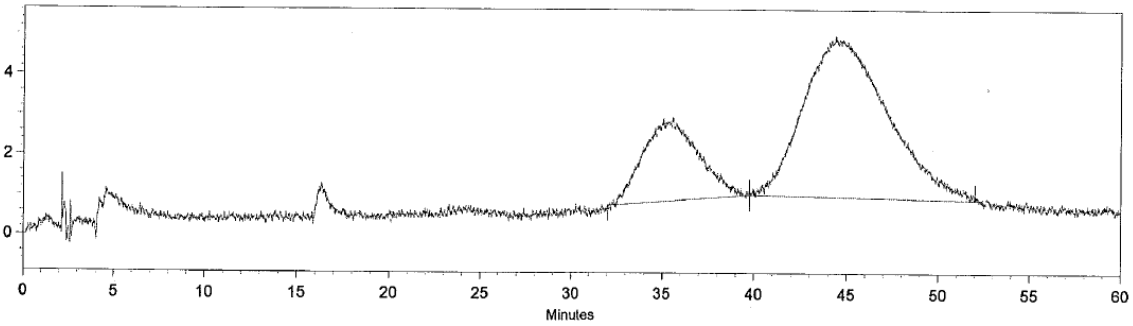

Column: ChiralCel OJ 4.6 x 250 mm, particle size 1 µm, 97.5:2.5 heptane/*i*-PrOH, 1.5 mL/min., temperature: 50 °C, PDA: 540 nm. Retention times: 35.6 and 44.4 min. In this example the ratio of the two enantiomers is 23:77 and the induction is 17%. See Note 2.

Chromatogram of *rac*-**2.1c-b**

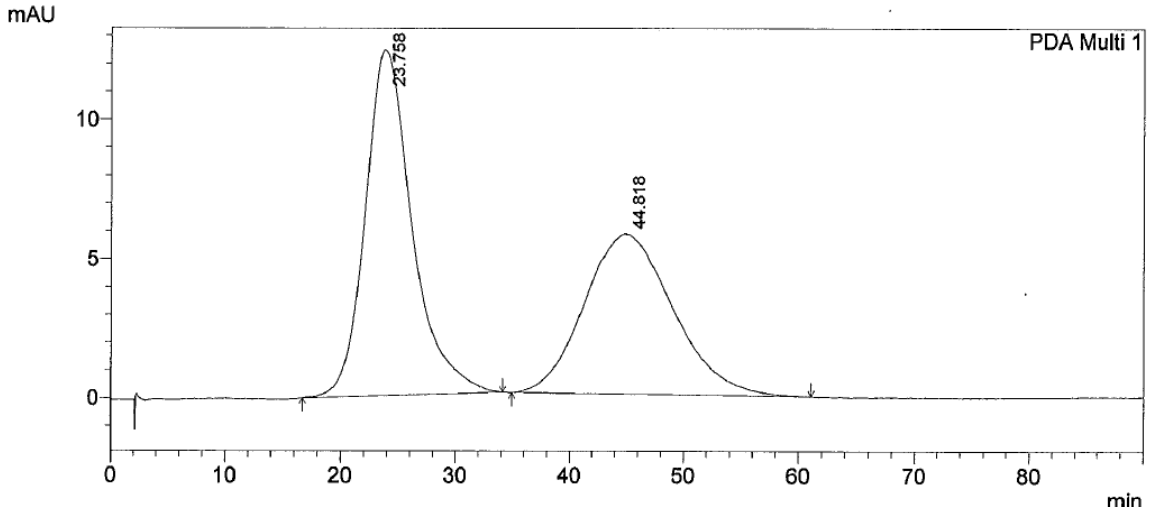

Column: ChiralCel OJ 4.6 x 250 mm, particle size 1 µm, 98:2 heptane/*i*-PrOH, 1.5 mL/min., temperature: 50 °C, PDA: 520 nm. Retention times: 23.8 and 44.8 min. In this example the ratio of the two enantiomers is 50:50 and the induction is 0%. See Note 2.

Example of Sergeant-Soldier experiment of **2.1o-b** with **2.1c*-b** (Sergeant % = 9%)

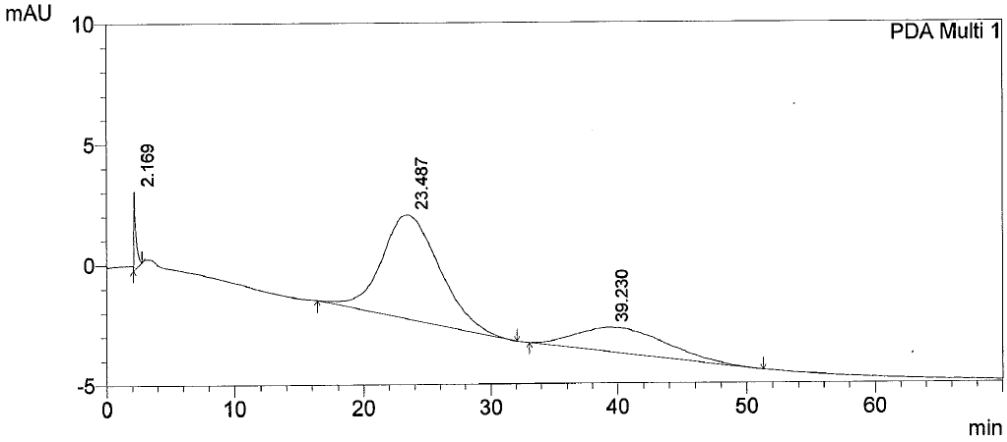

Column: ChiralCel OJ 4.6 x 250 mm, particle size 1 µm, 98:2 heptane/*i*-PrOH, 1.5 mL/min., temperature: 50 °C, PDA: 520 nm. Retention times: 23.5 and 39.2 min. In this example the ratio of the two enantiomers is 73:27 and the induction is 19%. See Note 2.

Notes

1 It is best to not evaporate the crude to dryness or dry-load the column as the gelator molecules will often not go back into solution easily for purification. Should the gelators precipitate or gel on the column, the yield drops tremendously.

2 It is important to set the PDA detector to detect at higher wavelength, otherwise the open photoswitch will be closed while it is eluted and may influence the outcome of the analysis.

2.9 Acknowledgements

We thank Dr. Paula de Mendoza and Dr. Jochem van Herpt for insightful comments and useful discussions.

2.10 References

[1] D. G. Blackmond, *Angew. Chem. Int. Ed.* **2009**, *48*, 2648–2654.
[2] S. Toxvaerd, *Int. J. Astrobiol.* **2005**, *4*, 43–48.
[3] D. G. Blackmond, *Proc. Natl. Acad. Sci. U. S. A.* **2004**, *101*, 5732–5736.
[4] A. J. Bissette, S. P. Fletcher, *Angew. Chem. Int. Ed.* **2013**, *52*, 12800–12826.
[5] F. C. Frank, *Biochim. Biophys. Acta* **1953**, *11*, 459–463.
[6] T. Shibata, H. Morioka, T. Hayase, K. Choji, K. Soai, *J. Am. Chem. Soc.* **1996**, *118*, 471–472.
[7] K. Soai, I. Sato, *Chirality* **2002**, *14*, 548–554.
[8] K. Soai, T. Shibata, H. Morioka, K. Choji, *Nature* **1995**, *378*, 767–768.
[9] T. Gehring, M. Busch, M. Schlageter, D. Weingand, *Chirality* **2010**, *22*, E173–E182.
[10] B. L. Feringa, R. A. van Delden, *Angew. Chem. Int. Ed.* **1999**, *38*, 3418–3438.
[11] D. G. Blackmond, C. R. McMillan, S. Ramdeehul, A. Schorm, J. M. Brown, *J. Am. Chem. Soc.* **2001**, *123*, 10103–10104.
[12] T. Gehring, M. Quaranta, B. Odell, D. G. Blackmond, J. M. Brown, *Angew. Chem. Int. Ed.* **2012**, *51*, 9539–9542.
[13] S. B. Tsogoeva, *Chem. Commun.* **2010**, *46*, 7662–7669.
[14] A. H. Alberts, H. Wynberg, *J. Am. Chem. Soc.* **1989**, *111*, 7265–7266.
[15] E. Yashima, T. Matsushima, Y. Okamoto, *J. Am. Chem. Soc.* **1997**, *119*, 6345–6359.
[16] E. Yashima, Y. Maeda, Y. Okamoto, *J. Am. Chem. Soc.* **1998**, *120*, 8895–8896.
[17] A. R. Palmans, J. A. Vekemans, E. E. Havinga, E. W. Meijer, *Angew. Chem. Int. Ed. Engl.* **1997**, *36*, 2648–2651.
[18] M. M. Green, M. P. Reidy, R. D. Johnson, G. Darling, D. J. O'Leary, G. Willson, *J. Am. Chem. Soc.* **1989**, *111*, 6452–6454.
[19] F. Helmich, M. M. Smulders, C. C. Lee, A. P. Schenning, E. W. Meijer, *J. Am. Chem. Soc.* **2011**, *133*, 12238–12246.
[20] F. García, P. M. Viruela, E. Matesanz, E. Ortí, L. Sánchez, *Chem. – Eur. J.* **2011**, *17*, 7755–7759.
[21] A. L. Nussbaumer, D. Studer, V. L. Malinovskii, R. Häner, *Angew. Chem. Int. Ed.* **2011**, *50*, 5490–5494.
[22] D. Ogata, T. Shikata, K. Hanabusa, *J. Phys. Chem. B* **2004**, *108*, 15503–15510.
[23] F. García, L. Sánchez, *J. Am. Chem. Soc.* **2012**, *134*, 734–742.
[24] S. J. George, Ž. Tomović, M. M. J. Smulders, T. F. A. de Greef, P. E. L. G. Leclère, E. W. Meijer, A. P. H. J. Schenning, *Angew. Chem. Int. Ed.* **2007**, *46*, 8206–8211.
[25] E. Yashima, K. Maeda, T. Nishimura, *Chem. – Eur. J.* **2004**, *10*, 42–51.
[26] A. Ajayaghosh, R. Varghese, S. J. George, C. Vijayakumar, *Angew. Chem. Int. Ed.* **2006**, *45*, 1141–1144.
[27] T. W. Anderson, J. K. Sanders, G. D. Pantos, *Org. Biomol. Chem.* **2010**, *8*, 4274–4280.
[28] A. Ajayaghosh, R. Varghese, S. Mahesh, V. K. Praveen, *Angew. Chem. Int. Ed.* **2006**, *45*, 7729–7732.
[29] T. Yamamoto, T. Fukushima, T. Aida, in *Self-Assembled Nanomaterials II*, Springer-Verlag Berlin, Heidelberg, Germany, **2008**, pp. 1–27.
[30] L. J. Prins, P. Timmerman, D. N. Reinhoudt, *J. Am. Chem. Soc.* **2001**, *123*, 10153–10163.
[31] K. -H. Ernst, *Curr. Opin. Colloid Interface Sci.* **2008**, *13*, 54–59.
[32] F. Vera, R. M. Tejedor, P. Romero, J. Barberá, M. B. Ros, J. L. Serrano, T. Sierra, *Angew. Chem. Int. Ed.* **2007**, *46*, 1873–1877.
[33] J. Wang, D. Ding, L. Zeng, Q. Cao, Y. He, H. Zhang, *New J. Chem.* **2010**, *34*, 1394–1400.

[34] T. Ishi-i, M. Crego-Calama, P. Timmerman, D. N. Reinhoudt, S. Shinkai, *J. Am. Chem. Soc.* **2002**, *124*, 14631–14641.

[35] T. Yamamoto, T. Fukushima, A. Kosaka, W. Jin, Y. Yamamoto, N. Ishii, T. Aida, *Angew. Chem.* **2008**, *120*, 1696–1699.

[36] F. Helmich, C. C. Lee, A. P. Schenning, E. W. Meijer, *J. Am. Chem. Soc.* **2010**, *132*, 16753–16755.

[37] M. Irie, *Chem. Rev.* **2000**, *100*, 1685–1716.

[38] M. Akazawa, K. Uchida, J. J. D. de Jong, J. Areephong, M. C. A. Stuart, G. Caroli, W. R. Browne, B. L. Feringa, *Org. Biomol. Chem.* **2008**, *6*, 1544–1547.

[39] J. J. D. de Jong, T. D. Tiemersma-Wegman, J. H. van Esch, B. L. Feringa, *J. Am. Chem. Soc.* **2005**, *127*, 13804–13805.

[40] L. N. Lucas, J. J. D. de Jong, J. H. van Esch, R. M. Kellogg, B. L. Feringa, *Eur. J. Org. Chem.* **2003**, *2003*, 155–166.

[41] J. J. D. de Jong, *PhD Thesis: Dithienylcyclopentene Optical Switches*, University of Groningen, **2006**.

[42] N. Katsonis, A. Minoia, T. Kudernac, T. Mutai, H. Xu, H. Uji-i, R. Lazzaroni, S. De Feyter, B. L. Feringa, *J. Am. Chem. Soc.* **2008**, *130*, 386–387.

[43] K. Matsuda, M. Irie, *J. Photochem. Photobiol. C-Photochem. Rev.* **2004**, *5*, 169–182.

[44] B. L. Feringa, W. R. Browne, *Molecular Switches*, John Wiley & Sons, Weinheim, Germany, **2011**.

[45] L. Frkanec, M. Žinić, *Chem. Commun.* **2010**, *46*, 522–537.

[46] J. J. D. de Jong, L. N. Lucas, R. M. Kellogg, J. H. Van Esch, B. L. Feringa, *Science* **2004**, *304*, 278–281.

[47] C. S. Snijder, J. C. deJong, A. Meetsma, F. vanBolhuis, B. L. Feringa, *Chem. – Eur. J.* **1995**, *1*, 594–597.

[48] N. Zweep, A. Hopkinson, A. Meetsma, W. R. Browne, B. L. Feringa, J. H. van Esch, *Langmuir* **2009**, *25*, 8802–8809.

[49] J. H. van Esch, *Langmuir* **2009**, *25*, 8392–8394.

[50] A. Mammana, G. T. Carroll, B. L. Feringa, in *Comprehensive Chiroptical Spectroscopy* (Eds.: N. Berova, P.L. Polavarapu, K. Nakanishi, R.W. Woody), John Wiley & Sons, Inc., **2012**, pp. 289–316.

[51] J. J. D. de Jong, B. L. Feringa, J. van Esch, in *Molecular Switches* (Eds.: B.L. Feringa, W.R. Browne), Wiley-VCH Verlag GmbH & Co. KGaA, Weinheim, Germany, **2011**, pp. 517–561.

[52] B. L. Feringa, in *From Non-Covalent Assemblies to Molecular Machines* (Eds.: J. -P. Sauvage, P. Gaspard), Wiley-VCH Verlag GmbH & Co. KGaA, Weinheim, Germany, **2010**, pp. 453–461.

[53] A. Friggeri, B. L. Feringa, J. van Esch, *J. Controlled Release* **2004**, *97*, 241–248.

[54] A. R. Hirst, I. A. Coates, T. R. Boucheteau, J. F. Miravet, B. Escuder, V. Castelletto, I. W. Hamley, D. K. Smith, *J. Am. Chem. Soc.* **2008**, *130*, 9113–9121.

[55] P. Terech, R. G. Weiss, *Chem. Rev.* **1997**, *97*, 3133–3160.

[56] J. van Esch, F. Schoonbeek, M. D. Loos, E. M. Veen, R. M. Kellogg, B. L. Feringa, in *Supramolecular Science: Where It Is and Where It Is Going* (Eds.: R. Ungaro, E. Dalcanale), Springer Netherlands, **1999**, pp. 233–259.

[57] J. J. D. de Jong, L. N. Lucas, R. M. Kellogg, J. H. van Esch, B. L. Feringa, *Science* **2004**, *304*, 278–281.

[58] J. J. D. de Jong, P. van Rijn, T. D. Tiemersma-Wegeman, L. N. Lucas, W. R. Browne, R. M. Kellogg, K. Uchida, J. H. Van Esch, B. L. Feringa, *Tetrahedron* **2008**, *64*, 8324–8335.

[59] W. Jin, T. Fukushima, M. Niki, A. Kosaka, N. Ishii, T. Aida, *Proc. Natl. Acad. Sci. U. S. A.* **2005**, *102*, 10801–10806.

[60] H. Miyasaka, S. Araki, A. Tabata, T. Nobuto, N. Malaga, M. Irie, *Chem. Phys. Lett.* **1991**, *230*, 249–254.

[61] J. Ern, A. T. Bens, H. -D. Martin, S. Mukamel, S. Tretiak, K. Tsyganenko, K. Kuldova, H. P. Trommsdorff, C. Kryschi, *J. Phys. Chem. A* **2001**, *105*, 1741–1749.

[62] P. Q. Huang, X. Zheng, X. M. Deng, *Tetrahedron Lett.* **2001**, *42*, 9039–9041.

[63] T. J. Mason, *Ultrasonics* **1992**, *30*, 192–196.

[64] R. Sutton, B. Rockett, P. G. Swindells, *Chemistry for the Life Sciences*, CRC Press, **2000**.

[65] J. Clayden, N. Greeves, S. Warren, P. Wothers, *Organic Chemistry*, OUP Oxford, Oxford ; New York, USA, **2001**.

[66] A. Horeau, *Tetrahedron Lett.* **1969**, *10*, 3121–3124.

[67] R. Wang, C. Geiger, L. Chen, B. Swanson, D. G. Whitten, *J. Am. Chem. Soc.* **2000**, *122*, 2399–2400.

[68] A. Takahashi, M. Sakai, T. Kato, *Polym. J.* **1980**, *12*, 335–341.

[69] A. J. Wilson, M. Masuda, R. P. Sijbesma, E. W. Meijer, *Angew. Chem. Int. Ed.* **2005**, *44*, 2275–2279.

[70] M. Masuda, P. Jonkheijm, R. P. Sijbesma, E. W. Meijer, *J. Am. Chem. Soc.* **2003**, *125*, 15935–15940.

[71] R. K. Uhrig, M. A. Picard, K. Beyreuther, M. Wiessler, *Carbohydr. Res.* **2000**, *325*, 72–80.

Chapter 3

Chirality Controlled Self-Assembled Nanotubes

In this chapter, a nanotube-forming, photoresponsive amphiphile is presented that co-assembles with its chiral counterpart to form nanotubes. We show how chirality can be used to effect in a controlled manner, the formation of either micrometer long, achiral nanotubes or shorter (~300 nm), chiral nanotubes that are bundled. We studied the assemblies using a variety of spectroscopic and microscopic techniques and show that the tubes can be disassembled, thereby allowing the chiral information to be erased, with light.

Part of the research presented in this chapter has been published:
D. J. van Dijken, P. Štacko, M. C. A. Stuart, W. R. Browne, B. L. Feringa, *manuscript in preparation*

A. C. Coleman, J. M. Beierle, M. C. A. Stuart, B. Maciá, G. Caroli, J. T. Mika, D. J. van Dijken, J. Chen, W. R. Browne, B. L. Feringa, *Nat. Nanotechnol.* **2011**, *6*, 547–552.

3.1 Introduction

A fascinating aspect and crucial feature of complex, multifunctional self-assembled objects found in Nature is that they are dynamic, allowing a multitude of biological processes to rely on feedback-controlled communication.[1] In other words, the self-assembled structure can adopt in response to an input signal. This adjustability in response to stimuli is crucial for correct functioning of many bioprocesses.[2] Therefore, the design and synthesis of similar systems that can respond to external stimuli is important in order to understand natural systems better, and they can provide novel biomimetic structures, for example, for sensing and drug delivery.[3–9]

Using chirality to affect or initiate self-assembly is a particularly interesting approach, as the world around us is made up of chiral molecules of a unique handedness. Many natural systems are extremely effective in discriminating enantiomers from each other. For example, enzymes often convert only one of two enantiomers, while leaving the other one untouched. Amplification of chirality is necessary for the emergence of homochirality from a pool of nearly racemic compound and is thought to play a crucial role in the origin of life.[10–12] In recent years, amplification of chirality has been exploited in the field of supramolecular chemistry and this principle has been applied in supramolecular polymers,[13–19] gels,[20–22] organic nanotubes,[23–25] liquid crystals[26–30] and other assemblies.[31–35]

Rigid systems are of special interest due to their homogeneity and the possibility to transfer information from the monomer to the self-assembled system as a whole. The groups of Aida and Meijer pioneered the possibility to amplify chirality in such rigid systems in parallel, using the "majority rules" principle,[25,36] where the major enantiomer determines the chirality of the entire assembly. In the system of Aida and coworkers, in an attempt to bias the helical sense of the nanotubes, two chiral derivatives of the originally reported hexa-*peri*-hexabenzocoronene (HBC) amphiphile,[37] have been designed that have stereogenic centers, bearing methyl groups in either the hydrophilic or the hydrophobic tails of the amphiphile (Figure 3.1).[25]

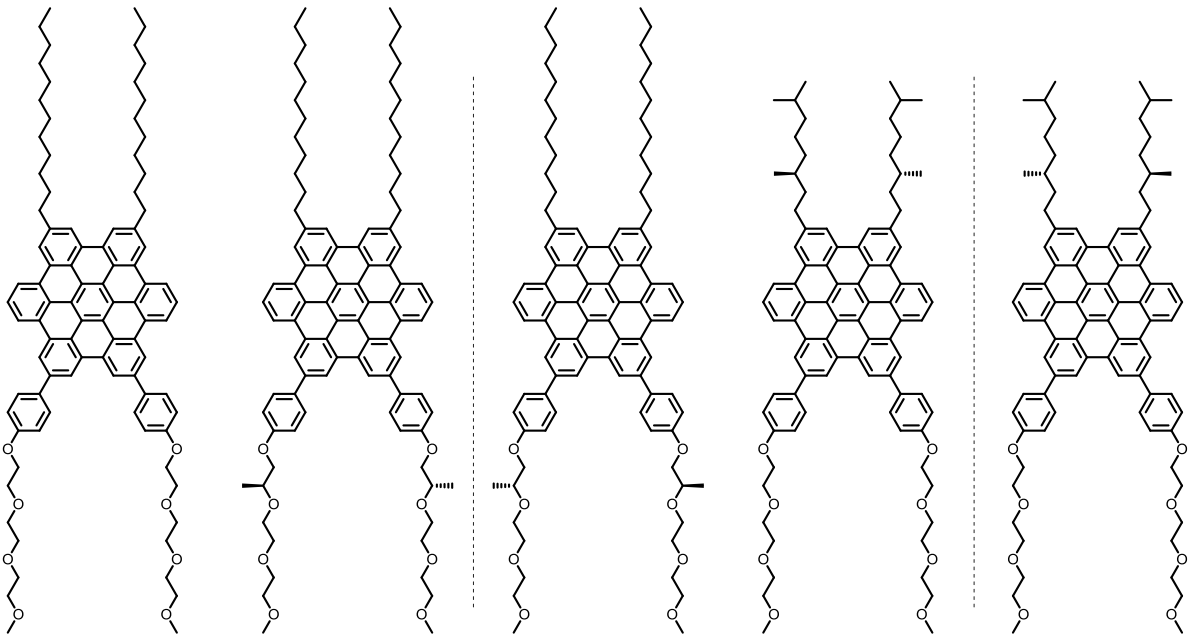

Figure 3.1. Hexa-*peri*-hexabenzocoronene amphiphile and chiral analogues reported by Aida and coworkers.[25]

Interestingly, when the two enantiomeric derivatives bearing the chiral information in the hydrophilic part of the amphiphile are co-assembled in MeTHF, nanotubes could be formed with either left- or right-handed helical senses, depending on the major enantiomer incorporated. When the chiral information is embedded in the interdigitating hydrophobic alkyl chains, however, nanotube formation is inhibited.[25] The authors state that this is due to the branched side chains that distort the packing and prevents the formation of a bilayer tape as was observed for the achiral HBC amphiphile and the chiral analogue with the stereogenic centers in the hydrophilic part of the amphiphile (Figure 3.1).

In addition to the majority rules principle, the "sergeant-soldier" principle has been reported for transfer of chirality from monomers to supramolecular aggregates. In the "sergeant-soldier principle", as introduced by Green and coworkers,[38] a minor amount of the chiral compound (sergeant), used as dopant, dictates the overall chirality of a polymer system that is made up of mainly achiral material (soldiers). Meijer and coworkers have reported supramolecular, chiral columnar stacks of disk-shaped molecules where the chirality of the supramolecular columns is governed through the majority rules[36] or sergeant-soldier[39–42] principle, depending on the system and conditions.

Previously, we have developed a complex, light-responsive, self-assembled nanotube system based on a photochemically active amphiphile (Fig. 3.2).

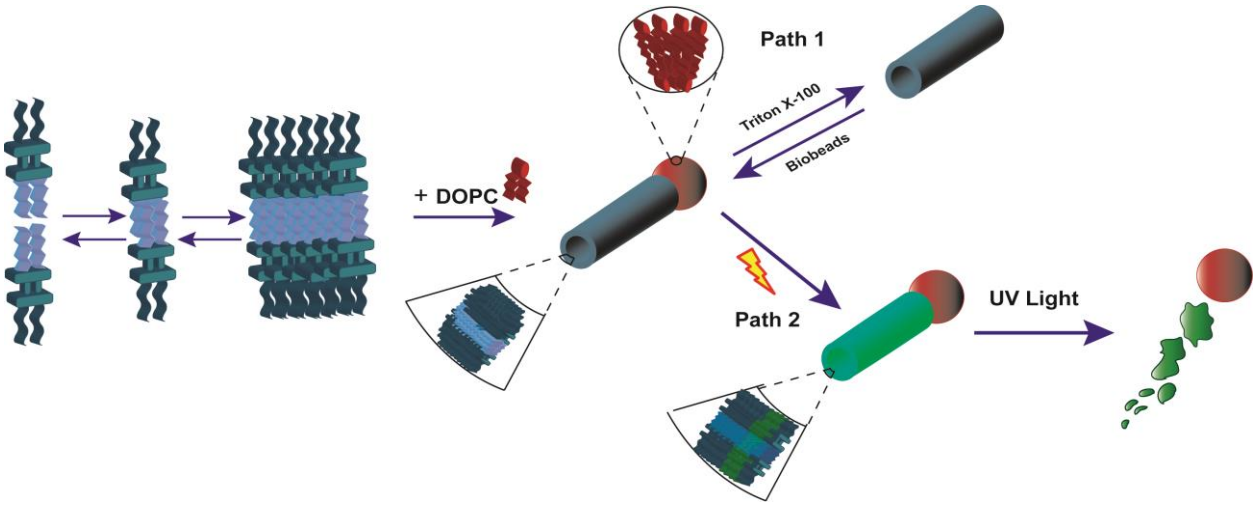

Figure 3.2. Schematic representation of assembly and disassembly of vesicle-capped, photoresponsive nanotubes.[43]

Figure 3.2 shows self-assembly of a photochemically active amphiphile in water, which initially forms interdigitated bilayers, followed by nanotube formation and capping of the nanotube with DOPC (1,2-dioleoyl-sn-glycero-3-phosphocholine) vesicles to give the hybrid end-capped nanotube system. Treatment of vesicle-capped nanotubes with detergent Triton X-100 (Figure 3.2; path 1) dissolves the phospholipid capping vesicle without affecting the nanotube. Subsequent removal of detergent with Biobeads followed by freeze-thaw cycles regenerates the vesicle-capped nanotubes. Alternatively, irradiation of the nanotubes (Figure 3.2; path 2) with UV light leads to disassembly of the nanotubes. This photochemically induced disassembly process offers a high degree of control, and can be followed in real time using confocal and epifluorescence microscopy.

The nanotubes disassemble into amorphous aggregates. Using confocal microscopy, the disassembly process was confirmed to occur due to the formation of the cyclized product of **3.1** upon irradiation with UV light (Figure 3.3).[43]

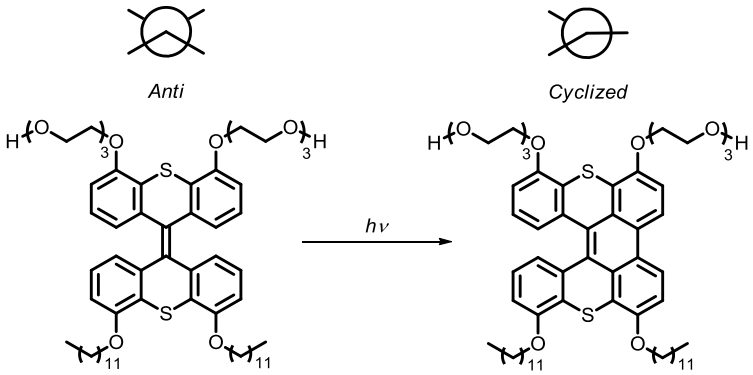

Figure 3.3. Antifolded structure of **3.1** prior to and cyclized form of **3.1** after irradiation with UV light.

The cyclized form of **3.1** is less flexible than the antifolded, uncyclized form and the nanotubes are believed to pack in such a tight manner, that loss of flexibility breaks up the tubes. Indeed, pure cyclized (before self-assembly) **3.1** formed vesicles upon self-assembly in water, rather than nanotubes, both in the presence and absence of DOPC, providing further evidence for the hypothesis that loss of flexibility, or a change in structure, leads to disassembly of the nanotubes.

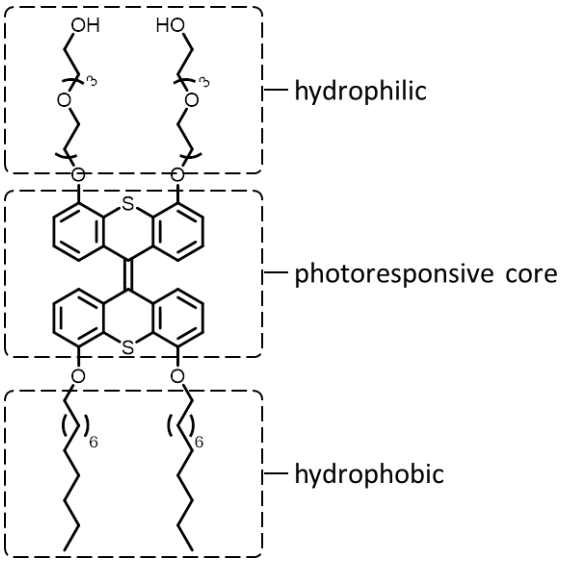

Figure 3.4. Structure and design of photoresponsive amphiphile **3.1**.

The structure of amphiphile **3.1** contains a photosensitive overcrowded alkene unit that links two hydrophilic oligo-ethyleneglycol headgroups with two hydrophobic alkyl tails. The bis-thioxanthylidene core provides a photoreactive and fluorescent functionality,[44,45] and the oligo-ethyleneglycol units facilitate solubility in water. The hydrophobic alkyl chains were shown to interact in a supramolecular fashion and interdigitate (confirmed by infrared spectroscopy and comparing bilayer thickness obtained by cryo-transmission electron microscopy (TEM) with calculated models, using Hyperchem) upon self-assembly to form a very robust bilayer that results in the formation of nanotubular assemblies.[43] We propose that the

interdigitation of the hydrophobic moieties of **3.1** occurs in order to maximize hydrophobic effects and van der Waals interaction.

We found that self-assembly of the nanotubes from **3.1** in the presence of DOPC was more reliable in terms of yield and practicality. When amphiphile **3.1** and DOPC were mixed (1:1) prior to assembly, well-defined nanotubes were obtained (see paragraph 3.4). In the absence of the phospholipid, pure **3.1** required more rigorous conditions, i.e. more freeze-thaw cycles and sonication, to give any well-defined aggregates. The fact that the addition of DOPC enhances the successful formation of well-defined structures indicates that co-assembly is key for the formation of the nanotubes and that (at least to some extent) DOPC molecules are likely embedded in the bilayers of the nanotubes. This observation led us to believe that co-assembly with other amphiphiles must also be possible. An intriguing possibility is the induction of chirality into rigid nano-objects and we envisioned that this might be possible using the sergeant-soldier principle as described in chapter 2.[39–42,46]

3.2 Concept

In contrast to the afore mentioned systems,[25,36,39–42] in natural phospholipids, the most abundant constituent of cell membranes, the chiral information is often present in the aliphatic tails.[47] The specific chiral information in these phospholipid backbones, present on the internal side of the self-assembled phospholipid bilayer, is of major importance. It is therefore remarkable that in most artificial systems, the chiral information is introduced in the part of the molecules that are not involved in the main interactions that lead to assembly into a larger aggregate.

The goal of the research presented in this chapter is to introduce chirality in the photoresponsive nanotubes, based on the previously studied amphiphile **3.1** from our group (Figure 3.2-3.4).[43] We envisioned introducing two stereocenters in the interdigitating, hydrophobic part of the amphiphile. Once synthesized, we reasoned that the amphiphile might form aggregates although we expected the methyl moieties to influence the (tight) packing of the amphiphiles to some extent. Following the sergeant-soldier principle, a small amount of the chiral amphiphile might be able to induce a structural change and chirality in the (otherwise achiral) nanotubes formed by amphiphile **3.1**.

If we could indeed apply the sergeant-soldier principle to our nanotubes, we might obtain a unique system that has several distinct differences to the systems described by the Meijer and Aida group. Firstly, the nanotubes described in this chapter are remarkably rigid, compared to the columnar systems reported by Meijer and coworkers. Secondly, the nanotubes are formed by self-assembly in water, whereas the HBC nanotubes of Aida and coworkers are in MeTHF.[25] Meijers hydrophobic, supramolecular columns are formed in dodecane and the hydrophilic analogues in water.[40] The fact that our nanotubes are also obtained in water, gives future opportunities for biocompatibility. Another advantage is that nanotubes formed from **3.1** are photoresponsive and can be disassembled with light.[43] The design of chiral analogue **3.2** is presented in Figure 3.5.

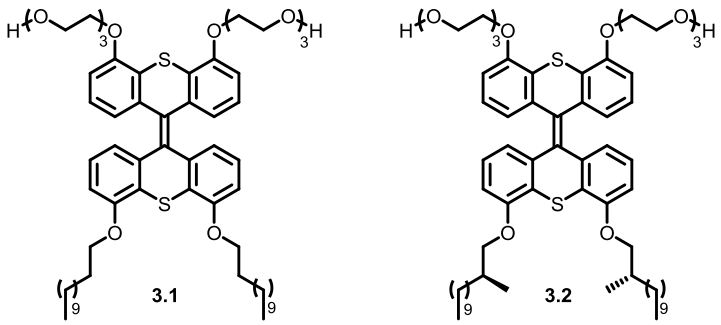

Figure 3.5. Structures of amphiphile **3.1** and chiral analogue **3.2**.

As the hydrophobic half of the molecule makes up the internal part of the bilayer after self-assembly and is most probably densely packed, we envisioned that the largest effect on the overall chirality could be obtained by introducing chirality in the hydrophobic alkyl chains. We furthermore reasoned that the packing of the molecules upon self-assembly would be least disturbed if the chirality is installed close to the aromatic core of the amphiphile. We therefore decided to introduce two methyl groups to generate pure enantiomers with the stereogenic information at the C2 position of the alkyl chains.

A major challenge in this project is the synthesis of both **3.1** and **3.2** in sufficient amounts to conduct the sergeant-soldier experiments. The synthesis of both amphiphiles is lengthy and contains some difficult steps. In this chapter, an optimized synthesis route is described as performed in a collaboration with Peter Štacko and the synthesis of the chiral analogue **3.2** will be described in his thesis in full.[48] Another challenge is the analysis of the nanotubes, as nano-objects can be different in shape and size from batch to batch and one has to be careful how to interpret the data obtained from visual techniques such as transmission electron microscopy.

3.3 Synthesis

We have optimized the synthesis of achiral analogue **3.1** since the original published procedure[43] considerably, increasing the overall yield from 7% to 58% (for the longest linear sequence), starting from the same starting materials (Schemes 3.1-3.4). Chiral analogue **3.2** was successfully synthesized in a similar way with an overall yield of 43% (for the longest linear sequence).[48]

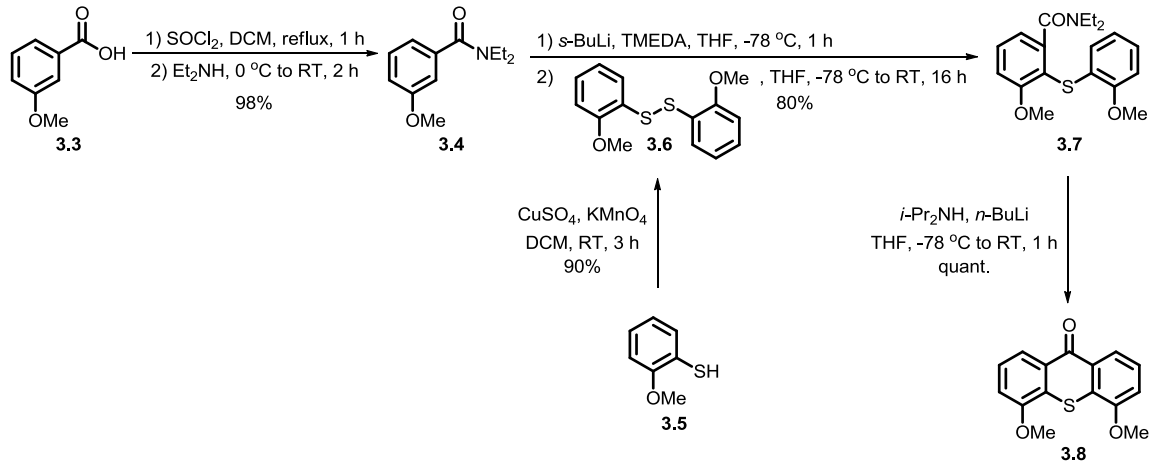

Scheme 3.1. Synthesis of key intermediate ketone **3.8** based on an adapted literature procedure.[49]

Following an adapted literature procedure,[49] 3-methoxybenzoic acid **3.3** was converted to its acid chloride, followed by treatment with diethylamine to give amide **3.4** (Scheme 3.1). In the original publication,[49] the acid chloride was added to a mixture of diethylamine and triethylamine. In our hands, this led to irreproducible results and by leaving out the triethylamine entirely, the yield was increased to a reproducible 98%. In parallel, oxidation of 2-methoxythiophenol **3.5** to disulfide **3.6** proceeded smoothly using a mixture of $CuSO_4$ and $KMnO_4$. *Ortho*-lithiation of amide **3.4** by adding the amide to a preformed complex of *sec*-BuLi and *N,N,N',N'*-tetramethylethylenediamine (TMEDA),[50] followed by addition of disulfide **3.6** gave thioether **3.7** in 85% yield. Counterintuitively, this reaction does not proceed without a trace of water present and while it has been reported that traces of water do not affect reaction rates for lithiation with lithium diisopropylamide (LDA),[51] we are currently not certain why water is needed for this reaction to give satisfactory yields. Subsequent treatment of **3.7** with LDA resulted in cyclization to afford thioxanthone **3.8** in quantitative yield. The overall yield of key building block **3.8** was improved from 71%[49] to 78% (Scheme 3.1) and this compound can be prepared on 20 g scale.

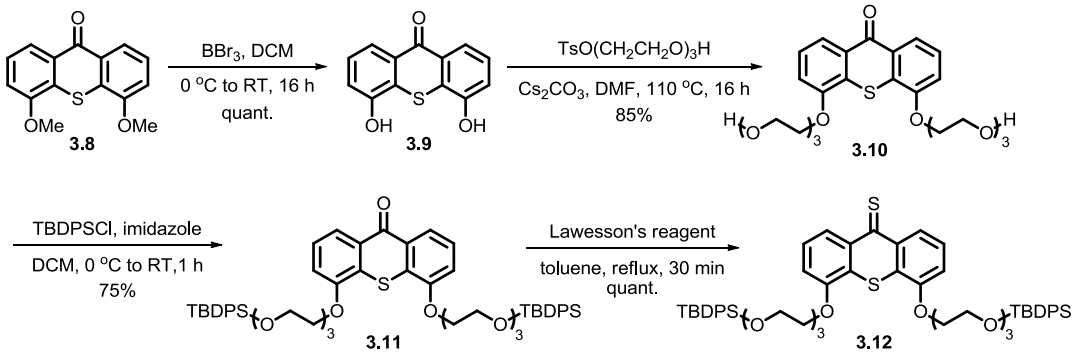

Scheme 3.2. Synthesis of the hydrophilic precursor, thioketone **3.12**, based on an adapted literature procedure.[43]

Deprotection of the phenol moieties of **3.8** with BBr_3 gives **3.9**, which reacts with monotosyl-tri-ethyleneglycol to give **3.10** (Scheme 3.2). The synthesis of the protected ethyleneglycol **4.13** is described in chapter 4 of this thesis. Protection of the ethyleneglycol chains with TBDPS-chloride occurs in good yield. Conversion of thioxanthone **3.11** to its thioketone, using Lawesson's reagent to increase its reactivity, is achieved in quantitative yield. By changing workups and purification methods slightly (see Experimental Section), the overall yield of **3.12**, starting from **3.8** was improved from 45%[43] to 64% yield (Scheme 3.2).

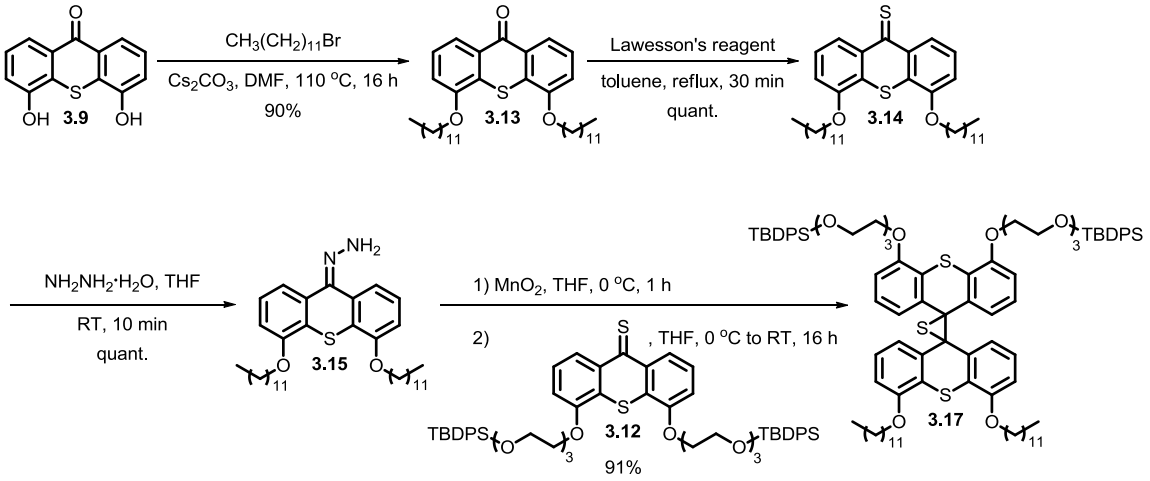

Scheme 3.3. Synthesis of the hydrophobic precursor, hydrazine **3.15** and coupling of **3.12** with **3.15** to give episulfide **3.17**, based on an adapted literature procedure.[43]

Reaction of diphenol **3.9** with laurylbromide in the presence of Cs_2CO_3 (the use of K_2CO_3 as the base gave identical results) gives **3.13** in excellent yield (Scheme 3.3). Conversion to hydrazone **3.15** using di-TBDMS protected hydrazine and *in situ* deprotection of the hydrazine is possible[43] but gave irreproducible results in our hands. Therefore, **3.13** was first converted into its thioketone **3.14**, using the same conditions as in Scheme 3.3 and subsequent conversion into hydrazone **3.15** was successful using hydrazine mono hydrate, in quantitative yield for both steps. Oxidation of the hydrazone, using MnO_2, and reaction with thioketone **3.12** yielded episulfide **3.17** in 91% yield (Scheme 3.3). In the original procedure,[43] hydrazone **3.15** was oxidized *in situ* using diacetoxyiodobenzene. This procedure led to irreproducible yields and scaling the reaction above 100 mg (0.170 mmol) of hydrazone was not possible without complete loss of conversion into desired product **3.17**. The new procedure for the synthesis of the episulfide using MnO_2 was successful at 350 mg (0.580 mmol) scale of hydrazone **3.15**, and not attempted at larger scale.

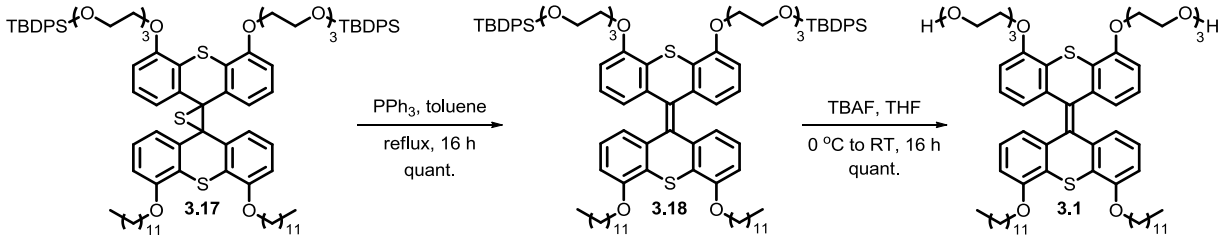

Scheme 3.4. Synthesis of nanotube forming amphiphile **3.1** based on an adapted literature procedure.[43]

Desulfurization of episulfide **3.17** with PPh_3 in toluene was achieved in quantitative yield (Scheme 3.4). We found that changing the solvent from *p*-xylene (original procedure[43]) to toluene, increased the yield considerably. Removal of the TBDPS groups with TBAF, using the literature procedure[43] gave amphiphile **3.1** in quantitative yield. The synthesis of amphiphile **3.2**, the chiral derivative of **3.1**, is described in the PhD thesis of Peter Štacko.[48]

3.4 Self-assembly

For the self-assembly experiments, the compounds (typically 1.0 mg) were weighed on an analytical balance (see Experimental Section) and dissolved in chloroform to give a 1 mg/mL stock solution. The stock solutions were never stored for more than a day and typically used immediately after preparation. Compounds **3.1**, **3.2** and DOPC were then mixed from the chloroform stock solutions in the desired ratio in a 2 mL glass vial and the mixture (typically 200-400 µL total volume) was vortexed for a few min. The mixture was subsequently dried under a low N_2-flow, while rotating the vial and after all chloroform evaporated, the vial was dried further for 1 h under vacuum. The dried thin film was then rehydrated in H_2O to give a suspension (1 mg/mL). The suspension was subjected to five freeze-thaw cycles in liquid nitrogen and a warm water bath (typically 40 °C), respectively, so that a homogeneous turbid solution was formed. During thawing, the samples were vortexed to stimulate homogenization.

For analysis by cryo-transmission electron microscopy (cryo-TEM), the turbid solution (2.5 µL) was placed on a glow-discharged holy carbon coated grid (Quantifoil 3.5/1, QUANTIFOIL Micro Tools GmbH, Großlöbichau, Germany). After blotting at room temperature, the grid was rapidly frozen in liquid ethane (Vitrobot, FEI, Eindhoven, The Netherlands) and stored in liquid nitrogen until observed. Grids were observed in a Gatan model 626 cryo-stage in a Philips CM120 cryo-electron microscope operating at 120 KeV. Images were recorded under low-dose conditions on a slow-scan CCD camera. The samples were used as described above for analysis by widefield fluorescence spectroscopy. For UV-vis and CD spectroscopy measurements, the samples were diluted after treated as described in the text (e.g. after irradiation of the concentrated sample).

Results

With enantiopure **3.2** in hand, aggregation was first confirmed by cryo-TEM measurements. Pure **3.2** did not give any aggregation in the absence of DOPC. However, starting from a 1:1 mixture of **3.2** and DOPC, the formation of nanotubes was observed (Figure 3.6c-d). Henceforth, assembly experiments were always conducted with DOPC in a ratio of 1:1 to the total amphiphile concentration. The nanotubes of **3.2** resemble the structures formed by amphiphile **3.1** (Figure 3.6a-b).

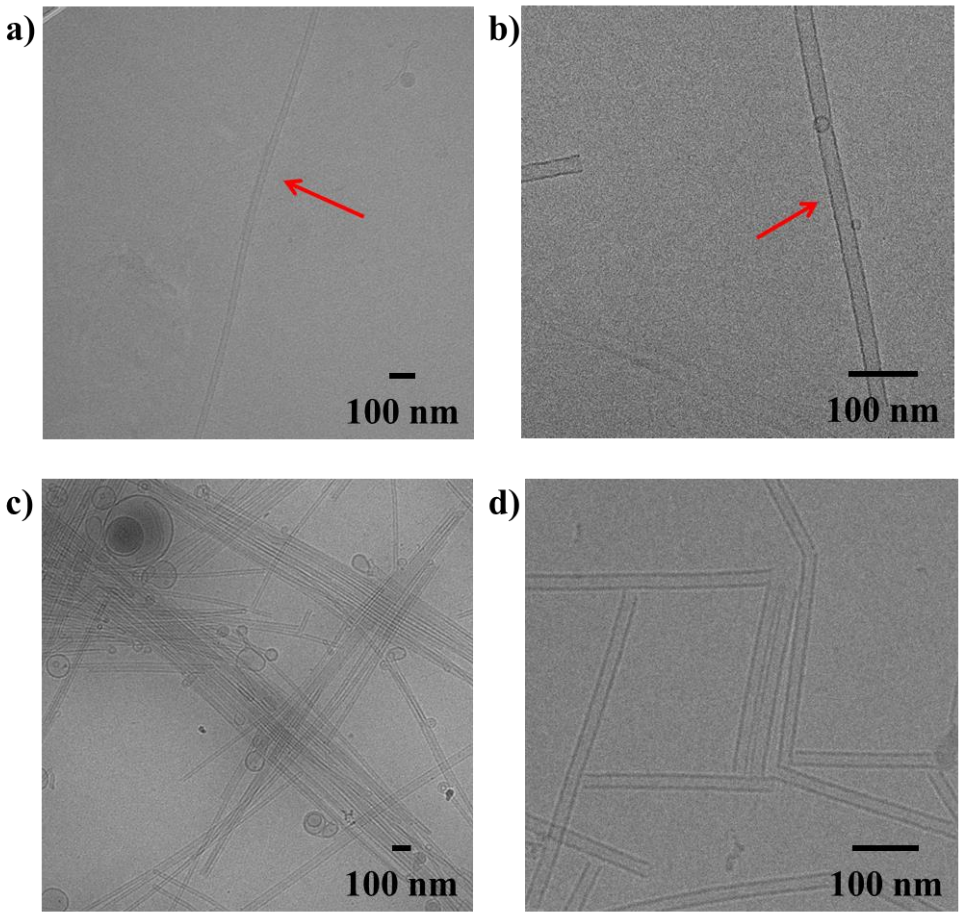

Figure 3.6. Cryo-TEM microscopy images of self-assembled nanotubes in water at a total concentration of 1 mg/mL. a-b) Images of nanotubes of achiral **3.1** with DOPC (1:1). Red arrows indicate a typical nanotube. c-d) Images of nanotubes of chiral **3.2** with DOPC (1:1).

The bilayers, making up the nanotube wall were found to be 3 nm thick for both tubes of pure achiral **3.1** and chiral **3.2** and differences could not be observed by cryo-TEM. No other types of aggregates were found for either **3.1** or **3.2**. Furthermore, the nanotubes are generally very straight and virtually no bends or turns were observed in nanotubes of **3.1**. Although we observed that for nanotubes of **3.2**, a higher amount of bent tubes were formed, compared to tubes of **3.1**, nanotubes of **3.2** were overall straight and uniform. A distinct difference between nanotubes of pure achiral **3.1** and chiral **3.2** is that nanotubes of **3.1** (Figure 3.6a-b; red arrows indicate the nanotube) are typically longer than a micrometer, while tubes of **3.2** (Figure 3.6c-d) are shorter and typically only ~300 nm long. In addition, we found that tubes of **3.2** tend to pack together more than those of **3.1** at the same concentration, as observed by cryo-TEM. Figure 3.6c for example, shows a type of network in which several nanotubes align and pack together and these "bundles" cross another bundle. Nanotubes of achiral **3.1** are typically more isolated and we found no evidence that they align with one another to a significant extent. While the reduced length of the nanotubes of **3.2** may be explained by a difference in packing, due to the presence of the two methyl moieties in the interacting hydrophobic tails (increase in hydrophobic volume), we do not currently know why the shorter tubes tend to bundle together. Nanotubes of both **3.1** and **3.2** that are capped with DOPC vesicles were found and the tubes are not different in this regard. After confirming that both enantiopure amphiphile **3.2** and achiral

amphiphile **3.1** form nanotubes, we set out to perform sergeant-soldier experiments by mixing varying ratios of **3.1** and **3.2**.

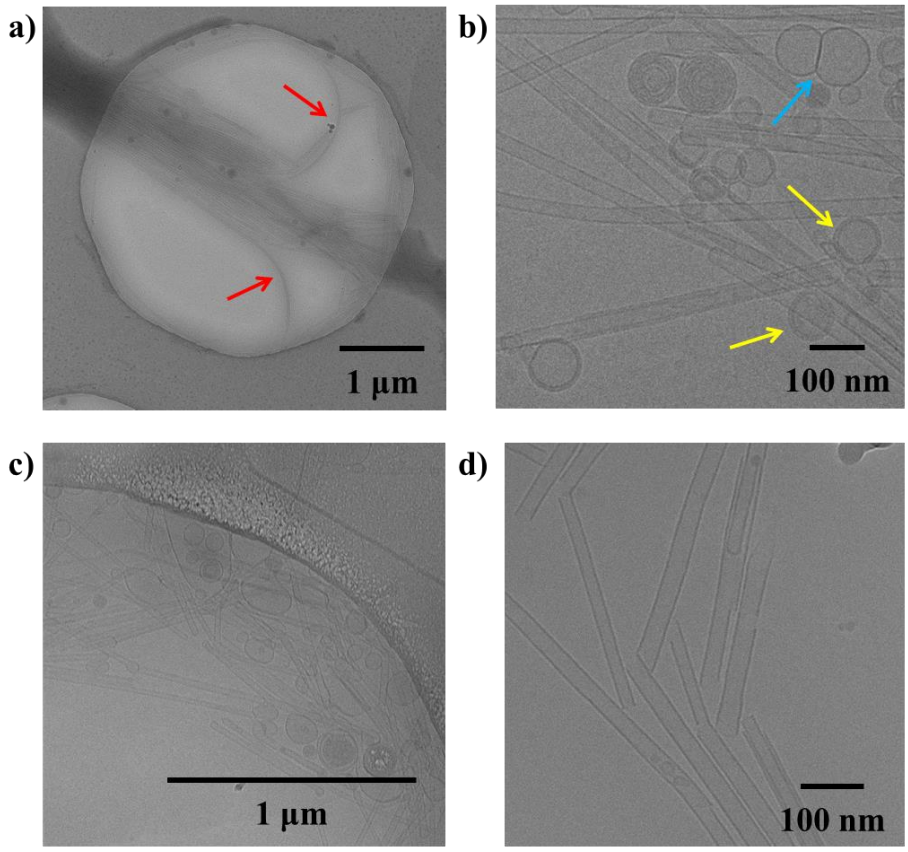

Figure 3.7. Cryo-TEM microscopy images of mixed nanotubes in water at a total concentration of 1 mg/mL. a-b) Images of nanotubes of **3.1** and **3.2** with DOPC (0.6:0.4:1). Red arrows indicate nanotubes bending away from the "bundle". Yellow arrows indicate vesicular aggregates. Blue arrow indicates DOPC vesicles. c-d) Images of nanotubes of **3.1** and **3.2** with DOPC (0.4:0.6:1).

In the mixed nanotubes (Figure 3.7), nanotube formation was not inhibited at any ratio of **3.1**:**3.2**. Increasing the fraction of **3.2** over 50% resulted in tubes that are shorter than nanotubes of pure **3.1**, typically ~300 nm in length, and more bundled, like the tubes of pure **3.2** (Figure 3.6c). Another observation is that the mixed tubes bend more as can be seen in Figure 3.7a (nanotubes are bending away from the "bundle" as indicated with red arrows) and that other (although to a small extent), vesicular aggregates are formed (Figure 3.7b; vesicles of DOPC with a bilayer thickness of 4 nm can be observed as indicated with the blue arrow, but also vesicles with a thicker bilayer of 7-8 nm as indicated with yellow arrows). After confirming that nanotubes could be formed at different ratios of **3.1** and **3.2**, we studied the spectroscopic properties.

3.5 Spectroscopy

The absorption properties of the different nanotubes were studied using UV-vis spectroscopy (Figure 3.8).

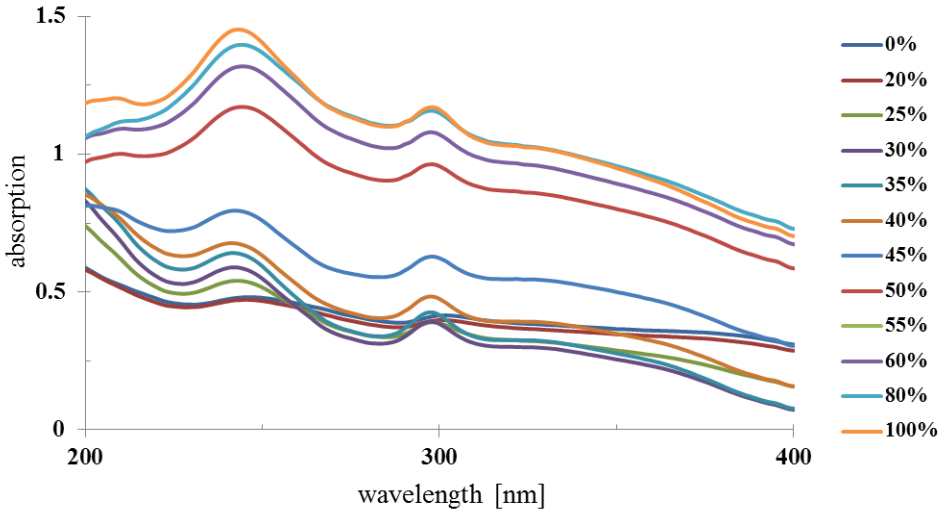

Figure 3.8. UV-vis absorption spectra of nanotubes in water, having different ratios of **3.1** and **3.2**, expressed as a percentage of **3.2**. The concentration of all samples is $1.6 \cdot 10^{-4}$ M and the total amphiphile to DOPC ratio is 1:1.

Larger aggregates scatter more light and consequently, the baseline in absorption spectra increases.[52] Self-assembled samples of pure **3.2** showed more scattering than those of pure **3.1** (Figure 3.9a), indicating the formation of the relatively large bundles of nanotubes, consistent with the observations by cryo-TEM. Mixed nanotubes that are composed of >50% achiral amphiphile **3.1**, show similar absorption spectra as pure **3.1**. Plotting the absorption (λ = 303 nm) as a function of the fraction of chiral amphiphile **3.2** in the mixed nanotubes, reveals a significant increase in scattering when the fraction of **3.2** exceeds 40% and with an undulation point at 47% (calculated by fitting a sigmoidal curve in Origin software; Figure 3.9b).

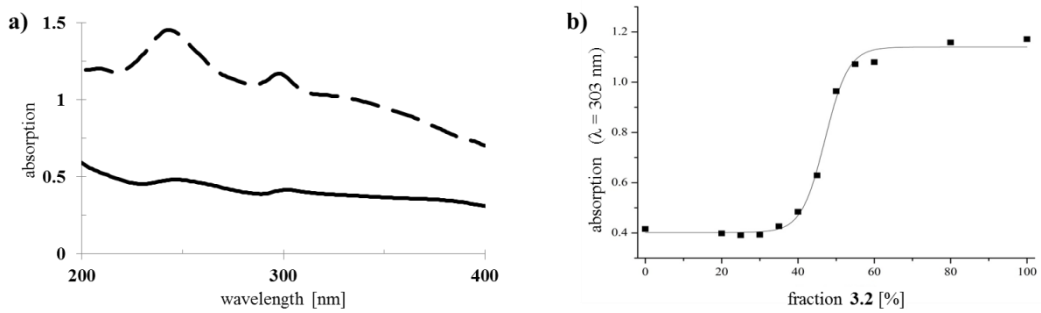

Figure 3.9. UV-vis absorption spectra of nanotubes of pure **3.1** and **3.2**. a) UV-vis absorption spectra of assemblies of **3.1** (solid line, $1.6 \cdot 10^{-4}$ M in water) and **3.2** (dashed line, $1.6 \cdot 10^{-4}$ M in water). b) Absorption at λ = 303 nm as a function of the fraction of **3.2** (data was fitted to sigmoidal line using Origin software).

When the nanotubes consist of >40% chiral amphiphile **3.2**, the absorption increases drastically, compared to tubes in which **3.1** is the major component (<50% **3.2**). Interestingly, the absorption remains nearly unchanged when increasing the fraction of **3.2** from 50% to 100%, and this leads us to propose that a homogeneous population of bundled, shorter

nanotubes is formed when **3.2** is the major component, while the formation of longer, isolated nanotubes is favored when the tubes are mainly made of **3.1**. This is in agreement with the finding of more bundled, shorter nanotubes for the same samples, as observed by cryo-TEM (Figures 3.6 and 3.7).

3.6 Induction of chirality

We next set out to probe the induction of chirality based on the sergeant-soldier principle as described earlier (Paragraph 3.4 of this chapter).[39–42] We found that a solution of **3.2** in $CHCl_3$ is CD silent (Figure 3.10), likely because the chromophore is too far away from, or not influenced by, the presence of the stereogenic centers. This offers good prospects for the concept of reading and erasing chiral information[33,53] if the nanotubes are not CD silent due to the nature of the photoactive amphiphile. On the other hand, CD spectroscopy shows that nanotubes of chiral amphiphile **3.2**, exhibit Cotton effects with negative maxima at λ = 303, 256 and 225 nm and a positive maximum at λ = 208 nm (Figure 3.10).

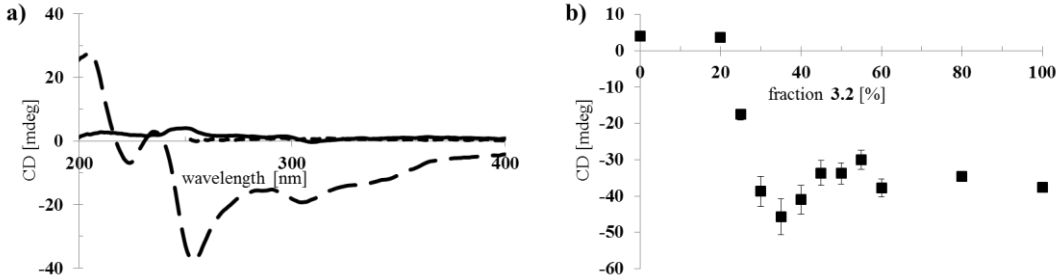

Figure 3.10. Circular dichroism spectra of nanotubes of **3.1** and **3.2**. a) Nanotubes of **3.1** (solid line, $1.6 \cdot 10^{-4}$ M in water) and **3.2** (dashed line, $1.6 \cdot 10^{-4}$ M in water) and a solution of **3.2** (dotted line, $2.5 \cdot 10^{-5}$ M in $CHCl_3$; cutoff for $CHCl_3$ is λ = 260 nm). b) CD maximum at λ = 303 nm as a function of the fraction **3.2**. Measurements were performed in triplo and error bars are shown.

We next performed the sergeant-soldier experiments and investigated if a small fraction of chiral **3.2** is able to induce chirality into the otherwise achiral nanotubes of **3.1**. To our delight, we found that mixed nanotubes that mainly consist of achiral **3.1** are chiral, due to the presence of **3.2** (Figure 3.10). On the other hand, nanotubes with less than 25% of **3.2**, do not show any CD signal. When the CD maximum (λ = 303 nm) is plotted as a function of the fraction of chiral component (Figure 3.10b), a similar relation is found as for the absorption (Figure 3.9) and nanotubes in which **3.2** is the major component (>50%) show an approximately constant CD value, independent of the ratio of **3.1** to **3.2**. In contrast to the absorption, which shows a sigmoidal relation with a sharp increase at 40% of **3.2** however, the CD signal increases when the fraction of chiral compound **3.2** exceeds 25% and reaches a maximum at 35%, after which it decreases and reaches a constant value. Above a fraction of 50% of **3.2**, the nanotubes appear to be homogeneous and no differences could be observed for tubes that consist of 50–100% of **3.2** (Figure 3.10b).

Cryo-TEM showed that the mixed nanotubes are micrometers long until **3.2** becomes the major component (>50%) and we hypothesize that mixtures of the amphiphiles, containing less than 50% **3.2**, leads to the formation of long, chiral nanotubes, which leads to a sharp increase in CD signal after exceeding a threshold of 20% **3.2** (Figure 3.10b). In the long nanotubes, the

CD signal is more pronounced than in the short nanotubes. Apparently, the long nanotubes have a higher preference for the absorption of light of one handedness over the other, compared to the shorter nanotubes, which leads to a maximum value for the CD signal at 35% **3.2**. Above this ratio, an increase in absorption is observed, signifying the appearance of shorter, bundled tubes and a consequent decrease in CD as in the short nanotubes, the chirality is less pronounced. When **3.2** is the major component (>50%) in the mixed tubes, both the UV-vis (Figure 3.9) and CD spectra (Figure 3.10) become approximately constant, indicating that further increasing the fraction of chiral component **3.2** in the mixed nanotubes does not lead to different self-assembled structures.

3.7 Disassembly

The core of amphiphiles **3.1** and **3.2** is photoresponsive and we were interested to see if nanotubes of **3.1**, **3.2** and mixtures of these compounds can be disassembled by light, given the formation of either long or short, more bundled nanotubes, depending on their composition (*vide supra*). In addition, as nanotubes of **3.2** and mixed nanotubes of **3.1** and **3.2**, where the fraction of **3.2** is higher than 25%, show a significant CD signal, and light-triggered disassembly of the chiral nanotubes would provide a way to erase the chiral information and this could be interesting for the development of memory devices.[54] We followed the disassembly of the different nanotubes in real time, using widefield fluorescence microscopy (Figure 3.11).

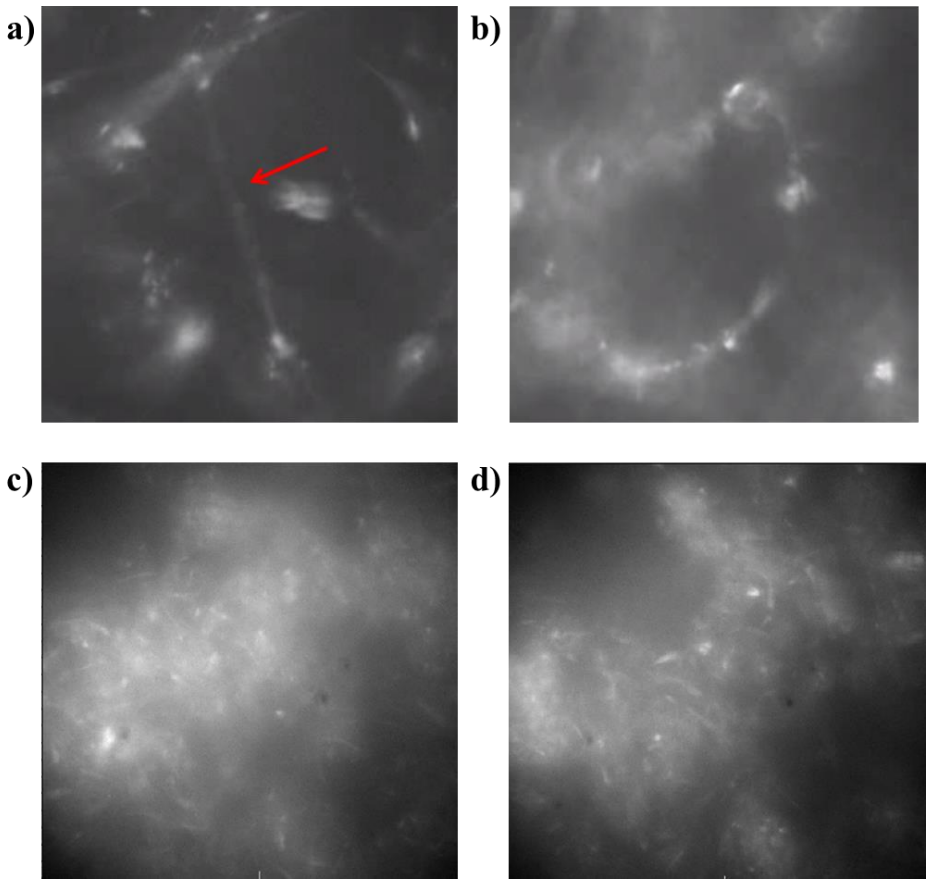

Figure 3.11. Widefield fluorescence microscopy images of self-assembled nanotubes in water at a total concentration of 1 mg/mL. a) Image of **3.1** with DOPC (1:1) before and b) after irradiation (t = 53 s, λ = 390 nm). c) Image of **3.2** with DOPC (1:1) before and d) after irradiation (t = 53 s, λ = 390 nm).

As shown in paragraph 3.1 of this chapter, irradiation of the nanotubes of **3.1** leads to photochemical ring-closure of the amphiphile and consequent disassembly of the nanotubes.[43,45] To our delight, upon irradiation, both long tubes of pure **3.1** (Figure 3.11a-b), short, clustered tubes of **3.2** (Figure 3.11c-d) and mixtures thereof (data not shown), disassemble and large, less defined aggregates are formed. For the short, bundled nanotubes, networks were observed and changes in morphology upon irradiation are therefore less clear, although reproducible and well-pronounced. This finding shows that by changing the chiral content of the nanotubes, the morphology changes, without affecting the photoresponsiveness of the tubular assemblies. Subsequently, the loss of CD signal upon low intensity UV irradiation was followed in time for mixed nanotube (**3.1** + **3.2**) samples consisting of 35% **3.2** (long chiral nanotubes) and 55% **3.2** (short chiral nanotubes) and is shown in Figure 3.12.

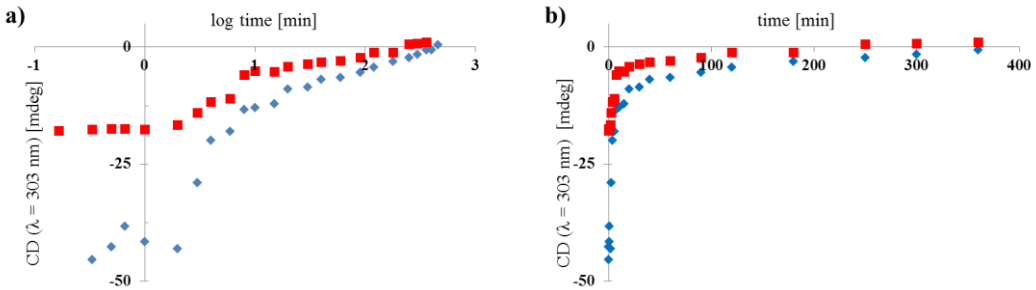

Figure 3.12. Low intensity UV irradiation (λ = 265 nm, 8W) of long chiral nanotubes consisting of 35% **3.2** (blue diamonds, $1.6 \cdot 10^{-4}$ M in water) and short chiral nanotubes consisting of 55% **3.2** (red squares, $1.6 \cdot 10^{-4}$ M in water), followed in time by CD spectroscopy (λ = 303 nm). The time is plotted on a) logarithmic scale and on b) linear scale.

Both long and short chiral nanotubes show a lag period for disassembly under the given conditions of 2 min. We hypothesize that upon initial irradiation, very little molecules are cyclized and disassembly of the nanotubes initiates after a certain threshold is reached. After the lag period, initial disassembly is relatively fast and slows down in time. After approximately 6–8 h, the samples are CD silent, the chiral information in the system erased due to disassembly of the tubes.

3.8 Conclusions

In summary, we present herein the design, synthesis and study of nanotubular objects in which chirality can be used as a means to control the morphology of self-assembled structures. To the best of our knowledge, this comprises the first example of such objects where the point chirality (stereogenic center) is present in the hydrophobic part of the amphiphiles, much like in natural membranes.

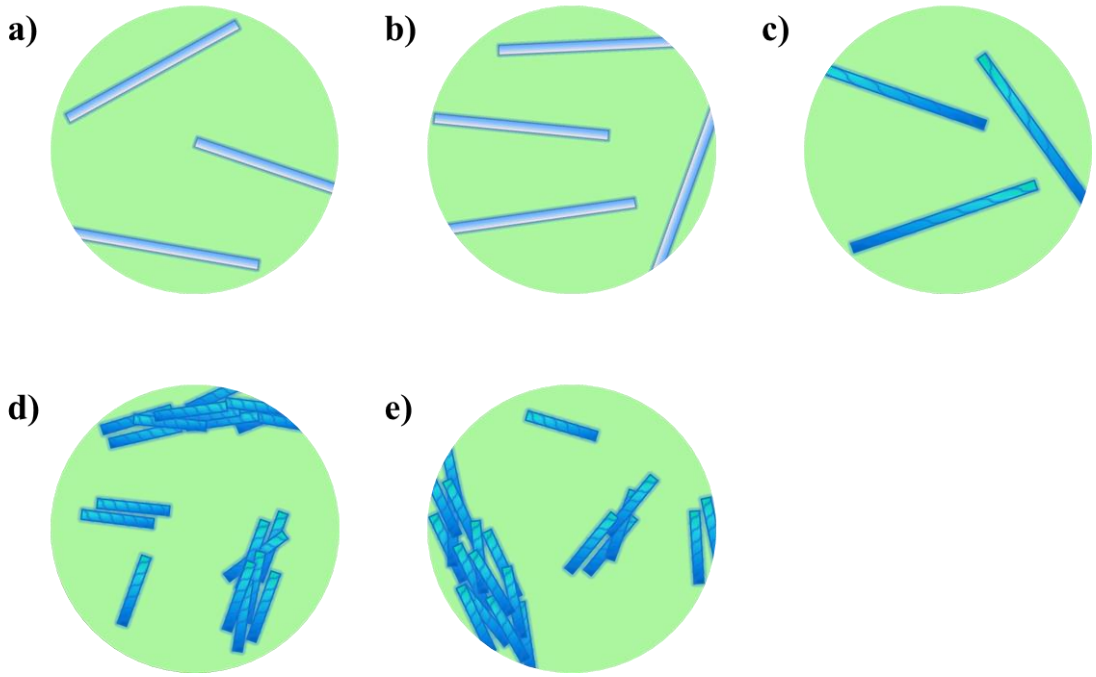

Figure 3.13. Schematic model for the observed behavior of nanotubes consisting of achiral **3.1** and chiral **3.2** (with DOPC in a ratio of 1:1 amphiphile:DOPC) as a function of the amount of **3.2**. a) pure **3.1**; long, isolated achiral nanotubes. b) <25% **3.2**; long, isolated achiral nanotubes. c) 25–50% **3.2**; long, isolated chiral nanotubes. d) >50% **3.2**; short, bundled chiral nanotubes. e) pure **3.2**; short, bundled chiral nanotubes.

Figure 3.13 shows a schematic model for the observed behavior and properties of nanotubes consisting of achiral **3.1** and chiral **3.2** (with DOPC in a ratio of 1:1 amphiphile:DOPC) as a function of the amount of **3.2**. Both achiral amphiphile **3.1** and its chiral analogue **3.2**, were found to form straight, photoresponsive nanotubes. While the tubes of **3.1** are typically micrometers long and isolated (Figure 3.13a), nanotubes of **3.2** are much shorter (~300 nm) and tend to align or pack together into "bundles" (Figure 3.13e). The molecular structure of the chiral amphiphile differs from the achiral amphiphile only by the presence of two methyl groups at stereogenic centers in the hydrophobic part of the amphiphile. For the mixed nanotubes, at low fractions of the chiral amphiphile (<50% **3.2**; Figure 3.13a-c), micrometer long distinct nanotubes were formed, similar to the nanotubes formed from pure achiral amphiphile **3.1**. When the fraction of chiral component **3.2** (which is CD silent in solution) is increased in the co-assembly, above a critical threshold (>25% **3.2**; Figure 3.13c-e), the tubes become chiral as was observed from CD measurements. Increasing the chiral fraction further (>50% **3.2**) or self-assembly of pure chiral amphiphile, results in the formation of shorter, bundled nanotubes (Figure 3.13d-e). We hypothesize that the hydrophobic volume of the chiral amphiphile **3.2** is increased, compared to that of the achiral amphiphile **3.1**, due to the two methyl moieties in C2 of the hydrophobic tails. The increase in hydrophobic volume distorts the packing of amphiphile

3.2, similar to the HBC amphiphiles reported by the group of Aida (Figure 3.1).[25] Remarkably, unlike in the system of Aida and coworkers, the formation of nanotubes is not inhibited by the presence of the methyl moieties in the hydrophobic chains and rather causes the formation of shorter nanotubes.

The chiral information can be erased by irradiation with light. This photo-induced disassembly process was followed in real time, using widefield fluorescence microscopy, showing the transition from nanotubes to less defined, larger aggregates.

It would be interesting to study the origin of the lag period in the irradiation experiment (Figure 3.12) as this may give valuable information and insight into the disassembly process of the nanotubes. Although the disassembly of the nanotubes is highly interesting, the underlying photochemical ring-closing reaction of the amphiphiles is irreversible. It would be highly desirable to have full control over the formation and deformation of the nanotubes by applying an external stimulus. In chapter 6 we describe amphiphiles that are based on molecular motors and show how they are able to undergo reversible changes in morphology upon irradiation with light. We also designed and synthesized amphiphiles that are analogous to the nanotube amphiphiles described in this chapter, bearing either quaternary ammonium groups or carboxylic acid groups as the hydrophilic moiety. This work will be described in the thesis of Peter Štacko.[48] The carboxylic acid derivative may be particularly interesting as it can in principle be deprotonated (once or twice) and protonated and this might cause triggerable aggregation and deaggregation, respectively.

3.9 Experimental section

General remarks

Starting materials and reagents were commercially available and used as obtained from Sigma-Aldrich or Acros without further purification. All solvents used for spectroscopic measurements, chromatography and the sergeant-soldier experiments were of analytical grade and degassed prior to use. Melting points were determined on a Büchi melting point B-545 apparatus. ^{1}H-NMR spectra were recorded on a Varian VXR-300 spectrometer (at 300 MHz) or a Varian MR400 (at 400 MHz) at ambient temperature. The splitting patterns are designated as follows: s (singlet); d (doublet); dd (double doublet); t (triplet); q (quartet); m (multiplet) and br (broad). ^{13}C-NMR spectra were recorded on a Varian VXR-300 spectrometer (at 75.4 MHz) or a Varian MR400 (100.6 MHz) at ambient temperature. Chemical shifts are denoted in δ (ppm), referenced to the residual protic solvent peak. Coupling constants *J*, are denoted in Hz. Masses were recorded with a Thermo scientific LTQ Orbitrap XL mass spectrometer. Silicycle Silicaflash P60, 40-63 m, (230–400 mesh) was used for column chromatography. Thin-layer chromatography (TLC) was performed on commercial Kieselgel 60F, 254 silica gel plates and compounds were visualized with UV light (λ = 254 nm) or $KMnO_4$ stain. Low intensity irradiations were performed with Spectroline ENB-280C/FE UV lamp. CD spectra were recorded on a JASCO J-715 spectropolarimeter and UV-vis measurements were performed on a Agilent 8453 UV-vis spectrophotometer. Weighing of small quantities was performed on a Mettler MT5 analytical microbalance. Wide field images were obtained using 60x oil immersion objective a Nikkon Ecllipse-Ti with an ANDOR EMCCD-Ixon-DU888 camera and an Andor laser combiner and AOTF unit for illumination at 488 nm.

Synthesis

***N*,*N*-Diethyl-3-methoxybenzamide (3.4)**

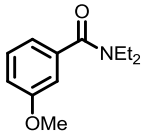

3-Methoxybenzoic acid (15.0 g, 98.6 mmol, 1.0 equiv) was dissolved in CH_2Cl_2 (100 mL) and $SOCl_2$ (27.3 mL, 237 mmol, 2.4 equiv) was slowly added. The mixture was heated to reflux for 1 h. After cooling down, the mixture was concentrated in vacuo and subsequently redissolved in CH_2Cl_2 (100 mL). The solution was slowly added to an ice bath cooled solution of Et_2NH (40.6 mL, 394 mmol, 4.0 equiv) in CH_2Cl_2 (100 mL) and stirred until all acid chloride had reacted (approximately 2 h). The mixture was then extracted with an 1 M aq. HCl solution (2 x 100 mL) and subsequently with saturated aq. $NaHCO_3$ (2 x 100 mL). Evaporation of the solvent under reduced pressure gave **3.4** as a yellow oil (20.0 g, 96.6 mmol, 98%). ^{1}H NMR (300 MHz, $CDCl_3$) δ = 7.34 (d, *J* = 8.8 Hz, 1H), 6.96 – 7.00 (m, 3H), 3.87 (s, 3H), 3.85 (br s, 2H), 3.59 (br s, 2H), 1.29 (br s, 3H), 1.17 (br s, 3H) ppm; ^{13}C NMR (75.4 MHz, $CDCl_3$) δ = 170.5, 159.1, 138.1, 129.1, 117.9, 114.5, 111.3, 54.8, 42.9, 38.8, 13.9, 12.5 ppm; HRMS-EI *m*/*z* calculated for $C_{12}H_{17}NO_2$ $[M]^+$ 207.1259, found 207.1257.

1,2-Bis(2-methoxyphenyl)disulfane (3.6)

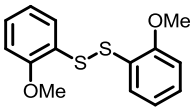

2-Methoxybenzenethiol (15.7 mL, 127 mmol, 1.0 equiv) was dissolved in CH_2Cl_2 (300 mL) and $KMnO_4$ (45.3 g, 286 mmol, 2.3 equiv) and $CuSO_4 \cdot 5\ H_2O$ (44.5 g, 178 mmol, 1.4 equiv) were added. The suspension was stirred at RT for 3 h. The mixture was filtered over celite and the cake washed with CH_2Cl_2 (100 mL). The filtrate was concentrated under vacuo and an off-white solid was obtained. After washing the solid with minimal amounts of CH_2Cl_2, disulfide **3.6** was obtained as a white solid (31.8 g, 114 mmol, 90%). m.p. 119.0 – 120.5 °C; ^{1}H NMR (300 MHz, $CDCl_3$) δ = 7.54 (dd, *J* = 7.7, 1.5 Hz, 1H), 7.16 – 7.22 (m, 1H), 6.88 – 6.94 (m, 1H), 6.85 (d, *J* = 8.1 Hz, 1H), 3.90 (s, 3H) ppm; ^{13}C NMR (75.4 MHz, $CDCl_3$) δ = 156.4, 137.6, 127.3, 124.2, 121.1, 110.3, 55.6 ppm; HRMS-EI *m*/*z* calculated for $C_{14}H_{14}O_2S_2$ $[M]^+$ 278.0435, found 278.0440.

***N*,*N*-Diethyl-3-methoxy-2-(2-methoxyphenylthio)benzamide (3.7)**

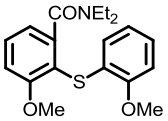

Dry THF (200 mL) was cooled to -80 °C under a nitrogen atmosphere. *s*-BuLi (18.5 mL, 21.2 mmol, 1.1 equiv) and TMEDA (3.2 mL, 21.2 mmol, 1.1 equiv) were subsequently added and the mixture stirred at -80 °C for 30 min. A solution of **3.4** (4.00 g, 19.3 mmol, 1.0 equiv) in dry THF (15 mL) was slowly added (5 min) and the mixture was stirred at -80 °C for 1 h. Compound **3.6** (6.5 g, 23.2 mmol, 1.2 equiv) was slowly added as a solid and the mixture was allowed to slowly warm to RT overnight. The mixture was diluted with Et_2O (200 mL) ,washed with 1 M aq. NaOH (200 mL) and concentrated in vacuo. The crude yellow solid was washed with a minimal amount of a mixture of *n*-pentane:EtOAc:CH_2Cl_2, 6:3:1 and the remaining off-white solid was purified by flash column chromatography (dry load, SiO_2, *n*-pentane:EtOAc:CH_2Cl_2, 6:3:1) to yield **3.7** as a white solid (5.30 g, 15.4 mmol, 80%). m.p. 140.9 – 142.6 °C; ^{1}H NMR (300 MHz, $CDCl_3$) δ = 7.41 – 7.46 (m, 1H), 7.02 – 7.07 (m, 1H), 6.93 – 6.95 (m, 2H), 6.80 (d, *J* = 8.4 Hz, 1H), 6.67 – 6.76 (m, 2H), 3.87 (s, 3H), 3.75 (s, 3H), 3.63 – 3.78 (m, 1H), 3.31 – 3.38 (m, 1H), 2.96 – 3.15 (m, 2H), 1.19 (t, *J* = 7.1 Hz, 3H), 0.98 (t, *J* = 7.1 Hz, 3H) ppm; ^{13}C NMR (75.4 MHz, $CDCl_3$) δ = 168.4, 160.3, 155.3, 144.8, 130.9, 126.5, 125.5, 125.1, 120.6, 118.3, 115.6, 111.0, 109.9, 55.8, 55.4, 42.4, 38.2, 13.6, 12.1 ppm; HRMS-EI *m*/*z* calculated for $C_{19}H_{23}NO_3S$ $[M]^+$ 345.1399, found 345.1390; elemental analysis calculated (%) for $C_{19}H_{23}NO_3S$: C, 66.10; H, 6.71; N, 4.05; S, 9.28; found (%): C, 66.00; H, 6.78; N, 4.04; S, 9.42.

4,5-Dimethoxy-9*H*-thioxanthen-9-one (3.8)

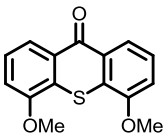

Compound **3.7** (15.0 g, 43.4 mmol, 1.0 equiv) was dissolved in dry THF (200 mL) under a nitrogen atmosphere and the solution added dropwise to a freshly prepared LDA solution (434 mL, 0.5 M, 5.0 equiv) cooled with an ice bath. The ice bath was removed and the mixture stirred at RT for 1 h. An 1 M aq. NH_4Cl solution (250 mL) was slowly added and the layers

separated. The water layer was extracted with CH_2Cl_2 (2 x 200 mL) and the combined organic phase dried over Na_2SO_4 and concentrated in vacuo. The crude solid was purified by flash column chromatography (dry load, SiO_2, *n*-pentane:EtOAc, 2:1) to yield **3.8** as a yellow cotton-like solid (11.8 g, 43.4 mmol, quant.). m.p. 250 – 255 °C (dec); ^{1}H NMR (300 MHz, $CDCl_3$) δ = 8.25 (dd, *J* = 8.2, 0.9 Hz, 2H), 7.42 – 7.47 (m, 2H), 7.14 (d, *J* = 7.7 Hz, 2H), 4.05 (s, 6H) ppm; ^{13}C NMR (75.4 MHz, $CDCl_3$) δ = 180.2, 154.8, 129.9, 127.6, 125.9, 121.4, 112.1, 56.4 ppm; HRMS-EI *m/z* calculated for $C_{15}H_{12}O_3S$ $[M]^+$ 272.0507, found 272.0506; elemental analysis calculated (%) for $C_{15}H_{12}O_3S$: C, 66.20; H, 4.44; S, 12.44; found (%): C, 66.30; H, 4.41; S, 11.77.***Note*****:** LDA was prepared by adding *n*-BuLi (8.40 mL, 13.5 mmol, 5.0 equiv) to a solution of *i*-Pr_2NH (1.90 mL, 13.5 mmol, 5.0 equiv) in dry THF (65 mL) at -80 °C under a nitrogen atmosphere. The solution was allowed to warm to RT and stirred for 1 h.

4,5-Dihydroxy-9*H*-thioxanthen-9-one (3.9)

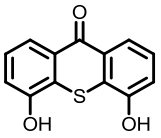

Compound **3.8** (2.0 g, 7.3 mmol, 1.0 equiv) was dissolved in dry CH_2Cl_2 (200 mL) under a nitrogen atmosphere and a 1 M boron tribromide solution (in CH_2Cl_2, 37 mL, 37 mmol, 5.0 equiv) was added dropwise at 0 °C. The mixture was allowed to warm to RT overnight. After cooling the mixture with an ice bath, water (150 mL) was slowly added and the layers separated. The organic layer was extracted with an 3 M aq. NaOH solution (3 x 150 mL). The waterlayer was subsequently acidified to pH = 1 with an 2 M aq. HCl solution and filtered through a glass filter. The residual cake was redissolved in acetone and concentrated in vacuo to yield **3.9** as a green solid (1.8 g, 7.3 mmol, quant.). m.p. 250 – 255 °C (dec); ^{1}H NMR (300 MHz, DMSO): δ = 10.98 (s, 2H, OH); 7.94 (d, *J* = 7.7 Hz, 2H); 7.38 (dd, *J* = 7.7, 7.7 Hz, 2H); 7.20 (d, *J* =7.7 Hz, 2H) ppm; ^{13}C NMR (50 MHz, DMSO): δ = 180.0, 153.7, 130.0, 127.0, 126.0, 119.9, 117.2 ppm; HRMS-APCI+ *m/z* calculated for $C_{13}H_9O_3S$ $[M + H]^+$ 245.0267, found 245.0259.

4,5-Bis(2-(2-(2-hydroxyethoxy)ethoxy)ethoxy)-9*H*-thioxanthen-9-one (3.10)

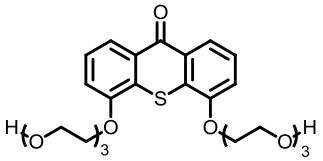

Compound **3.9** (5.80 g, 23.7 mmol, 1.0 equiv) was dissolved in DMF (150 mL). Cs_2CO_3 (16.5 g, 119 mmol, 5.0 equiv) and $TsO(CH_2CH_2O)_3H$ (14.1 g, 49.9 mmol, 2.0 equiv) were added and the mixture heated at 110 °C for 16 h. After cooling to room temperature, the reaction mixture was filtered over celite and the celite cake washed with CH_2Cl_2. The solvents were removed by rotary evaporation and the residue purified by flash column chromatography (SiO_2, 5% MeOH in CH_2Cl_2) to yield **3.10** as a yellow solid (10.3 g, 20.1 mmol, 85%). m.p. 36 °C; ^{1}H NMR (400 MHz, $CDCl_3$): δ = 8.18 (dd, *J* = 8.2, 1.1 Hz, 2H), 7.36 (td, *J* = 8.1, 1.0 Hz, 2H), 7.10 (d, *J* = 8.0 Hz, 2H), 4.34 – 4.26 (t, *J* = 5.1 Hz, 4H), 3.95 (t, *J* = 5.1 Hz, 4H), 3.84 – 3.75 (m, 4H), 3.72 – 3.65 (m, 8H), 3.63 – 3.52 (m, 4H), 3.14 (s, 2H) ppm; ^{13}C NMR (100.6 MHz, $CDCl_3$): δ = 180.0, 153.9, 129.8, 127.9, 125.8, 121.6, 113.4, 72.6, 72.5, 71.0, 70.3, 70.1, 69.3, 69.1, 61.5 ppm; HRMS-APCI+ *m/z* calculated for $C_{25}H_{33}O_9S$ $[M + H]^+$ 509.1839, found 509.1818.

4,5-Bis(2,2-dimethyl-3,3-diphenyl-4,7,10-trioxa-3-siladodecan-12-yloxy)-9*H*-thioxanthen-9-one (3.11)

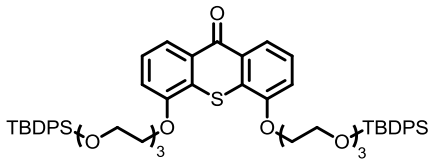

Compound **3.10** (7.60 g, 15.0 mmol, 1.0 equiv) was dissolved in CH_2Cl_2 (200 mL) and imidazole (3.40 g, 50.0 mmol, 3.3 equiv) was added at 0 °C. After 10 min, TBDPSCl (10.3 g, 37.4 mmol, 2.5 equiv) was added dropwise and after addition the icebath was removed. The reaction mixture was stirred at RT for 1 h. The reaction mixture was filtered over celite and the solvent was removed by rotary evaporation. Compound **3.11** was obtained after flash column chromatography (SiO_2, *n*-pentane:EtOAc, 7:3) as a yellow, viscous oil (11.2 g, 11.3 mmol, 75%). ^{1}H NMR (300 MHz, $CDCl_3$): δ = 8.23 (d, *J* = 8.0 Hz, 2H), 7.76 – 7.62 (m, 10H), 7.43 – 7.29 (m, 10H), 7.13 (d, *J* = 7.9 Hz, 2H), 4.30 (t, *J* = 4.9 Hz, 4H), 3.95 (t, *J* = 4.9 Hz, 4H), 3.86 – 3.57 (m, 16H), 1.03 (s, 18H) ppm; ^{13}C NMR (75.4 MHz, $CDCl_3$): δ = 180.4, 154.4, 135.8, 133.9, 130.2, 129.9, 128.4, 127.9, 126.1, 121.9, 113.9, 72.7, 71.4, 71.1, 69.8, 69.5, 63.7, 27.1, 19.4 ppm; HRMS-ESI- *m/z* calculated for $C_{57}H_{68}O_9SSi_2Cl$ $[M + Cl]^-$ 1019.3805, found 1019.3780.

4,5-Bis(2,2-dimethyl-3,3-diphenyl-4,7,10-trioxa-3-siladodecan-12-yloxy)-9*H*-thioxanthene-9-thione (3.12)

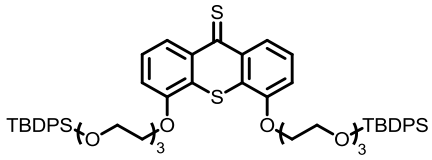

Compound **3.11** (4.0 g, 4.0 mmol, 1.0 equiv) was dissolved in dry toluene (100 mL) and Lawesson's reagent (5.0 g, 12 mmol, 3.0 equiv) was added. The reaction mixture was heated at reflux for 30 min. The solvent was removed by rotary evaporation and the crude material was purified by flash column chromatography (SiO_2, EtOAc:*n*-pentane, 2:1) to yield **3.12** as a viscous green oil (4.0 g, 4.0 mmol, quant.); ^{1}H NMR (400 MHz, $CDCl_3$): δ = 8.67 (d, *J* = 8.4 Hz, 2H), 7.70 – 7.66 (m, 10H), 7.42 – 7.31 (m, 14H), 7.14 (d, *J* = 7.9 Hz, 2H), 4.33 (t, *J* = 5.0 Hz, 4H), 3.97 (t, *J* = 5.0 Hz, 4H), 3.82 (t, *J* = 5.3 Hz, 4H), 3.77 – 3.73 (m, 4H), 3.72 – 3.65 (m, 4H), 3.62 (t, *J* = 5.3 Hz, 4H), 1.04 (s, 18H) ppm; ^{13}C NMR (100.6 MHz, $CDCl_3$) δ = 210.7, 154.2, 138.3, 135.6, 133.6, 129.6, 127.6, 126.3, 125.6, 112.8, 72.5, 71.2, 70.9, 69.5, 69.4, 63.4, 26.8, 19.2 ppm; HRMS-APCI+ *m/z* calculated for $C_{57}H_{69}O_8S_2Si_2$ $[M + H]^+$ 1001.3967, found 1001.3911.

4,5-Bis(dodecyloxy)-9*H*-thioxanthen-9-one (3.13)

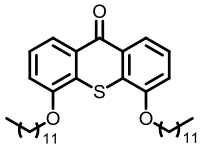

Compound **3.9** (0.50 mg, 2.0 mmol, 1.0 equiv) was dissolved in dry DMF (50 mL). Cs_2CO_3 (3.3 g, 10 mmol, 5.0 equiv) and dodecyl bromide (1.3 mL, 5.3 mmol, 2.6 equiv) were added and the mixture heated to 110 °C for 16 h. After cooling down to RT, the reaction mixture was filtered over celite and the solvent was removed by rotary evaporation. CH_2Cl_2 (50 mL) and H_2O (50 mL) were added and the layers separated. The water layer was extracted with CH_2Cl_2 (2 x 50 mL). The solvent was removed by rotary evaporation and the residue recrystallized from EtOH to yield **3.13** as a yellow solid (0.54 g, 1.8 mmol, 90%). m.p. 78 – 79 °C; ^{1}H NMR (400 MHz, $CDCl_3$): δ = 8.23 (dd, *J* = 8.1, 1.2 Hz, 2H), 7.41 (td, *J* = 8.1, 1.4 Hz, 2H), 7.12 (d, *J* = 8.0 Hz, 2H), 4.18 (t, *J* = 6.4 Hz, 4H), 2.00 – 1.85 (m, 4H), 1.65 – 1.55 (m, 4H), 1.44 – 1.20 (m, 16H), 0.87 (m, 6H) ppm; ^{13}C NMR (100.6 MHz, $CDCl_3$) δ = 180.4, 154.4, 130.0, 128.4, 125.8, 121.2, 113.0, 69.4, 31.9, 29.7, 29.6, 29.3, 29.0, 26.0, 22.7, 14.1 ppm; HRMS-APCI+ *m/z* calculated for $C_{37}H_{57}O_3S$ $[M + H]^+$ 581.4023, found 581.4002.

4,5-Bis(dodecyloxy)-9*H*-thioxanthen-9-thione (3.14)

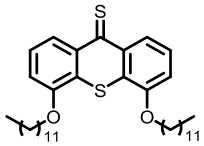

Compound **3.13** (2.0 g, 3.4 mmol, 1.0 equiv) was dissolved in toluene (100 mL) and Lawesson's reagent (4.17 g, 10.3 mmol, 3.0 equiv) was added. The reaction mixture was heated at reflux for 30 min. The solvent was subsequently removed by rotary evaporation. Purification by flash column chromatography (SiO_2, CH_2Cl_2:*n*-pentane, 1:2) gave **3.14** as a green solid (2.0 g, 3.4 mmol, quant.). m.p. 78 – 79 °C; ^{1}H NMR (400 MHz, $CDCl_3$): δ = 8.66 (d, *J* = 8.5 Hz, 2H), 7.36 (t, *J* = 8.2 Hz, 2H), 7.10 (d, *J* = 7.8 Hz, 2H), 4.19 (t, *J* = 6.4 Hz, 4H), 2.02 – 1.86 (m, 4H), 1.67 – 1.54 (m, 4H), 1.48 – 1.15 (m, 32H), 0.87 (t, *J* = 6.7 Hz, 6H) ppm; ^{13}C NMR (100.6 MHz, $CDCl_3$): δ = 210.8, 154.5, 138.3, 126.3, 125.1, 124.0, 112.1, 69.6, 31.9, 29.7, 29.7, 29.4, 29.1, 26.1, 22.7, 14.1 ppm; HRMS-ESI+ *m/z* calculated for $C_{37}H_{57}O_2S_2$ $[M + H]^+$ 597.3794, found 597.3783.

(4,5-Bis(dodecyloxy)-9*H*-thioxanthen-9-ylidene)hydrazine (3.15)

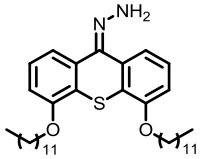

Compound **3.14** (2.14 g, 3.58 mmol, 1.0 equiv) was dissolved in THF (30 mL). The solution was treated at room temperature with 40% aq. hydrazine (8.00 mL, 140 mmol, 39 equiv). The solution decolorized to an orange solution within several min. The solvent and excess hydrazine were removed at reduced pressure. The residue was purified by flash column chromatography (SiO_2, *n*-pentane:EtOAc, 10:1) to yield **3.15** as a yellow solid (2.12 g, 3.56 mmol, quant.). m.p. 81 °C; ^{1}H NMR (300 MHz, $CDCl_3$): δ = 7.63 (d, *J* = 7.8 Hz, 1H), 7.43 (d, *J* = 7.8 Hz, 1H), 7.25 (m, 2H), 6.87 (d, *J* = 8.1 Hz, 1H), 6.82 (d, J = 7.9 Hz, 1H), 5.84 (s, 2H), 4.08 (dd, *J* = 14.2, 6.7 Hz, 4H), 1.88 (dd, *J* = 13.8, 6.9 Hz, 4H), 1.55 (m, 4H), 1.35 (m, 20H),

0.87 (t, *J* = 7.6 Hz, 6H) ppm; ^{13}C NMR (75.4 MHz, $CDCl_3$): δ = 155.9, 154.3, 142.0, 135.3, 127.0, 126.7, 125.7, 121.8, 120.1, 118.4, 111.2, 110.2, 69.4, 32.2, 29.9, 29.6, 29.4, 26.3, 22.9, 14.4 ppm; HRMS-APCI+ *m*/*z* calculated for $C_{37}H_{59}N_2O_2S$ $[M + H]^+$ 595.4292, found 595.4266.

Episulfide (3.17)

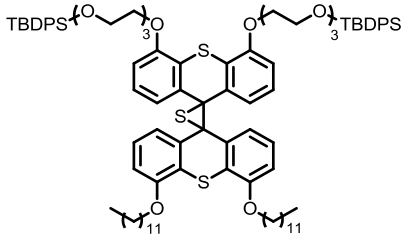

Solid MnO_2 (393 mg, 4.53 mmol, 10 equiv) was added to a solution of **3.15** (350 mg, 0.590 mmol, 1.3 equiv) in THF (50 mL) at 0 °C. The resulting solution was stirred for 1 h at 0 °C and filtered through a plug of silica gel. The plug was washed with a small amount of THF (10 mL). The light green solution was cooled to 0 °C. A solution of **3.12** (453 mg, 0.450 mmol, 1.0 equiv) in THF (2.4 mL) was added dropwise and the resulting mixture was stirred overnight. The solvents were evaporated under reduced pressure and the residue purified by flash column chromatography (SiO_2, *n*-pentane:EtOAc, 5:1) to yield **3.17** as a light yellow oil (638 mg, 0.41 mmol, 90%). ^{1}H NMR (400 MHz, $CDCl_3$) δ = 7.70 (d, *J* = 6.7 Hz, 10H), 7.40 – 7.33 (m, 12H), 7.32 (d, *J* = 7.9 Hz, 2H), 7.28 (d, *J* = 7.8 Hz, 2H), 6.85 (dd, *J* = 10.5, 5.4 Hz, 4H), 6.56 (d, *J* = 7.9 Hz, 2H), 6.51 (d, *J* = 8.0 Hz, 2H), 4.15 – 4.03 (m, 4H), 4.01 – 3.89 (m, 4H), 3.82 – 3.70 (m, 10H), 3.65 – 3.60 (m, 10H), 1.91 – 1.66 (m, 2H), 1.28 (m, 4H), 1.07 (s, 34H), 0.90 (t, *J* = 6.1 Hz, 6H) ppm; ^{13}C NMR (100.6 MHz, $CDCl_3$) δ = 154.1, 153.8, 135.8, 133.9, 132.6, 132.1, 129.8, 127.9, 126.0, 125.7, 125.2, 125.0, 124.0, 123.3, 120.1, 118.4, 111.6, 111.2, 110.3, 110.2, 72.7, 71.3, 71.0, 69.8, 69.5, 69.4, 63.6, 32.2, 30.0, 29.9, 29.8, 29.7, 29.6, 29.5, 29.4, 27.1, 26.3, 26.2, 23.0, 19.4, 14.4 ppm; HRMS-APCI+ *m*/*z* calculated for $C_{94}H_{123}O_{10}S_3Si_2$ $[M + H]^+$ 1564.7845, found 1564.7883.

12,12'-((4',5'-Bis(dodecyloxy)-[9,9'-bithioxanthenylidene]-4,5-diyl)bis(oxy))bis(2,2-dimethyl-3,3-diphenyl-4,7,10-trioxa-3-siladodecane) (3.18)

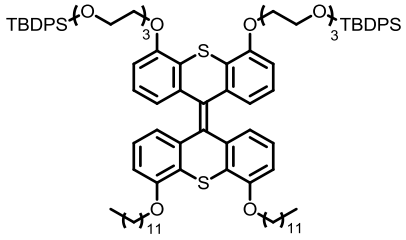

Compound **3.17** (3.6 g, 2.3 mmol, 1.0 equiv) was dissolved in toluene (140 mL) and PPh_3 (1.8 g, 6.9 mmol, 3.0 equiv) was added. The reaction mixture was heated at reflux for 16 h. The solvent was removed by rotary evaporation. Purification by flash column chromatography (SiO_2, *n*-pentane:EtOAc, 10:1) yielded **3.18** as a yellow solid (3.6 g, 2.3 mmol, quant.). ^{1}H NMR (400 MHz, $CDCl_3$): δ = 7.81 – 7.63 (m, 10H), 7.44 – 7.32 (m, 10H), 6.81 (t, *J* = 7.9 Hz, 4H), 6.67 (d, *J* = 5.1 Hz, 2H), 6.65 (d, *J* = 5.2 Hz, 2H), 6.44 (d, *J* = 7.8 Hz, 2H), 6.39 (d, *J* = 7.8 Hz, 2H), 4.36 – 4.25 (m, 2H), 4.15 (dt, *J* = 16.1, 5.6 Hz, 4H), 4.06 – 3.90 (m, 6H), 3.82 (m, 8H), 3.75 – 3.58 (m, 8H), 1.91 (m, 4H), 1.59 (m, 4H), 1.35 (m, 32H), 1.06 (s, 18H), 0.97 – 0.76 (m, 6H) ppm; ^{13}C NMR (100.6 MHz, $CDCl_3$): δ = 155.4, 155.1, 137.0, 136.6, 135.8, 133.9, 129.8, 127.9, 126.0, 125.9, 125.0, 122.8, 122.3, 109.6, 109.3, 72.7, 71.4, 71.1, 69.9, 69.2, 68.8, 63.6, 32.2, 30.0,

29.9, 29.8, 29.6, 29.5, 27.1, 26.4, 22.9, 19.4, 14.4 ppm; HRMS-ESI- *m/z* calculated for $C_{94}H_{123}O_{10}S_2Si_2Cl$ $[M - H + Cl]^-$: 1567.7813, found 1567.7879.

2,2'-((((((4',5'-Bis(dodecyloxy)-[9,9'-bithioxanthenylidene]-4,5-diyl)bis(oxy))bis(ethane-2,1-diyl))bis(oxy))bis(ethane-2,1-diyl))bis(oxy))diethanol (3.1)

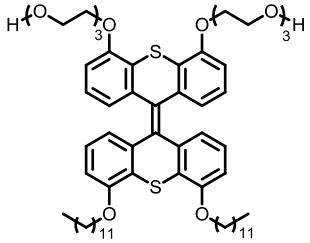

Compound **3.18** (90 mg, 0.059 mmol, 1.0 equiv) was dissolved in THF (5 mL) and TBAF (1 M in THF) (0.15 mL, 0.15 mmol, 2.5 equiv) was added at 0 °C. The reaction mixture was stirred at RT for 16 h. The solvent was removed by rotary evaporation and the residue purified by flash column chromatography (SiO_2, 5% MeOH in EtOAc) to yield **3.1** as an off-white solid (56 mg, 0.053 mmol, 90%). ^{1}H NMR (400 MHz, $CDCl_3$): δ = 6.82 (dd, *J* = 14.5, 7.8 Hz, 4H), 6.66 (t, *J* = 7.3 Hz, 4H), 6.44 (d, *J* = 7.7 Hz, 2H), 6.38 (d, *J* = 7.7 Hz, 2H), 4.31 (d, *J* = 4.4 Hz, 2H), 4.20 (d, *J* = 4.2 Hz, 2H), 4.13 (d, *J* = 9.0 Hz, 2H), 4.00 (dd, *J* = 9.5, 6.2 Hz, 6H), 3.90 (t, *J* = 4.6 Hz, 4H), 3.76 (d, *J* = 3.1 Hz, 8H), 3.70 – 3.63 (m, 4H), 2.95 (s, 1H), 1.96 – 1.85 (m, 4H), 1.70 (d, *J* = 2.8 Hz, 1H), 1.57 (dd, *J* = 13.9, 6.6 Hz, 4H), 1.43 – 1.21 (m, 32H), 0.88 (t, *J* = 6.7 Hz, 6H) ppm; ^{13}C NMR (75.4 MHz, $CDCl_3$): δ = 155.4, 155.0, 137.2, 136.5, 133.5, 132.8, 126.1, 125.9, 125.0, 124.8, 122.9, 122.3, 118.7, 109.5, 109.3, 73.0, 71.4, 70.8, 69.9, 69.2, 69.0, 62.0, 32.2, 29.9, 29.7, 29.63, 29.5, 26.4, 22.9, 14.4 ppm; HRMS-APCI+ *m/z* calculated for $C_{62}H_{89}O_{10}S_2$ $[M + H]^+$ 1057.5897, found 1057.5889.

2,2'-((((((4',5'-Bis(((*S*)-2-methyldodecyl)oxy)-[9,9'-bithioxanthenylidene]-4,5-diyl)bis(oxy))bis(ethane-2,1-diyl))bis(oxy))bis(ethane-2,1-diyl))bis(oxy))diethanol (3.2)

The synthesis of amphiphile **3.2** is described in the PhD Thesis of Peter Štacko.[48]

3.10 Acknowledgements

Dr. Marc Stuart has performed all the cryo-TEM measurements and is acknowledged for useful input. Peter Štacko is acknowledged for the pleasant collaboration in the synthesis of the described molecules. Wim Velema and Dr. Wiktor Szymański are gratefully acknowledged for helpful discussions.

3.11 References

[1] D. Roy, J. N. Cambre, B. S. Sumerlin, *Prog. Polym. Sci.* **2010**, *35*, 278–301.

[2] R. F. Service, *Science* **2005**, *309*, 95–95.

[3] G. Verma, P. A. Hassan, *Phys. Chem. Chem. Phys.* **2013**, *15*, 17016–17028.

[4] Y. -Z. Zhao, L. -N. Du, C. -T. Lu, Y. -G. Jin, S. -P. Ge, *Int. J. Nanomedicine* **2013**, *8*, 1621–1633.

[5] M. Zhang, X. Yan, F. Huang, Z. Niu, H. W. Gibson, *Acc. Chem. Res.* **2014**, *47*, 1995–2005.

[6] B. Zheng, F. Wang, S. Dong, F. Huang, *Chem. Soc. Rev.* **2012**, *41*, 1621–1636.

[7] R. Dong, Y. Zhou, X. Zhu, *Acc. Chem. Res.* **2014**, *47*, 2006–2016.

[8] L. Isaacs, *Acc. Chem. Res.* **2014**, *47*, 2052–2062.

[9] P. C. Ray, S. A. Khan, A. K. Singh, D. Senapati, Z. Fan, *Chem. Soc. Rev.* **2012**, *41*, 3193–3209.

[10] D. G. Blackmond, *Proc. Natl. Acad. Sci. U. S. A.* **2004**, *101*, 5732–5736.

[11] J. E. Hein, D. G. Blackmond, *Acc. Chem. Res.* **2012**, *45*, 2045–2054.

[12] K. Soai, T. Kawasaki, T. Shibata, in *Catalytic Asymmetric Synthesis*, John Wiley & Sons, Hoboken, N.J, USA, **2010**, pp. 891–930.

[13] F. Helmich, M. M. Smulders, C. C. Lee, A. P. Schenning, E. W. Meijer, *J. Am. Chem. Soc.* **2011**, *133*, 12238–12246.

[14] F. García, P. M. Viruela, E. Matesanz, E. Ortí, L. Sánchez, *Chem. – Eur. J.* **2011**, *17*, 7755–7759.

[15] A. L. Nussbaumer, D. Studer, V. L. Malinovskii, R. Häner, *Angew. Chem. Int. Ed.* **2011**, *50*, 5490–5494.

[16] D. Ogata, T. Shikata, K. Hanabusa, *J. Phys. Chem. B* **2004**, *108*, 15503–15510.

[17] F. Garcia, L. Sanchez, *J. Am. Chem. Soc.* **2012**, *134*, 734–742.

[18] S. J. George, Ž. Tomović, M. M. J. Smulders, T. F. A. de Greef, P. E. L. G. Leclère, E. W. Meijer, A. P. H. J. Schenning, *Angew. Chem. Int. Ed.* **2007**, *46*, 8206–8211.

[19] E. Yashima, K. Maeda, T. Nishimura, *Chem. – Eur. J.* **2004**, *10*, 42–51.

[20] A. Ajayaghosh, R. Varghese, S. J. George, C. Vijayakumar, *Angew. Chem. Int. Ed.* **2006**, *45*, 1141–1144.

[21] D. J. van Dijken, J. M. Beierle, M. C. A. Stuart, W. Szymański, W. R. Browne, B. L. Feringa, *Angew. Chem. Int. Ed.* **2014**, *53*, 5073–5077.

[22] J. J. D. de Jong, L. N. Lucas, R. M. Kellogg, J. H. van Esch, B. L. Feringa, *Science* **2004**, *304*, 278–281.

[23] T. W. Anderson, J. K. Sanders, G. D. Pantos, *Org. Biomol. Chem.* **2010**, *8*, 4274–4280.

[24] A. Ajayaghosh, R. Varghese, S. Mahesh, V. K. Praveen, *Angew. Chem. Int. Ed.* **2006**, *45*, 7729–7732.

[25] W. Jin, T. Fukushima, M. Niki, A. Kosaka, N. Ishii, T. Aida, *Proc. Natl. Acad. Sci. U. S. A.* **2005**, *102*, 10801–10806.

[26] R. Eelkema, B. L. Feringa, *Org. Biomol. Chem.* **2006**, *4*, 3729–3745.

[27] B. L. Feringa, R. A. van Delden, *Angew. Chem. Int. Ed.* **1999**, *38*, 3418–3438.

[28] K. Maeda, Y. Takeyama, K. Sakajiri, E. Yashima, *J. Am. Chem. Soc.* **2004**, *126*, 16284–16285.

[29] N. P. M. Huck, W. F. Jager, B. de Lange, B. L. Feringa, *Science* **1996**, *273*, 1686–1688.

[30] R. A. van Delden, N. Koumura, N. Harada, B. L. Feringa, *Proc. Natl. Acad. Sci. U. S. A.* **2002**, *99*, 4945–4949.

[31] L. J. Prins, P. Timmerman, D. N. Reinhoudt, *J. Am. Chem. Soc.* **2001**, *123*, 10153–10163.

[32] K. -H. Ernst, *Curr. Opin. Colloid Interface Sci.* **2008**, *13*, 54–59.

[33] F. Vera, R. M. Tejedor, P. Romero, J. Barberá, M. B. Ros, J. L. Serrano, T. Sierra, *Angew. Chem. Int. Ed.* **2007**, *46*, 1873–1877.
[34] J. Wang, D. Ding, L. Zeng, Q. Cao, Y. He, H. Zhang, *New J. Chem* **2010**, *34*, 1394–1400.
[35] T. Ishi-i, M. Crego-Calama, P. Timmerman, D. N. Reinhoudt, S. Shinkai, *J. Am. Chem. Soc.* **2002**, *124*, 14631–14641.
[36] J. van Gestel, A. R. Palmans, B. Titulaer, J. A. Vekemans, E. W. Meijer, *J. Am. Chem. Soc.* **2005**, *127*, 5490–5494.
[37] J. P. Hill, W. S. Jin, A. Kosaka, T. Fukushima, H. Ichihara, T. Shimomura, K. Ito, T. Hashizume, N. Ishii, T. Aida, *Science* **2004**, *304*, 1481–1483.
[38] M. M. Green, M. P. Reidy, R. D. Johnson, G. Darling, D. J. O'Leary, G. Willson, *J. Am. Chem. Soc.* **1989**, *111*, 6452–6454.
[39] A. R. Palmans, J. A. Vekemans, E. E. Havinga, E. W. Meijer, *Angew. Chem. Int. Ed.* **1997**, *36*, 2648–2651.
[40] J. K. Hirschberg, L. Brunsveld, A. Ramzi, J. A. Vekemans, R. P. Sijbesma, E. W. Meijer, *Nature* **2000**, *407*, 167–170.
[41] L. Brunsveld, A. Schenning, M. A. C. Broeren, H. M. Janssen, J. Vekemans, E. W. Meijer, *Chem. Lett.* **2000**, 292–293.
[42] M. M. Smulders, A. P. Schenning, E. W. Meijer, *J. Am. Chem. Soc.* **2008**, *130*, 606–611.
[43] A. C. Coleman, J. M. Beierle, M. C. A. Stuart, B. Macia, G. Caroli, J. T. Mika, D. J. van Dijken, J. Chen, W. R. Browne, B. L. Feringa, *Nat. Nanotechnol.* **2011**, *6*, 547–552.
[44] W. R. Browne, M. M. Pollard, B. de Lange, A. Meetsma, B. L. Feringa, *J. Am. Chem. Soc.* **2006**, *128*, 12412–12413.
[45] A. C. Coleman, J. Areephong, J. Vicario, A. Meetsma, W. R. Browne, B. L. Feringa, *Angew. Chem. Int. Ed.* **2010**, *49*, 6580–6584.
[46] see reference 21
[47] B. Alberts, A. Johnson, J. Lewis, M. Raff, K. Roberts, P. Walter, "Molecular Biology of the Cell," can be found under http://www.ncbi.nlm.nih.gov/books/NBK21054/, **2002**.
[48] P. Štacko, *PhD Thesis*, University of Groningen, **forthcoming**.
[49] M. M. Pollard, M. K. ter Wiel, R. A. van Delden, J. Vicario, N. Koumura, C. R. van den Brom, A. Meetsma, B. L. Feringa, *Chem. – Eur. J.* **2008**, *14*, 11610–11622.
[50] P. Beak, R. A. Brown, *J. Org. Chem.* **1982**, *47*, 34–46.
[51] L. Gupta, A. C. Hoepker, Y. Ma, M. S. Viciu, M. F. Faggin, D. B. Collum, *J. Org. Chem.* **2013**, *78*, 4214–4230.
[52] M. I. Viseu, A. S. Tatikolov, R. F. Correia, S. M. B. Costa, *J. Photochem. Photobiol. Chem.* **2014**, *280*, 54–62.
[53] A. Mammana, A. D'Urso, R. Lauceri, R. Purrello, *J. Am. Chem. Soc.* **2007**, *129*, 8062–8063.
[54] M. Irie, *Chem. Rev.* **2000**, *100*, 1685–1716.

Chapter 4

Synthesis and Morphology of Aromatic Amphiphiles

A range of aromatic amphiphiles was synthesized and the morphology of the self-assembled aggregates studied by cryo-TEM. The hydrophilic and hydrophobic moieties of the amphiphiles, as well as their aromatic cores, were systematically changed in order to study the differences in self-assembly and morphology as a function of molecular structure. The amphiphiles were found to have interesting properties and while the synthesis of thioxanthone-derived amphiphiles was readily accomplished, the preparation of xanthone- and anthrone-derived amphiphiles proved to be challenging. While classical surfactants aggregate according to packing parameter theory, for amphiphiles described in this chapter, the shape of the aromatic core and π-π interactions can contribute to the aggregation behavior. Synthetic approaches as well as morphological studies of the prepared amphiphiles are presented and discussed in this chapter.

Part of the research presented in this chapter will be published:
D. J. van Dijken, M. C. A. Stuart, A. Huizing, M. Jurgėlenas, W. Szymański, B. L. Feringa, *manuscript in preparation*

4.1 Introduction

The development of functional materials, based on supramolecular structures that are formed through self-assembly, has seen much attention since Charles Pedersen synthesized crown ethers, cyclic compounds that are able to complex cations.[1,2] The importance of supramolecular chemistry was further highlighted in 1987, when the Nobel prize in Chemistry was awarded to Pedersen,[3] Cram[4] and Lehn[5] for the development of this field.

Nanotechnology, a scientific field that deals with the synthesis, analysis and manipulation of matter at the molecular and supramolecular scale[6,7] has led to the development of sophisticated (supra)molecular systems of ever increasing complexity.[8–18] At the very basis of this exciting field lies the understanding and predictability of self-assembly.

A particularly interesting class of compounds that can undergo self-assembly are amphiphiles as described in chapter 1.[19] The amphiphile, or surfactant, industry is huge[20,21] and these molecules have found wide spread use, ranging from household detergents to explosives.[22,23] Briefly, amphiphilic molecules contain a hydrophilic (water soluble) and hydrophobic (water insoluble) part and generally have the tendency to self-assemble in water in order to minimize unfavorable interactions with the solvent. Amphiphilic molecules have the tendency to give well-defined aggregates upon self-assembly in water, leading to the formation of for example rods, micelles, vesicles and inversed micelles, depending on the amphiphile and the conditions.[24,25] The obtained morphology of the self-assembled amphiphile, depends on the way the amphiphiles organize in the solvent. This is directly correlated to their structure and the packing of the individual molecules, dependent on the so called “packing parameter” as introduced by Israelachvili and coworkers (see chapter 1).[24] This model, allows the prediction of aggregate morphology by calculating the headgroup area and the volume and length of the hydrophobic part of the amphiphile. While it gives a good estimate for relatively simple molecules and is very useful, it is often difficult to use for more complex molecules and synthesis and study of new classes of amphiphiles is often necessary. New models or adaptations to the existing models are being developed,[27–30] to improve the ability to explain, rationalize or even predict self-assembly based on the molecular structure of the amphiphile, but one will eventually always have to prepare any new amphiphiles in the lab and study their morphology.

An elegant example of the synthesis and investigation of self-assembly morphology is described by Kunitake and coworkers.[31] The synthesis of 62 single-chain amphiphiles, containing different rigid segments, was described and their morphology studied by electron microscopy (Figure 4.2).

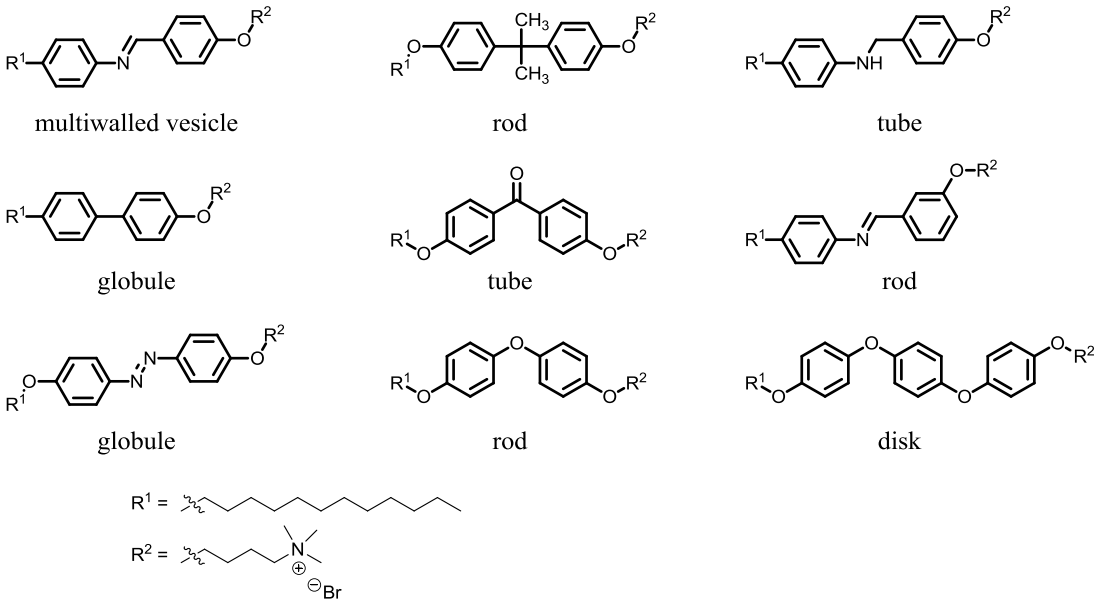

Figure 4.2. Variation of different single-chain amphiphiles and their morphologies as observed by electron microscopy.[31]

As can be seen from the overview presented in Figure 4.2, relatively small variations in one part of the molecule result in the formation of a large variety of different nano-structures. Given the shape of the amphiphiles in Figure 4.2, the aromatic moieties of the amphiphiles, building the rigid segment, play a key role in the morphology of these self-assembled molecules. Interactions such as π-π stacking[32] and cation-π interactions,[33,34] (given the charged polar headgroup) differ from molecule to molecule and will have an influence on the aggregation behavior of these different molecules.

Synthetic amphiphiles are interesting because a well-thought out synthetic route can allow for multigram scale synthesis of the desired amphiphiles as well as making structural variations in a late stage of the synthesis in order to introduce functionalities at wish. In addition, structures can be made that do not occur in Nature which is interesting but also useful in terms of possible new properties and bio-orthogonality. Gaining insight into changes in properties of self-assembled nanoscale objects, as a consequence of a change in the molecular structure, is therefore warranted and the goal of this chapter for a small library of molecules.

4.2 Concept

Inspired by previous results from our group[35] (see chapters 3 and 6), we envisioned to synthesize a range of amphiphiles with an aromatic core, connecting an oligo-ethyleneglycol chain to two aliphatic tails as the hydrophilic and hydrophobic moieties, respectively (Figure 4.3).

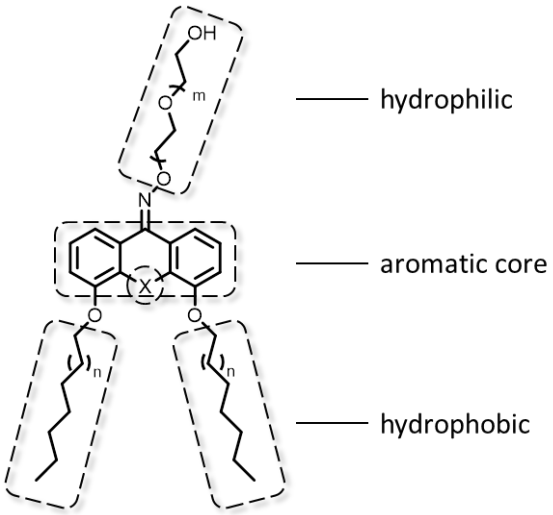

Figure 4.3. Basic structure of amphiphiles studied in this chapter and the different moieties indicated.

In the study described in this chapter, we employed ethyleneglycol chains of different lengths as the hydrophilic headgroups as to avoid the complexity that is related to the use of charged moieties regarding both synthesis but more importantly, effects that do not stem from the amphiphiles based on for example different counterions.

We envisioned different aromatic cores, i.e. thioxanthone, xanthone and anthrone (Figure 4.4). Due to the different heteroatoms in the core, the packing is expected to be different and this was supported by calculations.[36]

Based on literature precedence,[35] we envisioned that the alkyl chains of the thioxanthone-derived amphiphiles may interdigitate upon self-assembly. For simple amphiphiles, it is known that the structure of the hydrophobic tail, i.e. its length and branching has a large influence on aggregate morphology and properties.[37–40] The introduction of aromatic moieties into the hydrophobic tails of single tailed amphiphiles leads to large differences in the critical micelle concentration between the aromatic analogues and their parent compounds and shows that aromatic moieties can play an interesting role in morphological behavior.[41] We believe that the hydrophobic interactions in the supramolecular assembly might be increased by removing the ether functionalities and linking the alkyl chains directly to the aromatic thioxanthone core of the amphiphiles (henceforth referred to as C-C linked). To this end, we envisioned the synthesis of C-C linked hydrophobic tails and study the differences between all amphiphiles, giving 6 target amphiphile structures in total.

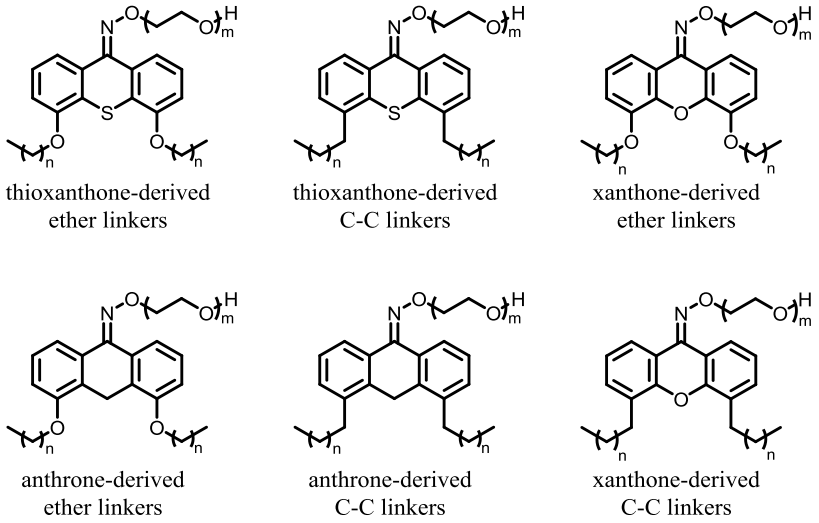

Figure 4.4. Target amphiphiles, having different aromatic cores and either ether-linked or C-C linked hydrophobic chains.

4.3 Self-assembly

For the self-assembly experiments, the amphiphile was dissolved in chloroform (1 mg/mL) in a 2 mL glass vial. The mixture was subsequently dried under a low N_2-flow, while rotating the vial and after all chloroform evaporated, the vial was dried further for 1 h under vacuum. The dried thin lipid-film was then rehydrated in H_2O to give a suspension (1 mg/mL). The suspension was subjected to three freeze-thaw cycles in liquid nitrogen and a warm water bath, respectively, so that a homogeneous turbid solution was formed. The sample was then subjected to one more freeze-thaw cycle in liquid nitrogen and a water bath at a set temperature (indicated below the images for each amphiphile in this chapter) and kept in the water bath for 30 min.

For analysis by cryo transmission electron microscopy (cryo-TEM), the turbid solution (2.5 µL) was placed on a glow-discharged holy carbon coated grid (Quantifoil 3.5/1, QUANTIFOIL Micro Tools GmbH, Großlöbichau, Germany). After blotting at the set temperature (indicated below the images for each amphiphile in this chapter), the grid was rapidly frozen in liquid ethane (Vitrobot, FEI, Eindhoven, The Netherlands) and stored in liquid nitrogen until observed. Grids were observed in a Gatan model 626 cryo-stage in a Philips CM120 cryo-electron microscope operating at 120 KeV. Images were recorded under low-dose conditions on a slow-scan CCD camera.

All samples were prepared and measured several times and the repetitive experiments gave consistent results, unless otherwise indicated.

4.4 Thioxanthone-derived amphiphiles

4.4.1 Synthesis of thioxanthene amphiphiles with ether-linked alkyl chains

Synthesis of key building block, thioxanthone **3.8** is described in chapter 3 and is readily achieved in 78% over 4 steps. Introduction of a range of alkyl chains of different length is facile and shown in Scheme 4.1.

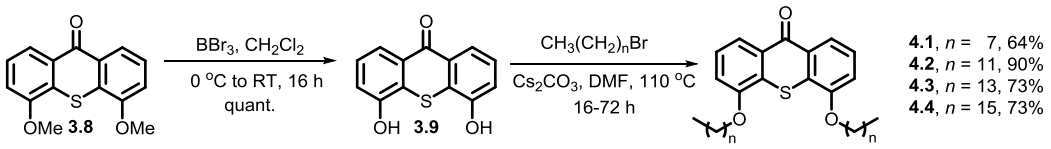

Scheme 4.1. Synthesis of hydrophobic thioxanthones **4.1**-**4.4**, bearing alkyl chains of different length.

Deprotection of the phenol moieties of **3.8** with BBr_3 gives **3.9**. Reaction of diphenol **3.9** with different alkylbromides in the presence of Cs_2CO_3 (use of K_2CO_3 as the base gave identical results) gives **4.1**-**4.4** in good yields (Scheme 4.1). Next, the ketone moiety needs to be transformed into an oxime in order to connect the hydrophilic oligo-ethyleneglycol chain to the thioxanthane core. Direct conversion of thioxanthones **4.1**-**4.4** to the corresponding oximes only proceeded in low yields, by reaction with hydroxylammonium chloride in the presence of pyridine. Prior conversion into the corresponding thioketones **4.5**-**4.8**, from thioxanthones **4.1**-**4.4**, however, increased the reactivity and subsequent reaction with hydroxylammonium chloride gave oximes **4.9**-**4.12** in good to excellent yields for both steps (Scheme 4.2).

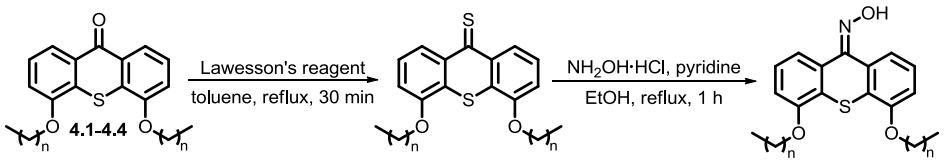

Scheme 4.2. Synthesis of oxime intermediates **4.9**-**4.12**, bearing alkyl chains of different length.

Installment of the hydrophilic oligo-ethyleneglycol headgroup requires monofunctionalized-ethyleneglycol with a leaving group. Following a procedure reported by Bouzide and coworkers, monotosyl-ethyleneglycol **4.13**-**4.16** were synthesized (Scheme 4.3).[42]

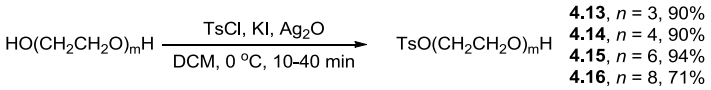

Scheme 4.3. Synthesis of monotosyl-ethyleneglycol intermediates **4.13**-**4.16** of different length.

Employing a mixture of Ag_2O, KI and TsCl in DCM at 0 °C, mainly monotosylated products were obtained in good to excellent yields.

Deprotection of the oxime, in the presence of the monotosyl-ethyleneglycol, with *t*-BuOK at ambient temperature and subsequent substitution, yields amphiphiles **4.17**-**4.25** (Scheme 4.4).

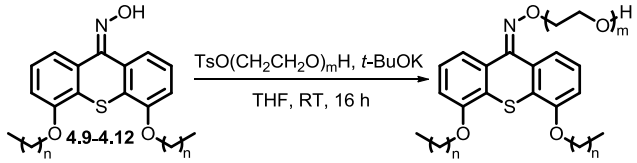

4.17, *n* = 7, *m* = 4, 80%
4.18, *n* = 7, *m* = 6, 82%
4.19, *n* = 11, *m* = 3, 80%
4.20, *n* = 11, *m* = 4, 90%
4.21, *n* = 11, *m* = 6, 96%
4.22, *n* = 13, *m* = 4, 60%
4.23, *n* = 13, *m* = 6, 61%
4.24, *n* = 15, *m* = 6, 70%
4.25, *n* = 15, *m* = 8, 56%

Scheme 4.4. Synthesis of amphihiles **4.17**-**4.25**.

4.4.2 Morphology of thioxanthene amphiphiles with ether-linked alkyl chains

With amphiphiles **4.17**-**4.25** in hand, we studied their morphology at different temperatures by cryo-TEM. Apart from studying how the morphology of the self-assembled amphiphiles changes as a function of structure, we were interested to obtain vesicles or bilayers of different sizes for other purposes (see for example chapter 5). For this purpose, we studied the self-assemblies at different temperatures (low, room temperature and elevated temperatures). At the end of this paragraph, the morphologies will be compared in more detail.

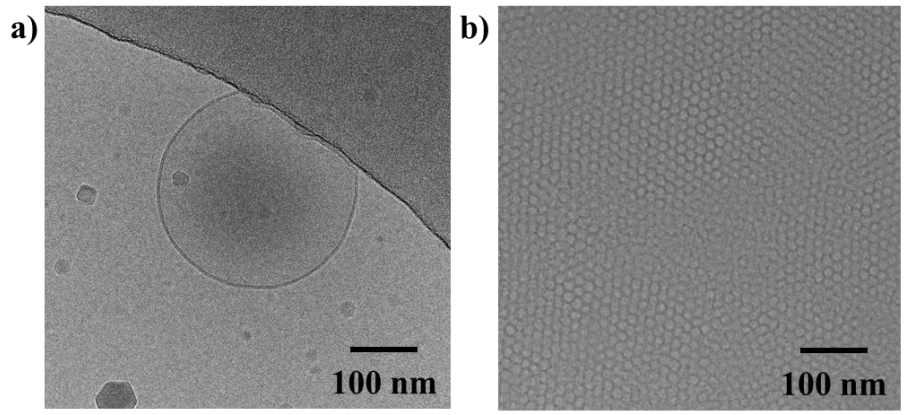

Figure 4.5. Cryo-TEM images of **4.17** (*n* = 7, *m* = 4) in water (1 mg/mL). a) At 4 °C; vesicles with a diameter of ~200 nm. b) At 20 °C; cubic phase.

At low temperature **4.17** (*n* = 7, *m* = 4) forms large vesicles with a diameter of ~200 nm. At room temperature, a cubic phase was observed (Figure 4.5).

For thioxanthone-derived amphiphile **4.18** (*n* = 7, *m* = 6), we were unable to detect any self-assembled structures. This is likely due to the fact that the hydrophilic part of the amphiphile is rather large with respect to the hydrophobic part and the amphiphile thereby becomes too soluble in water. For amphiphile **4.19** (*n* = 11, *m* = 3), on the other hand, we found the opposite, i.e. **4.19** is visually insoluble in water. Sonication and increasing the amount of freeze-thaw cycles from three to six, both techniques that usually help for the self-assembly of amphiphiles, did not result in any detectable aggregates for **4.19** (*n* = 7, *m* = 3) in water. Aggregates (micelles) might still be formed that are not observable by electron microscopy, but the majority of the sample stayed as a solid in the water.

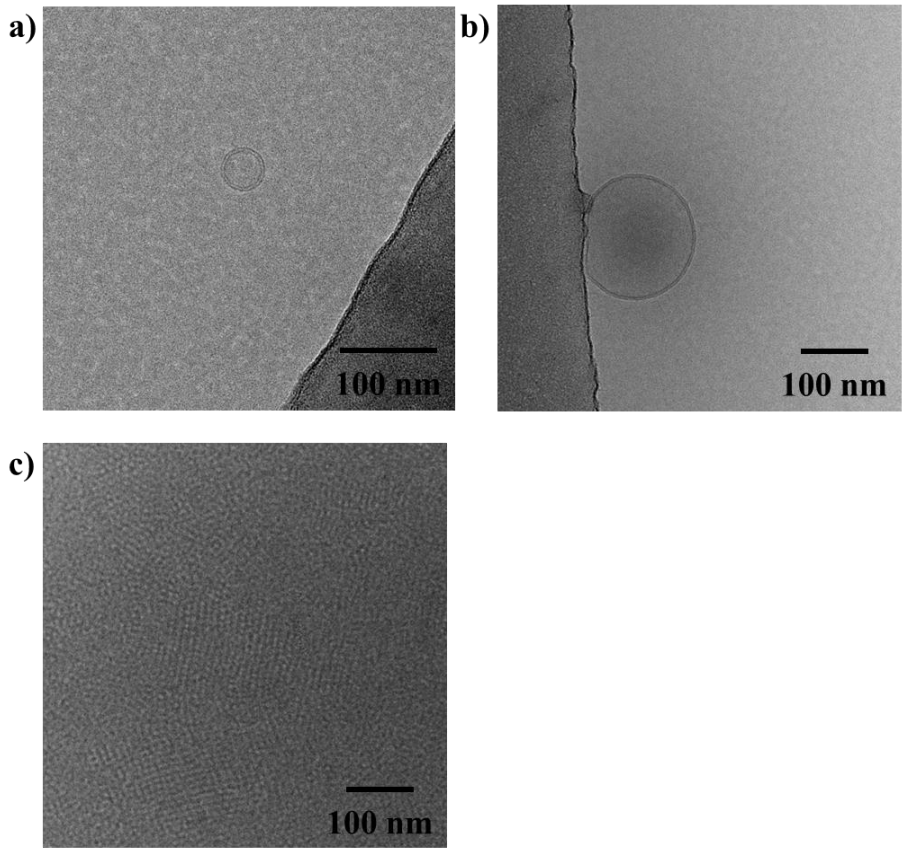

Figure 4.6. Cryo-TEM images of **4.20** (*n* = 11, *m* = 4) in water (1 mg/mL). a) At 10 °C; vesicles with a diameter of ~40 nm. b) At 25 °C; vesicles with a diameter of ~120 nm. c) At 35 °C; cubic phase.

At low temperature **4.20** (*n* = 11, *m* = 4) forms small vesicles with a diameter of ~40 nm. At room temperature, large vesicles with a diameter of ~120 nm were observed. At elevated temperature, a cubic phase was observed (Figure 4.6).

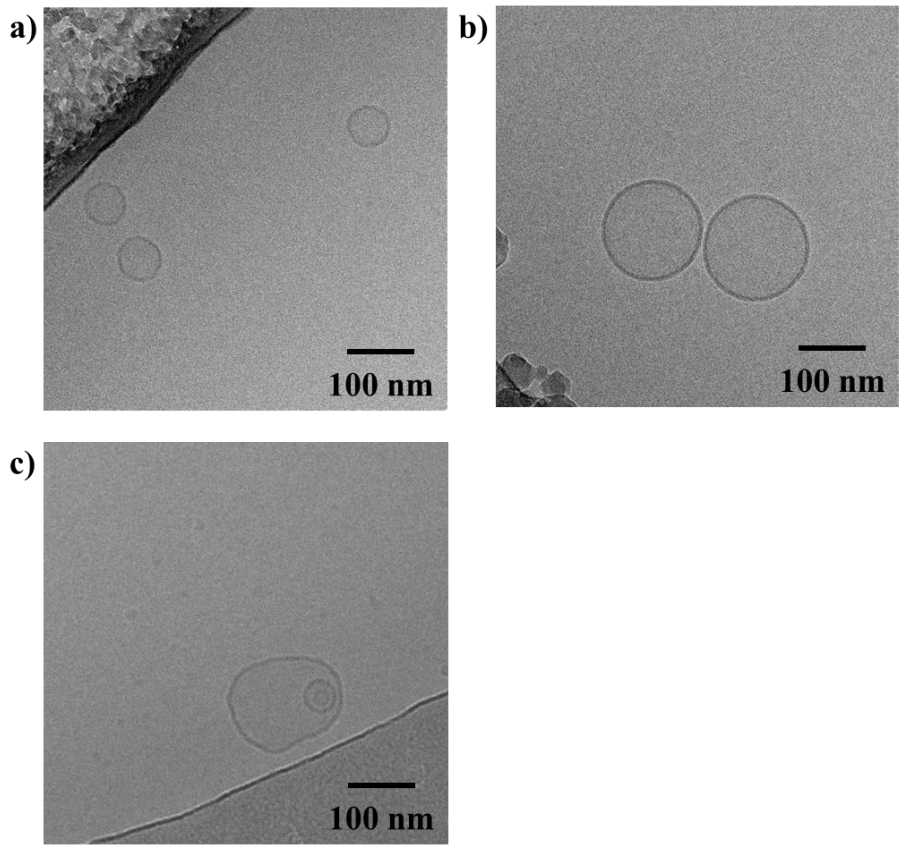

Figure 4.7. Cryo-TEM images of **4.21** (*n* = 11, *m* = 6) in water (1 mg/mL). a) At 4 °C; vesicles with a diameter of ~80 nm. b) At 4 °C; vesicles with a diameter of ~150 nm. c) At 20 °C; vesicles with a diameter of ~160 nm.

At low temperature **4.21** (*n* = 11, *m* = 6) forms vesicles with a diameter of 80–150 nm. At room temperature, only large vesicles with a diameter of ~160 nm were observed (Figure 4.7).

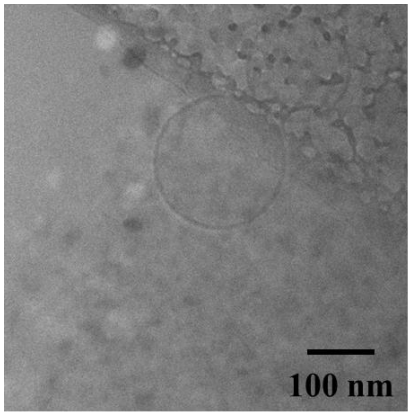

Figure 4.8. Cryo-TEM images of **4.22** (*n* = 13, *m* = 4) in water (1 mg/mL) at 40 °C; vesicles with a diameter of ~200 nm.

For amphihile **4.22** (*n* = 13, *m* = 4) at room temperature, no aggregates were observed. At elevated temperature, large vesicles with a diameter of ~200 nm were observed (Figure 4.8).

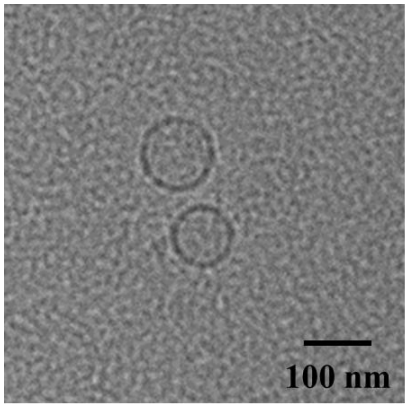

Figure 4.9. Cryo-TEM images of **4.23** (*n* = 13, *m* = 6) in water (1 mg/mL) at 40 °C; vesicles with a diameter of ~100 nm.

For **4.23** (*n* = 13, *m* = 6) at room temperature, no aggregates were observed. At elevated temperature, vesicles with a diameter of ~100 nm were observed (Figure 4.9).

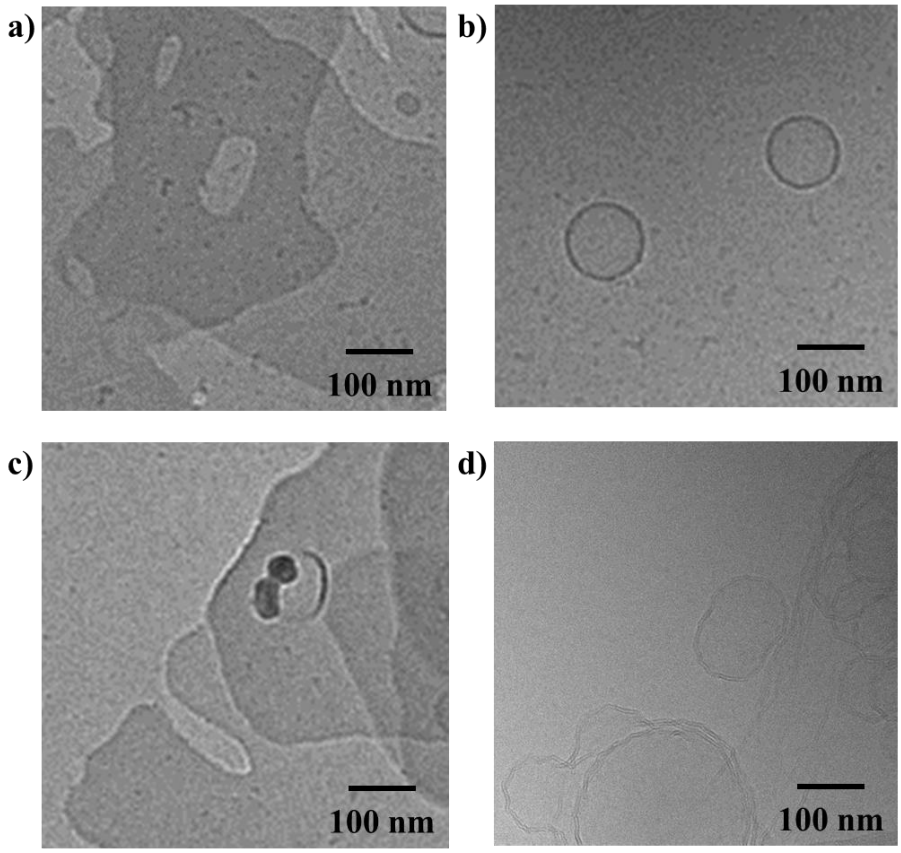

Figure 4.10. Cryo-TEM images of **4.24** (*n* = 15, *m* = 6) in water (1 mg/mL). a) At 25 °C; large plates. b-d) At 50 °C; vesicles with a diameter of ~100 nm, large plates and aggregated vesicles with irregular bilayers.

At room temperature **4.24** (*n* = 15, *m* = 6) forms large plates. At elevated temperature, vesicles with a diameter of ~100 nm were observed, but also large plates and other aggregates (Figure 4.10).

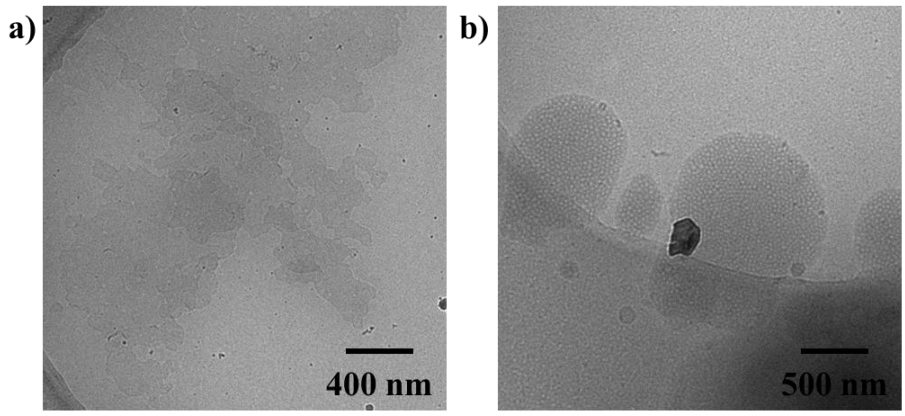

Figure 4.11. Cryo-TEM images of **4.25** (*n* = 15, *m* = 8) in water (1 mg/mL). a) At 25 °C; large plates. b) At 50 °C; cubic aggregates.

At room temperature **4.25** (*n* = 15, *m* = 8) forms large plates. At elevated temperature, very large cubic aggregates are observed (Figure 4.11).

Studying the differences in morphology for amphiphiles **4.17**-**4.25** as a function of their structure, certain trends were observed. Not surprisingly, the hydrophilicity of the amphiphiles, i.e. the number of ethyleneglycol units, needs to be balanced with the two hydrophobic alkyl chains and the aromatic core of the amphiphiles, in order to ensure self-assembly.

For thioxanthone-derived amphiphiles, bearing two saturated alkyl chains as the hydrophobic moiety and an ethyleneglycol chain as the hydrophilic moiety, some comparisons can be made as a small library of systematically altered amphiphiles could be synthesized. As expected,[27–30] a fine balance must be met between the hydrophilic and hydrophobic moieties. Amphiphile **4.19** (*n* = 11, *m* = 3) is too insoluble, for example and we could not observe any self-assembly. On the other extreme, **4.18** (*n* = 7, *m* = 6) is too soluble and no aggregates could be observed either.

Comparing the amphiphiles that bear tetra-ethyleneglycol chains as the hydrophilic moiety (**4.17**, **4.20** and **4.22**), we found that vesicles with a diameter of 120–200 nm formed consistently. Increasing the alkyl chain length, i.e. the hydrophobic part of these amphiphiles (from *n* = 7 to *n* = 11 to *n* = 13), increases the temperature needed to form these large vesicles. Aditionally, the temperature at which the molecules from a cubic phase, rather than vesicles, increases. These findings are in line with what has been reported for amphiphiles in general.[31,43,44]

For amphiphiles that bear hexa-ethyleneglycol chains (**4.21**, **4.23** and **4.24**), we found that vesicles were formed with a diameter of 80–150 nm. When the hydrophobic moieties, i.e. the alkyl chains, get too long (*n* = 15), however, the packing of the amphiphiles appears to become more efficient and more stable sheets, or “plates”, are formed. This appears to be a general phenomenon for the thioxanthone-derived amphiphiles described in this chapter and increasing the hydrophilic ethyleneglycol chain length does not lead to improved morphologies as was observed for **4.25** (*n* = 15, *m* = 8), for which vesicles could not be obtained; plates were formed at room temperature and a cubic phase was observed at higher temperatures. This observation in in agreement with general packing parameter theory (see chapter 1).[24,45] At higher temperatures, the hydrophilic headgroup is less hydrated and the diameter of the headgroup is

thereby smaller. At the same time, the effective volume of the hydrophobic tails is larger as their motion is increased at elevated temperatures. As a consequence, at higher temperature the packing parameter is larger, leading to an inverted shape of the amphiphiles and this fits with the observation of cubic phases.

In general, increasing the hydrophilic part increased the solubility, i.e. the ability of the amphiphile to be hydrated. We were able to increase the extent of hydration of **4.20** (*n* = 11, *m* = 4), which showed very promising ion-conductive properties as described in chapter 5, by synthesizing **4.21** (*n* = 11, *m* = 6). Compound **4.21** has similarly good properties as **4.20**, but was much easier to use in a practical sense. For details, the reader is referred to chapter 5 of this thesis. However, the change in hydration is not predictable enough to make good use of it in all cases. We expected **4.25** (*n* = 15, *m* = 8) to give better properties than **4.24** (*n* = 15, *m* = 6) for example, but observed similar ill-defined plates at useful temperatures.

4.4.3 Synthesis of thioxanthene amphiphiles with C-C linked alkyl chains

In **4.17**-**4.25**, the alkyl chains are linked to the aromatic core of the amphiphiles through an ether linker. For the amphiphiles with C-C linked alkyl chains, the selective alkylation of thioxanthone, *ortho* to the thioether moiety is the crucial step for the synthesis of the target amphiphiles. Attachment of the hydrophilic part of the amphiphile to the ketone functionality of the thioxanthone precurors would likely proceed without difficulty, as was shown for the synthesis of **4.17**-**4.25**. We envisioned to utilize lithium chemistry for the alkylation, specifically *ortho*-lithiation.[46–48]

Ortho-lithiation of thioxanthone mainly leads to addition of the lithium reagent to the ketone functionality and it needs to be protected to effect lithiation adjacent to the thioether functionality. To our surprise, no efficient protection procedures were reported in literature and we explored several protection groups and strategies (Schemes 4.5-4.7).

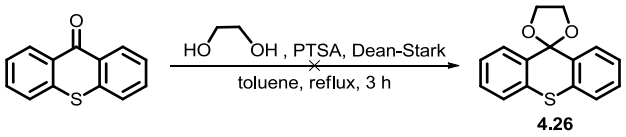

Scheme 4.5. Attempted protection of thioxanthone as a cyclic acetal.[49]

Protection of a ketone as a cyclic acetal is classic textbook chemistry.[49] Protection of thioxanthone with ethyleneglycol, in the presence of a catalytic amount of *para*-toluenesulfonic acid in toluene with a Dean-Stark trap, however, did not succeed. Starting material was quantitatively recovered and it appears that the ketone is not reactive enough.

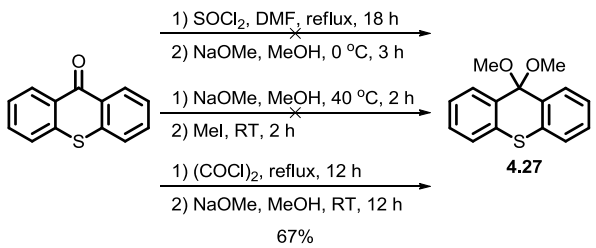

Scheme 4.6. Protection of thioxanthone as acetal **4.27**.

Xanthone can be protected as its dimethylketal using thionylchloride and subsequent reaction with sodium methoxide.[50] Under the conditions described, however, a complex mixture of products was obtained for thioxanthone. Using a strong nucleophile, i.e. sodium methoxide, and reaction with MeI, resulted in recovery of thioxanthone. Curiously, while the use of thionylchloride and subsequent reaction with sodium methoxide gave no product, when oxalylchloride is used, the dimethylketal product **4.27** can be obtained in 67% yield. Alternatively, thioxanthone can be protected as a mixed acetal as shown in Scheme 4.7.

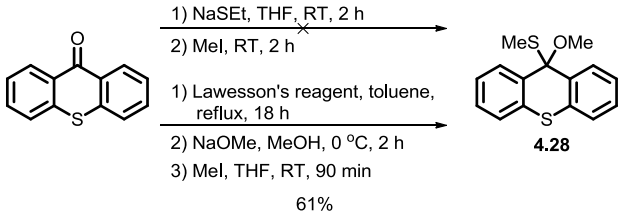

Scheme 4.7. Protection of thioxanthone as a mixed acetal.

Conversion of thioxanthone into its corresponding thioketone with Lawesson's reagent, increases its electrophilicity.[51] The thioketone now undergoes nucleophilic attack by sodium methoxide and can be alkylated with MeI to give mixed acetal **4.28** in 61% yield.

With protected thioxanthone in hand, we next studied the *ortho*-lithiation in order to attach alkyl chains to the aromatic rings, adjacent to the thioether moiety. *Ortho*-directed metalation with organolithium reagents is possible due to the interactions between the lone pair of the directing moiety, and the lithium species.[52] A wide variety of *ortho*-directing groups has been reported, including ethers, thioethers and acetals.[53–55] This could potentially pose a problem as **4.27** and **4.28** contain several moieties that are directing groups for the lithiation. As the moieties have different directing strengths, the choice of lithium reagent and reaction conditions will play a crucial role in the regioselectivity of the lithiation.[53–56]

To examine the *ortho*-lithiation of dimethylketal **4.27**, we subjected the substrate to different lithiation conditions and quenched the reaction with MeI, enabling us to analyze the thioxanthone after acidic workup and therefore the regioselectivity of the lithiation by ^{1}H NMR (Table 4.1). Tetrahydropyran (THP) was used as the solvent in most cases due to its unreactivity with lithium reagents,[57] whereas THF can react with lithium reagents at temperatures above 0 °C (in THF at 0 °C the half-life of *n*-BuLi is 23.5 h).[58,59] At temperatures below -40 °C, THP freezes and THF was used instead.

Table 4.1. Screening of lithiation conditions of acetal-protected thioxanthone **4.27**.

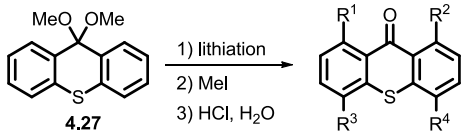

Entry	Conditions[a]	R^1 or R^2	R^3 or R^4	Conv.[b]
1	*n*-BuLi (2.0 equiv), THF, 0 °C, 2 h	Me	H	<10%
2	*n*-BuLi (6.0 equiv), THP, 0 °C, 2 h	Me	H	full
3[c]	*t*-BuLi (1.0 equiv), THP, 0 °C, 30 min	Me	Me	<10%
4	*t*-BuLi, *t*-BuOK (1:1, 3.0 equiv), THP, -40 °C, 30 min	Me	Me	full
5[d]	*s*-BuLi, TMEDA (1:1, 2.0 equiv), THF, -78 °C, 1 h	H	H	-
6	*n*-BuLi, TMEDA (1:1, 2.0 equiv), THP, -40 °C, 30 min	Me	H	<20 %

[a] Equivalents of lithium reagent, with respect to **4.27**. [b] Determined by ^{1}H NMR. [c] With 6.0 equivalents of *t*-BuLi, a complex mixture of products was obtained [d] At higher temperature, a complex mixture of products was obtained.

The results shown in table 4.1 indicate that the protons *ortho* to the acetal moieties (R^1 and R^2) are most reactive (Table 4.1, entry 1). Increasing the equivalents of *n*-BuLi from 2.0 to 6.0 (Table 4.1, entry 2), only the mono-methylated (in R^1 or R^2) product was obtained. The regioselectivity was not unexpected as the acetal moiety should be a better *ortho*-directing group than the thioether moiety in general.[53–56] The use of an equimolar amount of the more reactive *t*-BuLi (Table 4.1, entry 3) gave the dimethylated product with one methyl group *ortho* to both directing moieties in low conversion at 0 °C. Increasing the equivalents of *t*-BuLi led to a complex mixture of products. Use of Lochmann-Schlosser base[60] (Table 4.1, entry 4), which has been described to be selective[61] and is more reactive than *t*-BuLi, at -40 °C, gave the same product as *t*-BuLi (Table 4.1, entry 3) but with full conversion. Using a mixture of tetramethylethylenediamine (TMEDA) at low temperatures, which is known to increase the reactivity of lithium reagents, in combination with *s*-BuLi (Table 4.1, entry 5) or *n*-BuLi (Table 4.1, entry 6) led to poor conversions and selectivities.

For a more indebt study on selective lithiation of (thio)xanthone derivatives that are protected as acetals or thioacetals, the reader is referred to the Master thesis of Anja Huizing.[36] It was concluded at this stage that selective *ortho*-lithiation of (protected) thioxanthones is not a facile route to obtain di-alkylated thioxanthones that are substituted *ortho* to the thioether moiety.

4.5 Xanthone-derived amphiphiles

4.5.1 Synthesis of xanthene amphiphiles with C-C linked alkyl chains

Following a procedure described by Odrowaz and coworkers,[62] xanthone was protected as its dimethylketal (Scheme 4.8).

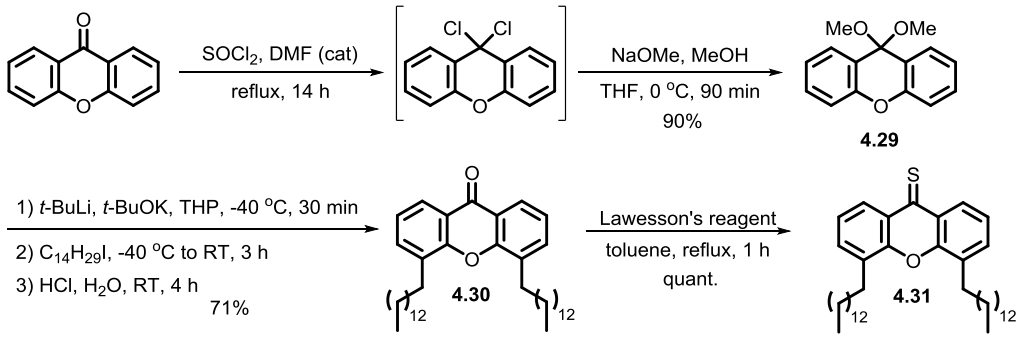

Scheme 4.8. Synthesis of hydrophobic thiated xanthone **4.31**.

Conversion of the ketone functionality in xanthone into its geminal dichloride can be achieved with thionylchloride. Slow addition of this intermediate to a methanolic solution of sodium methoxide yields dimethylketal **4.29** in 90% yield over the two steps. Following a modified literature procedure[62] regioselective *ortho*-lithiation of **4.29**, followed by quenching with the alkylhalide and subsequent acidic workup yielded **4.30** in 71% yield. Reaction with Lawesson's reagent gave thioketone **4.31** in quantitative yield.

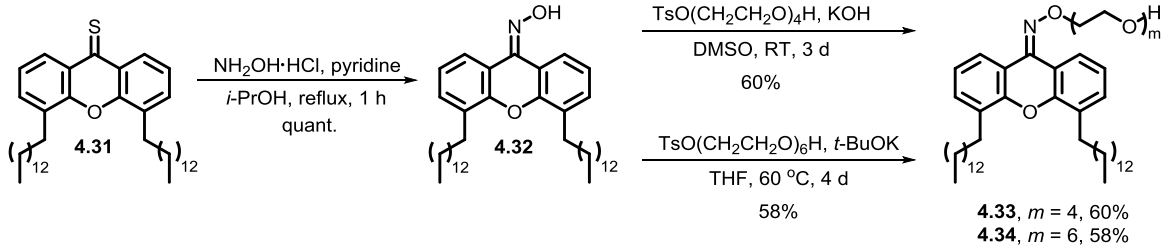

Scheme 4.9. Synthesis of amphihiles **4.33**-**4.34**.

The thioketone undergoes hydrolysis back to ketone **4.31** when stored and was converted into the oxime, immediately after purification to give **4.32** in quantitative yield (Scheme 4.9). Two different protocols could be employed for the preparation of amphiphiles **4.33** (*m* = 4) and **4.34** (*m* = 6). Reaction of oxime **4.32** with monotosyl-tetra-ethyleneglycol in the presence of KOH in DMSO gave amphiphile **4.33** (*m* = 4) in 60% yield. For the reaction of **4.32** with monotosyl-hexa-ethyleneglycol, *t*-BuOK was employed in THF at elevated temperature and **4.34** (*m* = 6) was obtained in 58% yield. Both procedures yield the respective amphiphilic product in moderate yield after several days, but due to the ease of removal of THF, the second route is preferred.

4.5.2 Morphology of xanthene amphiphiles with C-C linked alkyl chains

With amphiphiles **4.33**-**4.34** in hand, we studied their morphology in water at room temperature by cryo-TEM.

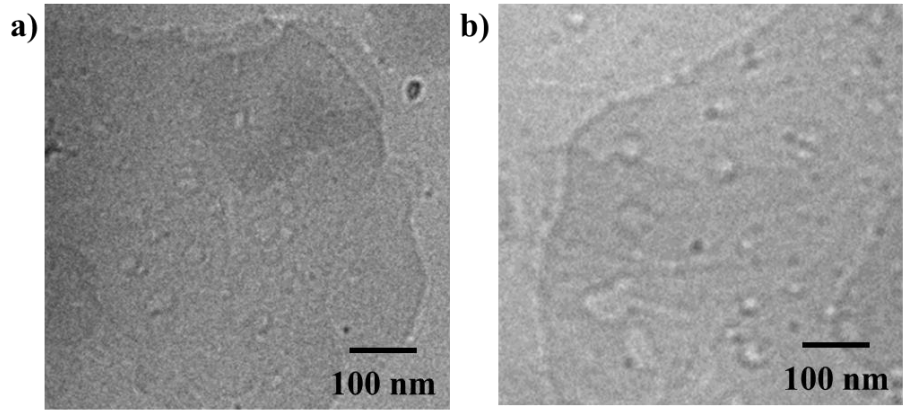

Figure 4.12. Cryo-TEM images of xanthone-derived amphiphiles in water (1 mg/mL) at room temperature. a) **4.33**; stacked sheets. b) **4.34**; stacked sheets.

Self-assemblies of both xanthone-derived amphiphiles **4.33** (*m* = 4) and **4.34** (*m* = 6) showed µm-size stacked sheets by cryo-TEM (Figure 4.12). The sheets were not very homogeneous and the longer hydrophilic ethyleneglycol chain did not have a pronounced effect on the morphology of the self-assembled structures.

4.6 Anthrone- and anthraquinone-derived amphiphiles

4.6.1 Synthesis of anthrone-derived amphiphiles with ether-linked alkyl chains

The envisioned synthesis of an anthrone-derived amphiphile is based on the two-step synthesis of dimethoxy anthrone **4.36** (Scheme 4.10), starting from 1,8-dihydroxy anthraquinone as described in literature.[63,64]

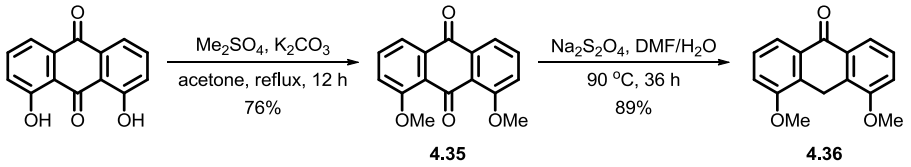

Scheme 4.10. Synthesis of dimethoxy anthrone precursor **4.36**.[63,64]

Protection of 1,8-dihydroxy anthraquinone was performed using dimethylsulfate and potassiumcarbonate in 76% yield.[64] It was found that the conversion drops if less than 2.0 equiv of K_2CO_3 were used, contrary to what is described in literature.[64] Reduction and selective elimination of **4.35** with an excess of sodium dithionite gave full conversion to **4.36**, which was obtained in 89% yield after crystallization from EtOAc.

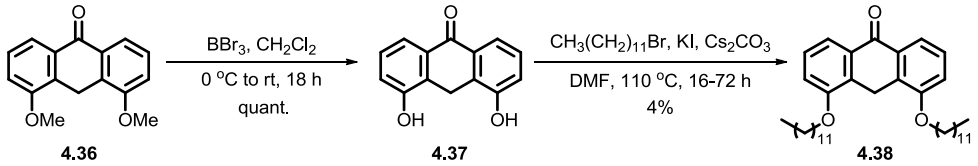

Scheme 4.11. Attempted synthesis of hydrophobic precursor **4.38**.

Deprotection of **4.36** is described in literature with $SnCl_2$ (67% yield), but we opted for the use of BBr_3, given our experience (*vide supra*). Indeed, **4.36** could be deprotected in quantitative yield (Scheme 4.11). The alkylation of diphenol **4.37**, using the procedure that worked well for thioxanthone and xanthone derivatives, gave **4.38** in very low yield (4%), although the conversion was >95%, likely due to the instability of **4.37**. We therefore designed a new route that does not require protection and deprotection of the phenol moieties, but is based on alkylation, followed by selective reduction, starting from 1,8-dihydroxy anthraquinone.

It is known that the phenol moieties of 1,8-dihydroxy anthraquinone are not very reactive due to ion-pairing of the deprotonated species, causing precipitation from organic solvent.[65] Robello and coworkers reported an approach based on phase-transfer, which circumvents the precipitation issue.[65] This reaction, utilizing KI, tetrabutylammoniumbromide (TBAB) and KOH in a biphasic chlorobenzene/water medium, resulted in alkylation of 1,8-dihydroxy anthraquinone with laurylbromide to give **4.39** in 94% yield (Scheme 4.12).

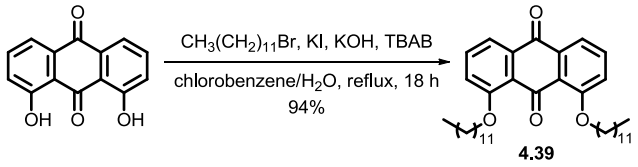

Scheme 4.12. Alkylation of 1,8-dihydroxy anthraquinone to give hydrophobic precursor **4.39**.

The proposed mechanism of this reaction is interesting and shown in Scheme 4.13.

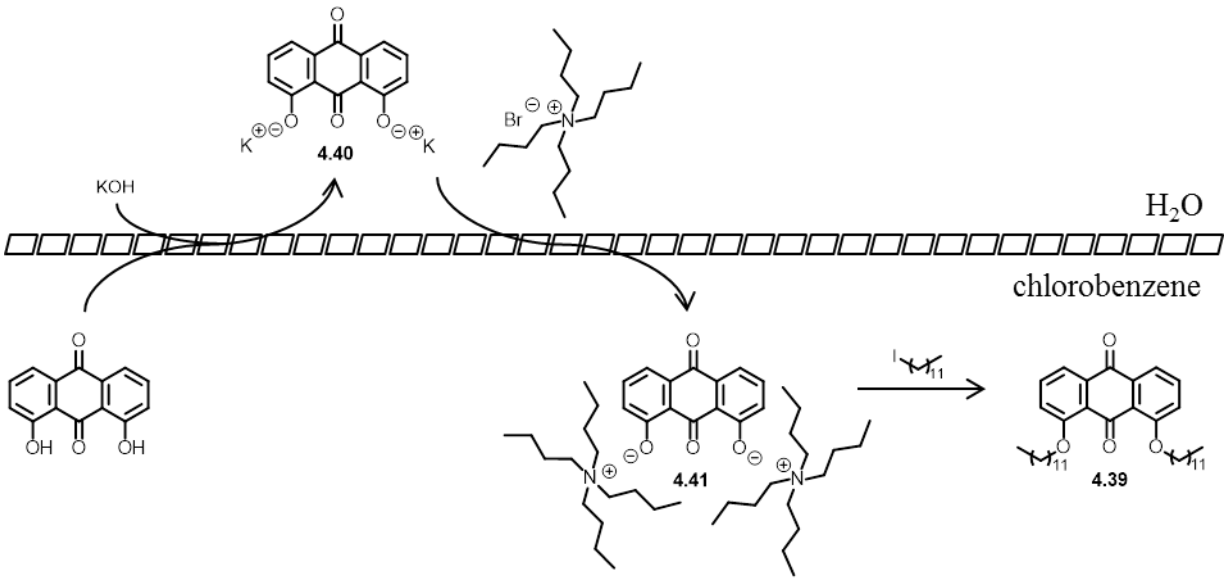

Scheme 4.13. Proposed mechanism of alkylation of 1,8-dihydroxy anthraquinone in a biphasic system.

After deprotonation of 1,8-dihydroxy anthraquinone, the ionic species, **4.40** dissolves in the water layer. Here, the potassium counterions are replaced by tetrabutylammonium cations, making the ionic species, **4.41**, soluble in the organic phase again. It now attacks lauryliodide, which was formed *in situ* by reaction of laurylbromide and KI, to give the product **4.39**.

With di-alkylated **4.39** in hand, the selective reduction with sodium dithionite was attempted, following the same procedure as in Scheme 4.10.

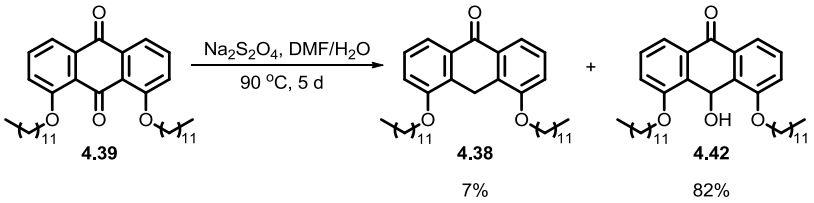

Scheme 4.14. Attempted reduction of anthraquinone **4.39** to anthrone **4.38**.[63]

While the reduction and subsequent elimination with sodium dithionite[63] worked well for dimethoxy substituted anthraquinone **4.35**, under the same conditions, no significant product formation for **4.39** (bearing two long alkyl chains) was accomplished (Scheme 4.14). We found that the reduction to the diol does not take place under these conditions, but stops after the mono-alcohol **4.42** is formed even in the presence of a large excess (40 equiv) of the reducing agent and after prolonging the reaction time from 36 h to 5 d.

Using $NaBH_4$ as the reducing agent instead, led to high conversion to the diol (Scheme 4.15).

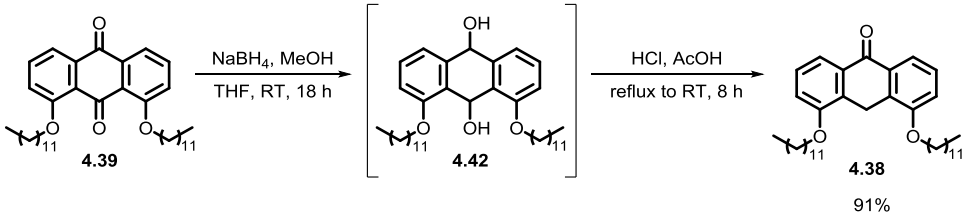

Scheme 4.15. Reduction of anthraquinone **4.39** and elimination to form anthrone **4.38**.

Adding several portions of $NaBH_4$ and MeOH over time to a solution of **4.39** in THF and subsequent workup gave presumed diol **4.42**. Stirring the crude solid in a 1:1 mixture of HCl and acetic acid yielded anthrone **4.38** in a convenient way and in 91% over the two steps (Scheme 4.15).

Conversion of **4.38** into the oxime derivative proved to be problematic (Scheme 4.16).

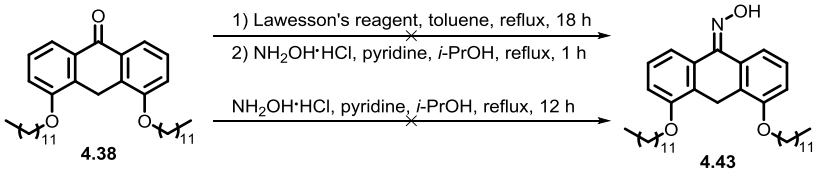

Scheme 4.16. Attempted synthesis of oxime intermediate **4.43**, bearing long alkyl chains.

Reaction of **4.38** with Lawesson's reagent, in order to generate the thioketone, resulted in a complex mixture of products. We employ this reaction to increase the reactivity of the ketone and subsequent conversion into the oxime with hydroxyl amine. Direct conversion into the oxime in *i*-PrOH under reflux did not lead to any conversion (Scheme 4.16). The issue with the conversion of ketone **4.38** into its corresponding oxime **4.43** is likely due to the tautomerization which favors the anthranol form under basic conditions or at high temperature (Scheme 4.17).[66–68]

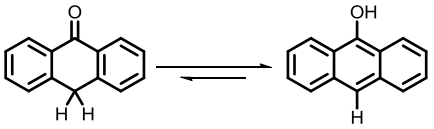

Scheme 4.17. Keto-enol tautomerization between anthrone and anthranol, favoring the enol form under basic conditions or at higher temperature.[66–68]

One solution would be to di-alkylate **4.38** so that the tautomerization is no longer possible.[69] This work has been partially successful, but is beyond the scope of this chapter and the reader is referred to the Master thesis of Anja Huizing.[36]

4.6.2 Synthesis of anthranone amphiphiles with ether-linked alkyl chains

As we were unsuccessful in the conversion of anthrone **4.38** into its oxime derivative **4.43**, we decided to convert anthraquinone **4.39** to the oxime and synthesize the envisioned amphiphile with an extra ketone functionality.

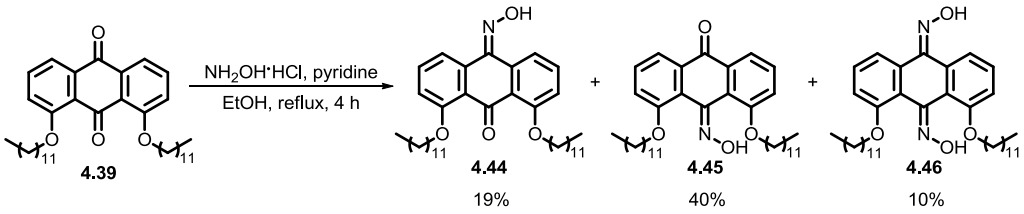

Scheme 4.18. Synthesis of anthraquinone oxime intermediate **4.44**.

When applying the conditions as described earlier, to convert **4.39** to the oxime, both regioisomers of the oxime **4.44** and **4.45** were obtained as well as the di-oxime **4.46** (Scheme 4.18). We did not identify which isomer of **4.46** was obtained and *cis*-**4.46** is drawn arbitrarily. This reaction can likely be optimized to favor the formation of **4.44** over the other products, but with 19% yield of the desired oxime, we proceeded to synthesize the target amphiphile.

The use of monotosyl-tetra-ethyleneglycol as the electrophile, led to purification problems and while amphiphile **4.48** could be synthesized, we were unable to separate it from the monotosyl-tetra-ethyleneglycol by column chromatography, washing or recrystallization. We opted for the use of monobromo-ethyleneglycol instead and the tosyl moiety was therefore converted into bromide with LiBr (Scheme 4.19).[70]

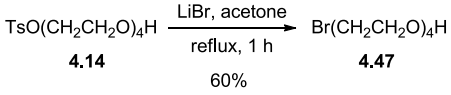

Scheme 4.19. Conversion of monotosyl-tetra-ethyleneglycol **4.14** into its bromide derivative **4.47**.[70]

Substitution of the tosyl moiety by bromine yields **4.47** in 60% yield. The monobromo-tetra-ethyleneglycol was now used as an electrophile in the reaction with oxime **4.44** (Scheme 4.20).

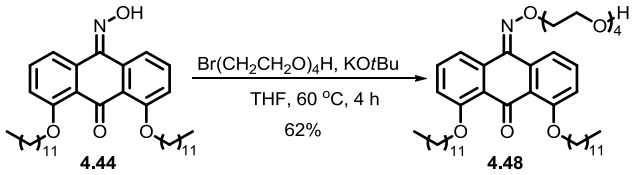

Scheme 4.20. Synthesis of amphiphile **4.48**.

Target anthraquinone-derived amphiphile **4.48** could be purified from the electrophile by column chromatography and was obtained in 62% yield. For future synthesis, the use of monobromo-ethyleneglycol would be recommended over the use of monotosyl-ethyleneglycol.

4.6.3 Morphology of anthranone amphiphiles with ether-linked alkyl chains

With amphiphile **4.48** in hand, we studied its self-assembly by Cryo-TEM. Unfortunately, however, we were unable to detect any self-assembled structures for the anthraquinone-derived amphiphile.

4.7 Conclusions

The synthesis of six different aromatic, amphiphilic structures was studied and the results are described in this chapter. We envisioned the synthesis of thioxanthone-, xanthone- and anthrone-derived amphiphiles bearing a hydrophilic ethyleneglycol headgroup and two hydrophobic alkyl chains, connected to the aromatic core through either an ether-linkage or a C-C linkage.

Convenient synthetic methods were developed for the preparation of thioxanthone-derived amphiphiles in which the hydrophobic tails are connected through an ether-linkage. The C-C linked analogues proved difficult to synthesize. In general, the synthesis of C-C linked alkyl-appended aromatic systems through *ortho*-lithiation proved to be a challenging task and was thus far only successful for xanthone-derived amphiphiles. Preparation of anthrone-based amphiphiles proved to be especially challenging and while we successfully synthesized an anthraquinone-based amphiphile, anthrone-derived amphiphiles could not be obtained due to the lack of reactivity of their carbonyl group.

We were able to synthesize C-C linked xanthone-, ether-linked thioxanthone- and ether-linked anthraquinone-derived amphiphiles. Of these, we prepared a small library of systematically varied thioxanthone-derived amphiphiles bearing hydrophobic and hydrophilic moieties of different length. This allows comparison of their morphologies. Making comparisons between the other amphiphiles, however, is not possible at this time due to lack of a sufficient amount of

different amphiphiles. Self-assembled structures of both xanthone-derived (**4.33** and **4.34**) and anthraquinone amphiphiles (**4.48**) were not homogeneous and ill-defined.

Furthermore, a fine balance between hydrophilicity and hydrophobicity must be found to ensure self-assembly.[27–30] If either the hydrophobic part is too large, the amphiphile is too insoluble and self-assembly will not be possible, as observed for **4.19** (thioxanthone-derived, n = 11, m = 3). On the other hand, if the amphiphile is too hydrophilic, the amphiphile is too soluble and no aggregates could be observed either, for example **4.18** (thioxanthone-derived, n = 7, m = 6).

Increasing the alkyl chain length, i.e. the hydrophobic part of these type of amphiphiles (from n = 7 to n = 11 to n = 13), increases the temperature needed to form the same type of aggregates. These findings are in line with what has been reported for amphiphiles in general.[31,43,44] Increasing the hydrophilic part increased the solubility, i.e. the ability of the amphiphile to be hydrated. However, the change in hydration is not predictable enough to make good use of it in all cases. We expected **4.25** (thioxanthone-derived, n = 15, m = 8) to give better properties than **4.24** (thioxanthone-derived, n = 15, m = 6) for example, but similar ill-defined plates were observed at useful temperatures.

In conclusion, a library of systematically varied amphiphiles was synthesized and studied. Within the different subclasses of these amphiphiles, based on their aromatic core, useful comparisons could be made. The obtained knowledge of the thioxanthone-based amphiphilic family has led to the development of highly interesting, conducting bilayer systems and is described in chapter 5.

4.8 Experimental section

General remarks

Starting materials were commercially available and used without further purification. Melting points were determined on a Büchi melting point B-545 apparatus. ^{1}H NMR spectra were recorded on a Varian MR400 (at 400 MHz) at ambient temperature. The splitting patterns are designated as follows: s (singlet); d (doublet); dd (double doublet); t (triplet); q (quartet); quint (quintet); m (multiplet) and br (broad). ^{13}C NMR spectra were recorded on a Varian MR400 (100.6 MHz) at ambient temperature. Chemical shifts are denoted in δ (ppm), referenced to the residual protic solvent peak. Coupling constants *J*, are denoted in Hz. Masses were recorded with a Thermo scientific LTQ Orbitrap XL mass spectrometer. Drying of solutions was performed with $MgSO_4$ or Na_2SO_4 and solvents were removed with a rotatory evaporator. Silicycle Siliaflash P60, 40-63 m, (230–400 mesh) was used for column chromatography. Thin-layer chromatography (TLC) was performed on commercial Kieselgel 60F, 254 silica gel plates and compounds were visualized with UV light (λ = 254 nm) or $KMnO_4$ stain. Reagents and starting materials were used as obtained from Sigma-Aldrich or Acros.

Synthesis

The synthesis of ketone **3.8** is described in chapter 3.

4,5-Dihydroxy-9*H*-thioxanthen-9-one (3.9)

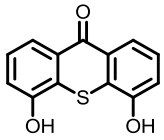

Compound **3.8** (2.0 g, 7.3 mmol, 1.0 equiv) was dissolved in dry CH_2Cl_2 (200 mL) under a nitrogen atmosphere and a 1 M boron tribromide solution (in CH_2Cl_2, 37 mL, 37 mmol, 5.0 equiv) was added dropwise at 0 °C. The mixture was allowed to warm to RT overnight. After cooling the mixture with an ice bath, water (150 mL) was slowly added and the layers separated. The organic layer was extracted with an 3 M aq. NaOH solution (3 x 150 mL). The waterlayer was subsequently acidified to pH = 1 with an 2 M aq. HCl solution and filtered through a glass filter. The residual cake was redissolved in acetone and concentrated in vacuo to yield **3.9** as a green solid (1.8 g, 7.3 mmol, quant.). m.p. 250 – 255 °C (dec); ^{1}H NMR (300 MHz, DMSO-d_6): δ = 10.98 (s, 2H, OH); 7.94 (d, *J* = 7.7 Hz, 2H); 7.38 (dd, *J* = 7.7, 7.7 Hz, 2H); 7.20 (d, *J* =7.7 Hz, 2H) ppm; ^{13}C NMR (50 MHz, DMSO-d_6): δ = 180.0, 153.7, 130.0, 127.0, 126.0, 119.9, 117.2 ppm; HRMS-APCI+ *m/z* calculated for $C_{13}H_9O_3S$ $[M + H]^+$ 245.0267, found 245.0259.

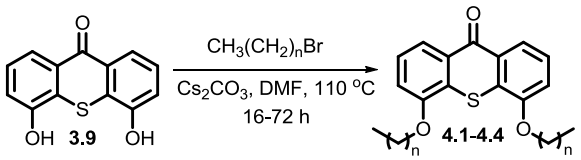

Scheme 4.21. General procedure for alkylation of diphenol **3.9**.

General procedure for the alkylation of 4,5-dihydroxy-9*H*-thioxanthen-9-one (3.9): Compound **3.9** (0.50 g, 2.0 mmol, 1.0 equiv) was dissolved in dry DMF (50 mL). Cs_2CO_3 (3.3 g, 10 mmol, 5.0 equiv) and alkylbromide (5.3 mmol, 2.6 equiv) were added and the mixture heated to 110 °C for 16 h. After cooling down to RT, the reaction mixture was filtered over celite and the solvent was removed by rotary evaporation. CH_2Cl_2 (50 mL) and H_2O (50 mL) were added and the layers separated. The aqueous layer was extracted with CH_2Cl_2 (2 x 50 mL) and the combined organic layers dried over $MgSO_4$, filtered and concentrated in vacuo.

4,5-Bis(octyloxy)-9*H*-thioxanthen-9-one (4.1)

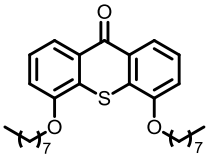

Synthesized according to the general procedure from **3.9** (0.21 g, 0.86 mmol, 1.0 equiv) and 1-bromooctane (0.40 mL, 2.2 mmol, 2.6 equiv). Purification by column chromatography (dry load, SiO_2, flash, CH_2Cl_2/*n*-pentane 1:1) gave **4.1** as a yellow solid (0.26 g, 0.55 mmol, 64%). ^{1}H NMR (400 MHz, $CDCl_3$) δ = 8.24 (d, *J* = 8.1 Hz, 2H), 7.42 (t, *J* = 8.0 Hz, 2H), 7.13 (d, *J* = 7.9 Hz, 2H), 4.19 (t, *J* = 6.4 Hz, 4H), 2.05 – 1.84 (m, 4H), 1.66 – 1.50 (m, 4H), 1.36 (m, 16H), 0.89 (t, *J* = 6.7 Hz, 6H) ppm; ^{13}C NMR (100.6 MHz, $CDCl_3$) δ = 180.4, 154.4, 130.0, 128.4, 125.8, 121.3, 113.1, 69.5, 31.8, 29.3, 29.3, 29.1, 26.1, 22.7, 14.1 ppm; HRMS-ESI+ *m*/*z* calculated for $C_{29}H_{41}O_3S$ $[M + H]^+$ 469.2771, found 469.2765.

4,5-Bis(dodecyloxy)-9*H*-thioxanthen-9-one (4.2)

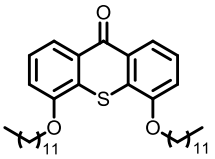

Synthesized according to the general procedure from **3.9** (0.50 g, 2.0 mmol, 1.0 equiv) and 1-bromododecane (1.3 mL, 5.3 mmol, 2.6 equiv). Purification by recrystallization from EtOH gave **4.2** as a yellow-brown solid (0.54 g, 1.8 mmol, 90%). mp 78 – 79 °C; ^{1}H NMR (400 MHz, $CDCl_3$) δ = 8.23 (d, *J* = 8.1 Hz, 2H), 7.41 (t, *J* = 8.1 Hz, 2H), 7.12 (d, *J* = 8.0 Hz, 2H), 4.18 (t, *J* = 6.4 Hz, 4H), 2.00 – 1.85 (m, 4H), 1.65 – 1.55 (m, 4H), 1.44 – 1.20 (m, 16H), 0.87 (m, 6H) ppm; ^{13}C NMR (100.6 MHz, $CDCl_3$) δ = 180.4, 154.4, 130.0, 128.4, 125.8, 121.2, 113.0, 69.4, 31.9, 29.7, 29.6, 29.3, 29.0, 26.0, 22.7, 14.1 ppm; HRMS-APCI+ *m*/*z* calculated for $C_{37}H_{57}O_3S$ $[M + H]^+$ 581.4023, found 581.4002.

4,5-Bis(tetradecyloxy)-9*H*-thioxanthen-9-one (4.3)

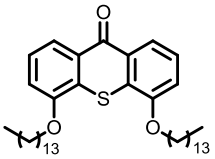

Synthesized according to the general procedure from **3.9** (0.55 g, 2.2 mmol, 1.0 equiv) and 1-bromotetradecane (1.7 mL, 5.8 mmol, 2.6 equiv). Purification by column chromatography (dry load, SiO_2, flash, CH_2Cl_2/*n*-pentane 1:1) gave **4.3** as a yellow solid (1.0 g, 1.6 mmol, 73%). mp 106 – 107 °C; ^{1}H NMR (400 MHz, $CDCl_3$) δ = 8.23 (d, *J* = 8.1 Hz, 2H), 7.42 (t, *J* = 8.0 Hz, 2H), 7.13 (d, *J* = 7.9 Hz, 2H), 4.19 (t, *J* = 6.5 Hz, 4H), 2.00 – 1.87 (m, 4H), 1.67 – 1.50 (m, 4H), 1.45 – 1.16 (m, 20H), 0.87 (t, *J* = 6.7 Hz, 6H) ppm; ^{13}C NMR (100.6 MHz, $CDCl_3$) δ = 180.4, 154.4, 130.0, 128.4, 125.8, 121.3, 113.0, 69.5, 31.9, 29.7, 29.7, 29.7, 29.5, 29.4, 29.1, 26.1, 22.7, 14.1 ppm; HRMS-ESI+ *m*/*z* calculated for $C_{41}H_{65}O_3S$ $[M + H]^+$ 637.4649, found 637.4637.

4,5-Bis(hexadecyloxy)-9*H*-thioxanthen-9-one (4.4)

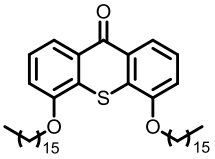

Synthesized according to the general procedure from **3.9** (1.3 g, 5.5 mmol, 1.0 equiv) and 1-bromohexadecane (4.4 mL, 14 mmol, 2.6 equiv). Purification by recrystallization from EtOH gave **4.4** as a yellow solid (2.8 g, 4.0 mmol, 73%). mp 101 – 102 °C; ^{1}H NMR (400 MHz, $CDCl_3$) δ = 8.23 (d, *J* = 8.2 Hz, 2H), 7.42 (t, *J* = 8.0 Hz, 2H), 7.13 (d, *J* = 7.9 Hz, 2H), 4.19 (t, *J* = 5.7 Hz, 4H), 2.03 – 1.88 (m, 4H), 1.64 – 1.54 (m, 4H), 1.50 – 1.16 (m, 48H), 0.88 (t, *J* = 7.0 Hz, 6H) ppm; ^{13}C NMR (100.6 MHz, $CDCl_3$) δ = 180.5, 154.4, 130.0, 128.5, 125.8, 121.3, 113.1, 69.5, 58.4, 31.9, 29.7, 29.7, 29.4, 29.1, 26.1, 22.7, 18.4, 14.1 ppm; HRMS-ESI+ *m*/*z* calculated for$C_{45}H_{73}O_3S$ $[M + H]^+$ 693.5275, found 693.5267.

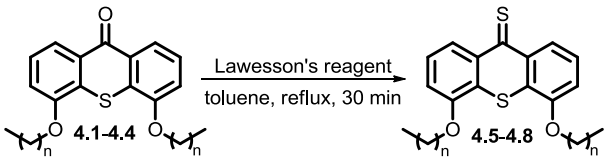

Scheme 4.22. General procedure for conversion of ketones **4.1**-**4.4** to thioketones **4.5**-**4.8**.

General procedure for the thiation of 4,5-bis(alkoxy)-9*H*-thioxanthen-9-one: The ketone starting material (3.4 mmol, 1.0 equiv) was dissolved in toluene (100 mL) and Lawesson's reagent (10.3 mmol, 3.0 equiv) was added. The reaction mixture was heated at reflux for 30 min. The solvent was subsequently removed by rotary evaporation.

4,5-Bis(octyloxy)-9*H*-thioxanthene-9-thione (4.5)

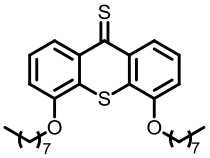

Synthesized according to the general procedure for thiation from **4.1** (0.26 g, 0.55 mmol, 1.0 equiv). Purification by column chromatography (SiO_2, flash, CH_2Cl_2/*n*-pentane 1:2) gave **4.5** as a green sticky solid (0.27 g, 0.55 mmol, quant.). ^{1}H NMR (400 MHz, $CDCl_3$) δ = 8.66 (d, *J* = 8.5 Hz, 2H), 7.34 (t, *J* = 7.1 Hz, 2H), 7.06 (d, *J* = 7.9 Hz, 2H), 4.13 (t, *J* = 6.4 Hz, 4H), 1.98 – 1.85 (m, 4H), 1.63 – 1.50 (m, 4H), 1.44 – 1.21 (m, 16H), 0.89 (t, *J* = 6.8 Hz, 6H) ppm; ^{13}C NMR (100.6 MHz, $CDCl_3$) δ = 210.7, 154.5, 138.3, 126.3, 125.1, 124.0, 112.1, 69.7, 31.9, 29.4, 29.4, 29.1, 26.1, 22.7, 21.5, 14.1 ppm; HRMS-ESI+ *m*/*z* calculated for $C_{29}H_{41}O_2S_2$ $[M + H]^+$ 485.2542, found 485.2535.

4,5-Bis(dodecyloxy)-9*H*-thioxanthen-9-thione (4.6)

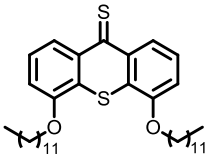

Synthesized according to the general procedure for thiation from **4.2** (2.0 g, 3.4 mmol, 1.0 equiv). Purification by column chromatography (SiO_2, flash, CH_2Cl_2/*n*-pentane 1:2) gave **4.6** as a green solid (2.0 g, 3.4 mmol, quant.). mp 78 – 79 °C; ^{1}H NMR (400 MHz, $CDCl_3$) δ = 8.66 (d, *J* = 8.5 Hz, 2H), 7.36 (t, *J* = 8.2 Hz, 2H), 7.10 (d, *J* = 7.8 Hz, 2H), 4.19 (t, *J* = 6.4 Hz, 4H), 2.02 – 1.86 (m, 4H), 1.67 – 1.54 (m, 4H), 1.48 – 1.15 (m, 32H), 0.87 (t, *J* = 6.7 Hz, 6H) ppm; ^{13}C NMR (100.6 MHz, $CDCl_3$) δ = 210.8, 154.5, 138.3, 126.3, 125.1, 124.0, 112.1, 69.6, 31.9, 29.7, 29.7, 29.4, 29.1, 26.1, 22.7, 14.1 ppm; HRMS-ESI+ *m*/*z* calculated for $C_{37}H_{57}O_2S_2$ $[M + H]^+$ 597.3794, found 597.3783.

4,5-Bis(tetradecyloxy)-9*H*-thioxanthene-9-thione (4.7)

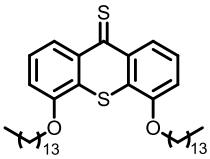

Synthesized according to the general procedure for thiation from **4.3** (0.40 g, 0.85 mmol, 1.0 equiv). Purification by column chromatography (SiO_2, flash, CH_2Cl_2/*n*-pentane 1:2) gave **4.7** as a green sticky solid (0.35 g, 0.72 mmol, 85%). ^{1}H NMR (400 MHz, $CDCl_3$) δ = 8.66 (d, *J* = 8.5 Hz, 2H), 7.36 (t, *J* = 8.2 Hz, 2H), 7.10 (d, *J* = 7.8 Hz, 2H), 4.18 (t, *J* = 6.4 Hz, 4H), 1.99 – 1.87 (m, 4H), 1.63 – 1.54 (m, 4H), 1.46 – 1.19 (m, 40H), 0.87 (t, *J* = 6.6 Hz, 6H) ppm; ^{13}C NMR (100.6 MHz, $CDCl_3$) δ = 210.7, 154.5, 138.3, 126.3, 125.1, 123.9, 12.1, 69.6, 31.9, 29.7, 29.7, 29.4, 29.1, 26.1, 22.7, 14.1 ppm; HRMS-ESI+ *m*/*z* calculated for $C_{41}H_{65}O_2S_2$ $[M + H]^+$ 653.4420, found 653,4427.

4,5-Bis(hexadecyloxy)-9*H*-thioxanthene-9-thione (4.8)

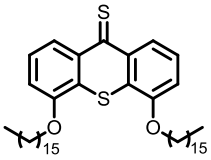

Synthesized according to the general procedure for thiation from **4.4** (2.0 g, 2.8 mmol, 1.0 equiv). Purification by column chromatography (SiO_2, flash, CH_2Cl_2/*n*-pentane 1:2) gave **4.8** as a green solid (1.4 g, 2.0 mmol, 71%). mp 101 – 102 °C; ^{1}H NMR (400 MHz, $CDCl_3$) δ = 8.66 (d, *J* = 8.5 Hz, 2H), 7.36 (t, *J* = 8.2 Hz, 2H), 7.10 (d, *J* = 7.9 Hz, 2H), 4.19 (t, *J* = 6.4 Hz, 4H), 2.03 – 1.87 (m, 4H), 1.68 – 1.55 (m, 4H), 1.47 – 1.19 (m, 48H), 0.88 (t, *J* = 6.8 Hz, 6H) ppm; ^{13}C NMR (100.6 MHz, $CDCl_3$) δ = 210.7, 154.5, 138.3, 126.3, 125.1, 124.0, 112.1, 69.6, 31.9, 29.7, 29.7, 29.4, 29.1, 26.1, 22.7, 14.1 ppm; HRMS-ESI+ *m*/*z* calculated for $C_{45}H_{73}O_2S_2$ $[M + H]^+$ 709.5047, found 709.5046.

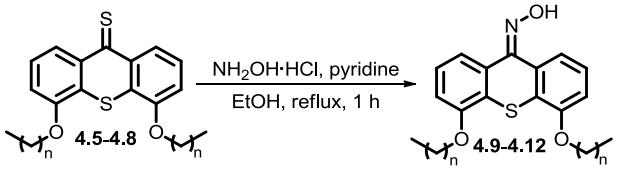

Scheme 4.23. General procedure for conversion of thioketones **4.5**-**4.8** to oximes **4.9**-**4.12**.

General procedure for oxime formation of 4,5-bis(alkoxy)-9*H*-thioxanthen-9-thione: The thioketone starting material (2.0 mmol, 1.0 equiv) was dissolved in EtOH (75 mL) and hydroxyl amine hydrochloride (0.54 g, 7.7 mmol, 4.0 equiv) and pyridine (1.6 mL, 19 mmol, 10 equiv) were added. The reaction mixture was heated at reflux for 4 h. The solvent was removed by rotary evaporation and CH_2Cl_2 (50 mL) and H_2O (25 mL) were added and the layers separated. The aqueous layer was extracted with CH_2Cl_2 (2 x 25 mL) and the combined organic layers dried over $MgSO_4$, filtered and concentrated in vacuo.

4,5-Bis(octyloxy)-9*H*-thioxanthen-9-one oxime (4.9)

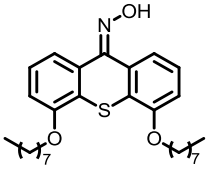

Synthesized according to the general procedure for oxime formation from **4.5** (0.27 g, 0.55 mmol, 1.0 equiv). Purification by column chromatography (dry load, SiO_2, flash, 10% – 20% EtOAc in *n*-pentane) gave **4.9** as a white solid (0.24 g, 0.51 mmol, 92%). mp 105 – 106 °C; ^{1}H NMR (400 MHz, $CDCl_3$) δ = 9.16 (br, 1H), 8.04 (d, *J* = 8.0 Hz, 1H), 7.46 (d, *J* = 7.8 Hz, 1H), 7.30 – 7.20 (m, 2H), 6.90 (t, *J* = 8.5 Hz, 2H), 4.14 – 4.04 (m, 4H), 1.99 – 1.81 (m, 4H), 1.70 – 1.48 (m, 4H), 1.48 – 1.20 (m, 16H), 0.89 (t, *J* = 6.8 Hz, 6H) ppm; ^{13}C NMR (100.6 MHz, $CDCl_3$) δ = 154.6, 154.2, 148.6, 131.0, 126.8, 125.7, 125.1, 124.4, 123.4, 122.7, 118.3, 111.6, 110.8, 69.3, 69.1, 31.9, 29.4, 29.3, 29.17, 29.16, 26.10, 26.09, 22.7, 14.2 ppm; HRMS-ESI+ *m*/*z* calculated for $C_{29}H_{42}NO_3S$ $[M + H]^+$ 484.2880, found 484.2876.

4,5-Bis(dodecyloxy)-9*H*-thioxanthen-9-one oxime (4.10)

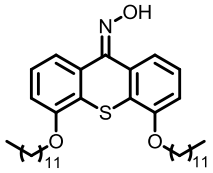

Synthesized according to the general procedure for oxime formation from **4.6** (1.0 g, 1.7 mmol, 1.0 equiv). Purification by column chromatography (dry load, SiO_2, flash, *n*-pentane/EtOAc 10:1) gave **4.10** as a white solid (0.91 g, 1.5 mmol, 90%). mp 103 – 104 °C; ^{1}H NMR (400 MHz, $CDCl_3$) δ = 8.02 (d, *J* = 8.1 Hz, 1H), 7.74 (br, 1H), 7.47 (d, *J* = 7.9 Hz, 1H), 7.33 – 7.17 (m, 2H), 6.90 (t, *J* = 8.4 Hz, 2H), 4.13 – 4.06 (m, 4H), 1.94 – 1.83 (m, 4H), 1.60 – 1.49 (m, 4H), 1.46 – 1.13 (m, 32H), 0.88 (t, *J* = 6.9 Hz, 6H) ppm; ^{13}C NMR (100.6 MHz, $CDCl_3$) δ = 154.6, 154.2, 149.1, 131.0, 126.6, 125.6, 125.0, 124.4, 123.3, 122.7, 118.4, 111.5, 110.7, 69.3, 69.1, 31.9, 29.71, 29.67, 29.64, 29.40, 29.37, 29.13, 26.05, 26.04, 22.7, 14.1 ppm; HRMS-ESI+ *m*/*z* calculated for $C_{37}H_{58}NO_3S$ $[M + H]^+$ 596.4132, found 596.4127.

4,5-Bis(tetradecyloxy)-9*H*-thioxanthen-9-one oxime (4.11)

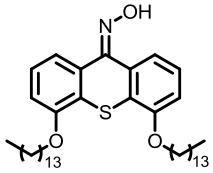

Synthesized according to the general procedure for oxime formation from **4.7** (0.35 g, 0.72 mmol, 1.0 equiv). Purification by column chromatography (dry load, SiO_2, flash, *n*-pentane/EtOAc 10:1) gave **4.11** as an off-white solid (0.38 g, 0.59 mmol, 82%). mp 114 – 115 °C; ^{1}H NMR (400 MHz, $CDCl_3$) δ = 8.01 (d, *J* = 7.1 Hz, 1H), 7.52 (br, 1H), 7.47 (d, *J* = 7.9 Hz, 1H), 7.25 – 7.20 (m, 2H), 6.90 (t, *J* = 8.9 Hz, 2H), 4.14 – 4.03 (m, 4H), 1.93 – 1.80 (m, 4H), 1.61 – 1.47 (m, 4H), 1.43 – 1.20 (m, 40H), 0.88 (t, *J* = 6.9 Hz, 6H) ppm; ^{13}C NMR (100.6 MHz, $CDCl_3$) δ = 154.6, 154.2, 149.0, 131.0, 126.6, 125.6, 125.0, 124.4, 123.3, 122.7, 118.4, 111.5, 110.8, 69.3, 69.1, 31.9, 29.72, 29.67, 29.65, 29.41, 29.37, 29.13, 26.05, 26.04, 22.7, 14.1 ppm; HRMS-ESI+ *m*/*z* calculated for $C_{41}H_{66}NO_3S$ $[M + H]^+$ 652.4758, found 652.4751.

4,5-Bis(hexadecyloxy)-9*H*-thioxanthen-9-one oxime (4.12)

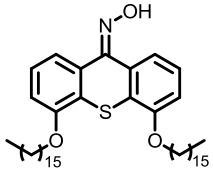

Synthesized according to the general procedure for oxime formation from **4.8** (1.4 g, 2.0 mmol, 1.0 equiv). Purification by column chromatography (dry load, SiO_2, flash, *n*-pentane/EtOAc 10:1) gave **4.12** as a white solid (1.2 g, 1.6 mmol, 82%). mp 118 – 119 °C; ^{1}H NMR (400 MHz, $CDCl_3$) δ = 8.02 (d, *J* = 8.1 Hz, 1H), 7.96 (br, 1H), 7.46 (d, *J* = 7.9 Hz, 1H), 7.29 – 7.20 (m, 2H), 6.90 (t, *J* = 8.4 Hz, 2H), 4.16 – 4.02 (m, 4H), 1.94 – 1.81 (m, 4H), 1.60 – 1.50 (m, 4H), 1.46 – 1.17 (m, 48H), 0.88 (t, *J* = 6.8 Hz, 6H) ppm; ^{13}C NMR (100.6 MHz, $CDCl_3$) δ = 154.6, 154.2, 149.1, 131.0, 126.6, 125.6, 125.0, 124.3, 123.3, 122.7, 118.4, 111.5, 110.7, 69.3, 69.1, 31.9, 29.72,

29.66, 29.65, 29.41, 29.36, 29.13, 26.05, 26.04, 22.7, 14.1 ppm; HRMS-ESI+ *m/z* calculated for $C_{45}H_{74}NO_3S$ [M + H]$^+$ 708.5384, found 708.5387.

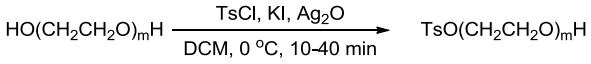

Scheme 4.24. General procedure for mono-tosylation of ethyleneclycols to give **4.13**-**4.16**.[42]

General procedure for mono-tosylation of ethyleneglycols: Mono-tosylated glycols were synthesized according to an adapted literature procedure.[42] *m*-Ethyleneglycol (0.83 mmol, 1.0 equiv) was dissolved in CH_2Cl_2 (15 mL) and the solution was cooled to 0 °C. Then, Ag_2O (0.29 g, 1.2 mmol, 1.5 equiv), tosylchloride (0.17 g, 0.91 mmol, 1.1 equiv) and KI (28 mg, 0.17 mmol, 0.20 equiv) were added. The reaction mixture was stirred at 0 °C until all tosylchloride had reacted. The suspension was then filtered through a silica plug and the plug washed with CH_2Cl_2. The solvent was removed by rotary evaporation.

Tri-ethyleneglycol-monotosylate (4.13)

$TsO(CH_2CH_2O)_3H$

Synthesized according to the general procedure for mono-tosylation of ethyleneglycols from tri-ethyleneglycol (30 mL, 33 mmol, 1.0 equiv). Purification by column chromatography (SiO_2, flash, 0% – 10% MeOH in CH_2Cl_2) gave **4.13** as a colorless oil (9.2 g, 30 mmol, 90%). Experimental data of **4.13** is in accordance with that reported.[42] ^{1}H NMR (400 MHz, $CDCl_3$) δ = 7.80 (d, *J* = 8.3 Hz, 2H), 7.34 (d, *J* = 8.4 Hz, 2H), 4.18 – 4.14 (m, 4H), 3.73 – 3.67 (m, 4H), 3.61 (s, 4H), 3.59 – 3.54 (m, 2H), 2.44 (s, 3H), 2.08 (br, 1H) ppm; HRMS-ESI+ *m/z* calculated for $C_{13}H_{21}O_6S$ [M + H]$^+$ 305.1053, found 305.1054.

Tetra-ethyleneglycol-monotosylate (4.14)

$TsO(CH_2CH_2O)_4H$

Synthesized according to the general procedure for mono-tosylation of ethyleneglycols from tetra-ethyleneglycol (2.5 g, 13 mmol, 1.0 equiv). Purification by column chromatography (SiO_2, flash, 0% – 10% MeOH in CH_2Cl_2) gave **4.14** as a colorless oil (4.0 g, 11 mmol, 90%). Experimental data of **4.14** is in accordance with that reported.[71] ^{1}H NMR (400 MHz, $CDCl_3$) δ = 7.80 (d, *J* = 8.3 Hz, 2H), 7.34 (d, *J* = 8.4 Hz, 2H), 4.19 – 4.14 (m, 2H), 3.80 – 3.53 (m, 14H), 2.45 (s, 3H), 1.85 (br, 1H) ppm; HRMS-ESI+ *m/z* calculated for $C_{15}H_{25}O_7S$ [M + H]$^+$ 349.1316, found 349.1311.

Hexa-ethyleneglycol-monotosylate (4.15)

$TsO(CH_2CH_2O)_6H$

Synthesized according to the general procedure for mono-tosylation of ethyleneglycols from hexa-ethyleneglycol (3.1 mL, 3.5 mmol, 1.0 equiv). Purification by column chromatography (SiO_2, flash, 0% – 10% MeOH in CH_2Cl_2) gave **4.15** as a colorless oil (1.4 g, 3.3 mmol, 94%). Experimental data of **4.15** is in accordance with that reported.[72] ^{1}H NMR (400 MHz, $CDCl_3$) δ = 7.80 (d, *J* = 8.2 Hz, 2H), 7.35 (d, *J* = 8.0 Hz, 2H), 4.20 – 4.13 (m, 2H), 3.80 – 3.46 (m, 22H), 2.80 (br, 1H), 2.45 (s, 3H) ppm; HRMS-ESI+ *m/z* calculated for $C_{19}H_{33}O_9S$ [M + H]$^+$ 437.1840, found 437.1830.

Octa-ethyleneglycol-monotosylate (4.16)

$TsO(CH_2CH_2O)_8H$

Synthesized according to the general procedure for mono-tosylation of ethyleneglycols from octa-ethyleneglycol (0.40 g, 1.1 mmol, 1.0 equiv). Purification by column chromatography (SiO_2, flash, 0% – 10% MeOH in CH_2Cl_2) gave **4.16** as a colorless oil (0.40 g, 0.76 mmol, 71%). ^{1}H NMR (400 MHz, $CDCl_3$) δ = 7.80 (d, *J* = 8.3 Hz, 2H), 7.34 (d, *J* = 8.0 Hz, 2H), 4.19 – 4.11 (m, 2H), 3.77 – 3.55 (m, 30H), 2.45 (s, 3H), 1.95 (br, 1H) ppm; ^{13}C NMR (100.6 MHz, $CDCl_3$) δ = 144.7, 132.9, 129.7, 127.8, 72.4, 70.6-69.9, 69.2, 68.5, 61.4, 21.6 ppm; HRMS-ESI+ *m*/*z* calculated for $C_{23}H_{41}O_{11}S$ $[M + H]^+$ 525.2364, found 525.2346.

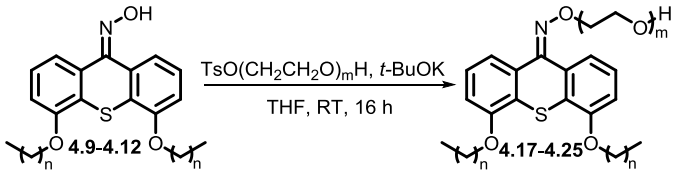

Scheme 4.25. General procedure for the synthesis of amphiphiles **4.17**-**4.25**.

General procedure for installing the glycol moiety: The oxime starting material (0.15 g, 0.21 mmol, 1.0 equiv) was dissolved in THF (15 mL) and *m*-glycol-monotosylate (0.25 mmol, 1.2 equiv) and *t*-BuOK (47 mg, 0.42 mmol, 2.0 equiv) were added and the reaction mixture was stirred at RT for 16 h. H_2O (50 mL) and CH_2Cl_2 (100 mL) were added and the layers were separated. The aqueous layer was extracted with CH_2Cl_2 (50 mL) and the combined organic layers dried over Na_2SO_4, filtered and concentrated in vacuo.

4,5-Bis(octyloxy)-9*H*-thioxanthen-9-one O-tetraethyleneglycol oxime (4.17)

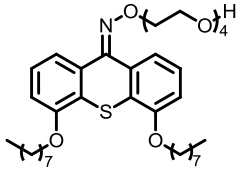

Synthesized according to the general procedure for installing the glycol moiety from **4.14** (50 mg, 0.10 mmol, 1.0 equiv) and **4.9** (44 mg, 0.13 mmol, 1.2 equiv). Purification by column chromatography (SiO_2, flash, 0% – 10% MeOH in CH_2Cl_2) gave **4.17** as a colorless oil (53 mg, 80 µmol, 80%). ^{1}H NMR (400 MHz, $CDCl_3$) δ = 8.01 (d, *J* = 8.1 Hz, 1H), 7.51 (d, *J* = 7.9 Hz, 1H), 7.25 – 7.17 (m, 2H), 6.88 (t, *J* = 7.9 Hz, 2H), 4.44 – 4.32 (m, 2H), 4.08 (t, *J* = 6.0 Hz, 4H), 3.88 – 3.82 (m, 2H), 3.75 – 3.52 (m, 12H), 2.46 (br, 1H), 1.95 – 1.81 (m, 4H), 1.61 – 1.49 (m, 4H), 1.44 – 1.24 (m, 16H), 0.89 (t, *J* = 6.7 Hz, 6H) ppm; ^{13}C NMR (100.6 MHz, $CDCl_3$) δ = 154.5, 154.1, 148.1, 131.2, 126.4, 126.2, 124.9, 124.2, 123.6, 122.5, 118.7, 111.3, 110.6, 74.1, 72.5, 70.66, 70.61, 70.58, 70.33, 69.61, 69.21, 69.11, 61.7, 31.9, 29.36, 29.29, 29.13, 29.11, 26.06, 26.03, 22.7, 14.1 ppm; HRMS-ESI+ *m*/*z* calculated for $C_{37}H_{58}NO_7S$ $[M + H]^+$ 660.3929, found 660.3920.

4,5-Bis(octyloxy)-9*H*-thioxanthen-9-one O-hexaethyleneglycol oxime (4.18)

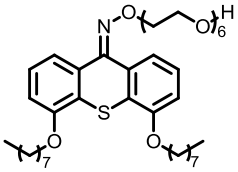

Synthesized according to the general procedure for installing the glycol moiety from **4.15** (40 mg, 0.080 mmol, 1.0 equiv) and **4.9** (43 mg, 0.10 mmol, 1.2 equiv). Purification by column chromatography (SiO_2, flash, 0% – 10 % MeOH in CH_2Cl_2) gave **4.18** as a yellow oil (49 mg, 0.066 mmol, 82%); ^{1}H NMR (400 MHz, $CDCl_3$) δ = 8.01 (d, *J* = 8.1 Hz, 1H), 7.51 (d, *J* = 7.9 Hz, 1H), 7.24 – 7.18 (m, 2H), 6.88 (t, *J* = 8.0 Hz, 2H), 4.41 – 4.34 (m, 2H), 4.09 (t, *J* = 6.5 Hz, 4H), 3.87 – 3.81 (m, 2H), 3.75 – 3.56 (m, 20H), 1.93 – 1.83 (m, 4H), 1.62 – 1.49 (m, 4H), 1.44 – 1.21 (m, 16H), 0.88 (t, *J* = 6.7 Hz, 6H) ppm; ^{13}C NMR (100.6 MHz, $CDCl_3$) δ = 154.5, 154.1, 148.0, 131.2, 126.4, 126.2, 124.9, 124.2, 123.6, 122.5, 118.7, 111.3, 110.6, 74.1, 72.6, 70.63, 70.59, 70.56, 70.54, 70.50, 70.49, 70.46, 70.22, 69.59, 69.21, 69.11, 61.7, 31.9, 29.69, 29.36, 29.29, 29.13, 29.11, 26.05, 26.03, 22.7, 14.1 ppm; HRMS-ESI+ *m*/*z* calculated for $C_{41}H_{66}NO_9S$ $[M + H]^+$ 748.4453, found 748.4456.

4,5-Bis(dodecyloxy)-9*H*-thioxanthen-9-one O-triethyleneglycol oxime (4.19)

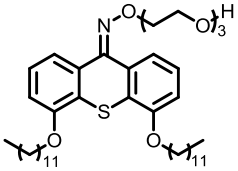

Synthesized according to the general procedure for installing the glycol moiety from **4.13** (56 mg, 94 µmol, 1.0 equiv) and **4.10** (34 mg, 0.11 mmol, 1.2 equiv). Purification by column chromatography (SiO_2, flash, 0% – 10% MeOH in CH_2Cl_2) gave **4.19** as a colorless oil (55 mg, 75 µmol, 80%). ^{1}H NMR (400 MHz, $CDCl_3$) δ = 8.02 (d, *J* = 8.1 Hz, 1H), 7.51 (d, *J* = 7.9 Hz, 1H), 7.24 – 7.19 (m, 2H), 6.88 (t, *J* = 7.9 Hz, 2H), 4.42 – 4.31 (m, 2H), 4.08 (t, *J* = 6.2 Hz, 4H), 3.88 – 3.84 (m, 2H), 3.74 – 3.51 (m, 8H), 2.46 (br, 1H), 1.94 – 1.81 (m, 4H), 1.60 – 1.46 (m, 4H), 1.43 – 1.17 (m, 32H), 0.89 (t, *J* = 6.7 Hz, 6H) ppm; ^{13}C NMR (100.6 MHz, $CDCl_3$) δ = 154.6, 154.1, 148.1, 131.1, 126.5, 126.1, 124.8, 124.1, 123.6, 122.6, 118.7, 111.3, 110.7, 74.1, 72.5, 70.65, 70.61, 70.57, 70.32, 69.61, 69.21, 69.10, 61.74, 31.7, 29.72, 29.68, 29.65, 29.40, 29.37, 29.14, 28.12, 26.05, 26.03, 22.6, 14.1 ppm; HRMS-ESI+ *m*/*z* calculated for$C_{43}H_{70}NO_6S$ $[M + H]^+$ 728.4918, found 728.4920.

4,5-Bis(dodecyloxy)-9*H*-thioxanthen-9-one O-tetraethyleneglycol oxime (4.20)

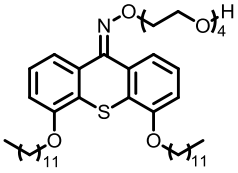

Synthesized according to the general procedure for installing the glycol moiety from **4.14** (0.20 g, 0.30 mmol, 1.0 equiv) and **4.10** (0.16 g, 0.36 mmol, 1.2 equiv). Purification by column chromatography (SiO_2, flash, 0% – 10% MeOH in CH_2Cl_2) gave **4.20** as a yellow oil (0.21 g, 0.27 mmol, 90%). ^{1}H NMR (400 MHz, $CDCl_3$) δ = 8.01 (d, *J* = 8.1 Hz, 1H), 7.51 (d, *J* = 7.9 Hz, 1H), 7.25 – 7.18 (m, 2H), 6.87 (t, *J* = 7.9 Hz, 2H), 4.42 – 4.32 (m, 2H), 4.08 (t, *J* = 6.2 Hz, 4H), 3.89 – 3.83 (m, 2H), 3.74 – 3.52 (m, 12H), 2.44 (br, 1H),

1.95 – 1.81 (m, 4H), 1.60 – 1.47 (m, 4H), 1.44 – 1.19 (m, 32H), 0.88 (t, *J* = 6.7 Hz, 6H) ppm; ^{13}C NMR (100.6 MHz, $CDCl_3$) δ = 154.5, 154.1, 148.1, 131.2, 126.4, 126.1, 124.9, 124.2, 123.6, 122.5, 118.7, 111.3, 110.6, 74.1, 72.5, 70.66, 70.61, 70.58, 70.33, 69.61, 69.21, 69.11, 61.74, 31.9, 29.72, 29.68, 29.65, 29.41, 29.38, 29.14, 29.12, 26.06, 26.04, 22.7, 14.1 ppm; HRMS-ESI+ *m*/*z* calculated for$C_{45}H_{74}NO_7S$ $[M + H]^+$ 772.5181, found 772.5174.

4,5-Bis(dodecyloxy)-9*H*-thioxanthen-9-one O-hexaethyleneglycol oxime (4.21)

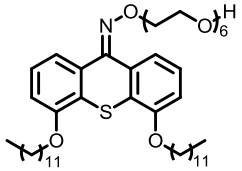

Synthesized according to the general procedure for installing the glycol moiety from **4.15** (0.25 g, 0.37 mmol, 1.0 equiv) and **4.10** (0.33 g, 0.45 mmol, 1.2 equiv). Purification by column chromatography (SiO_2, flash, 0% – 10% MeOH in CH_2Cl_2) gave **4.21** as a green oil (0.33 g, 0.35 mmol, 96%). ^{1}H NMR (400 MHz, $CDCl_3$) δ = 8.01 (d, *J* = 8.1 Hz, 1H), 7.51 (d, *J* = 7.9 Hz, 1H), 7.25 – 7.18 (m, 2H), 6.88 (t, *J* = 7.2 Hz, 2H), 4.40 – 4.34 (m, 2H), 4.08 (t, *J* = 6.4 Hz, 4H), 3.88 – 3.82 (m, 2H), 3.74 – 3.56 (m, 20H), 2.7 (br, 1H), 1.94 – 1.81 (m, 4H), 1.66 – 1.59 (m, 4H), 1.43 – 1.18 (m, 32H), 0.88 (t, *J* = 6.8 Hz, 6H) ppm; ^{13}C NMR (100.6 MHz, $CDCl_3$) δ = 154.5, 154.1, 148.0, 131.2, 126.4, 126.1, 124.9, 124.2, 123.6, 122.5, 118.7, 111.3, 110.6, 74.1, 72.6, 70.66, 70.63, 70.60, 70.55, 70.50, 70.47, 70.23, 69.6, 69.2, 69.1, 63.6, 61.7, 31.9, 29.72, 29.67, 29.65, 29.41, 29.38, 29.14, 29.11, 26.06, 26.04, 22.7, 21.0, 14.1 ppm; HRMS-ESI+ *m*/*z* calculated for $C_{49}H_{82}NO_9S$ $[M + H]^+$ 860.5705, found 860.5707.

4,5-Bis(tetradecyloxy)-9*H*-thioxanthen-9-one O-tetraethyleneglycol oxime (4.22)

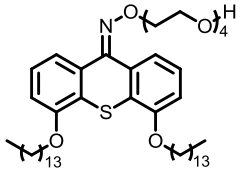

Synthesized according to the general procedure for installing the glycol moiety from **4.14** (50 mg, 0.070 mmol, 1.0 equiv) and **4.11** (30 mg, 0.090 mmol, 1.2 equiv). Purification by column chromatography (SiO_2, flash, 0% – 10% MeOH in CH_2Cl_2) gave **4.22** as an orange oil (35 mg, 0.040 mmol, 60%). ^{1}H NMR (400 MHz, $CDCl_3$) δ = 8.01 (d, *J* = 8.2 Hz, 1H), 7.51 (d, *J* = 8.0 Hz, 1H), 7.25 – 7.17 (m, 2H), 6.88 (t, *J* = 7.9 Hz, 2H), 4.43 – 4.32 (m, 2H), 4.08 (t, *J* = 5.7 Hz, 4H), 3.89 – 3.81 (m, 2H), 3.73 – 3.55 (m, 12H), 1.94 – 1.81 (m, 4H), 1.64 – 1.48 (m, 4H), 1.47 – 1.14 (m, 40H), 0.88 (t, *J* = 6.8 Hz, 6H) ppm; ^{13}C NMR (100.6 MHz, $CDCl_3$) δ = 154.5, 154.1, 148.1, 131.2, 126.4, 126.1, 124.9, 124.2, 123.6, 122.5, 118.7, 111.3, 110.6, 74.1, 72.5, 70.65, 70.60, 70.57, 70.32, 69.61, 69.21, 69.11, 61.7, 31.9, 29.73, 29.69, 29.68, 29.67, 29.66, 29.42, 29.37, 29.14, 29.12, 26.06, 26.04, 22.7, 14.1 ppm; HRMS-ESI+ *m*/*z* calculated for $C_{49}H_{82}NO_7S$ $[M + H]^+$ 828.5807, found 828.5802.

4,5-Bis(tetradecyloxy)-9*H*-thioxanthen-9-one O-hexaethyleneglycol oxime (4.23)

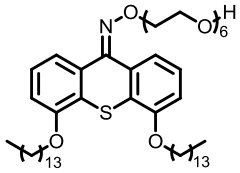

Synthesized according to the general procedure for installing the glycol moiety from **4.15** (50 mg, 0.070 mmol, 1.0 equiv) and **4.11** (38 mg, 0.090 mmol, 1.2 equiv). Purification by column chromatography (SiO_2, flash, 0% – 10% MeOH in CH_2Cl_2) gave **4.23** as a yellow oil (50 mg, 0.050 mmol, 61%). ^{1}H NMR (400 MHz, $CDCl_3$) δ = 8.01 (d, *J* = 8.1 Hz, 1H), 7.51 (d, *J* = 7.8 Hz, 1H), 7.25 – 7.18 (m, 2H), 6.88 (t, *J* = 7.9 Hz, 2H), 4.41 – 4.33 (m, 2H), 4.08 (t, *J* = 6.5 Hz, 4H), 3.88 – 3.82 (m, 2H), 3.74 – 3.52 (m, 20H), 2.01 (br, 1H), 1.93 – 1.83 (m, 4H), 1.74 – 1.61 (m, 4H), 1.44 – 1.22 (m, 40H), 0.88 (t, *J* = 5.8 Hz, 6H) ppm; ^{13}C NMR (100.6 MHz, $CDCl_3$) δ = 154.5, 154.1, 148.0, 131.2, 126.4, 126.2, 124.9, 124.2, 123.6, 122.5, 118.7, 111.3, 110.6, 74.1, 72.6, 70.62, 70.59, 70.55, 70.54, 70.49, 70.48, 70.45, 70.21, 69.59, 69.21, 69.11, 61.7, 31.9, 29.72, 29.69, 29.68, 29.67, 29.42, 29.37, 29.14, 29.12, 26.1, 22.7, 14.1 ppm; HRMS-ESI+ *m*/*z* calculated for $C_{53}H_{90}NO_9S$ $[M + H]^+$ 916.6331, found 916.6324.

4,5-Bis(hexadecyloxy)-9*H*-thioxanthen-9-one O-hexaethyleneglycol oxime (4.24)

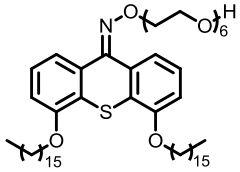

Synthesized according to the general procedure for installing the glycol moiety from **4.15** (0.26 g, 0.35 mmol, 1.0 equiv) and **4.12** (0.30 g, 0.42 mmol, 1.2 equiv). Purification by column chromatography (SiO_2, flash, 0% – 10% MeOH in CH_2Cl_2) gave **4.24** as a bright yellow oil (0.28 g, 0.29 mmol, 70%). ^{1}H NMR (400 MHz, $CDCl_3$) δ = 8.01 (d, *J* = 8.0 Hz, 1H), 7.51 (d, *J* = 7.9 Hz, 1H), 7.25 – 7.18 (m, 2H), 6.88 (t, *J* = 7.9 Hz, 2H), 4.43 – 4.32 (m, 2H), 4.08 (t, *J* = 6.4 Hz, 4H), 3.91 – 3.80 (m, 2H), 3.77 – 3.51 (m, 20H), 2.67 (br, 1H), 1.94 – 1.81 (m, 4H), 1.68 – 1.48 (m, 4H), 1.43 – 1.18 (m, 48H), 0.88 (t, *J* = 6.8 Hz, 6H) ppm; ^{13}C NMR (100.6 MHz, $CDCl_3$) δ = 154.5, 154.1, 148.0, 131.2, 126.4, 126.2, 124.9, 124.2, 123.6, 122.5, 118.7, 111.3, 110.6, 74.1, 72.6, 70.64, 70.61, 70.59, 70.57, 70.53, 70.51, 70.48, 70.25, 69.59, 69.21, 69.11, 61.7, 31.9, 29.72, 29.69, 29.67, 29.42, 29.37, 29.15, 29.12, 26.07, 26.04, 22.7, 14.1 ppm; HRMS-ESI+ *m*/*z* calculated for $C_{57}H_{98}NO_9S$ $[M + H]^+$ 972.6957, found 972.6958.

4,5-Bis(hexadecyloxy)-9*H*-thioxanthen-9-one O-octaethyleneglycol oxime (4.25)

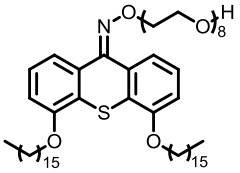

Synthesized according to the general procedure for installing the glycol moiety from **4.16** (0.15 g, 0.21 mmol, 1.0 equiv) and **4.12** (0.13 g, 0.25 mmol, 1.2 equiv). Purification by column chromatography (SiO_2, flash, 0% – 10% MeOH in CH_2Cl_2) gave **4.25** as a colorless oil (0.13 g, 12 mmol, 56%). ^{1}H NMR (400 MHz, $CDCl_3$) δ = 8.01 (d, *J* = 8.1 Hz, 1H), 7.51 (d, *J* = 7.9 Hz, 1H), 7.24 – 7.17 (m, 2H), 6.88 (t, *J* = 7.9 Hz, 2H), 4.40 – 4.34 (m, 2H), 4.08 (t, *J* = 5.8 Hz, 4H), 3.87 – 3.81 (m, 2H), 3.75 – 3.54 (m, 28H), 2.71 (br, 1H), 1.97 – 1.82 (m, 4H), 1.61 – 1.47 (m, 4H), 1.44 – 1.17 (m, 48H), 0.88 (t, *J* = 6.7 Hz, 6H) ppm; ^{13}C NMR (100.6 MHz, $CDCl_3$) δ = 154.5, 154.1, 148.0, 131.2, 126.4, 126.1, 124.9, 124.2, 123.6, 122.5, 118.7, 111.3, 110.6, 74.1, 72.6, 70.63, 70.58, 70.55, 70.53, 70.52, 70.49, 70.46, 70.43, 70.18, 69.58, 69.21, 69.11, 61.6, 31.9, 29.73, 29.69, 29.67, 29.65, 29.42, 29.37, 29.15, 29.12, 26.07, 26.04, 22.7, 14.1 ppm; HRMS-ESI+ *m/z* calculated for $C_{61}H_{106}NO_{11}S$ $[M + H]^+$ 1060.7481, found 1060.7490.

9,9-Dimethoxy-9*H*-thioxanthene (4.27)

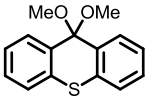

Thioxanthone (1.5 g, 7.0 mmol, 1.0 equiv) was added to oxalyl chloride (20 mL) and the mixture was heated at reflux for 5 h. After cooling the mixture to room temperature, the excess oxalyl chloride was removed on the rotaray evaporator. A red solid was obtained, which was assumed to be 9,9-dichloro-9*H*-thioxanthene. The crude solid was dissolved in dry THF (15 mL) under a nitrogen atmosphere and the solution was added dropwise to a methanolic solution of fresh NaOMe (0.48 g, 21 mmol, 3.0 equiv Na in 10 mL MeOH) and the solution was stirred at RT for 12 h. Subsequently, the solvents were removed under reduced pressure and the resulting yellow solid was recrystallized from MeOH to yield **4.27** as pink needles (1.2 g, 4.7 mmol, 67%). m.p. 122 – 124 °C; ^{1}H NMR (400 MHz, $CDCl_3$): δ = 7.88 – 7.82 (m, 2H), 7.44 – 7.38 (m, 2H), 7.37 – 7.28 (m, 4H), 3.10 (s, 6H) ppm; ^{13}C NMR (100.6 MHz, $CDCl_3$): δ = 133.4, 131.3, 128.3, 127.9, 125.9, 125.8, 99.7, 51.9 ppm; HRMS-ESI+ *m/z* calculated for $C_{15}H_{14}O_2SNa$ $[M + Na]^+$ 281.0612, found 281.0609.

9-Methoxy-9-(methylthio)-9*H*-thioxanthene (4.28)

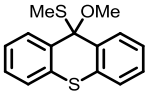

A methanolic solution of fresh NaOMe (0.13 g, 3.0 mmol, 6.8 equiv Na in 10 mL MeOH) was cooled in an ice bath. Compound **4.49** (0.10 g, 0.44 mmol, 1.0 equiv), dissolved in THF (5 mL) was added dropwise and the mixture stirred at RT for 2 h. Subsequently, MeI (21 mg, 3.0 mmol, 6.8 equiv) in THF (5 mL) was added slowly and the mixture stirred at RT for 90 min. The solvents were then removed under reduced pressure and the residue was dissolved in CH_2Cl_2 (50 mL). This solution was washed with aq. saturated $NaHCO_3$ (30 mL), dried over $MgSO_4$ and concentrated in vacuo. Recrystallization from MeOH yielded **4.28** as pink crystals (75 mg, 0.27 mmol, 61%). m.p. 150 – 152 °C; ^{1}H NMR (400 MHz, $CDCl_3$):

δ = 7.70 (dd, *J* = 7.7, 1.6 Hz, 2H), 7.40 – 7.27 (m, 6H), 3.31 (s, 3H), 1.86 (s, 3H) ppm; ^{13}C NMR (100.6 MHz, $CDCl_3$): δ = 131.8, 131.0, 128.0, 127.7, 126.0, 125.8, 86.8, 54.0, 13.7 ppm; HRMS-ESI+ *m/z* calculated for $C_{15}H_{14}O_2S_2$ $[M + H]^+$ 274.0486, found 274.0488.

9,9-dimethoxy-9*H*-xanthene (4.29)

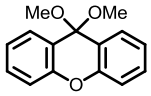

Xanthone (10 g, 51 mmol, 1.0 equiv) was added to thionylchloride (20 mL) and a catalytic amount of DMF and the mixture was heated at reflux for 18 h. After cooling the mixture to room temperature, the excess thionylchloride was removed on the rotaray evaporator. A red solid was obtained, which was assumed to be 9,9-dichloro-9*H*-xanthene. The crude solid was dissolved in dry THF (30 mL) under a nitrogen atmosphere and the solution was added dropwise to an ice bath cooled methanolic solution of fresh NaOMe (3.5 g, 0.15 mol, 3.0 equiv Na in 40 mL MeOH) and the solution was stirred at RT for 90 min. Subsequently, the solvents were removed under reduced pressure and the residue was dissolved in CH_2Cl_2 (40 mL). This solution was washed with aq. saturated $NaHCO_3$ (3 x 20 mL), dried over $MgSO_4$ and concentrated in vacuo to yield **4.29** as a yellow solid (12 g, 48 mmol, 95%), containing trace amounts of xanthone. ^{1}H NMR (400 MHz, $CDCl_3$): δ = 2.94 (s, 6H), 7.19 – 7.25 (m, 4H), 7.43 (td, *J* = 8.0, 2.0 Hz, 2H), 7.73 (dd, *J* = 7.8, 1.6 Hz, 2H) ppm. Data is in accordance with literature.[50,62]

4,5-Ditetradecyl-9*H*-xanthen-9-one (4.30)

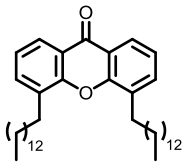

This compound was prepared following an adapted literature procedure.[62] Compound **4.29** (0.50 g, 2.0 mmol, 1.0 equiv) was dissolved in THP (6 mL) and *t*-BuOK (0.67 g, 6.0 mmol, 3.0 equiv) was added. The reaction was cooled to -40 °C and *t*-BuLi (3.5 mL, 6.0 mmol, 3.0 equiv, 1.7 M in hexanes) was added dropwise. After 30 min, iodotetradecane **4.50** (2.0 g, 6.0 mmol, 3.0 equiv) was added slowly and the mixture stirred at -40 °C for 1 h. The mixture was then allowed to warm to RT and stirred for 2 h after which H_2O (50 mL) was added. The reaction was acidified with 1 M aq. HCl until pH <2 and the mixture was stirred at RT for 4 h. The aqueous layer was extracted with Et_2O (3 x 50 mL) and the combined organic layers dried over $MgSO_4$ and concentrated in vacuo. The resulting mixture was filtered through a plug of silica gel. The plug was washed with *n*-pentane and the product washed off with EtOAc. After evaporation of the EtOAc, the product was recrystallized from Et_2O to yield **4.30** as a white solid (0.82 g, 1.4 mmol, 71%). m.p. 80 – 81 °C; ^{1}H NMR (400 MHz, $CDCl_3$): δ = 8.20 (dd, *J* = 8.0, 1.7 Hz, 2H), 7.57 (dd, *J* = 7.3, 1.6 Hz, 2H), 7.30 (m, 2H), 2.97 (t, *J* = 7.6 Hz, 4H), 1.76 (quint, *J* = 7.6 Hz, 4H), 1.50 – 1.16 (m, 44H), 0.88 (t, *J* = 7.6 Hz, 6H) ppm; ^{13}C NMR (100.6 MHz, $CDCl_3$): δ = 178.0, 154.0, 134.8, 132.0, 124.4, 123.4, 121.6, 31.9, 30.3, 30.2, 29.9, 29.8, 29.6, 29.4, 22.7, 14.1 ppm; HRMS-ESI+ *m/z* calculated for $C_{41}H_{65}O_2$ $[M + H]^+$ 589.4979, found 589.4964.

4,5-Ditetradecyl-9*H*-xanthene-9-thione (4.31)

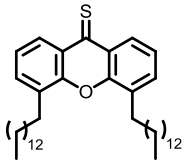

A mixture of compound **4.30** (0.15 g, 0.24 mmol, 1.0 equiv) and Lawesson's reagent (0.40 g, 1.0 mmol, 4.2 equiv) in dry toluene (20 mL) was heated at reflux under nitrogen atmosphere for 18 h. The resulting green solution was cooled to room temperature and concentrated under reduced pressure. Purification by flash column chromatography (SiO_2, *n*-pentane:Et_2O 20:1) gave **4.31** as a green solid (0.13 g, 0.22 mmol, 92%). ^{1}H NMR (400 MHz, $CDCl_3$): δ = 8.62 (dd, *J* = 8.3, 1.6 Hz, 2H), 7.60 (dd, *J* = 5.2 Hz, 1.6 Hz, 2H), 7.31 – 7.26 (m, 2H), 2.99 (t, *J* = 8.0 Hz, 4H), 1.76 (quint, *J* = 7.6 Hz, 4H), 1.49 – 1.23 (m, 24 H), 0.88 (t, *J* = 6.8 Hz, 6H) ppm.

4,5-Ditetradecyl-9*H*-xanthen-9-one oxime (4.32)

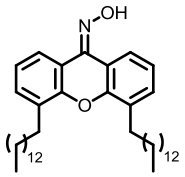

Compound **4.31** (0.13 g, 0.22 mmol, 1.0 equiv) was dissolved in *i*-PrOH (10 mL) and hydroxyl amine hydrochloride (68 mg, 1.0 mmol, 4.5 equiv) and pyridine (0.10 mL, 1.2 mmol, 5.5 equiv) were added. The reaction mixture was heated at reflux for 18 h. When cooling to RT, a white solid precipitated and H_2O (50 mL) was added to the mixture. The aqueous layer was extracted with EtOAc (3 x 50 mL) and the combined organic layers were washed with brine (50 mL), dried over $MgSO_4$, filtered and concentrated in vacuo, yielding **4.32** as a white solid (0.12 g, 0.19 mmol, 86%). ^{1}H NMR (400 MHz, $CDCl_3$): δ = 8.81 (dd, *J* = 8.2, 1.4 Hz, 1H), 7.86 (dd, *J* = 8.0, 1.4 Hz, 1H), 7.38 – 7.32 (m, 1H), 7.30 – 7.26 (m, 1H), 7.17 – 7.07 (m, 2H), 2.89 – 2.80 (m, 4H), 7.75 – 1.65 (m, 4H), 1.50 – 1.19 (m, 44H), 0.88 (t, *J* = 6.8 Hz, 6H) ppm.

4,5-Ditetradecyl-9*H*-xanthen-9-one O-(2-(2-(2-(2-hydroxyethoxy)ethoxy)ethoxy)ethyl) oxime (4.33)

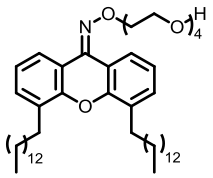

Compound **4.32** (35 mg, 0.058 mmol, 1.0 equiv) was dissolved in DMSO (5 mL) and Cs_2CO_3 (28 mg, 0.087 mmol, 1.5 equiv) was added and the reaction mixture was stirred at RT for 30 min. Subsequently, monotosyl-tetra-ethyleneglycol **4.14** (26 mg, 0.074 mmol, 1.3 equiv) was added and the mixture was stirred at 60 °C for 72 h. After cooling down to RT, EtOAc (40 mL) was added. The mixture was washed with H_2O (3 x 50 mL) and concentrated in vacuo to yield **4.33** as a yellow solid (31 mg, 0.040 mmol, 69%). m.p. 55 – 56 °C; ^{1}H NMR (400 MHz, $CDCl_3$): δ = 8.73 (d, *J* = 7.2 Hz, 1H), 7.89 (d, *J* = 6.9 Hz, 1H), 7.30 (d, *J* = 7.3 Hz, 1H), 7.23 (d, *J* = 6.9 Hz, 1H), 7.12 – 7.01 (m, 2H), 4.47 – 4.40 (m, 2H), 3.94 – 3.84 (m, 2H), 3.76 – 3.54 (m, 12H), 2.87 – 2.76 (m, 4H), 1.74 – 1.62 (m), 1.49 – 1.18 (m, 48H), 0.88 (t, *J* = 6.8Hz, 6H) ppm; ^{13}C NMR (100.6 MHz, $CDCl_3$): δ = 150.5, 149.3, 141.2, 132.0, 130.9, 130.7, 129.1, 123.1, 122.0,

121.9, 119.2, 116.1, 74.3, 72.4, 70.7, 70.6, 70.6, 70.4, 69.8, 61.7, 31.9, 30.8 – 29.4, 22.7, 14.1 ppm; HRMS-ESI+ *m/z* calculated for $C_{49}H_{82}NO_6$ $[M + H]^+$ 780.6137, found 780.6140.

4,5-Ditetradecyl-9*H*-xanthen-9-one O-(17-hydroxy-3,6,9,12,15-pentaoxaheptadecyl) oxime (4.34)

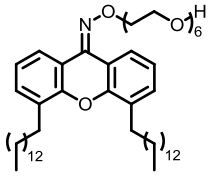

Compound **4.32** (50 mg, 0.080 mmol, 1.0 equiv) was dissolved in THF (5 mL) and *t*-BuOK (17 mg, 0.15 mmol, 1.9 equiv) was added and the reaction mixture was stirred at RT for 30 min. Subsequently, monotosyl-hexa-ethyleneglycol **4.15** (58 mg, 0.15 mmol, 1.9 equiv) was added and the mixture was stirred at RT for 4 d. After concentrating the mixture on the rotary evaporator, H_2O (50 mL) was added and the aqueous layer extracted with Et_2O (3 x 50 mL) and the combined organic layers concentrated in vacuo. Purification by flash column chromatography (SiO_2, CH_2Cl_2:MeOH 9:1) gave **4.34** as a yellow solid (26 mg, 0.030 mmol, 37 %). m.p. 60 – 61 °C; ^{1}H NMR (400 MHz, $CDCl_3$): δ = 8.73 (dd, *J* = 8.2, 1.3 Hz, 1H), 7.89 (d, *J* = 8.0, 1.4 Hz, 1H), 7.30 (d, *J* = 8.4 Hz, 1H), 7.23 (d, *J* = 8.8 Hz, 1H), 7.10 – 7.02 (m, 2H), 4.41 (t, *J* = 5.2 Hz, 2H), 3.89 (t, *J* = 5.2 Hz, 2H), 3.74 – 3.57 (m, 16H), 2.86 (m, 4H), 1.73 – 1.63 (m, 4H), 1.47 – 1.20 (m, 48H), 0.88 (t, *J* = 6.8 Hz, 6H) ppm; ^{13}C NMR (100.6 MHz, $CDCl_3$): δ = 150.5, 149.0, 141.2, 132.0, 130.9, 130.7, 130.6, 129.1, 123.1, 122.0, 121.9, 119.2, 116.1, 74.3, 72.5, 70.7, 70.63, 70.60, 70.58, 70.56, 70.54, 70.52, 70.3, 69.7, 61.7, 31.9, 30.8, 30.3, 30.22, 30.16, 29.89, 29.85, 29.78, 29.64, 22.7, 14.1 ppm; HRMS-ESI+ *m/z* calculated for $C_{53}H_{90}NO_8$ $[M + H]^+$ 868.6661, found 868.6673.

1,8-Dimethoxyanthracene-9,10-dione (4.35)

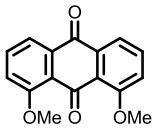

This compound was prepared as described in literature.[63,64] To a vigorously stirred solution of 1,8-dihydroxy anthraquinone (4.0 g, 16 mmol, 1.0 equiv) in acetone (250 mL), K_2CO_3 (15 g, 0.10 mol, 6.3 equiv) was added. The mixture was heated at reflux and upon changing colour from yellow to red, a precipitate was formed. Dimethylsulfate (5.0 mL, 56 mmol, 3.5 equiv) was added slowly and the reaction was stirred at reflux for 14 h. After cooling down to RT, the suspension was filtered and the residue washed with acetone (2 x 100 mL). The filtrate was concentrated in vacuo and purification by flash column chromatography (SiO_2, *n*-pentane:Et_2O 1:1) gave **4.35** (3.1 g, 12 mmol, 72%). ^{1}H NMR (400 MHz, $CDCl_3$): δ = 7.84 (d, *J* = 7.7 Hz, 2H), 7.64 (t, *J* = 8.0 Hz, 2H), 7.30 (d, *J* = 8.4 Hz, 2H), 4.01 (s, 6H) ppm. Data is in accordance with literature.[63,64]

4,5-Dimethoxyanthracen-9(10*H*)-one (4.36)

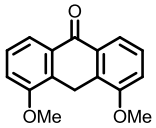

This compound was prepared as described in literature.[63] Compound **4.35** (1.0 g, 3.7 mmol, 1.0 equiv) was dissolved in a 1:1 mixture of DMF (50 mL) and H_2O (50 mL). Sodium dithionite (7.0 g, 40 mmol, 11 equiv) was added and the mixture was heated at reflux for 30 h. After cooling down to RT, the mixture was poured into H_2O (500 mL) and the layers separated. The aqueous layer was extracted with EtOAc (3 x 100 mL) and the combined organic layers were washed with H_2O (3 x 250 mL) and concentrated in vacuo. Purification by recrystallization from EtOAc gave **4.36** as white crystals (0.85 g, 3.3 mmol, 89%). ^{1}H NMR (400 MHz, $CDCl_3$): δ = 7.98 (d, *J* = 8.0 Hz, 2H), 7.44 (t, *J* = 8.0 Hz, 2H), 7.13 (d, *J* = 8.0 Hz, 2H), 4.06 (s, 2H), 3.98 (s, 6H) ppm. Data is in accordance with literature.[63]

4,5-Dihydroxyanthracen-9(10*H*)-one (4.37)

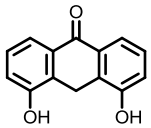

This compound was prepared as described in literature.[63] Compound **4.36** (0.50 g, 2.0 mmol, 1.0 equiv) was dissolved in dry CH_2Cl_2 (50 mL) under a nitrogen atmosphere and the reaction was cooled using an ice bath. BBr_3 (0.95 mL, 10 mmol, 5.0 equiv) was added slowly and the reaction was stirred in an ice bath for 18 h. Subsequently, H_2O (10 mL) was added slowly and the suspension was poured in EtOAc (250 mL) and the mixture filtered. The residue was washed with EtOAc (80 mL) and the combined organic layers were washed with brine (100 mL), dried over $MgSO_4$, filtered and concentrated in vacuo to give **4.37** as a red solid (0.43 g, 1.9 mmol, 95%). The product was used without further purification in subsequent steps. ^{1}H NMR (400 MHz, $CDCl_3$): δ = 10.19 (s, 2H), 7.72 (dd, *J* = 7.8, 1.0 Hz, 2H), 7.39 (t, *J* = 7.9 Hz, 2H), 7.21 (dt, *J* = 16.4, 8.2 Hz, 2H), 4.00 (s, 2H) ppm. Data is in accordance with literature.[63]

4,5-Bis(dodecyloxy)anthracen-9(10*H*)-one (4.38)

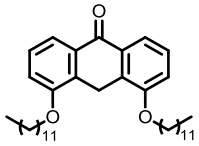

Method A ($Na_2S_2O_4$): Compound **4.39** (0.20 g, 0.35 mmol, 1.0 equiv) was dissolved in a 1:1 mixture of DMF (15 mL) and H_2O (15 mL). Sodium dithionite (1.4 g, 8.0 mmol, 23 equiv) was added and the mixture was stirred at 90 °C for 24 h. Two additional batches of $Na_2S_2O_4$ (2 x 2.0 g, 11 mmol, 31 equiv) were added after 14 h and 18 h, respectively. After cooling down to RT, the mixture was poured into H_2O (50 mL) and the layers separated. The aqueous layer was extracted with EtOAc (2 x 150 mL) and the combined organic layers were dried over $MgSO_4$ and concentrated in vacuo. Purification by flash column chromatography (SiO_2, *n*-pentane:EtOAc 9:1) gave **4.38** as white crystals (7.0 mg, 0.030 mmol, 4%).
Method B ($NaBH_4$): Compound **4.39** (0.60 g, 1.0 mmol, 1.0 equiv) was dissolved in THF (20 mL). $NaBH_4$ (4 x 0.33 g, 8.7 mmol, 8.7 equiv) was added in 4 batches every hour for the next 4 h and the reaction was stirred at RT for 14 h. Subsequently, H_2O (10 mL) was added dropwise and the mixture stirred at RT for 1 h, after which the mixture was poured into water (50 mL). The

mixture was filtered and the residue washed with H_2O (100 mL). The white solid was assumed to be the diol and used without further purification. The solid was added to a 1:1 mixture of HCl (37%, 9 mL) and AcOH (9 mL) and the mixture was stirred at reflux for 30 min. After cooling to RT, the mixture was stirred for an additional 7 h. The mixture was filtered and the residue washed with H_2O (10 mL), aq. saturated $NaHCO_3$ (15 mL) and H_2O (10 mL). The crude solid was purified by flash column chromatography (SiO_2, *n*-pentane:EtOAc 9:1) to give **4.38** as a white solid (0.53 g, 0.95 mmol, 91%). ^{1}H NMR (400 MHz, $CDCl_3$): δ = 7.88 (dd, *J* = 7.9, 0.8 Hz, 2H), 7.32 (t, *J* = 8.0 Hz, 2H), 7.02 (d, *J* = 8.0 Hz, 2H), 4.20 – 3.82 (m, 6H), 1.92 – 1.70 (m, 4H), 1.59 – 1.41 (m, 4H), 1.19 (s, 32H), 0.80 (t, *J* = 6.9 Hz, 6H) ppm; ^{13}C NMR (100.6 MHz, $CDCl_3$): δ = 184.6, 156.4, 132.6, 130.3, 127.1, 118.9, 114.0, 68.2, 31.9, 31.4, 30.2, 29.7-29.3, 26.2, 22.7, 22.5, 14.1 ppm; HRMS-ESI+ *m/z* calculated for $C_{38}H_{59}O_3$ $[M + H]^+$ 563.4459, found 563.4449.

1,8-Bis(dodecyloxy)anthracene-9,10-dione (4.39)

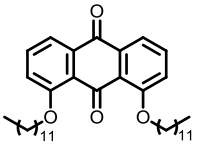

1,8-Dihydroxy anthraquinone (1.0 g, 3.6 mmol, 1.0 equiv) was dissolved in chlorobenzene (50 mL). TBAB (0.13 g, 0.40 mmol, 0.11 equiv), KI (0.10 g, 0.60 mmol, 0.17 equiv) and laurylbromide (2.4 g, 9.4 mmol, 2.6 equiv) were added, followed by addition of aq. 3 M KOH (7.5 mL). The mixture was stirred at reflux for 18 h. After cooling down to RT, the layers were separated and the aqueous layer was extracted with CH_2Cl_2 (3 x 80 mL). The combined organic layers were concentrated in vacuo and purification of the crude solid by recrystallization from EtOAc, gave **4.39** (1.9 g, 3.3 mmol, 94%). m.p. 109 – 110 °C; ^{1}H NMR (400 MHz, $CDCl_3$): δ = 7.80 (dd, *J* = 7.7, 0.9 Hz, 2H), 7.58 (t, *J* = 8.0 Hz, 2H), 7.29 – 7.24 (m, 2H), 4.12 (t, *J* = 6.6 Hz, 4H), 1.97 – 1.81 (m, 4H), 1.63 – 1.48 (m, 4H), 1.43 – 1.14 (m, 32H), 0.88 (t, *J* = 6.8 Hz, 6H) ppm; ^{13}C NMR (100.6 MHz, $CDCl_3$): δ = 184.3, 182.1, 158.9, 134.8, 133.4, 124.7, 119.6, 118.8, 113.8, 69.8, 31.9, 29.7, 29.7, 29.7, 29.6, 29.4, 29.4, 29.1, 25.9, 22.7, 14.1 ppm; HRMS-ESI+ *m/z* calculated for $C_{38}H_{57}O_4$ $[M + H]^+$ 577.4251, found 577.4240.

1,8-Bis(dodecyloxy)-10-(hydroxyimino)anthracen-9(10*H*)-one (4.44)

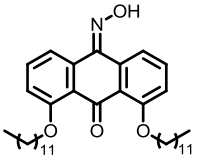

Compound **4.39** (0.25 g, 0.43 mmol, 1.0 equiv) was dissolved in MeOH (5 mL) and hydroxyl amine hydrochloride (45 mg, 0.65 mmol, 1.5 equiv) and pyridine (0.15 mL, 1.8 mmol, 4.2 equiv) were added. The reaction mixture was heated at reflux for 4 h. After cooling to RT, the mixture was poured into CH_2Cl_2 (40 mL) and washed with H_2O (30 mL). The aqueous layer was extracted with CH_2Cl_2 (30 mL), dried over $MgSO_4$, filtered and concentrated in vacuo. Purification by flash column chromatography (SiO_2, *n*-pentane:EtOAc 9:1) gave **4.44** as a white solid (49 mg, 0.083 mmol, 19%). ^{1}H NMR (400 MHz, $CDCl_3$): δ = 8.19 (d, *J* = 7.9 Hz, 1H), 7.47 (t, *J* = 8.2 Hz, 1H), 7.45 – 7.35 (m, 2H), 7.07 (d, *J* = 8.5 Hz, 1H), 6.99 (d, *J* = 7.4 Hz, 1H), 4.11 – 4.01 (m, 4H), 1.93 – 1.78 (m, 4H), 1.56 – 1.44 (m, 4H), 1.39 – 1.16 (m, 32H), 0.88 (t, *J* = 6.7 Hz, 6H) ppm; ^{13}C NMR (100.6 MHz, $CDCl_3$): δ = 183.6, 157.8, 157.7, 146.6, 136.5, 132.7, 132.0, 130.0, 125.0, 123.8, 122.0, 116.1, 115.6, 114.0, 69.6, 69.4, 31.9, 29.7, 29.7, 29.7,

29.5, 29.4, 29.1, 25.9, 25.9, 22.7, 14.1 ppm; HRMS-ESI+ m/z calculated for $C_{38}H_{58}NO_4$ $[M + H]^+$ 592.4360, found 592.4360.

Tetraethyleneglycol-monobromide (4.47)

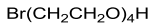

This compound was prepared as described in literature.[70] Compound **4.14** (0.15 g, 0.43 mmol, 1.0 equiv) was dissolved in acetone (5 mL) and LiBr (0.39 g, 4.5 mmol, 10 mmol) was added and the reaction mixture was heated at reflux for 2.5 h. After concentrating the mixture on the rotary evaporator, $CHCl_3$ (10 mL) was added and the solution washed with H_2O (2 x 5 mL), dried over $MgSO_4$, filtered and concentrated in vacuo to yield **4.47** as a colorless oil (95 mg, 0.37 mmol, 86%). ^{1}H NMR (400 MHz, $CDCl_3$): δ = 3.81 (t, *J* = 6.3 Hz, 2H), 3.75 – 3.71 (m, 2H), 3.71 – 3.64 (m, 8H), 3.64 – 3.58 (m, 2H), 3.48 (t, *J* = 6.3 Hz, 2H) ppm. Data is in accordance with literature.[70]

1,8-Bis(dodecyloxy)-10-((2-(2-(2-(2-hydroxyethoxy)ethoxy)ethoxy)ethoxy)imino) anthracen-9(10*H*)-one (4.48)

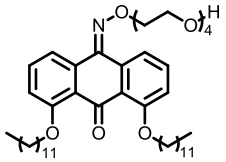

Compound **4.44** (60 mg, 0.10 mmol, 1.0 equiv) was dissolved in THF (3 mL) and *t*-BuOK (38 mg, 0.31 mmol, 3.1 equiv) and monobromo-tetra-ethyleneglycol **4.47** (38 mg, 0.16 mmol, 1.6 equiv) were added and the reaction mixture was stirred at RT for 3 h. After concentrating the mixture on the rotary evaporator, the product was purified by flash column chromatography (SiO_2, CH_2Cl_2:MeOH 9:1) to give a mixture or **4.48** and **4.47**. Crystallization from Et_2O gave **4.48** as an off-white solid (60 mg, 0.078 mmol, 78%). m.p. 43 – 46 °C; ^{1}H NMR (400 MHz, $CDCl_3$): δ = 8.11 (d, *J* = 7.9 Hz, 1H), 7.51 (d, *J* = 7.8 Hz, 1H), 7.48 – 7.30 (m, 2H), 7.05 (d, *J* = 8.4 Hz, 1H), 6.98 (d, *J* = 8.3 Hz, 1H), 4.61 – 4.33 (m, 2H), 4.06 (t, *J* = 6.5 Hz, 4H), 3.92 – 3.80 (m, 2H), 3.74 – 3.60 (m, 10H), 3.60 – 3.50 (m, 2H), 1.96 – 1.70 (m, 4H), 1.49 (dd, *J* = 14.5, 7.0 Hz, 4H), 1.42 – 1.05 (m, 32H), 0.87 (t, *J* = 6.8 Hz, 6H) ppm; ^{13}C NMR (100.6 MHz, $CDCl_3$): δ = 183.5, 157.7, 157.5, 145.9, 136.5, 132.4, 131.9, 130.3, 125.1, 123.8, 122.1, 116.3, 115.6, 113.9, 74.9, 72.4, 70.7, 70.6, 70.6, 70.3, 69.6, 69.6, 69.4, 61.7, 31.9, 29.7, 29.7, 29.7, 29.5, 29.4, 29.2, 25.9, 22.7, 14.1 ppm; HRMS-ESI+ m/z calculated for $C_{46}H_{74}NO_8$ $[M + H]^+$ 768.5409, found 768.5415.

9*H*-Thioxanthene-9-thione (4.49)

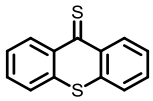

This compound was prepared as described in literature.[73] A mixture of thioxanthone (1.0 g, 4.7 mmol, 1.0 equiv) and Lawesson's reagent (4.0 g, 10 mmol, 2.1 equiv) in toluene (40 mL) was heated at reflux under a nitrogen atmosphere for 18 h. The resulting green solution was cooled to RT and filtered through a plug of silica gel. The plug was washed with *n*-pentane until the filtrate was colorless. The solvents were evaporated and **4.49** was obtained as a brown solid (0.64 g, 2.8 mmol, 60%). ^{1}H NMR (400 MHz, $CDCl_3$): δ = 9.01 (dd, *J* = 13.0, 0.6 Hz, 2H), 7.55 – 7.65 (m, 4H), 7.44 (dd, *J* = 8.4, 1.8 Hz, 2H) ppm. Data is in accordance with literature.[73]

1-Iodododecane (4.50)

This compound was prepared as described in literature.[74] 1-Bromotetradecane (9.8 g, 31 mmol, 1.0 equiv) was dissolved in acetone (18 mL) and NaI (11 g, 76 mmol, 2.5 equiv) was added and the reaction mixture was heated at reflux for 4 h. After filtration, the filtrate was concentrated under reduced pressure and the resulting oil was diluted with aq. saturated Na_2SO_3 (20 mL). The solution was extracted with Et_2O (3 x 50 mL) and the organic layer washer with brine (20 mL), dried over $MgSO_4$, filtered and concentrated in vacuo to yield a yellow oil. The crude product was purified by vacuum distillation (155 °C at 0.5 mbar) to give **4.50** as a colorless oil (7.9 g, 27 mmol, 86%). ^{1}H NMR (400 MHz, $CDCl_3$): δ = 3.19 (t, *J* = 7.1 Hz, 2H), 1.82 (m, 2H), 1.45 – 1.20 (m, 20 H), 0.88 (t, *J* = 6.8 Hz, 3H) ppm. Data is in accordance with literature.[74]

4.9 Acknowledgements

Anja Huizing is gratefully acknowledged for her major contribution to this chapter as part of her Master thesis.[36] She has performed most of the synthesis and analysis on the xanthone- and anthrone-derived amphiphiles. Dr. Marc Stuart has performed all the cryo-TEM measurements on the thioxanthone-derived amphiphiles and is acknowledged for useful input. Dr. Wiktor Szymański is acknowledged for helpful discussions.

4.10 References

[1] C. J. Pedersen, *J. Am. Chem. Soc.* **1967**, *89*, 7017–7036.
[2] M. Zhang, X. Yan, F. Huang, Z. Niu, H. W. Gibson, *Acc. Chem. Res.* **2014**, *47*, 1995–2005.
[3] C. J. Pedersen, *Angew. Chem. Int. Ed. Engl.* **1988**, *27*, 1021–1027.
[4] D. J. Cram, *Angew. Chem. Int. Ed. Engl.* **1988**, *27*, 1009–1020.
[5] J. -M. Lehn, *Angew. Chem. Int. Ed. Engl.* **1988**, *27*, 89–112.
[6] R. P. Feynman, *Eng. Sci.* **1960**, *23*, 22–36.
[7] E. Drexler, *Engines of Creation: The Coming Era of Nanotechnology*, Anchor, New York, USA, **1987**.
[8] S. I. Stupp, L. C. Palmer, *Chem. Mater.* **2014**, *26*, 507–518.
[9] V. Balzani, A. Credi, M. Venturi, in *Molecular Devices and Machines – A Journey into the Nano World*, Wiley-VCH Verlag GmbH & Co. KGaA, Weinheim, Germany, **2003**, pp. 1–18.
[10] J. D. Badjić, V. Balzani, A. Credi, S. Silvi, J. F. Stoddart, *Science* **2004**, *303*, 1845–1849.
[11] T. J. Huang, B. Brough, C. -M. Ho, Y. Liu, A. H. Flood, P. A. Bonvallet, H. -R. Tseng, J. F. Stoddart, M. Baller, S. Magonov, *Appl. Phys. Lett.* **2004**, *85*, 5391–5393.
[12] O. M. Yaghi, M. O'Keeffe, N. W. Ockwig, H. K. Chae, M. Eddaoudi, J. Kim, *Nature* **2003**, *423*, 705–714.
[13] J. C. Love, L. A. Estroff, J. K. Kriebel, R. G. Nuzzo, G. M. Whitesides, *Chem. Rev.* **2005**, *105*, 1103–1169.
[14] G. M. Whitesides, B. Grzybowski, *Science* **2002**, *295*, 2418–2421.
[15] W. R. Browne, B. L. Feringa, *Nat. Nanotechnol.* **2006**, *1*, 25–35.
[16] J. H. van Esch, B. L. Feringa, *Angew. Chem. Int. Ed.* **2000**, *39*, 2263–2266.
[17] N. Koumura, R. W. J. Zijlstra, R. A. van Delden, N. Harada, B. L. Feringa, *Nature* **1999**, *401*, 152–155.

[18] T. Kudernac, N. Ruangsupapichat, M. Parschau, B. Maciá, N. Katsonis, S. R. Harutyunyan, K. -H. Ernst, B. L. Feringa, *Nature* **2011**, *479*, 208–211.
[19] R. Nagarajan, *Amphiphiles: Molecular Assembly and Applications*, American Chemical Society, Washington, DC, USA, **2011**.
[20] E. W. Flick, *Industrial Surfactants: An Industrial Guide*, William Andrew, Park Ridge, N.J., U.S.A, **1994**.
[21] L. L. Schramm, *Surfactants. Fundamentals and Applications in the Petroleum Industry.*, Cambridge University Press, Cambridge, UK, **2010**.
[22] P. L. Swisstack, *Aerated Aqueous Explosive Composition with Surfactant*, **1966**, US3288661 (A).
[23] T. F. Tadros, in *Applied Surfactants*, Wiley-VCH Verlag GmbH & Co. KGaA, Weinheim, Germany, **2005**, pp. 1–17.
[24] J. N. Israelachvili, D. J. Mitchell, B. W. Ninham, *J. Chem. Soc. Faraday Trans. 2 Mol. Chem. Phys.* **1976**, *72*, 1525–1568.
[25] K. Velonia, J. J. L. M. Cornelissen, M. C. Feiters, A. E. Rowan, R. J. M. Nolte, in *Nanoscale Assemblies* (Ed.: W.T.S. Huck), Springer US, New York, USA **2005**, pp. 119–185.
[26] D. Vriezema, H. Elemans, E. Pierson, H. Geurts, "Amphiphiles," can be found under http://www.vcbio.science.ru.nl/en/fesem/applets/amphiphiles/, **2014**.
[27] R. Nagarajan, *Langmuir* **2002**, *18*, 31–38.
[28] G. K. Bourov, A. Bhattacharya, *J. Chem. Phys.* **2007**, *127*, 2449051–2449057.
[29] C. -I. Huang, Y. -J. Chiou, Y. -K. Lan, *Polymer* **2007**, *48*, 877–886.
[30] R. Lipowsky, E. Sackmann, *Structure and Dynamics of Membranes: I. From Cells to Vesicles/II. Generic and Specific Interactions*, Elsevier, Amsterdam, The Netherlands **1995**.
[31] T. Kunitake, Y. Okahata, M. Shimomura, S. Yasunami, K. Takarabe, *J. Am. Chem. Soc.* **1981**, *103*, 5401–5413.
[32] C. A. Hunter, J. K. M. Sanders, *J. Am. Chem. Soc.* **1990**, *112*, 5525–5534.
[33] J. C. Ma, D. A. Dougherty, *Chem. Rev.* **1997**, *97*, 1303–1324.
[34] D. A. Dougherty, *Acc. Chem. Res.* **2013**, *46*, 885–893.
[35] A. C. Coleman, J. M. Beierle, M. C. A. Stuart, B. Macia, G. Caroli, J. T. Mika, D. J. van Dijken, J. Chen, W. R. Browne, B. L. Feringa, *Nat. Nanotechnol.* **2011**, *6*, 547–552.
[36] A. Huizing, *Master Thesis: Synthesis of Xanthone-Derived Amphiphiles*, University of Groningen, **2014**.
[37] B. J. Ravoo, J. B. F. N. Engberts, *Langmuir* **1994**, *10*, 1735–1740.
[38] P. J. Missel, N. A. Mazer, G. B. Benedek, M. C. Carey, *J. Phys. Chem.* **1983**, *87*, 1264–1277.
[39] J. J. H. Nusselder, T. J. De Groot, M. Trimbos, J. B. F. N. Engberts, *J. Org. Chem.* **1988**, *53*, 2423–2426.
[40] J. J. H. Nusselder, J. B. F. N. Engberts, *J. Org. Chem.* **1991**, *56*, 5522–5527.
[41] I. Visscher, *PhD Thesis: Amphiphiles Containing Aromatic Groups in the Hydrophobic Part*, University of Groningen, **2004**.
[42] A. Bouzide, G. Sauvé, *Org. Lett.* **2002**, *4*, 2329–2332.
[43] E. Lee, Y. -H. Jeong, J. -K. Kim, M. Lee, *Macromolecules* **2007**, *40*, 8355–8360.
[44] Y. Okahata, S. Tanamachi, M. Nagai, T. Kunitake, *J. Colloid Interface Sci.* **1981**, *82*, 401–417.
[45] J. T. van Herpt, *PhD Thesis: Photo- and Mechano-Responsive Supramolecular Systems*, University of Groningen, **2013**.

[46] J. Clayden, *Organolithiums: Selectivity for Synthesis*, Elsevier, Amsterdam, The Netherlands **2002**.
[47] P. Beak, A. Basu, D. J. Gallagher, Y. S. Park, S. Thayumanavan, *Acc. Chem. Res.* **1996**, *29*, 552–560.
[48] M. C. Whisler, S. MacNeil, V. Snieckus, P. Beak, *Angew. Chem. Int. Ed.* **2004**, *43*, 2206–2225.
[49] P. G. M. Wuts, T. W. Greene, *Greene's Protective Groups in Organic Synthesis*, John Wiley & Sons, Hoboken, N.J, USA, **2006**.
[50] C. B. Reese, H. Yan, *J. Chem. Soc. [Perkin 1]* **2001**, *15*, 1807–1815.
[51] H. -N. Trân, T. -N. Pham, *Tetrahedron* **2001**, *57*, 1289–1295.
[52] V. Snieckus, *Chem. Rev.* **1990**, *90*, 879–933.
[53] H. P. Plaumann, B. A. Keay, R. Rodrigo, *Tetrahedron Lett.* **1979**, *20*, 4921–4924.
[54] H. Gilman, F. J. Webb, *J. Am. Chem. Soc.* **1949**, *71*, 4062–4066.
[55] S. Cabiddu, S. Melis, P. P. Piras, M. Secci, *J. Organomet. Chem.* **1977**, *132*, 321–326.
[56] S. Cabiddu, S. Melis, P. P. Piras, F. Sotgiu, *J. Organomet. Chem.* **1979**, *178*, 291–300.
[57] P. Tomboulian, K. Stehower, *J. Org. Chem.* **1968**, *33*, 1509–1512.
[58] M. Schlosser, *Organometallics in Synthesis, Third Manual*, John Wiley & Sons, Weinheim, Germany, **2013**.
[59] M. Schlosser, *Organomet. Synth. Man.* **1994**, 1–166.
[60] M. Schlosser, *Pure Appl. Chem.* **2009**, *60*, 1627–1634.
[61] F. Mongin, R. Maggi, M. Schlosser, *Chim. Int. J. Chem.* **1996**, *50*, 650–652.
[62] M. R. Odrowaz-Sypniewski, P. G. Tsoungas, G. Varvounis, P. Cordopatis, *Tetrahedron Lett.* **2009**, *50*, 5981–5983.
[63] H. Prinz, W. Wiegrebe, K. Müller, *J. Org. Chem.* **1996**, *61*, 2853–2856.
[64] C. W. Hui, T. C. W. Mak, H. N. C. Wong, *Tetrahedron* **2004**, *60*, 3523–3531.
[65] D. R. Robello, T. D. Eldridge, E. J. Urankar, *Org. Prep. Proced. Int.* **1999**, *31*, 433–439.
[66] H. Prinz, P. Schmidt, K. J. Böhm, S. Baasner, K. Müller, M. Gerlach, E. G. Günther, E. Unger, *Bioorg. Med. Chem.* **2011**, *19*, 4183–4191.
[67] C. Gao, D. Cao, S. Xu, H. Meier, *J. Org. Chem.* **2006**, *71*, 3071–3076.
[68] H. Baba, T. Takemura, *Tetrahedron* **1968**, *24*, 4779–4791.
[69] M. M. Pollard, M. Lubomska, P. Rudolf, B. L. Feringa, *Angew. Chem. Int. Ed.* **2007**, *46*, 1278–1280.
[70] A. R. McCarthy, L. Pirrie, J. J. Hollick, S. Ronseaux, J. Campbell, M. Higgins, O. D. Staples, F. Tran, A. M. Z. Slawin, S. Lain, et al., *Bioorg. Med. Chem.* **2012**, *20*, 1779–1793.
[71] M. Rubinshtein, C. R. James, J. L. Young, Y. J. Ma, Y. Kobayashi, N. C. Gianneschi, J. Yang, *Org. Lett.* **2010**, *12*, 3560–3563.
[72] M. K. Müller, L. Brunsveld, *Angew. Chem. Int. Ed.* **2009**, *48*, 2921–2924.
[73] A. C. Coleman, J. Areephong, J. Vicario, A. Meetsma, W. R. Browne, B. L. Feringa, *Angew. Chem. Int. Ed.* **2010**, *49*, 6580–6584.
[74] C. J. Newcomb, T. J. Moyer, S. S. Lee, S. I. Stupp, *Curr. Opin. Colloid Interface Sci.* **2012**, *17*, 350–359.

Chapter 5

Ion-Conducting Lipid Bilayers

In this chapter, novel amphiphiles that self-assemble into ion-conducting bilayers are described. The molecular structures comprise of a thioxanthane core that connects two hydrophobic alkyl chains with the hydrophilic oligo-ethyleneglycol chain and these amphiphiles form highly stable planar bilayers as well as spherical nano-containers of different sizes. Conductance and fluorescence dequenching ensemble measurements together with single molecule electrophysiology show that the bilayers allow the passage of small ions but retain large anions, and can accommodate a biological ion channel in its functional form. A mimic for a biological membrane that is biocompatible and permeable to certain ions holds promise for the generation of an electrochemical gradient across the lipid bilayer and is a significant step toward the development of artificial cellular systems.

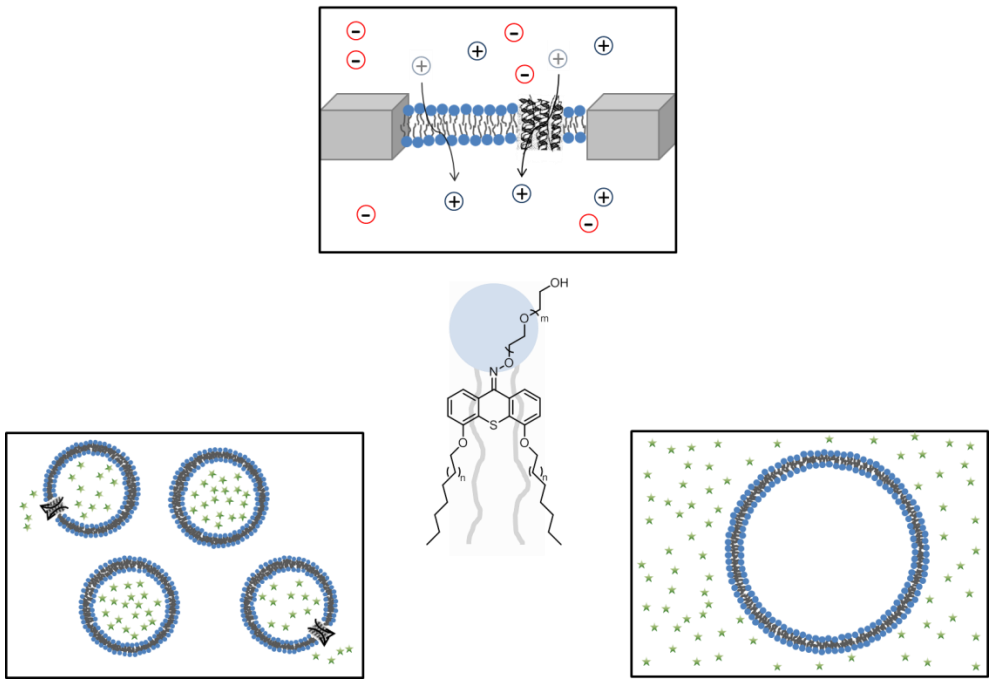

Part of the research presented in this chapter will be published:
D. J. van Dijken, D. Yilmaz, A. Koçer, B. L. Feringa *submitted*

5.1 Introduction

The cell membrane is a biological membrane that separates the interior of the cell from the environment on the outside (Figure 5.1). The membrane itself is extremely complex and effectively controls the selective passage of materials in and out of the cell. Biological membranes not only define the boundaries of the cells and cellular compartments but also have an important function in governing membrane transport and maintaining electrical and chemical potential differences between both sides of the membrane at a resting state.[1]

In addition to the cell membrane, many other lipid membranes can be found inside the cell, compartmentalizing the different parts of the cell. The main constituents of these biological membranes are proteins and lipids.[2] The lipids found in biological membranes are mainly phospholipids but non-phospholipids are also known.

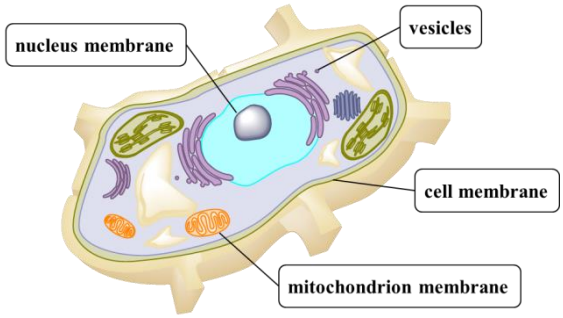

Figure 5.1. Schematic drawing of a typical cell and some of its external and internal membranes.

The cell membrane itself is composed of a 3 – 5 nm thick lipid bilayer,[2] which is an electrical insulator due to its low intrinsic permeability to ions, and its conductivity comes from the ion channels embedded in it. The transmembrane ionic concentration difference, together with the difference in the degree of permeability of the membrane to specific ions provided by its ion channels, establishes the transmembrane potential.[1,3] The transient changes in the transmembrane potential energetically drive many crucial physiological functions of the cells ranging from cellular communication and muscle contraction to energy generation.[1,3]

Due to the complexity of the cell membrane, artificial membrane systems have been developed and studied as models for the natural cell membrane. The basis of model membrane systems was established in 1965 by Alec Bangham and coworkers.[4] In the following years, a variety of closed-shell phospholipid liposomes, based on single bilayers, were reported.[5] The idea that these liposomes could encapsulate drugs and be used as drug delivery systems followed shortly after.[6–8] In 1976, Mayhew and coworkers showed that liposome-entrapped cytosine arabinoside (an anti-cancer drug) shows *in vivo* activity in animal models, increasing survival of mice bearing L1210 leukemia by over 90%.[9] The free drug on the other hand, had no effect on the survival of mice. This finding led to the development of other liposome-entrapped drugs[10,11] and in 2012, more than a dozen liposomal drugs were clinically approved.

The importance of liposomes is mostly associated with their ability to encapsulate a wide variety of substances and function as target-oriented carriers.[9,12,13] In addition, liposomes can serve as a models for cells, mimicking cell membranes due to having similar components and a similar structure. The properties of the liposomes are strongly dependent on the properties,

i.e. the molecular structure, of the lipids that make up the bilayers of the liposomes. Having control over the molecular structure, and therefore the properties of the lipid, offers fascinating opportunities for artificial, synthetic amphiphiles.

In addition to liposomes, planar bilayer lipid membranes (BLMs) have found extensive use. BLMs can be viewed as immobilized bilayers, attached to a support, separating two compartments from each other (Figure 5.2). One of the main advantages is that both sides of the bilayer are accessible and this enables full control over the environment of both sides after formation of the planar bilayer.

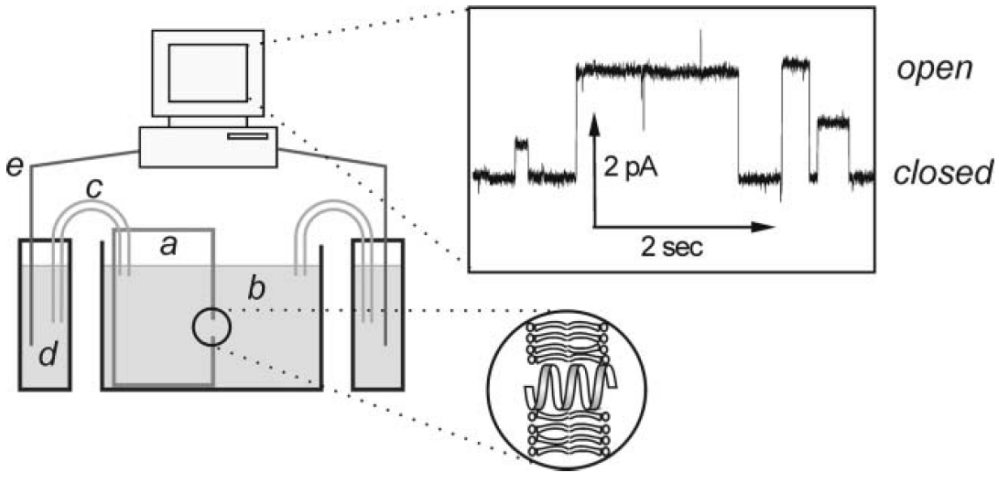

Figure 5.2. Schematic representation of a BLM setup.[14] A cup (a), with a small hole cut into one face, is immersed in an electrolyte (b) and the bilayer is formed by painting lipid across the hole. Electrical contact with Ag/AgCl reference electrodes (e) in a reference electrolyte (d) is achieved *via* Agar salt-bridges (c). A potential is applied and the current measured as a function of time. Ion channel activity appears as abrupt transitions, as shown. (Figure reproduced from reference 14)

Mimicking the controlled permeability of biological membranes in synthetic systems would be a significant step forward in artificial cell design. To this end, there have been major efforts to make synthetic ion channels that have similar sensitivity, permeability, and selectivity as their biological counterparts.[15–28] As a result, recently, synthetic channels with ion selectivity started to emerge.[15–30] Alternatively, there have been efforts toward the engineering of the bilayer itself.[31] In these studies, the goal is to control the permeability of the membrane by stimuli responsive changes in membrane structure and surface characteristics.

5.2 Concept

The research presented in this chapter describes a lipid membrane comprising of non-phospholipid amphiphiles that self-assemble into stable bilayers in aqueous environment. The synthesis of the amphiphiles was readily accomplished and the bilayer properties were studied, using a variety of analytical techniques. Unlike biological lipid bilayers, these membranes conduct positive and negative ions by themselves at applied voltages without the need for any ion channels, pumps or transporters. The lipid bilayer also allows the insertion of a pore forming peptide, alamethicin. Interestingly, the membranes do not allow the passage of larger, charged dye molecules in aqueous environments.

Despite developments on synthetic ion channels and responsive membranes, there is still no simple system that could generate a transmembrane potential in an artificial cell. The lipid mimic described in this chapter is a promising candidate to mimic the Gibbs-Donnan equilibrium system (Figure 5.3) seen in muscle cells.[32] In these cells, the membrane is permeable to specific anions and cations *via* specific ion channels and the ratio of the transmembrane ion concentration for diffusible anions and cations is equal. However, a transmembrane potential is created by the presence of non-diffusible negatively charged intracellular molecules that attract positively charged ions and repel negative ones, generating an ion gradient across the bilayer for the diffusible ions.[33] Our simple system shows promise to generate transbilayer potentials.

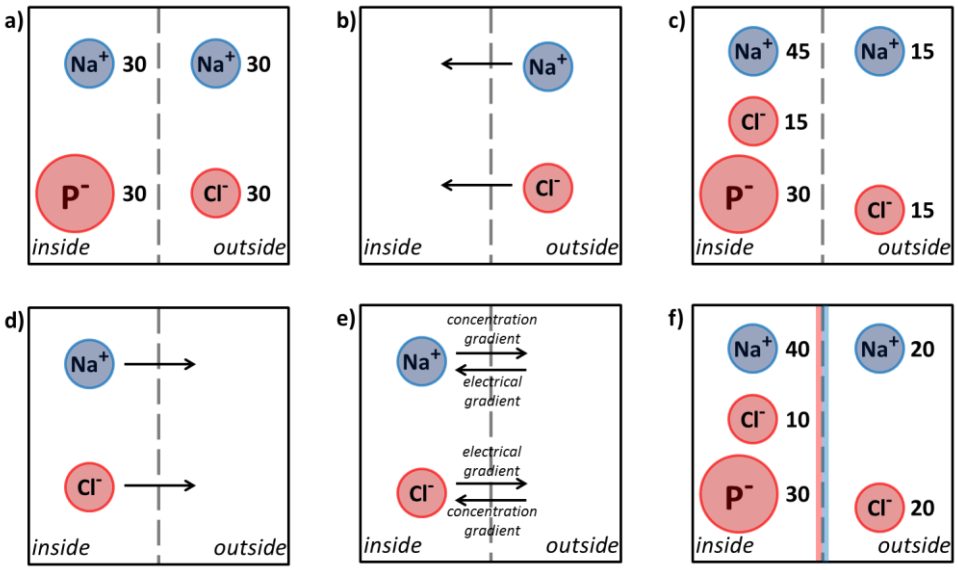

Figure 5.3. Gibbs-Donnan equilibrium.[3] a) A hypothetical situation, the semipermeable membrane dividing inside and outside is permeable to Na^+ and Cl^-, but impermeable to P^-. b-e) Conceptual stages that eventually lead to an equilibrium. f) Equilibrium situation.

The Gibbs-Donnan equilibrium can be explained by picturing a situation where a semipermeable membrane separates two electrolyte solutions, such as the plasma membrane that separates the inside and outside of the cell.[3] The electrolyte solutions consist of permeable ions such as Na^+ and Cl^- and impermeable charged molecules such as P^- that are trapped on the inside side of the bilayer. At the start (Figure 5.3a), all ions and molecules are present in a certain concentration (in Figure 5.3a, Na^+ is present in 30 mM on both the inside and outside of the membrane, Cl^- is only present on the outside and the impermeate charged molecule P^- is only present on the inside of the membrane, both in a concentration of 30 mM). The concentration gradient leads to diffusion of Cl^- from the outside to the inside. That will, however, create an electrical gradient that leads to diffusion of Na^+ from the outside to the inside. Basically, every Cl^- ion is accompanied by a Na^+ ion (Figure 5.3b). This results in a situation as shown in Figure 5.3c. As the concentration of Na^+ is higher (45 mM) on the inside than on the outside (15 mM), Na^+ will diffuse from the inside to the outside and to maintain electrical neutrality, Cl^- also diffuses (Figure 5.3d). Overall, diffusion of Na^+ from inside to outside creates a net positive charge on the outside of the membrane so that an equilibrium is reached when the concentration gradient from inside to outside matches the electrical gradient

for Na^+ from outside to inside (Figure 5.3e). In the same way, the concentration gradient for Cl^- from outside to inside balances the electrical gradient from inside to outside (Figure 5.3e), resulting in a net negative charge on the inside of the membrane. In the equilibrium situation (Figure 5.3f), a potential difference has developed between the two surfaces of the membrane, the outside being positive compared to the inside. The positivity on the outside prevents further diffusion of Na^+ and the negativity on the inside prevents further diffusion of Cl^-. In the end situation, the concentration of Na^+ is higher on the inside and the concentration of Cl^- is higher on the outside, generating the membrane potential across the semipermeable lipid bilayer.

The design of the amphiphile presented in this chapter is inspired by our recent work on responsive, self-assembled nanotubes.[34] The nanotubes were shown to be remarkably rigid and this was attributed to the interdigitating alkyl chains of the nanotube-forming amphiphile. This prompted us to design an analogue that would be more soluble and of which the synthesis is more scalable and facile. We envisioned that by introducing more flexibility into the system, while keeping the hydrophobic half (which makes up the internal part of the bilayer) of the molecule similar to that of the nanotube amphiphile, amphiphiles with interesting properties may be obtained. The amphiphiles presented in this chapter are based on a simple building block that can be synthesized on large scale. Amphiphile **5.1** (Figure 5.4) contains a thioxanthane core that connects two hydrophobic alkyl chains with the hydrophilic oligo-ethyleneglycol headgroup.

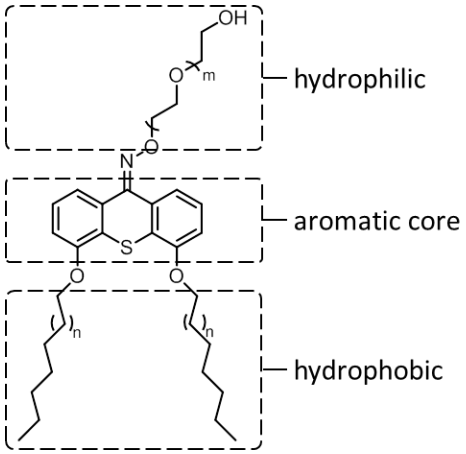

Figure 5.4. Design and structural features of non-phospholipid amphiphile **5.1**.

5.3 Synthesis

Synthesis of key building block, thioxanthone **3.8** is described in chapter 3 and is readily achieved in 78% over 4 steps and can be obtained in large quantities (verified up to 20 g in one batch). Starting from **3.8**, the synthesis of amphiphile **5.1a** (**4.20** in chapter 4) and **5.1b** (**4.21** in chapter 4) can be achieved in five steps and is described in detail in chapter 4. A brief description is given below (Scheme 5.1).

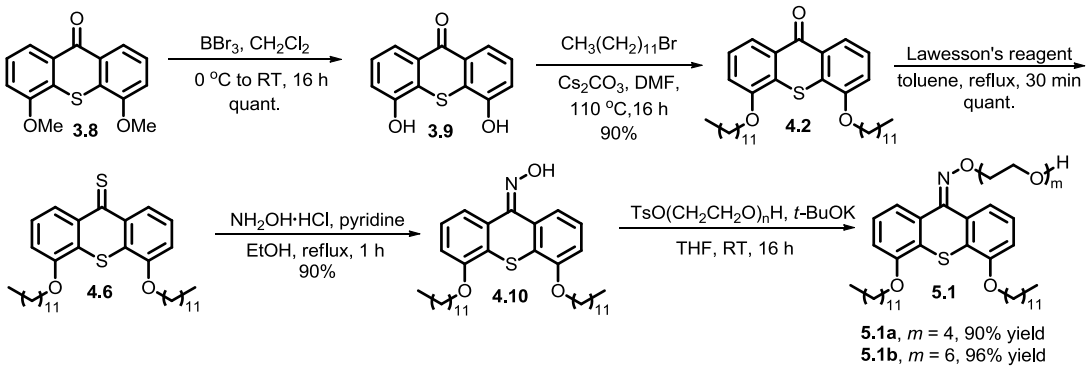

Scheme 5.1. Synthesis of amphiphile **5.1**.

Deprotection of the ether groups with BBr_3 provides diphenol **3.9**, which reacts with laurylbromide to yield the hydrophobic half **4.2** of the target amphiphile. Conversion into the corresponding thioketone **4.6** increases the reactivity, and subsequent reaction with hydroxylamine, gives **4.10**. The oxime was then functionalized with an appropriate oligo-ethyleneglycol chain to give amphiphile **5.1** (73–78% overall yield from **3.8**). The nature of the amphiphile can be readily modified by changing the alkylhalide as well as monotosyl-ethyleneglycol for a different electrophile. This was demonstrated by the synthesis of **5.1a** and **5.1b**, bearing tetra-ethyleneglycol and hexa-ethyleneglycol as the hydrophilic chains, respectively.

5.4 Self-assembly and membrane properties

With amphiphiles **5.1a** and **5.1b** in hand, bilayer formation was confirmed by cryo-transmission electron microscopy (TEM) measurements. Employing standard protocols, vesicles of **5.1a** with a diameter of ~160 nm and ~120 nm for **5.1b** were obtained (Figure 5.5).

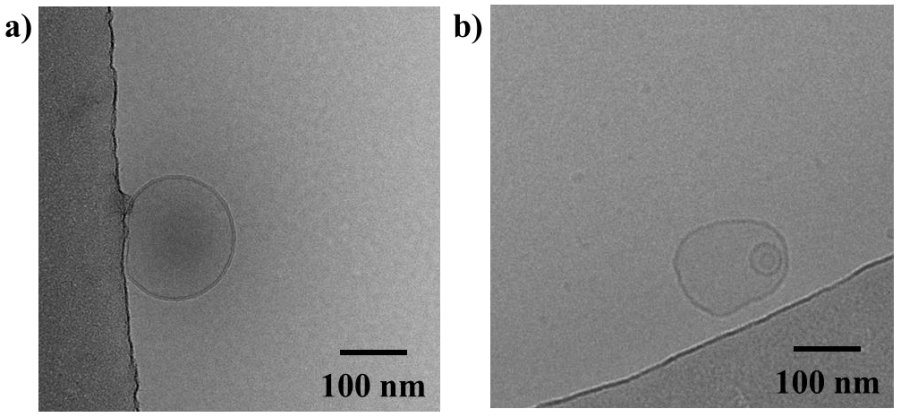

Figure 5.5. Cryo-TEM measurements of **5.1**. a) Vesicles of **5.1a**, with diameters of ~160 nm. b) Vesicles of **5.1b**, with diameters of ~120 nm.

Next, we studied the bilayer properties by using standard black lipid membrane (BLM) measurements.[35,36] To this end, bilayers were formed with **5.1a** and control lipids, i.e. commonly used phospholipid 1,2-dioleoyl-sn-glycero-3-phosphocholine (DOPC), or a 3:7 mixture of DOPC and 1,2-dioleoyl-sn-glycero-3-phosphoethanolamine (DOPE) across a 250 μm aperture, separating two compartments filled with an 50 aq. mM NaCl solution, by using

the painting method.[35–37] Membrane formation was followed by measuring the bilayer capacitance[38] (Figure 5.6, left panel). Biological membranes behave as a capacitor by serving as an insulator separating two conducting solutions. In order to examine the formation of the lipid bilayer, the capacitance test function of the instrument (BC-535 amplifier) was used. Upon applying a triangular wave to the membrane, a square wave in which the amplitude is proportional to the membrane capacitance was observed, as expected for a capacitor. While the control lipid mixture gave flat-top square waves (Figure 5.6a, left panel), **5.1a** showed imperfect square waves, in which the top of the squares are not flat (Figure 5.6b, left panel), indicating that membranes of **5.1a** are less insulating than those of bilayers based on control lipids DOPC/DOPE (Figure 5.6c, left panel).

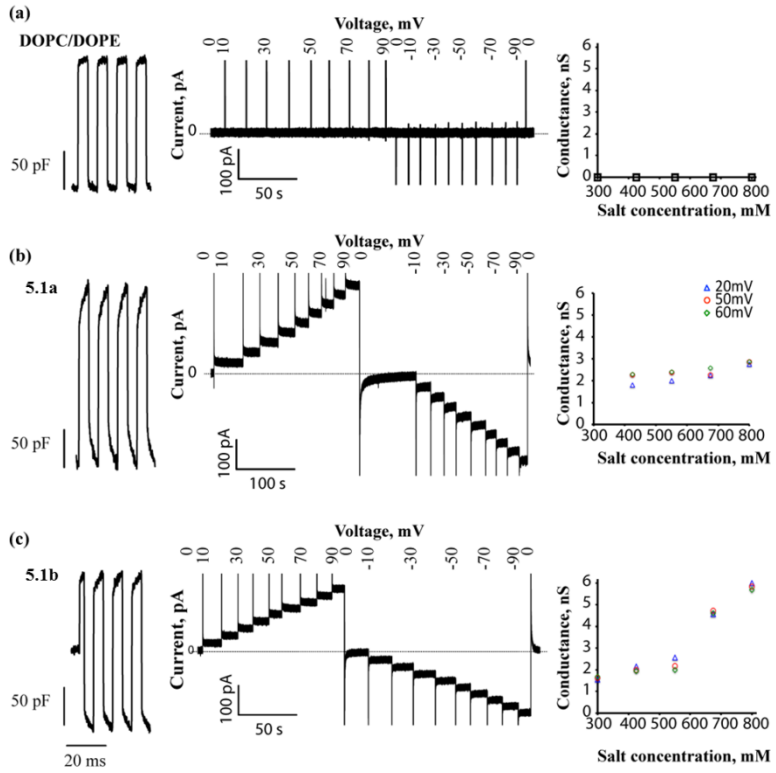

Figure 5.6. Planar bilayer formation and its ionic conductance properties for a) DOPC/DOPE. b) **5.1a**. c) **5.1b**. The left panel shows representative capacitance traces of the planar bilayers. The current response of the bilayers at positive and negative applied voltages, and the dependence of the ionic conductance to different salt (NaCl) concentrations are indicated in the middle and the right panels, respectively.

In practice, it turned out to be slightly more difficult to form a bilayer of **5.1a**, i.e., more painting[35–37] attempts are generally required to form a bilayer of **5.1a**, compared to formation of a bilayer from DOPC/DOPE. However, once formed, they presented reproducible characteristics. To further improve the bilayer formation, we envisioned to increase the hydrophilicity of the headgroup to allow for better hydration. In amphiphile **5.1b**, the headgroup was extended by two ethyleneglycol units, while the hydrophobic part of the amphiphile, and therefore the internal part of the bilayer, was kept identical. Bilayers of amphiphile **5.1b** formed more readily, compared to **5.1a**. As for **5.1a**, the capacitance measurements gave non-perfect square waves for **5.1b** (Figure 5.6c, left panel), suggesting that bilayers formed from **5.1a** and **5.1b** are not good insulators compared to biological membranes. Indeed, when we applied voltage to the bilayer, while the control lipid DOPC/DOPE did not

allow the passage of ions and hence gave zero current (Figure 5.6a, middle panel), both **5.1a** and **5.1b** conducted ions at both positive and negative applied voltages (Figure 5.6, middle panel). The current increased linearly with increasing applied voltage. Furthermore, the bilayers of **5.1a** and **5.1b** were very stable; they did not rupture for at least 2 h and relatively high voltages (up to 0.35 V for **5.1a** and 1.0 V for **5.1b**) could be applied for 5 min, with no influence on the membrane properties. The response of the membranes proved to be highly reversible and no significant changes in conductance were observed for several cycles of switching between positive and negative voltages (Figure 5.7).

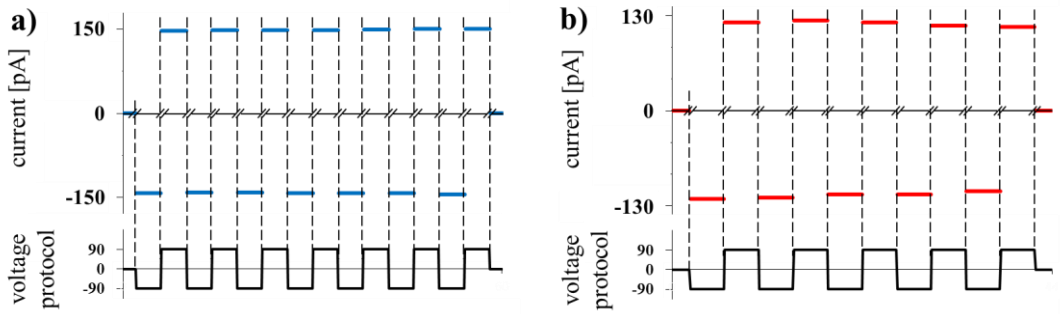

Figure 5.7. Reversibility of the response in current to a change in voltage for lipid bilayers of **5.1**. The voltage was alternated between -90 and 90 mV several times and the resulting current is plotted. a) **5.1a**; bilayer capacitance 116 pF. b) **5.1b**; bilayer capacitance 86 pF. Between the changes in voltage, the voltage was kept constant for 10 s.

Next, we examined the salt dependence by measuring the ionic current at different salt concentrations. While the control lipid bilayer (Figure 5.6a, right panel) did not conduct any ions at any salt (NaCl) concentrations, both **5.1a** (Figure 5.6b, right panel) and **5.1b** (Figure 5.6c, right panel) had increasing conductances with increasing salt concentration. Furthermore, at a given salt concentration, the conductance did not change at various applied voltages (Figure 5.6b-c, right panel, tested up to 60 mV), indicating that the conducting behavior of the lipid bilayer does not originate from the applied voltage. These results demonstrate that **5.1a** and **5.1b** form lipid bilayers and allow the passage of ions without disrupting the membrane.

The biocompatibility of these conducting membranes was tested by the incorporation of a model, pore forming peptide, i.e. alamethicin.[39] Membranes with a capacitance of >70 pF were used throughout the study. To this end, 5 µL of alamethicin from a 1 mg/mL stock (in methanol), was added into the buffer (50 mM aq. NaCl) on the *cis* side of the bilayer in a standard BLM setup. When a voltage was applied, the membrane became conducting as described earlier. A few min after applying a voltage across the bilayer, distinct alamethicin channels could be observed in membranes of both **5.1a** and **5.1b** (Figure 5.8a and 5.8b), which confirms that the membrane protein retained its functionality in these bilayers, just like in the control bilayers (Figure 5.8c).

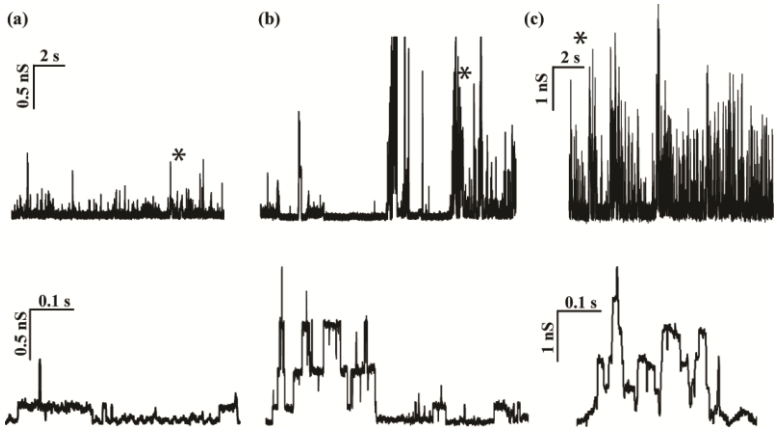

Figure 5.8. Representative activity of functional alamethicin pores in planar bilayers formed from amphiphiles **5.1a** (a) and **5.1b** (b) at 230 and 240 mV applied voltage, respectively, in 50 mM aq. NaCl and the control lipids DOPC/DOPE (c) at 20 mV applied voltage in 1 M aq. NaCl. The channel openings are shown as upward deflections. The asterisk (*) in the top panel marks the position shown magnified in the bottom panel.

The conductance of the membrane itself did not change upon addition of alamethicin. In order to study the function of ion channels in more detail or possibly exploit the sensitivity and functionality of ion channels, stable bilayers are a key prerequisite[40,41] and bilayer membranes of **5.1** proved to be suitable for this purpose.

Additionally, we investigated if the addition of **5.1** to DOPC/DOPE (3:7) could lead to conducting patches in the otherwise non-conducting planar bilayer of DOPC/DOPE. Addition of either **5.1a** or **5.1b** to a pre-formed membrane of DOPC/DOPE did not lead to conductivity, presumably due to inefficient incorporation of the synthetic amphiphiles into the membrane. Prolonged waiting periods or stirring may lead to better mixing and formation of conducting patches in the existing phospholipid bilayer, but this was not investigated further. However, when forming a membrane of pre-mixed DOPC/DOPE with **5.1a** or **5.1b** (3:7:5 w/w in both cases), conductivity is observed albeit to a lesser extent than for membranes formed from pure **5.1a** or **5.1b**. This suggests that mixed membranes are formed. More experiments would be required to confirm these observations.

5.5 Liposomes

As amphiphiles **5.1** form stable, conducting and biocompatible lipid bilayers, the possibility to create cell-sized containers from **5.1** was investigated. These liposomes can encapsulate a variety of hydrophilic substances, be decorated with different molecules and not only form a basis for artificial cell mimics, but also have prospect as nano-reactors[42,43] or target-oriented carriers.[12] For loading and delivery applications, large unilamellar vesicles (LUVs) are the most promising type of liposomes because of their homogeneity and high encapsulating efficiency.[44] In order to generate LUVs, first a thin layer of **5.1** was formed, from a chloroform solution, on the walls of a glass vial under a low N_2-flow, while rotating the sample. Then, the resulting lipid film was rehydrated with sodium phosphate buffer (10 mM sodium phosphate, pH = 8.0, 150 mM NaCl). After freeze-thawing the sample three times and subsequent homogenization, the lipid suspension was extruded through a 400 nm filter in the presence of the self-quenching fluorescent dye calcein The LUVs were purified from external calcein by size exclusion

chromatography. The membrane integrity of the LUVs was measured by following the leakage of calcein using a fluorescence dequenching assay.[45]

The principle of the assay is that if the lipid vesicle, containing self-quenching concentrations of calcein, does not leak the dye under isosmotic conditions, no significant fluorescence signal is measured. However, if calcein leaks out of the vesicles, it dilutes in the measurement buffer, thereby generating a fluorescence signal. At the end of each experiment, the total fluorescence of the sample was determined by dissolving the vesicles by adding a detergent; Triton X-100 (Figure 5.9).

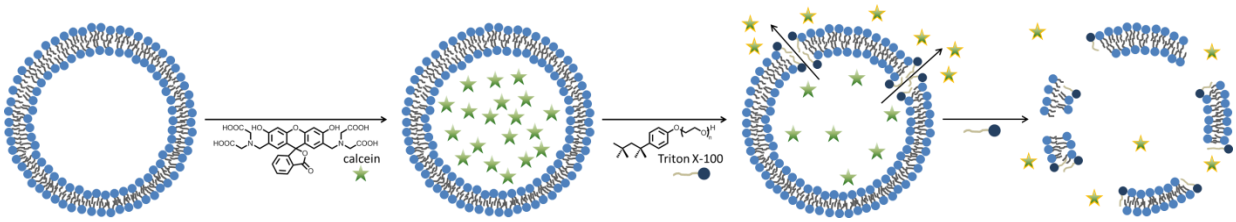

Figure 5.9. Schematic representation of fluorescent dequenching assay of LUVs, using self-quenching calcein.

The detergent incorporates in the bilayer membranes of the LUVs and makes it possible for calcein to leak out and eventually bursts the LUVs so that all calcein is released into the bulk solution. Because an excess is used, the LUVs burst instantly upon addition of the detergent (Figure 5.10). As **5.1b** presumably hydrates better, more liposomes are formed and the amount of calcein released (and therefore the fluorescence) after addition of detergent was higher than for **5.1a**.

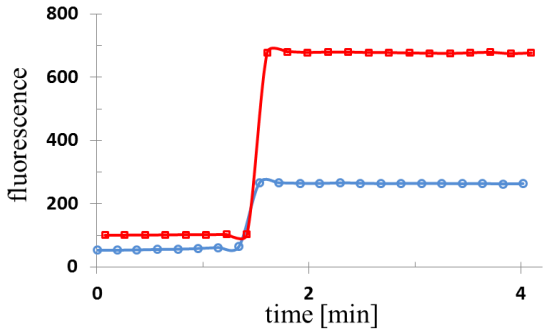

Figure 5.10. Fluorescent dequenching assay of LUVs of **5.1a** (circles, blue line) and **5.1b** (squares, red line). Triton X-100 was added after 90 s.

In our experiments, calcein stayed encapsulated as cargo inside the LUVs and no detectable leakage was observed over a time period of 3 d for LUVs of either **5.1a**, **5.1b** or the control LUVs, stored at room temperature (Figure 5.11). This observation is remarkable and shows that unlike its permeability to small ions, the bilayer membranes of **5.1** are not permeable to bigger, charged molecules such as calcein, similar to membrane impermeant charged molecules in biological cells. This may provide a basis for the generation of a membrane potential across the membranes, based on the Gibbs-Donnan effect.[3,46]

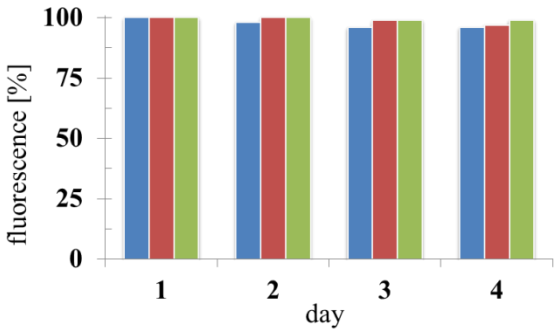

Figure 5.11. Normalized fluorescence after storage of LUVs of **5.1a** (blue), **5.1b** (red) and DOPC/DOPE 3:7 (green) at room temperature.

Next, we tested if alamethicin could be incorporated in LUVs of **5.1**. Alamethicin showed good incorporation in planar BLMs, but is known to be sensitive to membrane properties.[39] As LUVs are spherical, the surface tension of the membrane is different than for planar bilayers of the same amphiphiles. A schematic representation of the experiment is shown in Figure 5.12. Alamethicin is added to dye-loaded LUVs. If alamethicin inserts and retains its function as a channel or pore, calcein can flow out of the LUVs to some extent. By adding detergent after the efflux of calcein has stabilized, the remaining calcein is released from the LUVs.

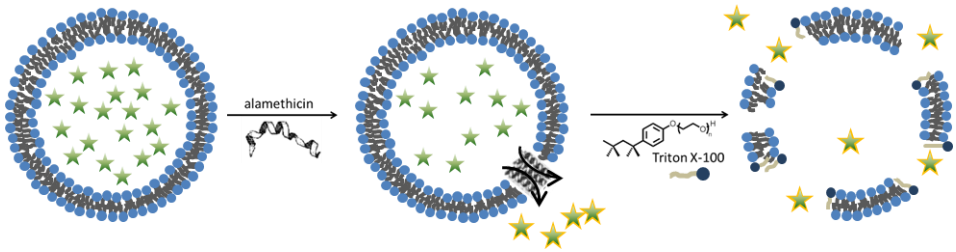

Figure 5.12. Schematic representation of fluorescent dequenching assay of LUVs to study the insertion of alamethicin.

LUVs of all lipids were prepared and after separation of the external dye by size exclusion chromatography, 50 µL of LUVs was added into 2 mL of buffer (10 mM sodium phosphate, pH = 8.0, 150 mM NaCl, 1 mM EDTA). Upon addition of alamethicin (final concentration: 5 µg/mL) at t = 45 s, calcein was released from the LUVs of both **5.1a** and **5.1b** and the control LUVs (Figure 5.13).

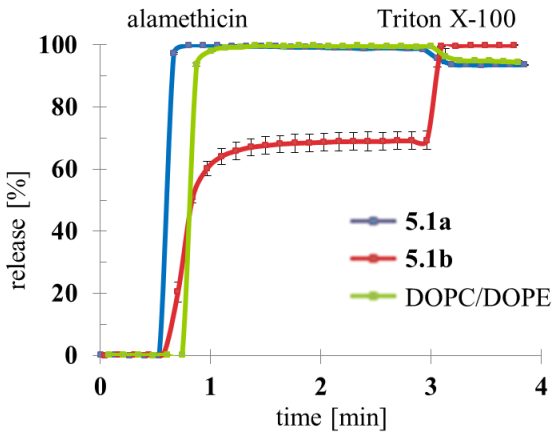

Figure 5.13. Normalized fluorescence upon insertion of alamethicin in LUVs of **5.1a** (blue line), **5.1b** (red line) and DOPC/DOPE 3:7 (green line) loaded with calcein. Alamethicin was added at t = 45 s. Once the signal stabilizes (t = 3 min), Triton X-100 (excess) was added to dissolve the LUVs. The experiment was performed in triplo and error bars are shown.

While the release from **5.1a** and control[47] DOPC/DOPE LUVs could reach 100% with the amount of alamethicin used, **5.1b** LUVs gave only 60% release. Addition of more alamethicin also resulted in 100% release from **5.1b** LUVs. The requirement for higher alamethicin concentrations to reach 100% release for **5.1b** LUVs is attributed to better hydration of **5.1b** compared to **5.1a**, i.e. the presence of more **5.1b** LUVs in a given volume, relative to **5.1a** LUVs.

After initial release, no significant leakage was observed from LUVs of **5.1b**. Next, a detergent (Triton X-100) was added and the LUVs burst, releasing the remaining encapsulated calcein into solution (Figure 5.13). This shows that alamethicin was able to incorporate into the LUVs bilayers and that its function as a channel is retained in these closed, spherical nano-containers, in addition to functioning in planar bilayers of **5.1a** and **5.1b**.

In addition to voltage gated ion channels such as alamethicin, mechanosensitive channels, such as the mechanosensitive channel of large conductance (MscL) are of interest. These channels are versatile and protein engineering has made it possible to change the sensory characteristics of MscL. Important properties such as modality have been successfully modified and new properties can be introduced, e.g., light-activatable nanovalves based on MscL have been developed,[45] showing that manipulation of ion channels is indeed feasible. The properties of MscL can be controlled to a better extent than alamethicin and therefore, the insertion of MscL into bilayers of **5.1a** and **5.1b** was attempted.

Following standard protocols,[48–50] the reconstitution of MscL into bilayers of type **5.1** was, however, unsuccessful thus far. Varying the amount of detergent or increasing the temperature (up to 50 °C) during reconstitution did not yield any incorporated MscL channels in LUVs of **5.1** as determined by calcein efflux measurements. In addition, gel electrophoresis of the liposomes, after pelleting down the samples, did not confirm the presence of MscL in LUVs of **5.1** in all cases.

Noting that stable LUVs can be formed from **5.1**, the next goal was to form giant unilamellar vesicles (GUVs). GUVs have similar size and membrane curvature as cells (typically 1-100 μm).[51] However, unlike biological cells, increasing the size of lipid vesicles usually makes them more fragile and less easy to handle. The preparation and physical properties of GUVs have been studied extensively, but the relative poor stability is the major limiting factor for practical applications and use as cell mimics.[52] The development of GUVs that are as stable as GUVs formed from DOPC, but have added properties or functionalities is therefore warranted. Here, using the electroformation method,[53] we could form highly stable GUVs from pure amphiphiles **5.1a** and **5.1b** using standard protocols (Figure 5.14).

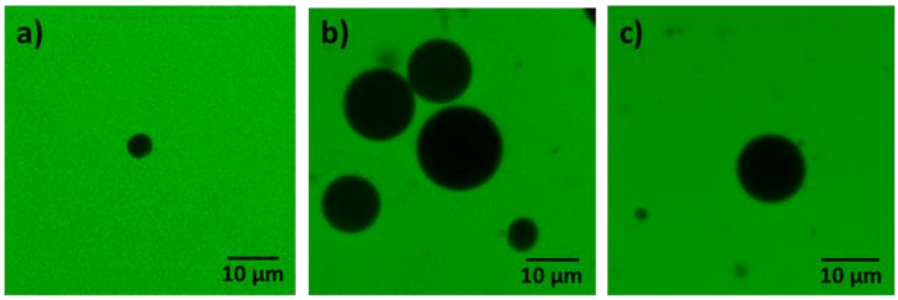

Figure 5.14. Giant unilamellar vesicles (GUVs), formed by electroformation.[53] GUV sizes within the same image appear different due to different focal planes. a) GUVs of **5.1a**. b) GUVs of **5.1b**. c) GUVs of DOPC.

The GUVs formed from **5.1a** were relatively small (diameter ≈ 5 μm) and therefore more mobile, compared to GUVs of DOPC (diameter ≈ 15 μm). Amphiphile **5.1b**, which is more hydrophilic than **5.1a**, gave large GUVs (diameter ≈ 15 – 20 μm), similar to GUVs from DOPC, in high yield. In all samples, we consistently observed a lower number of GUVs for **5.1a** than for **5.1b** and DOPC. Both synthetic amphiphiles form a homogeneous solution of GUVs, using standard protocols. The difference between GUVs of **5.1a** on one hand and GUVs of **5.1b** and DOPC on the other hand, demonstrates that a small change in the molecular structure of the amphiphilic molecule leads to a significant change in the self-assembled bilayer and therefore the biomimetic system.

Intact GUVs could still be observed after storage of the GUVs from **5.1a** and **5.1b** for 4 d at room temperature. It should be emphasized that after heating the GUVs in water up to 70 °C for 30 min in the presence of calcein, no influx was observed, indicating that the GUVs are stable at elevated temperatures and impermeable to calcein (identical observations were made for the reference GUVs of DOPC).

We hypothesized that by preparing GUVs from mixtures of amphiphile **5.1a** and **5.1b**, different properties might be obtained. GUVs could be formed from 1:1 and 4:1 mixtures of **5.1a** and **5.1b**, however, the properties, i.e. the size and stability, were found to be identical to GUVs consisting of pure **5.1b**. It cannot be concluded that **5.1b** stabilizes the GUVs consisting of **5.1a** however, since it may also be that GUVs of **5.1a** simply did not form from the mixture, even though **5.1a** was present in excess. More experiments would have to be conducted to show the possible stabilizing effect of **5.1b**.

5.6 Conclusions

In conclusion, novel, synthetic amphiphiles that form ion-conducting membranes were developed. Not only highly stable planar lipid bilayers are obtained, but also cell-sized containers. While ions can pass through the bilayer, large charged molecules such as calcein stay on one side of the membrane. Furthermore, we have shown that a functioning membrane protein can be embedded in the bilayer membrane. The conducting properties of the highly stable, functional membrane with no need for specific ion channels, pumps and transporters, combined with the protein compatibility, offers fascinating opportunities toward the design of primitive, functional artificial cells.[54] This simple system has prospects for the generation of transbilayer potentials and thereby energizing processes in such artificial systems, ranging from ion channel functioning to transport.

While the conduction mechanism is not known at this moment, we speculate that the molecules may function as ionophores.[55,56] The ethyleneglycol headgroup may function as a crown ether, hiding the complexed ion's charge from the inner part of the bilayer. The complexed amphiphile disturbs the membrane to allow transport or shuttles to the other side of the membrane, driven by the applied voltage, and releases the ion. An important experiment would be the use of different ions in aqueous solutions, such as KCl, $CaCl_2$ and Na_2CO_3 in the BLM experiment to investigate if there is a preference for certain ions over others and how the different ions affect the conductance. If **5.1** is indeed acting as an ionophore, it should be selective for cations over anions and an effect of the size and valency of the cation on the conductance would be expected.[57,58] This experiment could give a good hint to the mechanism by which the membranes are conducting ions and would be a step forward towards utilizing the Gibbs-Donnan effect.

5.7 Experimental section

General remarks

Reagents were commercially available and used as obtained from Sigma-Aldrich or Acros. Alamethicin was obtained from Fermentek Biotechnology.

Synthesis

Synthesis of amphiphile **5.1a** (**4.20** in chapter 4) and **5.1b** (**4.21** in chapter 4) is described in detail in chapter 4.

Bilayer lipid membranes

Electrophysiology measurements were performed with a Warner Instruments planar lipid bilayer workstation. Both chambers of the instrument were filled with an aq. solution of NaCl (50 mM for **5.1a** and **5.1b** and 1 M for the control lipid). Planar bilayers were formed across the 250 μm aperture (Delrin cup; Warner Instruments, Hamden CT) using the painting method[35–37] from an *n*-decane solution of amphiphiles. The bilayer formation was followed by measuring the capacitance.[38]

Ionic currents passing through the alamethicin channels were measured by a Warner Instruments planar lipid bilayer workstation. Data were amplified and filtered at 10 kHz (BC-535D Bilayer Amplifier; Warner Instruments, Hamden, CT), sampled at 33 kHz (DigiData 1440A; Axon Instruments, Foster City, CA), and stored on a computer using the Axoscope program (version 9.0; Axon Instruments, Foster City, CA). Data analysis was performed using pClamp suite software (version 10.2; Axon Instruments, Foster City, CA).

The functional insertion of membrane proteins into the bilayer was tested by using the self-inserting peptide alamethicin. 5 µL Of alamethicin (Fermentek Ltd, Israel), dissolved in methanol (final concentration: 1 mg/mL), was added to the buffer (50 mM NaCl for **5.1a** and **5.1b** and 1 M for the control lipid) on the *cis* side of the bilayer. A few min after applying a voltage across the bilayer (230 mV and 240 mV for **5.1a** and **5.1b**, respectively, and 20 mV for the control lipid, sampling at 50 kHz and filtering at 5 kHz), conductance typical for distinct alamethicin channels could be observed (see main text, Figure 5.8).

For the linearity measurements, the voltage was increased from -90 mV to 90 mV in steps of 10 mV. Between the increments, the voltage was kept constant for 10 s.

The reversibility of membranes made from **5.1a** and **5.1b** was confirmed by switching between -90 mV and 90 mV or -70 mV and 70 mV for **5.1a** and **5.1b**, respectively. Between the changes in voltage, the voltage was kept constant for 10 s. The capacitance of the membranes was monitored between each cycle and remained unchanged (209 pF for **5.1a** and 279 pF for **5.1b**).

Large unilamellar vesicles

In order to prepare the LUVs, the amphiphiles were dissolved in chloroform (4 mg/mL) and then vacuum-dried under reduced pressure. The dried thin lipid-film was rehydrated in aq. sodium phosphate buffer (10 mM sodium phosphate, pH = 8.0, 150 mM NaCl in H_2O) and the suspension was subjected to three freeze-thaw cycles in liquid nitrogen and a 25 °C water bath, respectively. Then, the lipid suspension was mixed with self-quenching dye calcein in 1:1 (v/v) ratio. The mixture was then homogenized using a mini-extruder (Avanti Polar Lipids) by eleven passages through a polycarbonate filter with a pore size of 400 nm.

Before the fluorescent dequenching assay, the mixture was purified by size exclusion column chromatography (Sephadex G50 Pharmacia) to remove the external dye. Dye-loaded vesicles were collected in eppendorfs.

All elution fractions were assayed in a Varian Cary Eclipse Fluorometer at an excitation wavelength of λ = 495 nm and recording the emission at λ = 515 nm.

Alamethicin incorporation
All elution fractions were assayed in a Varian Cary Eclipse Fluorometer at an excitation wavelength of λ = 495 nm and recording the emission at λ = 515 nm.

In a standard assay, 50 µL calcein-filled vesicles of **5.1a**, **5.1b** or DOPC/DOPE (3:7) were diluted into 2.0 mL efflux buffer (10 mM sodium phosphate, pH = 8.0, 150 mM NaCl, 1 mM EDTA). At t = 45 s, alamethicin (final concentration: 5 µg/mL) was added. The fluorescence was measured continuously, and the total fluorescence of the sample was determined by bursting the vesicles with 0.5% (v/v) Triton X-100 at t = 3 min. As a control, the same batch of vesicles was recorded in the absence of alamethicin. The data sets were normalized by setting the initial fluorescence of each sample as 0% and the signal after the Triton X-100 addition as 100%.

Giant unilamellar vesicles
GUVs were prepared by electroformation according to a standard literature protocol with small adaptations.[53] 20 µL of amphiphiles, dissolved in chloroform (4 mg/mL), was spotted onto the conducting side of an indium tin oxide plate and dried under a N_2-flow. Then, the lipid films were rehydrated in 300 mM sucrose by electroformation using the Vesicle Prep Pro instrument (Nanion Technologies). Electroformation was carried out with AC electrical field applied (10 Hz, 1.1 V) through electrodes sealed on the glass coverslides at 4 °C for 1 h. Subsequently, the GUVs were monitored under a fluorescence microscope.

GUVs were visualized with a fluorescence microscope equipped with a Zeiss C-Apochromat infinity-corrected 1.2 NA 633 water immersion objective and a charge-coupled device camera. For the detection of GUVs, calcein (a fluorescent dye) was mixed with the sample containing GUVs. The laser beam (488 nm, argon ion laser, Innova 99, Coherent, Louisville, CO) was used for excitation of the calcein.

Cryo-transmission electron microscopy
For analysis by cryo transmission electron microscopy (cryo-TEM), the turbid solution (2.5 µL) was placed on a glow-discharged holy carbon coated grid (Quantifoil 3.5/1, QUANTIFOIL Micro Tools GmbH, Großlöbichau, Germany). After blotting, the grid was rapidly frozen in liquid ethane (Vitrobot, FEI, Eindhoven, The Netherlands) and stored in liquid nitrogen until observed. Grids were observed in a Gatan model 626 cryo-stage in a Philips CM120 cryo-electron microscope operating at 120 KeV. Images were recorded under low-dose conditions on a slow-scan CCD camera.

5.8 Acknowledgements

We thank Dr. Martin Walko and and Dr. Gemma Moiset for helpful discussions. Dr. Marc Stuart is acknowledged for Cryo-TEM measurements.

5.9 References

[1] B. Alberts, A. Johnson, J. Lewis, M. Raff, K. Roberts, P. Walter, *Molecular Biology of the Cell, 4th Edition*, Garland Science, New York, USA, **2002**.

[2] H. T. Tien, A. Ottova-Leitmannova, *Membr. Sci. Technol.* **2003**, *7*, 1–73.

[3] R. L. Bijlani, S. Manjunatha, *Understanding Medical Physiology: A Textbook for Medical Students*, Jaypee Bros. Medical Publishers, London, UK, **2010**.

[4] A. D. Bangham, M. M. Standish, J. C. Watkins, *J. Mol. Biol.* **1965**, *13*, 238–252.

[5] G. Sessa, G. Weissmann, *J. Lipid Res.* **1968**, *9*, 310–318.

[6] G. Gregoriadis, B. E. Ryman, *Eur. J. Biochem.* **1972**, *24*, 485–491.

[7] G. Gregoriadis, C. P. Swain, E. J. Wills, A. S. Tavill, *The Lancet* **1974**, *303*, 1313–1316.

[8] G. Gregoriadis, D. Neerunjun, *Biochem. Biophys. Res. Commun.* **1975**, *65*, 537–544.

[9] E. Mayhew, D. Papahadjopoulos, Y. M. Rustum, C. Dave, *Cancer Res.* **1976**, *36*, 4406–4411.

[10] G. Lopez-Berestein, V. Fainstein, R. Hopfer, K. Mehta, M. P. Sullivan, M. Keating, M. G. Rosenblum, R. Mehta, M. Luna, E. M. Hersh, *J. Infect. Dis.* **1985**, *151*, 704–710.

[11] A. Gabizon, T. Peretz, A. Sulkes, S. Amselem, R. Ben-Yosef, N. Ben-Baruch, R. Catane, S. Biran, Y. Barenholz, *Eur. J. Cancer Clin. Oncol.* **1989**, *25*, 1795–1803.

[12] D. Peer, J. M. Karp, S. Hong, O. C. Farokhzad, R. Margalit, R. Langer, *Nat. Nanotechnol.* **2007**, *2*, 751–760.

[13] A. D. Bangham, M. M. Standish, J. C. Watkins, *J. Mol. Biol.* **1965**, *13*, 238–IN27.

[14] T. M. Fyles, *Chem. Soc. Rev.* **2007**, *36*, 335–347.

[15] T. Kiwada, K. Sonomura, Y. Sugiura, K. Asami, S. Futaki, *J. Am. Chem. Soc.* **2006**, *128*, 6010–6011.

[16] J. Montenegro, M. R. Ghadiri, J. R. Granja, *Acc. Chem. Res.* **2013**, *46*, 2955–2965.

[17] J. Sánchez-Quesada, M. P. Isler, M. R. Ghadiri, *J. Am. Chem. Soc.* **2002**, *124*, 10004–10005.

[18] N. Sakai, S. Matile, *Langmuir* **2013**, *29*, 9031–9040.

[19] N. Sakai, S. Matile, *Angew. Chem. Int. Ed.* **2008**, *47*, 9603–9607.

[20] X. Li, B. Shen, X. -Q. Yao, D. Yang, *J. Am. Chem. Soc.* **2009**, *131*, 13676–13680.

[21] K. S. Iqbal, M. C. Allen, F. Fucassi, P. J. Cragg, *Chem. Commun.* **2007**, 3951–3953.

[22] Y. E. Ghoul, R. Renia, I. Faye, S. Rassou, N. Badi, V. Bennevault-Celton, C. Huin, P. Guégan, *Chem. Commun.* **2013**, *49*, 11647–11649.

[23] T. Liu, C. Bao, H. Wang, Y. Lin, H. Jia, L. Zhu, *Chem. Commun.* **2013**, *49*, 10311–10313.

[24] L. Movileanu, S. Howorka, O. Braha, H. Bayley, *Nat. Biotechnol.* **2000**, *18*, 1091–1095.

[25] J. R. Burns, K. Göpfrich, J. W. Wood, V. V. Thacker, E. Stulz, U. F. Keyser, S. Howorka, *Angew. Chem. Int. Ed.* **2013**, *52*, 12069–12072.

[26] M. A. Holden, L. Jayasinghe, O. Daltrop, A. Mason, H. Bayley, *Nat. Chem. Biol.* **2006**, *2*, 314–318.

[27] M. Ma, D. Bong, *Acc. Chem. Res.* **2013**, *46*, 2988–2997.

[28] C. R. Martin, Z. S. Siwy, *Science* **2007**, *317*, 331–332.

[29] G. W. Gokel, S. Negin, *Acc. Chem. Res.* **2013**, *46*, 2824–2833.

[30] D. Wandera, S. R. Wickramasinghe, S. M. Husson, *J. Membr. Sci.* **2010**, *357*, 6–35.

[31] W. Szymański, D. Yilmaz, A. Koçer, B. L. Feringa, *Acc. Chem. Res.* **2013**, *46*, 2910–2923.

[32] D. J. Aidley, *The Physiology of Excitable Cells*, Cambridge University Press, Cambridge, UK, **1998**.

[33] C. Tanford, *Science* **1986**, *233*, 898–898.

[34] A. C. Coleman, J. M. Beierle, M. C. A. Stuart, B. Maciá, G. Caroli, J. T. Mika, D. J. van Dijken, J. Chen, W. R. Browne, B. L. Feringa, *Nat. Nanotechnol.* **2011**, *6*, 547–552.

[35] P. Mueller, D. Rudin, H. Tien, W. Wescott, *Nature* **1962**, *194*, 979–&.
[36] E. T. Castellana, P. S. Cremer, *Surf. Sci. Rep.* **2006**, *61*, 429–444.
[37] P. Mueller, W. Wescott, D. Rudin, H. Tien, *J. Phys. Chem.* **1963**, *67*, 534–&.
[38] W. F. Wonderlin, A. Finkel, R. J. French, *Biophys. J.* **1990**, *58*, 289–297.
[39] B. Leitgeb, A. Szekeres, L. Manczinger, C. Vagvolgyi, L. Kredics, *Chem. Biodivers.* **2007**, *4*, 1027–1051.
[40] A. Hirano-Iwata, M. Niwano, M. Sugawara, *Trends Anal. Chem.* **2008**, *27*, 512–520.
[41] M. Sugawara, A. Hirano, P. Bühlmann, Y. Umezawa, *Bull. Chem. Soc. Jpn.* **2002**, *75*, 187–201.
[42] P. Tanner, P. Baumann, R. Enea, O. Onaca, C. Palivan, W. Meier, *Acc. Chem. Res.* **2011**, *44*, 1039–1049.
[43] Q. Chen, H. Schönherr, G. J. Vancso, *Small* **2009**, *5*, 1436–1445.
[44] T. M. Allen, P. R. Cullis, *Adv. Drug Deliv. Rev.* **2013**, *65*, 36–48.
[45] A. Kocer, M. Walko, B. L. Feringa, *Nat. Protoc.* **2007**, *2*, 1426–1437.
[46] B. Alberts, A. Johnson, J. Lewis, M. Raff, K. Roberts, P. Walter, "Membrane Transport of Small Molecules and the Electrical Properties of Membranes," can be found under http://www.ncbi.nlm.nih.gov/books/NBK21044/, **2002**.
[47] G. van Meer, D. R. Voelker, G. W. Feigenson, *Nat. Rev. Mol. Cell Biol.* **2008**, *9*, 112–124.
[48] G. van den Bogaart, V. Krasnikov, B. Poolman, *Biophys. J.* **2007**, *92*, 1233–1240.
[49] J. H. A. Folgering, J. M. Kuiper, A. H. de Vries, J. B. F. N. Engberts, B. Poolman, *Langmuir* **2004**, *20*, 6985–6987.
[50] R. Rigler, Ü. Mets, J. Widengren, P. Kask, *Eur. Biophys. J.* **1993**, *22*, 169–175.
[51] K. Carvalho, L. Ramos, C. Roy, C. Picart, *Biophys. J.* **2008**, *95*, 4348–4360.
[52] A. Jesorka, O. Orwar, *Annu. Rev. Anal. Chem.* **2008**, *1*, 801–832.
[53] L. Mathivet, S. Cribier, P. F. Devaux, *Biophys. J.* **1996**, *70*, 1112–1121.
[54] T. M. S. Chang, *Artificial Cells*, World Scientific Publishing Co. Pte. Ltd., Singapore, Singapore, **2007**.
[55] F. De Riccardis, I. Izzo, D. Montesarchio, P. Tecilla, *Acc. Chem. Res.* **2013**, *46*, 2781–2790.
[56] I. Alfonso, R. Quesada, *Chem. Sci.* **2013**, *4*, 3009–3019.
[57] F. Vögtle, E. Weber, E. Weber, J. L. Toner, I. Goldberg, F. Vögtle, D. A. Laidler, J. F. Stoddart, R. A. Bartsch, C. L. Liotta, in *Crown Ethers Analogs*, John Wiley & Sons, Inc., Chichester, UK, **1989**, pp. 207–304.
[58] G. W. Gokel, *Crown Ethers and Cryptands, 3rd Edition*, Royal Society Of Chemistry, Cambridge, UK, **1991**.

Chapter 6

Amphiphilic Molecular Motors

In this chapter, amphiphilic molecular motors are described that self-assemble into tubular structures in water. Two different molecular motors, having distinct rotation speeds, were designed, synthesized and their dynamic self-assembly properties examined. The self-assembled aggregates and their function as a motor were studied using cryo-TEM microscopy and UV-vis spectroscopy. The slow motor assembles into nanotubes, which showed reversible behavior and reorganization into different morphologies. The changes could be reversibly induced by going through the rotation cycle of the motor, i.e. alternating light-irradiation and heating of the system. This is, to the best of our knowledge, the first example in which a molecular motor forms well-defined structures in water and in which the molecular component causes a reversible change in morphology when exposed to external stimuli.

Part of the research presented in this chapter will be published:
D. J. van Dijken, J. Chen, M. C. A. Stuart, L. Hou, W. R. Browne, B. L. Feringa, *manuscript in preparation*

6.1 Introduction

The formation of well-defined nanoscale objects that are dynamic in nature and can be visualized with techniques such as electron microscopy, fluorescence or scanning probe techniques is a challenge that would bring artificial systems one step closer to resembling natural systems. In addition to pushing the boundaries of functional systems by utilizing molecular self-assembly, such a system may lead to better understanding of complex dynamic processes found in Nature.[1] The cell is an astonishing example of how Nature utilizes self-assembly and sophisticated processes to create this complex, multicomponent entity. Designing and controlling self-assembling, dynamic systems is a daunting task, however, and molecular self-assembly has therefore mainly focused on equilibrium systems, rather than systems that are out of equilibrium.

Increasing the complexity of molecules and molecular assemblies at the nanoscale to enhance functions has been a long standing goal of many research groups. With varying success, this has led to the design and development of a wide variety of functional molecules and supramolecular assemblies.[2] While supramolecular chemistry offers great ways to increase complexity in a system, it is also intrinsically dynamic due to the lability of the interactions between the molecular units that are held together in the supramolecular assembly and this can make the design and study of such assemblies a difficult task.[1,3,4]

In order to develop a system that can undergo dynamic changes in response to external stimuli, we envisioned to use a molecular motor that is able to assemble into nanoscale objects. Several types of molecular motors have been developed over the years,[5,6] however, in this chapter only overcrowded alkenes that undergo light-induced isomerization around a central double bond, as shown in Figure 6.1 are treated and henceforth referred to as molecular motors. An important feature of these molecular motors is that, apart from the *trans-cis* isomerization upon irradiation with light, a thermal helix inversion can be induced. It is the irreversibility of the thermal steps that ensures that the rotation of the upper half of the molecular motor, with respect to the lower half, is unidirectional.[7]

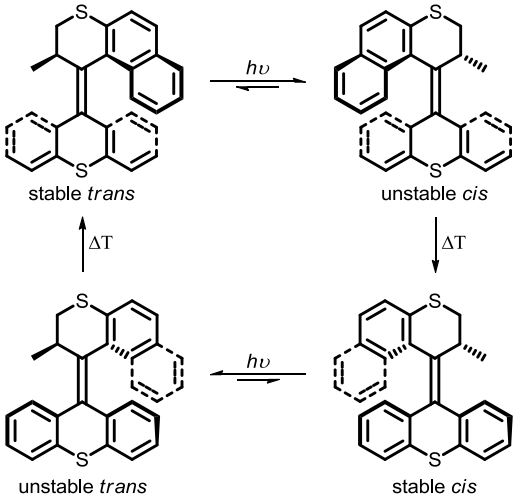

Figure 6.1. Unidirectional rotary cycle of a molecular motor based on an overcrowded alkene.

In the 4-step rotary cycle (Figure 6.1), the steric crowding around the central tetrasubstituted alkene bond (the rotary axle) forces the molecule to adapt a non-planar shape in order to minimize the steric repulsion. In the stable *trans* isomer, the substituent at the stereogenic centre (Me-moiety in Figure 6.1) adopts a pseudo-axial conformation. Upon a photochemical isomerization from the stable *trans* to the unstable *cis* isomer, the Me-substituent adopts an unfavored pseudo-equatorial orientation. Upon heating, the molecular motor can undergo a thermal helix inversion to form the stable *cis* isomer, releasing the conformational strain as the stereogenic methyl moiety adopts a pseudo-axial conformation. Repetition of the photochemical and thermal steps completes the 360° rotation cycle *via* the unstable *trans* isomer.[5,8] For the molecular motor in Figure 6.1, due to the symmetry of the lower half, the stable *trans* and *cis* isomers, as well as the unstable *trans* and *cis* isomers, are identical

Molecular motors have been studied in solution extensively and effects on their kinetics as a function of their structure has been studied in detail.[9–11] Using the molecular motors' unique properties and utilizing their unidirectional motion at the nanoscale to induce macroscopic changes in a system poses a significant challenge and such examples are scarce.[12,13] One example in which such macroscopic changes could be effected, shows the employment of a molecular motor to induce dynamic, helical organization in a liquid-crystal (LC) film (Figure 6.2).[12] The rotation of the motor and the subsequent reorganization of the liquid-crystal film could be used to move a micrometre-sized glass rod, placed on top of the film.

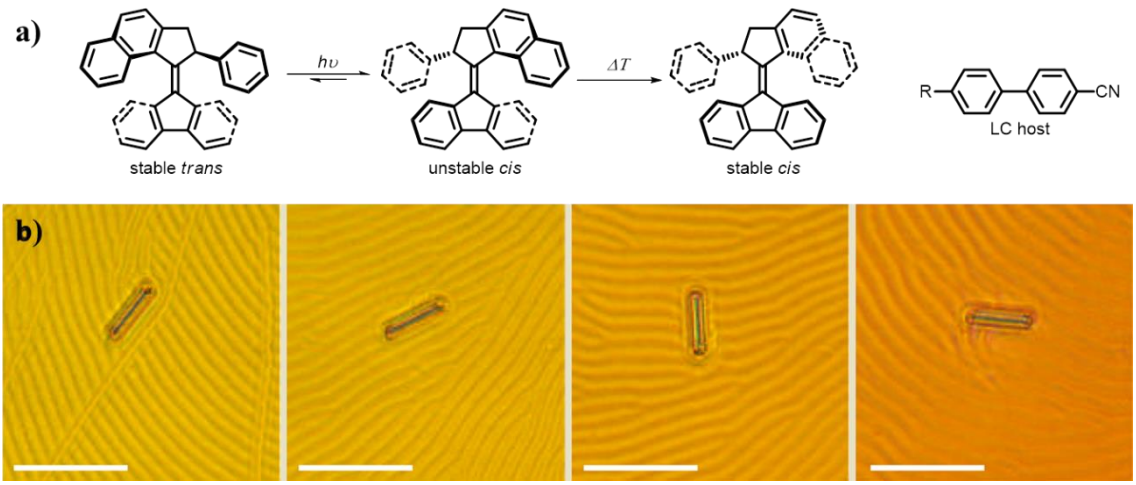

Figure 6.2. A liquid-crystal doped with molecular motor, showing that a glass rod can be moved upon reorganization of the liquid-crystal film as a consequence of the rotation of the molecular motor dopant.[12] a) Structural change in the molecular motor upon irradiation with light and structure of the liquid-crystal host. b) Glass rod rotating on the liquid-crystal film, doped with the molecular motor (shown in (a)), as a consequence of the motor undergoing rotation. Scale bars are 50 μm. (Figure reproduced from reference 12)

Apart from the unidirectional rotation of these motors, an interesting property is that, in principle, four distinct isomers can be addressed of the same molecular motor. In another example from our group, it was shown that a molecular motor, that is appended with two catalytic moieties, could be used as an organocatalyst which utilizes three distinct functional forms (Figure 6.3).[14]

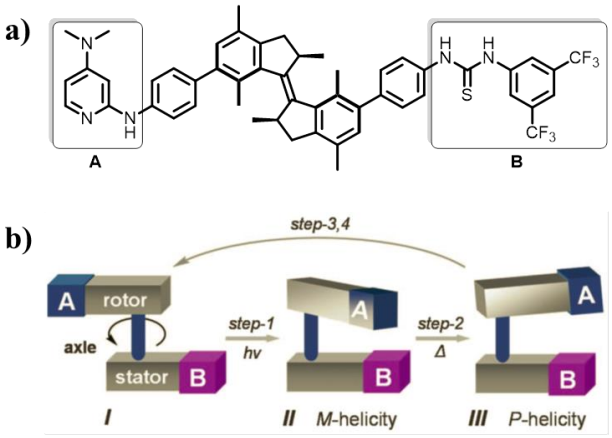

Figure 6.3. Molecular structure and schematic representation of a light-driven bifunctional organocatalyst.[14] a) Molecular structure of the organocatalyst, comprising of dimethylaminopyridine (A) and thiourea (B) moieties that function as Brønsted base and hydrogen bond donor during the catalysis, respectively. b) Schematic representation of the function of the bifunctional catalyst. The less active catalyst (I) and the two forms of the catalyst that give a product of different chirality (II and III) are shown. (Figure reproduced from reference 14)

The unique feature of the catalyst shown in Figure 6.3, is that it allows control over both catalytic activity and stereoselectivity. The Michael addition of 2-methoxythiophenol to cyclohexenone was chosen as the model reaction and when the *trans* isomer of the molecular motor (Figure 6.3, I) was used as the catalyst, racemic product was obtained at a low rate (7% conversion after 15 h). After photoisomerization to the (*M*,*M*)-*cis* isomer (Figure 6.3, II) the two catalytic moieties cooperate and as a consequence speed up the reaction and the (*S*)-product was isolated in 50% yield after 15 h. The (*P*,*P*)-*cis* isomer of the catalyst (Figure 6.3, III, obtained after thermal isomerization) speeds up the reaction even more and the opposite (*R*)-enantiomer is obtained in 83% yield after 15 h. This is an elegant example of how a molecular motor, having 3 distinct functional isomers, can be used in a responsive manner.

In addition to the selected examples shown, significant advancement has been made by "simplifying" the molecular machine systems, i.e. going from solution-based systems to molecules that are bound to surfaces or operate on interfaces so that the environment of the molecules is better understood and controlled.[8,15–27]

We envision that amhiphilic molecular motors, having several addressable states (isomers) that can be controlled by two orthogonal stimuli (light and heat) hold great prospect for the development of self-assembled systems, bearing unique properties. In our group, much knowledge has been gathered on how to change important properties such as thermal stability (half-life) and rotation speed, by changing the molecular structure of the motor[6,7,10,11,18,28–32] and we propose that once well-defined supramolecular architectures can be formed by design, the properties of these functional nano-objects may be fine-tuned by changing the molecular structure of the individual components. Upon applying an external stimulus, we hoped that morphological changes would occur in the nano-objects due to changes in shape of the motor or the movement of the molecular components in the self-assembled objects. Our approach and results are described in this chapter.

6.2 Concept and design

The goal of the research, presented in this chapter, is the design, synthesis and study of amphiphilic molecular motors. We envisioned to incorporate a motor that structurally resembles amphiphiles that we have studied previously[33] as closely as possible in order to ensure self-assembly into well-defined nano-objects. We designed a "fast" and "slow" molecular motor in which the light-responsive overcrowded alkene core connects two hydrophobic dodecyl tails with a hydrophilic charged, quaternary ammonium moiety that is attached to the aromatic core through an ethyleneglycol linker. With the knowledge from chapter 4, we envisioned a thioxanthane hydrophobic lower half for the molecular motors as we predicted that self-assembly would be facile.

Given the specific, tight packing of the thioxanthane-based amphiphiles described in chapter 3, where we showed that inducing structural changes in the amphiphiles by irradiation with light, disrupted the packing of the self-assembled nanotubes,[33] it was postulated that the molecular motors might not be able to undergo isomerization. The light-induced isomerization might sterically affect the neighbouring aggregated amphiphilic motor molecules and therefore be unfavorable. Additionally, other processes, such as inter- or intramolecular photochemical reactions may occur, if the motors are in close proximity to each other while aggregated, with respect to molecules in solution. We therefore designed molecular motor **6.1** (Figure 6.4), with a five-membered cyclopentene upper-half that we predicted to have a very short half-life, based on previous results.[9–11] Additionally, slow molecular motor **6.2** (Figure 6.4), bearing a six-membered dihydrothiopyran upper-half was designed.

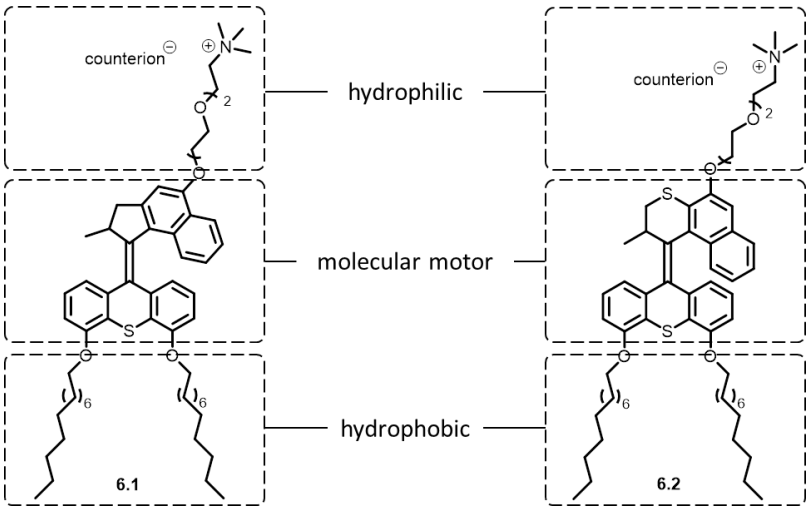

Figure 6.4. Design and structural features of amphiphiles based on a fast (**6.1**) and slow (**6.2**) molecular motor.

In water, the hydrophobic lower half of **6.1** and **6.2** would make up the internal part of the bilayer and we envisioned an interdigitated bilayer as seen for the nanotubes described previously.[33] The core consists of the motor functionality and the water-solubilizing, hydrophilic part is the quaternary ammonium moiety, linked through and ethyleneglycol chain.

6.3 Synthesis

The synthesis of the two amphiphilic motors **6.1** and **6.2** was accomplished by applying procedures developed in our group previously and will be described in detail in the PhD thesis of J. Chen.[34] Both **6.1** and **6.2** bear a tosylate ion as the counterion for synthetic reasons. In order to study the possible effect of the counterion, the TsO^- counterion of **6.1a** was exchanged for Cl^- (**6.1b**) using Amberlite ion-exchange resin, yielding a second amphiphilic, fast molecular motor **6.1b**.

6.4 Self-assembly and photochromic properties

For the self-assembly experiments, the compounds (typically 0.50 mg) were weighed on an analytical balance (see Experimental Section) and dissolved in chloroform (typically 0.20 mL) to give a homogeneous solution. From a fresh stock solution of phospholipid 1,2-dioleoyl-sn-glycero-3-phosphocholine (DOPC) in chloroform (1.0 mg/mL), DOPC (to give 1:1 w/w% amphiphile/DOPC) was added to the amphiphilic motor solution. The compounds were then mixed in a 2 mL glass vial by shaking the sample for a few min. The mixture was subsequently dried under a low N_2-flow, while rotating the vial and after all chloroform evaporated, the vial was dried further for 1 h under vacuum. The dried thin film was then rehydrated in H_2O to give a suspension (1 mg/mL). The suspension was subjected to three freeze-thaw cycles in liquid nitrogen and a warm water bath at 40 °C, respectively, so that a homogeneous turbid solution was formed. During thawing, the samples were vortexed to stimulate homogenization.

For analysis by cryo-transmission electron microscopy (cryo-TEM), the turbid solution (2.5 µL) was placed on a glow-discharged holy carbon coated grid (Quantifoil 3.5/1, QUANTIFOIL Micro Tools GmbH, Großlöbichau, Germany). After blotting, the grid was rapidly frozen in liquid ethane (Vitrobot, FEI, Eindhoven, The Netherlands) and stored in liquid nitrogen until measured. Grids were observed in a Gatan model 626 cryo-stage in a Philips CM120 cryo-electron microscope operating at 120 KeV. Images were recorded under low-dose conditions on a slow-scan CCD camera.

With both fast (**6.1a-b**) and slow (**6.2**) amphiphilic molecular motors in hand, aggregation was first confirmed by cryo-TEM measurements. The charged quaternary ammonium group ensures partial water solubility and we found that with a simple tri-ethyleneglycol chain, the amphiphiles are not soluble enough to give any well-defined aggregation in water. Pure **6.1a** did not give well-defined aggregates and only small pieces of bilayer could be observed. Previous work from our group has shown that the addition of phospholipids can increase the tendency of amphiphiles to form well-defined self-assemblies.[33] Addition of DOPC as described above, indeed led to the formation of torroided nanotubular structures (Figure 6.5).

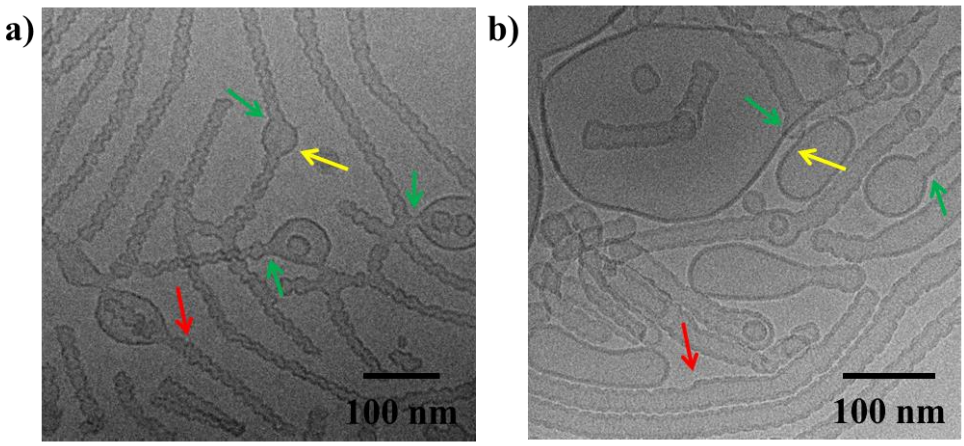

Figure 6.5. Cryo-TEM microscopy images of a) Co-assemblies of amphiphile **6.1a** and DOPC (1:1) in water at a total concentration of 1 mg/mL. b) Sample was extruded (pore size 200 nm). Red arrows indicate torroided nanotubes; yellow arrows indicate DOPC bilayers; green arrows indicate the merging DOPC and nanotube structures.

Reminiscent of the nanotubes described in chapter 3, a phase separation is observed between the DOPC lipid bilayers and the tubular structures formed by the amphiphilic motor. The DOPC vesicles and stretched vesicles have a smooth bilayer (indicated with a yellow arrow in Figure 6.5) whereas the tube-like aggregates of amphiphilic motor **6.1a** have uneven, "torroided" bilayer walls (indicated with a red arrow in Figure 6.5) and the tubes as a whole are less straight than those reported in chapter 3. The tubes are generally several micrometers long and 15–25 nm in diameter, with a typical bilayer wall of approximately 3 nm thick. Although the diameter differs within this range from tube to tube, within the same tube it is generally homogeneous. To the best of our knowledge, there is no literature precedence for this type of torroided nanotubular structures. Unlike with the nanotubes described in chapter 3 of this thesis, the torroided nanotubes made of motor amphiphile **6.1a** and DOPC, "connect" to DOPC vesicles (indicated with green arrows in Figure 6.5).

Given the fact that more well-defined tube-like aggregates form from **6.1a** when DOPC (1:1) was added, we conclude that DOPC is (at least to some extent) integrated into the bilayer walls of the aggregates. In an attempt to create a more homogeneous system (where no phase separation would be observed) and thereby perhaps change the properties of the aggregates, we attempted to homogenize the sample by extruding it. For the extrusion, the mixture of **6.1a**/DOPC (1:1) was homogenized using a mini-extruder (Avanti Polar Lipids) by eleven passages through a polycarbonate filter with a pore size of 200 nm, as is often done in the field of ion channels, where lipid bilayers are treated following this procedure.[35,36] For our system, no significant effects could be observed, however, and the phase separation remained unchanged (Figure 6.5b). The use of more DOPC (1:4 amphiphile/DOPC) gave the same tube-like aggregates. As the concentration of DOPC is higher in this case, much more vesicles from DOPC were observed and we decided to add DOPC in a 1:1 ratio for our experiments.

After confirming that aggregates could be formed, we studied the molecular motor using UV-vis spectroscopy. Both a MeOH solution (Figure 6.6a) and nanotubes of **6.1a** in water (Figure 6.6b) showed the typical absorption spectrum for a molecular motor of this type.[29,37]

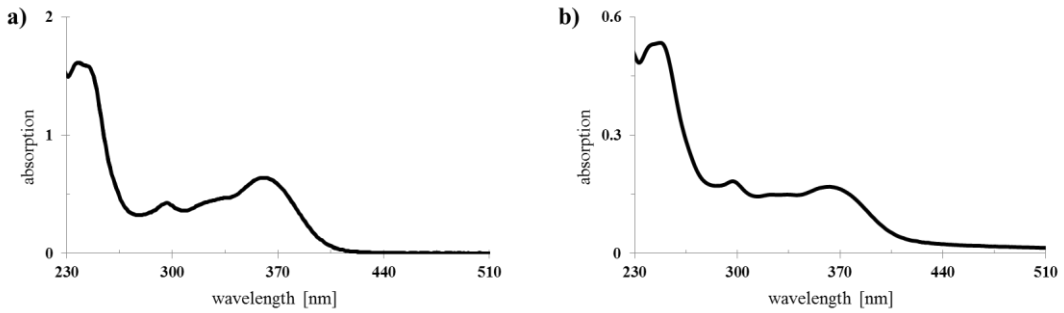

Figure 6.6. UV-vis absorption spectra of **6.1a**. a) In MeOH solution ($2.5 \cdot 10^{-6}$ M) before and after irradiation (10 min, λ = 365 nm), the spectra overlap. b) Aggregates of **6.1a** with DOPC (1:1) in water (1 mg/mL) before and after irradiation (10 min, λ = 365 nm), the spectra overlap.

Independent of the irradiation time (confirmed for up to 2 h, λ = 365 nm) of nanotubes of **6.1a**, no changes were observed in the UV-vis spectra (Figure 6.6). Similarly, a MeOH solution of **6.1a** did also not show any spectral changes upon irradiation. Transient absorption measurements (performed by Dr. Lili Hou) showed that the half-life ($\tau_{1/2}$) of **6.1a-b** in MeOH solution is 40 ns at 20 °C, making **6.1** one of the fastest light-driven molecular motors of this type, to the best of our knowledge.[11,32] The high rotation speed of the molecular motor explains why the absorption spectrum in solution does not show any change upon irradiation, as the unstable *cis* isomer of the motor isomerizes back to the stable *trans* isomer before the absorption spectrum can be measured using standard equipment (see Experimental Section). The solution studies of the amphiphilic motors were performed by Dr. Lili Hou and J. Chen and will be described in his PhD thesis.[34]

Regardless of the absence of spectroscopic changes, we were interested to see if morphological changes occurred upon irradiation of aggregates of **6.1a** as the movement of the molecular motor may still cause a change in morphology. Therefore we next probed the effect of irradiation on the morphology of the nanotubes of **6.1a** and DOPC (1:1) by cryo-TEM (Figure 6.7).

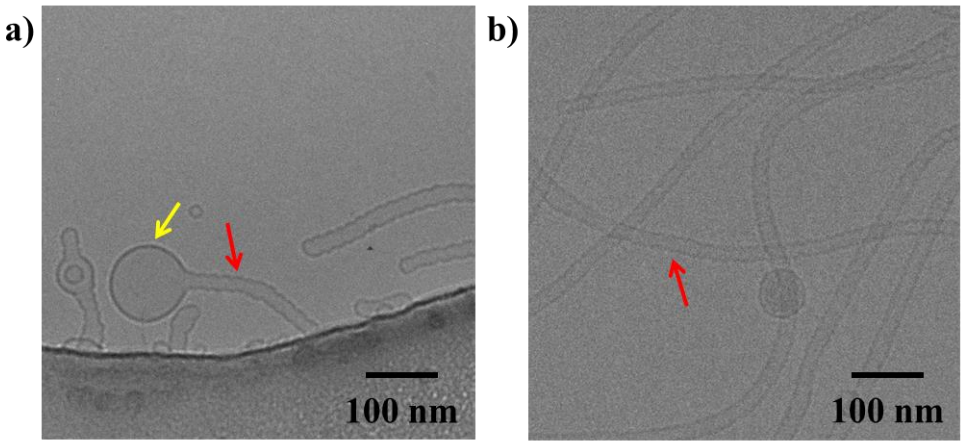

Figure 6.7. Cryo-TEM microscopy images of co-assemblies of amphiphile **6.1a** and DOPC (1:1) in water at a total concentration of 1 mg/mL. a) After irradiation (10 min, λ = 365 nm). b) Heated at 60 °C for 1 h. Red arrows indicate nanotubes; yellow arrows indicate DOPC bilayers.

Consistent with the lack of changes in the UV-vis spectra, cryo-TEM did not show changes in morphology upon irradiation (10 min, λ = 365 nm) of tubes (generally several micrometer long and 15–25 nm in diameter) of self-assembled **6.1a** and DOPC (1:1) in water (Figure 6.7a). Heating of nanotubes of **6.1a** and DOPC (1:1) in water (1 mg/mL) at 60 °C for 1 h (Figure 6.7b) did not have an effect on the morphology either, showing the stability of the tubes.

Changing the counterion from TsO^- to Cl^- (**6.1b**),[34] increases the propensity of **6.1** to self-assemble (i.e. after the first freeze-thaw cycle, a homogeneous turbid solution for **6.1b** is obtained, whereas it takes three cycles for **6.1a**/DOPC 1:1; all samples were freeze-thawed three times regardless). To our surprise, vesicles (50–140 nm in diameter) could be formed from **6.1b** without the need for the presence of additional DOPC lipid (Figure 6.8). When DOPC is added to **6.1b**, much bigger vesicles with a diameter of 120–800 nm are formed. The same amphiphilic molecular motor with a tosylate counterion (**6.1a**) does not show well-defined aggregation without DOPC and the observation that the exchange for a chloride counterion (**6.1b**) gave vesicles in the absence of DOPC was remarkable to us.

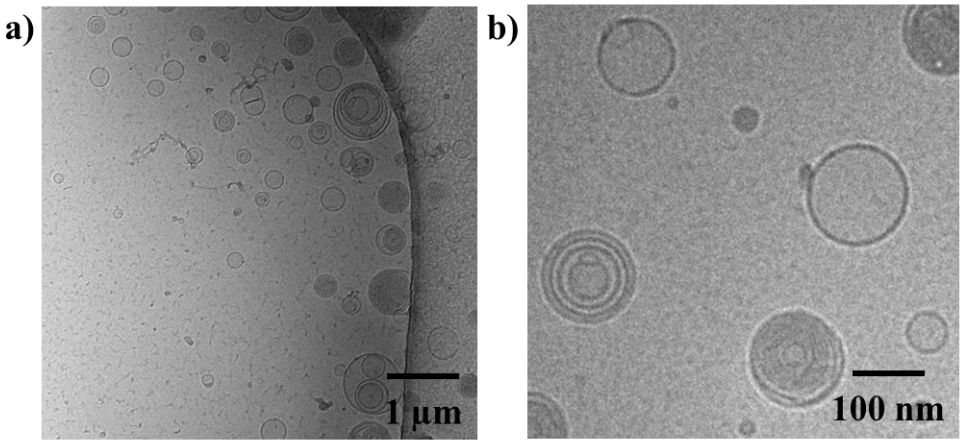

Figure 6.8. Cryo-TEM microscopy images of a) Co-assemblies of amphiphile **6.1b** and DOPC (1:1). b) Self-assembly of pure **6.1b**. Samples are in water and the total concentration of amphiphile is 1 mg/mL. Note that the scalebar in (a) is 1 µm.

Several groups have reported the effect of different counterions on changes in aggregation of surfactants.[38–41] Using viscosity measurements, Gamboa and coworkers studied sphere to rod transitions for micelles of cetyltrimethylammonium.[42,43] It was found that tosylate interacts with micelles of cetyltrimethylammonium both electrostatically and hydrophobically. By comparing a large variety of counterions, remarkably subtle differences were found, for example a difference in binding between tosylate and benzenesulfonate. In a separate, elaborate study, using conductometry, microcalorimetry and ^{1}H NMR, the group of Engberts reported a comparison between several classes of counterions including halides, alkanesulfonates and aromatic counterions.[44–46] It was shown that all aromatic counterions studied, intercalate in the headgroups of the (aromatic) pyridinium amphiphiles. Furthermore, it was shown that the growth of spherical micelles of alkylpyridinium surfactants into wormlike micelles, is strongly dependent on the structure of the (aromatic) counterion. The differences in aggregation are dependent on the substitution pattern of the aromatic counterion as well as its size and hydration.

While the interactions between the alkylpyridinium surfactants and the counterions on one hand and amphiphile **6.1** and the counterion (tosylate or chloride) on the other hand, are likely different, as **6.1** does not bear an alkylpyridinium headgroup, several types of interactions between **6.1** and tosylate can be envisioned, such as π-π interactions[47] between tosylate and the aromatic core of **6.1** as well as cation-π interactions[48,49] between the tosylate and the tertiary ammonium headgroup. To the best of our knowledge, there is no literature precedent for counterion effects on complex (photoresponsive) systems nor the observation of the worm-like nanotubular strucures that are formed upon self-assembly of **6.1a** and DOPC (1:1).

As for **6.1a**, aggregates of **6.1b** (vesicles with a diameter 50–140 nm) did not show any detectable differences in morphology or absorption upon irradiation (10 min, λ = 365 nm). The speed of the amphiphilic molecular motor **6.1** ($\tau_{1/2}$ = 40 ns at 20 °C) is somewhat surprising as the core of the same motor, without any substituents in the lower or upper half was found to have a half-life $\tau_{1/2}$ of 270 ns at 20 °C.[29,37,50] Given the high speed of the motor, a possibility is that **6.1** can undergo isomerization, but the change in molecular structure does not affect the morphology of the aggregates or the aggregates re-assemble to the original morphology faster than we are able to measure.

We next investigated the slower amphiphilic molecular motor, **6.2** of which the half-life $\tau_{1/2}$ was determined to be 7 d at 20 °C and the photostationary state (PSS) ratio 95:5 (see PhD thesis J. Chen).[34] Cryo-TEM showed that **6.2** assembles with DOPC (1:1) to form tubular structures in water (Figure 6.9a). The tubes are significantly shorter (100–200 nm in length) and wider (diameter of 30 nm) compared to amphiphile **6.1a**, which formed micrometer long tubes with a diameter of 15–25 nm. In addition, nanotubes of **6.2** are not torroided, unlike the tubes of **6.1a**, but straight. When the amount of DOPC is decreased (ratio **6.2**:DOPC is 4:1), identical nanotubes are formed (Figure 6.9b). Without DOPC however, as with **6.1a**, well-defined structures of **6.2** were not observed. In order to be able to make fair comparisons, further experiments were carried out with 1:1 mixtures of **6.2** and DOPC.

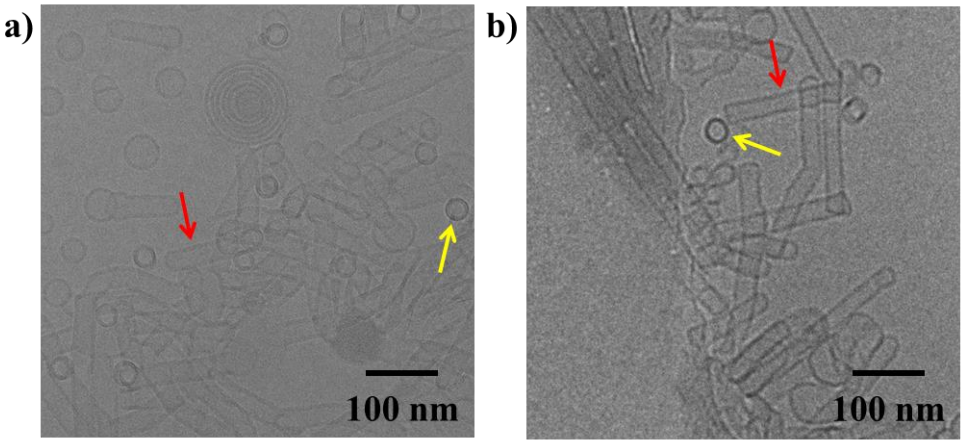

Figure 6.9. Cryo-TEM microscopy images of a) Co-assemblies of amphiphile **6.2** and DOPC (1:1). b) Amphiphile **6.2** and DOPC (4:1). Samples are in water and the total concentration of amphiphile is 1 mg/mL. Red arrows indicate nanotubes in the focal plane; yellow arrows indicate nanotubes perpendicular ("standing up") to the focal plane.

After confirming that tubular structures can be formed from **6.2**, the photochromic properties of the amphiphile were studied in solution and in the aggregates (Figure 6.10).

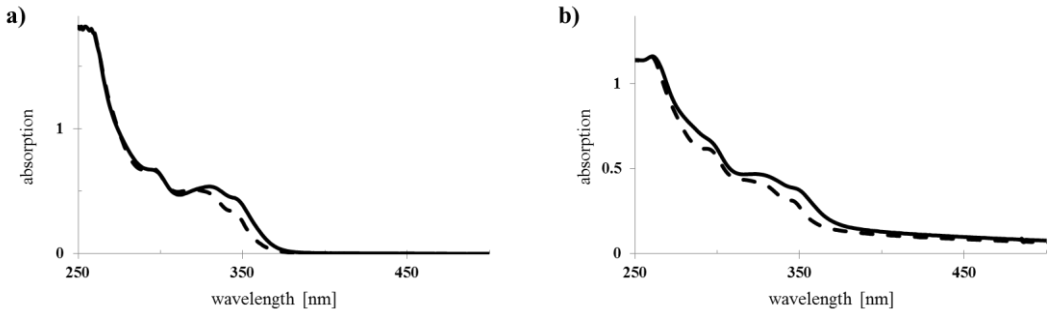

Figure 6.10. UV-vis absorption spectra of **6.2**. a) In CH_2Cl_2 solution ($2.5 \cdot 10^{-6}$ M) before (solid line) and after (dashed line) irradiation (2 h, λ = 365 nm). b) Aggregates of **6.2** with DOPC (1:1) in water (1 mg/mL) before (solid line) and after (dashed line) irradiation (10 min, λ = 365 nm).

Upon irradiation of **6.2** in solution (CH_2Cl_2, 2 h, λ = 365 nm), the spectrum shows a hypsochromic shift (Figure 6.10a), indicating the well-established isomerization of the stable *trans* to the unstable *cis* isomer of the molecular motor,[5,6,8,11,32] showing the same change in absorption as the unsubstituted molecular motor.[29,37,50] For **6.2**, CH_2Cl_2 was used as solvent for comparison reasons.[29] The half-life $\tau_{1/2}$ was calculated and found to be 7 d at 20 °C and 4.3 h at 50 °C (see PhD thesis of J. Chen).[34] Due to the unique photochemical and thermal stability of the molecular motors based on overcrowded alkenes,[5] the long half-life should allow us to see the different *trans* and *cis* isomers, and any consequential different aggregates, individually.[5] For the self-assembled molecular motor, a similar characteristic hypsochromic shift was observed (Figure 6.10b) as in solution, indicating that the motor still undergoes isomerization while aggregated. Since a change in absorption was observed upon irradiation of **6.2** (Figure 6.10), we investigated if morphological changes occur when irradiating the aggregated samples of **6.2** (Figure 6.11). As the PSS of **6.2** is very high (95:5),[34] we believe that effects on the morphology due to small amounts of the other isomer present can be neglected.

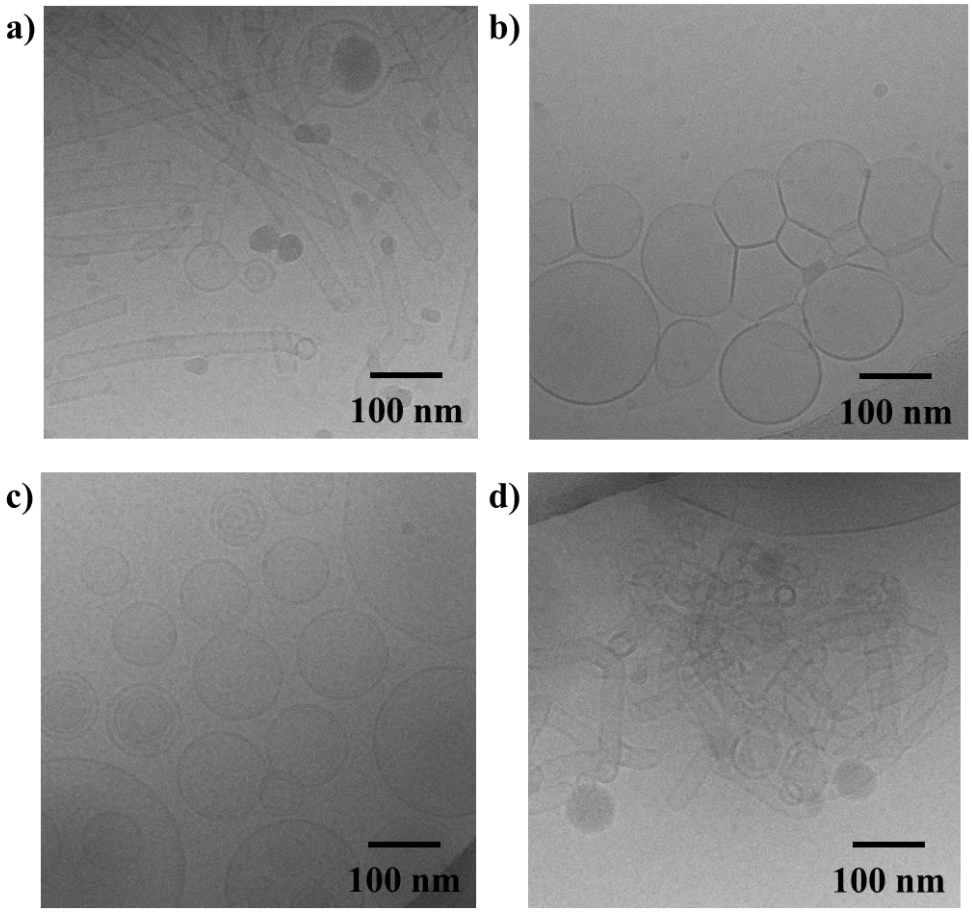

Figure 6.11. Cryo-TEM microscopy images of co-assemblies of amphiphile **6.2** and DOPC (1:1) in water at a total concentration of 1 mg/mL. The consecutive process is: a) Before irradiation. b) After irradiation (15 min, λ = 365 nm). c) After heating at 50 °C for 16 h. d) After freeze-thawing 3 times.

After irradiation (10 min, λ = 365 nm) of tubes of **6.2**/DOPC (1:1; total concentration is 1 mg/mL) in water (Figure 6.11a), cryo-TEM reveals that the tubular structures disappear completely and only vesicles (diameters of 130 nm to micrometers) and pieces of bilayer are observed (Figure 6.11b). UV-vis absorption measurements on the same sample shows a hypsochromic shift upon irradiation of the sample (Figure 6.12, from solid to dashed line) that is indicative for the formation of the unstable *cis* isomer of the molecular motor and we propose that the isomerization of the amphiphilic motor induces the morphological change of the aggregates.

If molecular motor **6.2** retains its functionality, heat should induce the thermal isomerization to the stable *trans* isomer. After heating the irradiated self-assembled sample (vesicles) at 50 °C for 16 h, no change in morphology is observed by cryo-TEM (Figure 6.11c). This is remarkable as the UV-vis absorption spectra of the same sample, show a decrease of the absorption over the entire spectrum (Figure 6.12, dotted line), indicating a change in the aggregates. If the isomerization did occur, it did not cause morphological changes to the vesicular aggregates. Another possibility is that a change in aggregation occurred, but the difference between the vesicles is not detectable by cryo-TEM.

When given the chance to reorganize, we envisioned that the tubes of **6.2** would be reformed. Indeed, upon freeze-thawing the irradiated and subsequently heated sample (3 x), as initially used to prepare the original nanotubes, the same tube-like structures are reformed (Figure 6.11d) with identical dimensions (100–200 nm in length, 30 nm in diameter), and the absorption spectrum of the aggregates is restored. This is a strong indication that aggregated amphiphilic motor **6.2** retains its functionality and the isomerization by irradiation (10 min, λ = 365 nm) from the stable *trans* to the unstable *cis* isomer causes the nanotubes to change morphology to vesicles. Proposed thermal back isomerization of **6.2** (50 °C, 16 h) to the stable *trans* isomer and subsequent freeze-thawing reforms the nanotubes. This completes the rotary cycle of the amphiphilic molecular motor.

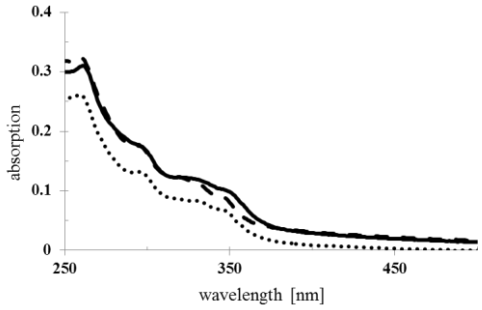

Figure 6.12. UV-vis absorption spectra of co-assemblies of amphiphile **6.2** and DOPC (1:1) in water at a total concentration of 1 mg/mL. The consecutive process is: 1) Before irradiation (solid line); 2) After irradiation for 10 min, λ = 365 nm (dashed line); 3) After heating at 50 °C for 16 h (dotted line).

In order to investigate the reversibility of this process, nanotubes of **6.2** were irradiated (10 min, λ = 365 nm) to induce the stable *trans* to unstable *cis* isomerization. Then, the aggregates were heated (50 °C for 16 h) to form the stable *trans* isomer (due to the symmetry of the lower half of **6.2**, the stable *trans* and *cis* isomers, as well as the unstable *trans* and *cis* isomers, are identical). This cycle was then repeated and the results are shown in Figure 6.13.

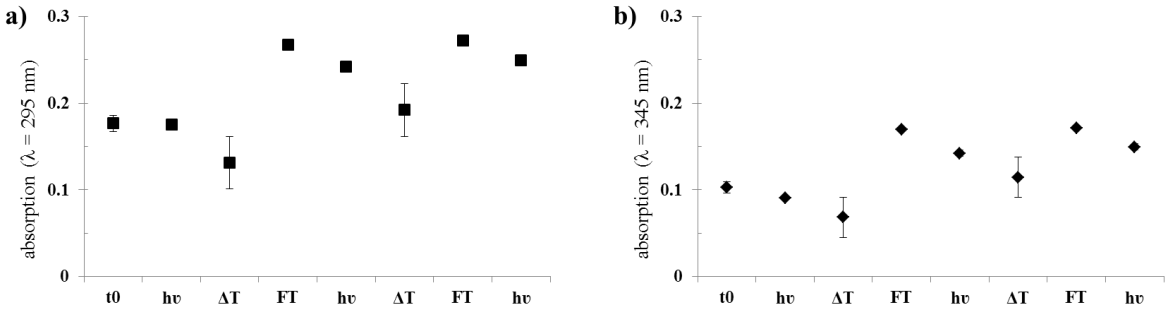

Figure 6.13. Reversibility of isomerization of co-assemblies of **6.2** and DOPC (1:1) in water at a total concentration of 1 mg/mL. a) UV-vis absorption maximum at λ = 295 nm and b) UV-vis absorption maximum at λ = 345 nm. t0 = starting point; hυ = sample irradiated for 10 min at λ = 365 nm; ΔT = sample heated at 50 °C for 16 h; FT = sample freeze-thawed 3 times. The experiment was performed in triplo and error bars are shown.

After confirming the formation of nanotubes from **6.2** (1:1 with DOPC at a total concentration of 1 mg/mL in water) by cryo-TEM (Figure 6.11a), a UV-vis spectrum was taken (Figure 6.10b) and λ_{max} was measured at two wavelengths (λ = 295 and 345 nm). This was set as t = 0 (Figure 6.13, t0). After irradiation of the nanotubes of **6.2** and DOPC with UV light (10 min, λ = 365 nm), the tubular structures disappeared and only vesicles were observed by cryo-TEM (Figure 6.11b). The UV-vis spectrum of the aggregates shows a hypsochromic shift (Figure 6.10b), causing λ_{295} and λ_{345} to decrease slightly (Figure 6.13, hυ). Upon heating, λ_{295} and λ_{345} decrease (Figure 6.13, ΔT), but cryo-TEM shows vesicles, as before heating. After freeze-thawing the samples, the nanotube structures are restored (Figure 6.11d) and λ_{295} and λ_{345} increase significantly (Figure 6.13, FT). This cycle was repeated and both cryo-TEM and UV-vis spectroscopy data show remarkably reproducible results for the reversible triggered changes between nanotubes and vesicles of **6.2** and DOPC (1:1) in water (1 mg/mL). The experiment was conducted in triplo and all data are consistent. Curiously, the initial nanotubes have a lower absorption than after reformation through irradiation and subsequent heating. After the first cycle, the UV-vis spectra are identical for the repetitive steps and the system seems to change morphology upon isomerization in a very reproducible manner. The reason for the lower intensity of the initial spectra (Figure 6.13, t0) is currently not known, but reproducible.

In order to exclude the possibility that the unstable *cis* isomer of **6.2** also forms tubes when given the chance to reorganize, we performed a freeze-thaw cycle on the irradiated sample (vesicles, *vide supra*) 3 times and no changes in morphology could be observed. This confirms that only the stable *trans* isomer of the molecular motor forms tubular structures. As a further control, as **6.2** needs to be mixed with DOPC to assemble into well-defined aggregates, in order to exclude the possibility that the change in morphology of the co-assemblies is due to DOPC, we irradiated pure DOPC vesicles and heated them under identical conditions and checked the morphology by cryo-TEM (Figure 6.14).

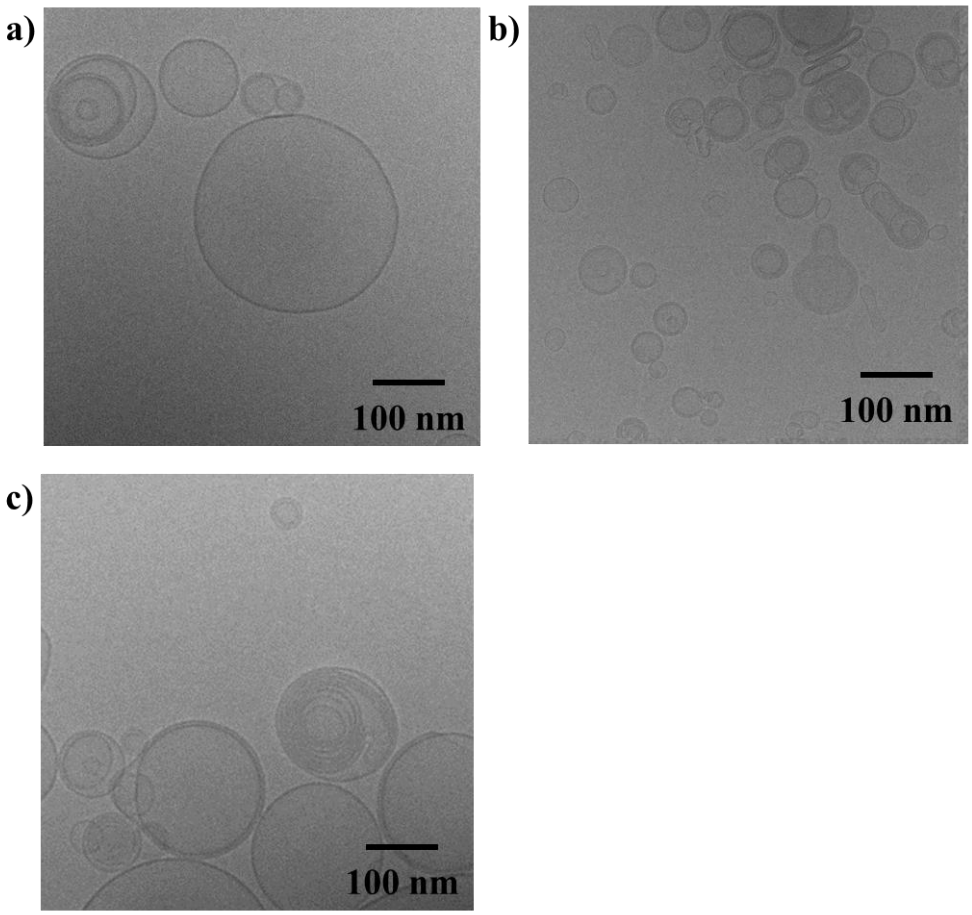

Figure 6.14. Cryo-TEM microscopy images of self-assembled DOPC. a) Before irradiation. b) After irradiation (15 min, λ = 365 nm). c) After irradiation (15 min, λ = 365 nm) and subsequent heating (50 °C, 16 h). All samples are in water at a concentration of 1 mg/mL.

As shown in Figure 6.14, vesicles consisting of pure DOPC did not change morphology when irradiated (Figure 6.14b; 15 min, λ = 365 nm) or heated (Figure 6.14c; 16 h, 50 °C) under identical conditions as the co-assemblies of molecular motor **6.2** and DOPC. Vesicles were observed in all cases, indicating that the observed changes in the co-aggregated nanotubes are due to the molecular motor constituent and not DOPC.

In order to determine the composition of the vesicles, observed after irradiation of nanotubes of **6.2** and DOPC (1:1) in water (Figure 6.11b), we performed energy-dispersive X-ray spectroscopy (EDX) and the results are shown in Figure 6.15. This technique is used for the elemental analysis of a sample and shows the atomic consistence, based on the interaction of different atoms with electron beam excitation[51] and is used as a qualitative technique to show the presence of certain atoms in the analysis of for example thin films,[52] nanotapes[53] and nanotubes.[54] We envisioned that EDX analysis could give information that indicates if the vesicles, formed after irradiation (Figure 6.11b) of the nanotubes consisting of amphiphilic motor **6.2** and DOPC (1:1), contain both **6.2** and DOPC. Unfortunately, the samples could only be analyzed after drying the samples for practical reasons. As only DOPC contains phosphorous, and sulfur is unique to molecular motor **6.2** in the sample, the content of these two atoms in the dried aggregates is directly related to the content of DOPC and **6.2**.

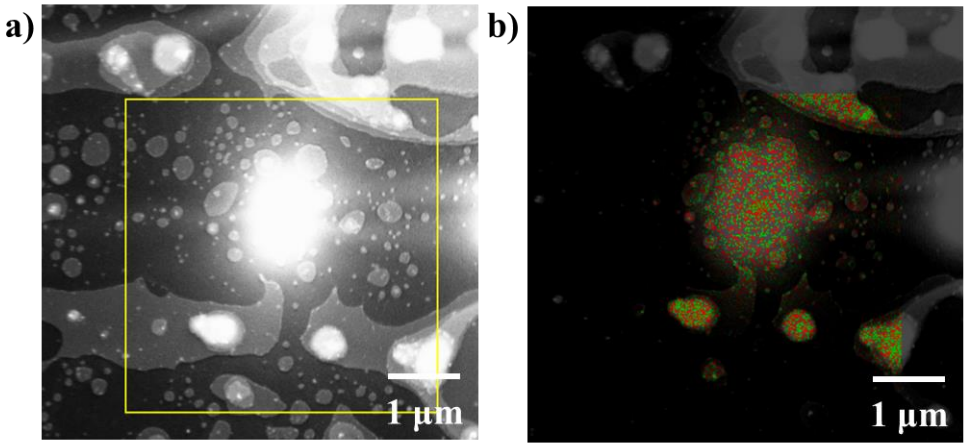

Figure 6.15. Mapped EDX analysis of self-assembled **6.2** with DOPC (1:1) after irradiation with UV light (15 min, λ = 365 nm) and subsequent drying of the sample from water (1 mg/mL). a) Mapped area. b) Atomic analysis for S (green) and P (red). Ratio (S:P) = 46:54.

Mapping an area after EDX analysis (Figure 6.15) shows the S:P ratio to be 46:54, indicating 2 DOPC molecules per molecule of **6.2** (molar ratio of **6.2**:DOPC is 45:55 and **6.2** contains two S-atoms per molecule, while DOPC contains one P-atom per molecule). Due to the fact that the sample has to be dried and the mapping of only a small volume of the sample, this data does not give any quantitative results. However, it does suggest that **6.2** and DOPC are still mixed as there are no isolated areas of either S or P (Figure 6.15; green and red dots, respectively).

6.5 Conclusions

We have developed the first three amphiphilic molecular motors with different rotation rates. All three motors are able to form well-defined nano-objects in water by self-assembly. The fast molecular motor ($\tau_{1/2}$ = 40 ns at 20 °C) **6.1a**, containing a cyclopentene upper half and bearing a tosylate counterion, assembled with DOPC (1:1) in water (1 mg/mL) to form torroided nanotubular structures that are generally several micrometer long and 15–25 nm in diameter. Although the diameter differs within this range from tube to tube, it is typically the same within a single tube. To the best of our knowledge, there is no literature precedence for this type of torroided nanotubular structures. Additionally, the tube bilayers connect to DOPC vesicles. When the counterion was changed from tosylate to chloride, the solubility of amphiphile **6.1b** ($\tau_{1/2}$ = 270 ns at 20 °C) was increased and DOPC was not required to form well-defined vesicles with a typical diameter of 50–140 nm. The effect of the counterion on morphology is interesting and has been reported in the literature with other amphiphiles.[38–46] To the best of our knowledge, there is no literature precedence for counterion effects on complex, responsive systems however. For future studies, it would be highly interesting to change the counterion of **6.2** (currently tosylate) for other anions such as halides or alkanesulfonates and study the morphological effects and, perhaps more importantly, the effect of the morphology on the responsiveness of the system.

When nanotubes or vesicles of **6.1** were irradiated (10 min, λ = 365 nm), no changes in absorption were observed and the morphology of the aggregates did not change. Due to the low half-life of **6.1** ($\tau_{1/2}$ = 40 ns for **6.1a** and $\tau_{1/2}$ = 270 ns for **6.1b** at 20 °C) a possibility is that **6.1** can undergo isomerization, but the change in molecular structure does not affect the

morphology of the aggregates or, alternatively, that the aggregates re-assemble to the original morphology faster than we are able to measure.

Slow amphiphilic molecular motor **6.2** ($\tau_{1/2}$ = 7 d at 20 °C and 4.3 h at 50 °C) assembled with DOPC (1:1) in water (1 mg/mL) to form straight nanotubes with a typical length of 100–200 nm and a diameter of 30 nm. Isomerization was followed by UV-vis spectroscopy and λ_{max} was measured at two wavelengths (λ = 295 and 345 nm) and the changes in aggregation were studied by cryo-TEM of the same samples.

To our delight, upon irradiation of nanotubes of **6.2** with UV light (10 min, λ = 365 nm), the tubular structures disappeared and vesicles (diameters of 130 nm to several micrometers) were observed instead. The UV-vis spectrum of the aggregates shows a hypsochromic shift, indicative for the isomerization from the stable *trans* to the unstable *cis* isomer for molecular motors of this type.[5,6,8,11,32] When heated subsequently, the vesicles did not show any changes by cryo-TEM, while the absorption decreased over the entire spectrum, indicating a change in the aggregates. It is likely that a change in aggregation occurred, given the change in absorption, but the difference between the vesicles is not detectable by cryo-TEM. After freeze-thawing the vesicles, nanotubes with identical dimensions as in the initial sample (100–200 nm in length, 30 nm in diameter) were restored. This process was repeated two times with the same sample (in triplo) and proved to be highly reversible and reproducible (UV-vis spectroscopy and cryo-TEM). Curiously, the only anomaly is that the initial nanotubes have a lower absorption than after reformation through irradiation and subsequent heating and freeze-thawing. After the first cycle, the UV-vis spectra are identical for the repetitive steps and the system changes morphology upon isomerization in a reproducible manner. The reason for the lower intensity of the initial spectra is currently not known, but reproducible.

Control experiments showed that DOPC is not responsible for the changes in morphology as vesicles of pure DOPC did not show any changes when subjected to the same conditions (irradiation and heating) as the nanotubes and vesicles formed by molecular motor **6.2** and DOPC (1:1). Furthermore, EDX analysis of the vesicles that form when the nanotubes are irradiated, showed no isolated areas of only DOPC or amphiphile **6.2**, indicating that the two are mixed.

As the lower half of **6.2** is symmetric, it only has two distinct isomers (stable *trans* and unstable *cis*) and both isomers could be addressed by the typical irradiation and heating cycles for this class of molecular motors.[5–11] For future studies, it would be interesting to study the effect of different counterions on the morphology of self-assembled **6.2** as we saw a large difference in morphology when changing the tosylate counterion for chloride. In addition, amphiphilic molecular motors with an asymmetric lower half would be very interesting to study as distinct morphologies might be obtained for all four isomers of the same molecular motor. It would also be interesting to perform inclusion and release experiments with the fast molecular motor **6.1**, to probe if substances can leave the aggregates when irradiated. This could be done by loading vesicles for example with calcein and performing fluorescence dequenching essays to see the effect of irradiation of the (by size exclusion chromatography purified) vesicles. Currently, it is not clear if the fast molecular motors are able to undergo isomerization while aggregated, however.

Providing the proof of concept in this chapter, we envision that amhiphilic molecular motors with an unsymmetrical lower half, having four addressable states (isomers) that can be controlled by two orthogonal stimuli (light and heat) hold great prospect for the development of self-assembled systems, having unique properties. By changing the molecular structure as well as the counterion and additives such as DOPC, multiresponsive, tunable aggregates may be obtained.

6.6 Experimental section

General remarks

All solvents used for spectroscopic measurements were degassed prior to use. Synthesized derivatives are light-sensitive and were therefore stored in the dark. Irradiations were performed with Spectroline ENB-280C/FE UV lamps (8 W). UV-vis measurements were performed on an Agilent 8453 UV-vis Spectrophotometer. Weighing of small quantities was performed on a Mettler MT5 analytical microbalance.

Synthesis

The synthesis of two amphiphilic motors **6.1** and **6.2** was accomplished by applying procedures developed in our group previously and will be described in detail in the PhD thesis of J. Chen.[34]

Transient absorption and photostationary state measurements

The half-life of the amphiphilic motors, described in this chapter, in solution, were determined by Dr. L. Hou and the photostationary states were determined by J. Chen and will be discussed in his PhD thesis.[34]

6.7 Acknowledgements

Dr. Lili Hou is acknowledged for the transient absorption measurements of the fast molecular motor. Dr. Wiktor Szymański is gratefully acknowledged for helpful discussions.

6.8 References

[1] G. M. Whitesides, M. Boncheva, *Proc. Natl. Acad. Sci. U. S. A.* **2002**, *99*, 4769–4774.

[2] M. M. Boyle, R. A. Smaldone, A. C. Whalley, M. W. Ambrogio, Y. Y. Botros, J. F. Stoddart, *Chem. Sci.* **2011**, *2*, 204–210.

[3] J. -M. Lehn, *Top. Curr. Chem.* **2012**, *322*, 1–32.

[4] J. -M. Lehn, *Angew. Chem. Int. Ed.* **2013**, *52*, 2836–2850.

[5] B. L. Feringa, *Acc. Chem. Res.* **2001**, *34*, 504–513.

[6] W. R. Browne, B. L. Feringa, *Nat. Nanotechnol.* **2006**, *1*, 25–35.

[7] E. M. Geertsema, S. J. van der Molen, M. Martens, B. L. Feringa, *Proc. Natl. Acad. Sci. U. S. A.* **2009**, *106*, 16919–16924.

[8] N. Koumura, R. W. J. Zijlstra, R. A. van Delden, N. Harada, B. L. Feringa, *Nature* **1999**, *401*, 152–155.

[9] B. L. Feringa, *J. Org. Chem.* **2007**, *72*, 6635–6652.

[10] M. M. Pollard, M. Klok, D. Pijper, B. L. Feringa, *Adv. Funct. Mater.* **2007**, *17*, 718–729.

[11] M. K. J. ter Wiel, R. A. van Delden, A. Meetsma, B. L. Feringa, *J. Am. Chem. Soc.* **2003**, *125*, 15076–15086.

[12] R. Eelkema, M. M. Pollard, J. Vicario, N. Katsonis, B. S. Ramon, C. W. M. Bastiaansen, D. J. Broer, B. L. Feringa, *Nature* **2006**, *440*, 163–163.

[13] T. Kudernac, N. Ruangsupapichat, M. Parschau, B. Maciá, N. Katsonis, S. R. Harutyunyan, K. -H. Ernst, B. L. Feringa, *Nature* **2011**, *479*, 208–211.

[14] J. Wang, B. L. Feringa, *Science* **2011**, *331*, 1429–1432.

[15] A. M. Schoevaars, W. Kruizinga, R. W. J. Zijlstra, N. Veldman, A. L. Spek, B. L. Feringa, *J. Org. Chem.* **1997**, *62*, 4943–4948.

[16] T. R. Kelly, H. De Silva, R. A. Silva, *Nature* **1999**, *401*, 150–152.

[17] T. R. Kelly, X. Cai, F. Damkaci, S. B. Panicker, B. Tu, S. M. Bushell, I. Cornella, M. J. Piggott, R. Salives, M. Cavero, et al., *J. Am. Chem. Soc.* **2007**, *129*, 376–386.

[18] A. A. Kulago, E. M. Mes, M. Klok, A. Meetsma, A. M. Brouwer, B. L. Feringa, *J. Org. Chem.* **2010**, *75*, 666–679.

[19] Y. Liu, A. H. Flood, P. A. Bonvallet, S. A. Vignon, B. H. Northrop, H. -R. Tseng, J. O. Jeppesen, T. J. Huang, B. Brough, M. Baller, et al., *J. Am. Chem. Soc.* **2005**, *127*, 9745–9759.

[20] T. D. Nguyen, H. -R. Tseng, P. C. Celestre, A. H. Flood, Y. Liu, J. F. Stoddart, J. I. Zink, *Proc. Natl. Acad. Sci. U. S. A.* **2005**, *102*, 10029–10034.

[21] B. K. Juluri, A. S. Kumar, Y. Liu, T. Ye, Y. -W. Yang, A. H. Flood, L. Fang, J. F. Stoddart, P. S. Weiss, T. J. Huang, *ACS Nano* **2009**, *3*, 291–300.

[22] S. Angelos, N. M. Khashab, Y. -W. Yang, A. Trabolsi, H. A. Khatib, J. F. Stoddart, J. I. Zink, *J. Am. Chem. Soc.* **2009**, *131*, 12912–12914.

[23] R. Klajn, L. Fang, A. Coskun, M. A. Olson, P. J. Wesson, J. F. Stoddart, B. A. Grzybowski, *J. Am. Chem. Soc.* **2009**, *131*, 4233–4235.

[24] M. A. Olson, A. Coskun, R. Klajn, L. Fang, S. K. Dey, K. P. Browne, B. A. Grzybowski, J. F. Stoddart, *Nano Lett.* **2009**, *9*, 3185–3190.

[25] R. Klajn, M. A. Olson, P. J. Wesson, L. Fang, A. Coskun, A. Trabolsi, S. Soh, J. F. Stoddart, B. A. Grzybowski, *Nat. Chem.* **2009**, *1*, 733–738.

[26] C. P. Collier, J. O. Jeppesen, Y. Luo, J. Perkins, E. W. Wong, J. R. Heath, J. F. Stoddart, *J. Am. Chem. Soc.* **2001**, *123*, 12632–12641.

[27] S. J. van der Molen, P. Liljeroth, *J. Phys. Condens. Matter* **2010**, *22*, 133001.

[28] M. M. Pollard, P. V. Wesenhagen, D. Pijper, B. L. Feringa, *Org. Biomol. Chem.* **2008**, *6*, 1605–1612.
[29] M. Klok, N. Boyle, M. T. Pryce, A. Meetsma, W. R. Browne, B. L. Feringa, *J. Am. Chem. Soc.* **2008**, *130*, 10484–10485.
[30] J. Vicario, M. Walko, A. Meetsma, B. L. Feringa, *J. Am. Chem. Soc.* **2006**, *128*, 5127–5135.
[31] J. Vicario, A. Meetsma, B. L. Feringa, *Chem. Commun.* **2005**, *47*, 5910–5912.
[32] N. Koumura, E. M. Geertsema, M. B. van Gelder, A. Meetsma, B. L. Feringa, *J. Am. Chem. Soc.* **2002**, *124*, 5037–5051.
[33] A. C. Coleman, J. M. Beierle, M. C. A. Stuart, B. Maciá, G. Caroli, J. T. Mika, D. J. van Dijken, J. Chen, W. R. Browne, B. L. Feringa, *Nat. Nanotechnol.* **2011**, *6*, 547–552.
[34] J. Chen, *PhD Thesis*, University of Groningen, **forthcoming**.
[35] G. van den Bogaart, V. Krasnikov, B. Poolman, *Biophys. J.* **2007**, *92*, 1233–1240.
[36] A. Koçer, M. Walko, B. L. Feringa, *Nat. Protoc.* **2007**, *2*, 1426–1437.
[37] M. Klok, L. P. Janssen, W. R. Browne, B. L. Feringa, *Faraday Discuss.* **2009**, *143*, 319–334.
[38] W. H. Ansari, J. Aslam, U. S. Siddiqui, Kabir-ud-Din, *J. Mol. Liq.* **2012**, *174*, 5–10.
[39] D. Bartet, C. Gamboa, L. Sepulveda, *J. Phys. Chem.* **1980**, *84*, 272–275.
[40] S. K. Ghosh, V. A. Raghunathan, *Langmuir* **2009**, *25*, 2622–2628.
[41] S. Kumar, A. Z. Naqvi, Kabir-ud-Din, *Langmuir* **2000**, *16*, 5252–5256.
[42] C. Gamboa, H. Rios, L. Sepulveda, *J. Phys. Chem.* **1989**, *93*, 5540–5543.
[43] C. Gamboa, L. Sepúlveda, *J. Colloid Interface Sci.* **1986**, *113*, 566–576.
[44] K. Bijma, J. B. F. N. Engberts, *Langmuir* **1997**, *13*, 4843–4849.
[45] K. Bijma, M. J. Blandamer, J. B. F. N. Engberts, *Langmuir* **1998**, *14*, 79–83.
[46] K. Bijma, E. Rank, J. B. F. N. Engberts, *J. Colloid Interface Sci.* **1998**, *205*, 245–256.
[47] C. A. Hunter, J. K. M. Sanders, *J. Am. Chem. Soc.* **1990**, *112*, 5525–5534.
[48] J. C. Ma, D. A. Dougherty, *Chem. Rev.* **1997**, *97*, 1303–1324.
[49] P. C. Kearney, L. S. Mizoue, R. A. Kumpf, J. E. Forman, A. McCurdy, D. A. Dougherty, *J. Am. Chem. Soc.* **1993**, *115*, 9907–9919.
[50] M. K. J. ter Wiel, J. Vicario, S. G. Davey, A. Meetsma, B. L. Feringa, *Org. Biomol. Chem.* **2005**, *3*, 28–30.
[51] J. Goldstein, D. E. Newbury, D. C. Joy, C. E. Lyman, P. Echlin, E. Lifshin, L. Sawyer, J. R. Michael, *Scanning Electron Microscopy and X-Ray Microanalysis, 3rd Edition*, New York, USA, **2003**.
[52] T. Jiao, M. Liu, *Thin Solid Films* **2005**, *479*, 269–276.
[53] P. J. Meadows, E. Dujardin, S. R. Hall, S. Mann, *Chem. Commun.* **2005**, *29*, 3688–3690.
[54] M. Reches, E. Gazit, *Science* **2003**, *300*, 625–627.

List of Abbreviations

γ-CD	γ-cyclodextrin
BLM	black lipid membrane *or* planar bilayer lipid membrane
CB[n]	cucurbituril of *n* repeating units
CD	circular dichroism
CTAB	cetyltrimethylammonium bromide
CTV	cyclotriveratrylene
DNA	deoxyribonucleic acid
DOPC	1,2-dioleoyl-sn-glycero-3-phosphocholine
EDX	energy-dispersive X-ray spectroscopy
exTTF	2-[9-(1,3-dithiol-2-ylidene)anthracen-10(9*H*)-ylidene]-1,3-dithiole
GUV	giant unilamellar vesicle
HBC	hexa-*peri*-hexabenzocoronene
LC	liquid crystal
LMWG	low molecular weight gelator
LUV	large unilamellar vesicle
MscL	mechanosensitive channel of large conductance
PDA	photodiode array
PSS	photostationary state
SDS	sodium dodecylsulphate
TBAB	tetrabutylammoniumbromide
TEM	transmission electron microscopy
THP	tetrahydropyran
TMEDA	tetramethylethylenediamine

Summary

The formation of well-defined nanoscale objects that are dynamic in nature and that can be visualized with techniques such as electron microscopy, fluorescence or scanning probe techniques is a challenge that would bring artificial systems one step closer to resembling natural systems. In addition to pushing the boundaries of functional systems by utilizing molecular self-assembly, such a system may lead to better understanding of complex dynamic processes found in Nature. The cell is an astonishing example of how Nature utilizes self-assembly and sophisticated processes to create this complex, multicomponent entity. Increasing the complexity of molecules and molecular assemblies at the nanoscale to enhance functions has been a longstanding goal of many research groups. With varying success, this has led to the design and development of a wide variety of functional molecules and supramolecular assemblies. While supramolecular chemistry provides a great tool to increase complexity in a system, it is also intrinsically dynamic due to the lability of the interactions between the molecular units that are held together in the supramolecular assembly and this can make the design and study of such assemblies a difficult task.

The research described in this thesis deals with new supramolecular systems that were designed to have specific functions. The properties of the molecular constituent of a supramolecular aggregate provides functional handles to address the supramolecular system as a whole and in this thesis we have utilized a variety of responsive molecules and studied their properties as well as the properties of the supramolecular systems as a whole. In addition, transfer of information between molecules in the supramolecular assemblies has been used to achieve various goals. Recurring themes in this thesis are *chirality*, *responsiveness*, and *aggregation*.

In *chapter 2*, the concept of autoamplification of molecular chirality *via* induction of supramolecular chirality is described. Diarylethene photohemical switches were used in autocatalytic induction. A small amount of chiral enantiopure ring-closed diarylethene sergeant was added to its precursor prochiral open diarylethene soldier. The mixture was then gelated and the chirality of the gel is controlled by the chiral sergeant, favoring the formation of either (*P*)- or (*M*)-helical gel depending on the chirality of the sergeant. The chirality is thus transferred from the molecular to the supramolecular level. Subsequently, irradiation of the gel with UV light leads to ring-closing of the prochiral diarylethene soldiers. As the soldiers are preorganized in the gel fibers, one enantiomer is formed in excess and the chiral information is locked at the molecular level as a consequence of the ring-closing. This completes the cycle from molecular chirality *via* supramolecular chiralty back to molecular chirality of the same molecules and places this system among the very few examples where a chiral product of a reaction can template its own asymmetric synthesis. This process is reminiscent of so-called “autocatalytic reactions”, however here the autoamplification takes place in a kinetically trapped state.

Chapter 3 describes the design, synthesis and study of nanotubular objects in which chirality can be used as a means to control the morphology of self-assembled structures. To the best of our knowledge, this comprises the first example of such objects where the point chirality (stereogenic centre) is present in the hydrophobic part of the amphiphiles, much like in natural membranes. The morphology of well-defined nanotubes in water can be fully controlled by adjusting the fraction of chiral component in a co-assembly of chiral and achiral nanotube-forming amphiphile. Three distinct types of assemblies can be addressed and have been analyzed with a variety of spectroscopic and microscopic techniques. The fact that the nanotubes form in water and that chirality is employed to control the morphology of the self-assembled nanotubes, takes the complexity of supramolecular systems one step closer to natural systems. In addition, the nanotubes can be disassembled with light and this feature offers prospects for the development of memory systems.

The synthesis of six different aromatic, amphiphilic structures was studied and the results are described in *chapter 4*. The synthesis of thioxanthone-, xanthone- and anthrone-derived amphiphiles was envisioned, bearing a hydrophilic ethyleneglycol headgroup and two hydrophobic alkyl chains, connected to the aromatic core through either an ether-linkage or a C-C linkage. Methodology was developed for the synthesis of a variety of aromatic amphiphiles. Of these, a small library of systematically varied thioxanthone-derived amphiphiles, bearing hydrophobic and hydrophilic moieties of different length, were studied by cryo-TEM. Within the different subclasses of the described amphiphiles, based on their aromatic core, useful comparisons could be made. The obtained knowledge of the thioxanthone-based amphiphilic family has led to the development of highly interesting, conducting bilayer systems and is described in chapter 5.

In *chapter 5*, novel, synthetic amphiphiles that form ion-conducting membranes were developed. Not only highly stable planar lipid bilayers were obtained, but also cell-sized containers. While ions can pass through the bilayer, large charged molecules such as calcein stay on one side of the membrane. Furthermore, we showed that a functioning membrane protein can be embedded in the bilayer membrane. The conducting properties of the highly stable, functional membrane with no need for specific ion channels, pumps and transporters, combined with the protein compatibility, offers fascinating opportunities toward the design of primitive, functional artificial cells. This simple system has prospects for the generation of transbilayer potentials and thereby energizing processes in such artificial systems, ranging from ion channel functioning to transport.

Chapter 6 describes, to the best of our knowledge, the first examples in which a molecular motor forms well-defined supramolecular structures upon self-assembly in water and in which the molecular component causes a reversible change in morphology when exposed to external stimuli. A slow ($\tau_{1/2}$ = 7 d at 20 °C) and fast ($\tau_{1/2}$ = 40 ns at 20 °C) amphiphilic molecular motor were designed, synthesized and studied using cryo-TEM microscopy and UV-vis spectroscopy. The fast motor forms torroided nanotubes when co-assembled with DOPC in water and is one of the fastest molecular motors reported to date. Therefore, its half-life is too low to observe any changes upon irradiation of the motor. The slow molecular motor self-assembles into nanotubes in water and upon irradiation with light, isomerization of the molecular component from *trans* to *cis* causes the tubular structures to reorganize into vesicles. Heating the system induces the

isomerization of the molecular motor from *cis* to *trans* and the nanotubes are subsequently reformed.

Since supramolecular chemistry was introduced some decades ago, the field has become increasingly more popular. The main reason for this is the ability of supramolecular chemistry to increase complexity of artificial systems by design. In addition, over the years, more sophisticated techniques have been developed to analyze supramolecular structures and their morphology. By incorporating functional molecules into supramolecular assemblies, responsiveness into the larger system as a whole can be introduced, based on the molecular building block. While supramolecular chemistry has contributed to our understanding of Nature and allowed us to develop increasingly complex artificial systems, its true potential has yet to be unlocked. This thesis contains a small contribution to the development of the next generation of responsive supramolecular systems.

Samenvatting

Het vormen van gedefinieerde nano-objecten die dynamisch van natuur zijn en die kunnen worden gevisualiseerd met technieken zoals electronenmicroscopie, fluorescentie of scanning probe technieken, is een uitdaging die kunstmatige systemen een stap in de richting van natuurlijke systemen zou brengen. Bovendien leidt de ontwikkeling van dergelijke kunstmatige systemen tot betere inzichten in ingewikkelde, dynamische processen in de Natuur. De cel is een verbluffend voorbeeld van hoe de Natuur "zelf-organisatie" (meerdere moleculen ondergaan interacties met elkaar, waardoor ze samen één groot systeem vormen) en ingewikkelde processen benut om deze complexe, uit meerdere componenten bestaande, eenheid te verwezenlijken. Het vergroten van de complexiteit van moleculen en supramoleculaire systemen om zo functionele systemen te optimaliseren is een doel waar veel wetenschappelijke groepen zich mee bezig houden. Dit heeft met variërende mate van succes geleid tot het ontwerp en de verwezenlijking van een breed scala aan functionele moleculen en supramoleculaire systemen. Ondanks het feit dat supramoleculaire chemie veel mogelijkheden biedt om de complexiteit van systemen te vergroten, brengt de inherente labiliteit van de interacties tussen de moleculaire eenheden en het feit dat het systeem als geheel dynamisch is ook uitdagingen met zich mee. Het ontwerpen, maken en bestuderen van zulke systemen is daardoor geen eenvoudige opgave.

Het onderzoek dat is beschreven in dit proefschrift beschrijft nieuwe supramoleculaire systemen die ontworpen zijn om verscheidene specifieke functies te hebben. De eigenschappen van de moleculaire bouwstenen in de supramoleculaire aggregaten zorgen voor functionele handvaten waarmee het supramoleculaire systeem als geheel beïnvloed kan worden. Dit proefschrift beschrijft het ontwerp, de synthese en de studie van een variëteit aan responsieve moleculen en de responsieve systemen die gevormd worden door zelf-organisatie van deze moleculen. Daarnaast is het doorgeven van informatie tussen moleculen in de supramoleculaire structuren een thema dat terug te vinden is in meerdere hoofdstukken van dit proefschrift. *Chiraliteit*, *responsiviteit* en *aggregatie* zijn de rode lijnen die door dit proefschrift lopen.

In *hoofdstuk 2* is het concept van auto-amplificatie van moleculaire chiraliteit *via* inductie van supramoleculaire chiraliteit beschreven. Diaryletheen fotochemische schakelaars werden gebruikt in auto-katalytische inductie. Een kleine hoeveelheid van chiraal enantiozuiver ring-gesloten diaryletheen (sergeant) werd toegevoegd aan zijn prochirale ring-geopende diaryletheen precursor (soldaat). Vervolgens werd een gel van het mengsel gemaakt waarin de chiraliteit van de gel bepaald wordt door de chirale sergeant, dat als sjabloon dienst doet, en waarop de formatie van (*P*)- of (*M*)-helische gel volgt, afhankelijk van de chiraliteit van de sergeant. De chiraliteit wordt op deze manier overgebracht van het moleculaire op het supramoleculaire niveau. Vervolgens werd de gel bestraald met UV licht, wat leidt tot ring-sluiting van de prochirale diaryletheen soldaten. Omdat de soldaten door de invloed van de sergeant gerangschikt zijn in de gel fibers, wordt één enantiomeer in overmaat gevormd en op

deze manier wordt de chirale informatie opgeslagen op moleculair niveau, als gevolg van de ring-sluiting. Dit voltooit de cyclus van moleculaire chiraliteit *via* supramoleculaire chiraiteit en terug naar moleculaire chiraliteit van dezelfde moleculen. Dit systeem is één van de weinige voorbeelden waarin het chirale product van een reactie zijn eigen asymmetrische vorming katalyseert. Dit proces lijkt op zogenoemde "auto-katalytische reacties", maar in dit geval vindt de auto-amplificatie plaats in een kinetisch bevroren toestand.

Hoofdstuk 3 beschrijft het ontwerp, de synthese en de studie van nanobuizen waarin chiraliteit gebruikt wordt als middel om de morfologie van de zelf-georganiseerde structuren te beïnvloeden. Voor zover ons bekend, is dit het eerste voorbeeld waarin in zulke objecten, de chiraliteit in het hydrofobe deel van de amfifielen is ingebouwd, net zoals in natuurlijke membranen. De morfologie van de nanobuizen in water kan volledig worden bepaald door de fractie van de chirale component aan te passen in het mengsel van chirale en achirale amfifielen. Drie type aggregaten kunnen reproduceerbaar gevormd worden en zijn geanalyseerd met behulp van een variëteit aan spectroscopische en microscopische technieken. Het feit dat de nanobuizen gevormd worden in water en dat chiraliteit gebruikt wordt om de morfologie van de aggregaten te bepalen, brengt dit systeem één stap dichter bij natuurlijke systemen. Bovendien kunnen de nanobuizen ontmanteld worden onder invloed van licht en dit biedt wellicht mogelijkheden voor de ontwikkeling van geheugensystemen.

De synthese van zes verschillende aromatische amfifiele structuren werd bestudeerd, waarvan de resultaten zijn beschreven in *hoofdstuk 4*. Het doel was de synthese van amfifiele aromatische derivaten met een hydrofiele ethyleenglycol kopgroep en twee hydrofobe alkylketens, verbonden met de aromatische kern door ether of koolstof-koolstof bindingen. De benodigde methodologie werd ontwikkeld en verscheidene amfifielen konden gesynthetiseerd worden. Een verzameling van systematisch verschillende amfifiele thioxanthon-derivaten met ethyleenglycol kopgroepen en alkylstaarten met verschillende lengte werden bestudeerd met behulp van cryo-TEM. Binnen deze subklasse, onderverdeeld naar de aromatische kern, konden nuttige vergelijkingen worden gemaakt. De verkregen kennis van de thioxanthon-derivaten heeft geleid tot de ontwikkeling van zeer interessante, geleidende bilaag systemen en is beschreven in hoofdstuk 5.

In *hoofdstuk 5* worden nieuwe synthetische amfifielen die ion-geleidende membranen vormen beschreven. Naast zeer stabiele vlakke bilagen konden ook cel-achtige containers gevormd worden. Interessant genoeg bleek dat hoewel ionen de bilagen kunnen passeren, dit voor grote geladen moleculen zoals calceïne niet mogelijk is. Daarnaast hebben we laten zien dat een functionerend membraaneiwit in het membraan kan worden ingebouwd. De geleidende eigenschappen van deze zeer stabiele functionele membranen, in afwezigheid van specifieke ionkanalen, -pompen en -transporters, samen met de compatibiliteit voor eiwitten, bieden fascinerende mogelijkheden voor het ontwerp van primitieve functionele kunstmatige cellen. Het simpele systeem dat hier beschreven is vindt mogelijk toepassing voor het genereren van een potentiaal over de bilaag en kan hiermee mogelijk energie leveren voor processen zoals ion kanaal werking en transport in kunstmatige systemen.

Hoofdstuk 6 beschrijft het, voor zover ons bekend, eerste voorbeeld waarin een moleculaire motor zelf-organisatie ondergaat en gedefinieerde structuren in water vormt en waarin de moleculaire component in de supramoleculaire systemen een reversibele verandering in morfologie bewerkstelligt wanneer het blootgesteld wordt aan externe stimuli. Een langzame ($\tau_{1/2}$ = 7 d bij 20 °C) en een snelle ($\tau_{1/2}$ = 40 ns bij 20 °C) amfifiele moleculaire motor werden ontworpen, gesynthetiseerd en bestudeerd met cryo-TEM miscroscopie en UV-vis spectroscopie. De snelle motor vormt getordeerde nanobuizen als deze geassembleerd wordt met DOPC in water en is één van de snelste moleculaire motoren die tot op heden bekend zijn. Door zijn snelheid is de halfwaardetijd te kort om eventuele veranderingen waar te nemen na bestraling van de motor. De langzame moleculaire motor daarentegen, vormt nanobuizen in water en ondergaat isomerisatie van *trans* naar *cis* als gevolg van bestraling met licht. Deze isomerisatie heeft als gevolg dat de nanobuizen herorganiseren en vesicles gevormd worden. Verwarmen van het systeem induceert de isomerisatie van de moleculaire motor van *cis* naar *trans* en de nanobuizen worden vervolgens weer gevormd.

Sinds supramoleculaire chemie voor het eerst beschreven werd, enige decennia geleden, is het onderzoeksveld steeds populairder geworden. De belangrijkste reden hiervoor is de mogelijkheden die supramoleculaire chemie biedt om kunstmatige systemen steeds complexer te maken. Bovendien zijn over de jaren heen steeds betere technieken ontworpen en beschikbaar geworden voor de analyse van zulke systemen en hun morfologie. Door het inbouwen van functionele moleculen in supramoleculaire assemblages kan responsiviteit in het grotere systeem als geheel geïntroduceerd worden, gebaseerd op de eigenschappen van de moleculaire bouwstenen. Supramoleculaire chemie heeft bijgedragen aan het beter begrijpen van de Natuur en stelt ons in staat om steeds complexere kunstmatige systemen te bouwen. Desondanks is het ware potentieel nog niet bereikt. Dit proefschrift draagt een kleine steen bij aan de verdere ontwikkeling van responsieve supramoleculaire systemen.

Acknowledgements

Doing research is not more difficult, time consuming or frustrating than any other profession. Perhaps it has more ups and downs and maybe the lows are lower, but the highs are higher in return. What makes performing research really worth it to me are the new experiences and knowledge that are gained and shared over the years. By that, I do not only mean scientific expertise, but also the many things one learns from the people you meet, having different backgrounds, points of view and opinions. I have a lot of respect for many people I have met during this period in my life and am grateful for having had this opportunity. With the writing of these acknowledgements, my time as a PhD draws to an end and I would like to thank those that have contributed to it and my personal knowledge.

Let me start by thanking all past and present members of the Stratingh institute in the time that I was part of this amazing group. In particular, I would like to thank my many labmates over the years. From the first lab I was in, with only Francesca and Paula, to the last period of my time in the green building. My labmates there have made the 'laatste loodjes' much more enjoyable. Thank you for this, Claudia, Wim, Wiktor, Mickel, Gosia, Anja, Maria and Yange. My gratitude is of course extended to the people in the surrounding labs of the Minnaard, Hirsch and Witte groups. You have been gone for quite some time now Dr. Guacamole, but I often recall the sausage parties and learned many life-lessons from you. I apologize for whatever it was that made you hate me in the beginning.

Beste Ben, het was een waar genoegen om deel uit te maken van de Feringa groep en jou als mentor te hebben. Ik heb veel van je geleerd en jouw enthousiasme, nieuwsgierigheid, kritiek en scherpe blik op dingen heb ik altijd op prijs gesteld. Ik waardeer de vrijheid die ik gehad heb tijdens mijn onderzoek en de mogelijkheden die je geboden hebt in de breedste zin van het woord.

Wesley, thank you for your critical input and the many questions you have asked over the years regarding different projects in this thesis as well as the projects that did not make it into this thesis. You have your own way of keeping people sharp and alert and I appreciate that you are always approachable and willing to help. I would also like to thank the other members of the reading committee for their critical reading of my thesis, Prof. Roeland Nolte and Prof. Jeroen Cornelissen. Niet minder belangrijk, Tineke; zonder jouw kordate en daadkrachtige bemiddelen had dit boekje hier nu waarschijnlijk niet in deze vorm gelegen, bedankt.

The two people that have provided most of the much needed daily distraction over these last years in the lab and office are Wim and Claudia and I want to thank you two for being my paranymphs. Claudia, you have a big heart and are most often in for a laugh. It was a lot of fun to share the lab and office with you. Wim, ik ben blij dat we altijd een gezonde balans vonden van humor en serieus, werk en vrije tijd. Het verbaast me steeds weer hoeveel dingen we eigenlijk gemeen hebben. Ik vind het passend en ben blij dat we op dezelfde dag verdedigen en kijk uit naar het feest en hopelijk dat lang beloofde casino uitje en een rondje in de turbo polyp.

During my PhD I had the opportunity to guide several students and I have learned a lot from this experience. Anja, je bent gegroeid tijdens onze lange samenwerking (sorry ik kon het niet laten) en je bent nu een zelfverzekerde jonge wetenschapper en ik wens je veel succes toe. Marius, you are one of the most stubborn persons I know. Luckily, you are also very talented and critical and I am convinced you will do well in your PhD and future career. It was truly a pleasure to work with you. Anniek, onderzoek doen was niet altijd even makkelijk voor jou, maar ik denk je er uiteindelijk veel van geleerd hebt en ik wens je veel succes toe als docent.

Gerald en Cati, you are a wonderful couple and I am still amazed how well it "clicks" between the four of us in any given combination. I am curious where our paths will meet again, because I am convinced they will.

I have been very fortunate in the many collaborations I have participated in during my PhD. Marc, we hebben veel discussies over wetenschap en andere dingen gehad en ik vind het altijd interessant hoe jij tegen dingen aan kijkt. Ik heb veel geleerd van de projecten waar je in betrokken bent geweest en (tot mijn schrik) staat er in alle hoofdstukken van dit boekje een TEM plaatje. Armağan, I enjoyed discussing with you as we have very different backgrounds and therefore different ways of looking at the same thing. Likewise, I learned much from discussing things with you Duygu. My "shitty lipids", as you referred to them, have caused much frustration but also happiness when things worked. I never felt our collaboration was difficult or fruitless although the equipment was not always on our side. Peter and Jiawen, thank you both for our massive synthetic cooperations. Dear Jack, you have left an impression and you have inspired me beyond what you may think, thank you and I wish you and your family all the best.

Ik ben dankbaar dat ons gezin altijd voor elkaar klaar staat en dat jullie meestal naar mijn verhalen en (soms slechte) grappen willen luisteren. Ma, ik waardeer de ongecompliceerde manier waarop jij in het leven staat en geniet van elke dag, ook al komen er soms nare dingen om de hoek kijken. Pa, we lijken veel op elkaar en dat botst soms wat, maar je onvoorwaardelijke steun is veel waard. Heb ik toch nog die boom geplant en ik vind het grappig dat ik uiteindelijk toch de stofjas aan heb waar je altijd voor waarschuwde. Lieve Joke, jij kent me op sommige vlakken het beste en ik heb ontzettend veel respect voor je doorzettingsvermogen en no-nonsense houding. Ik ben benieuwd wat de toekomst brengt en wanneer onze wegen weer overlappen. Bouke, Sandra en Dyon, jullie natuurlijk ook bedankt voor alles gedurende de jaren.

Paula, I could fill many pages here to thank you for everything, but I know you know. Life is not always fair and yet you always see the positive thing in anything and anyone. I am convinced life will smile at you and us in the future. You make me happy and life is better and more fun with you.

"This it is, and nothing more."
(E. A. Poe, 1845)